# ISOTOPES AND RADIATION TECHNOLOGY

*A Quarterly Technical Progress Review*

Prepared for DIVISION OF TECHNICAL INFORMATION / DIVISION OF ISOTOPES DEVELOPMENT, U. S. ATOMIC ENERGY COMMISSION,
By ISOTOPES INFORMATION CENTER, OAK RIDGE NATIONAL LABORATORY

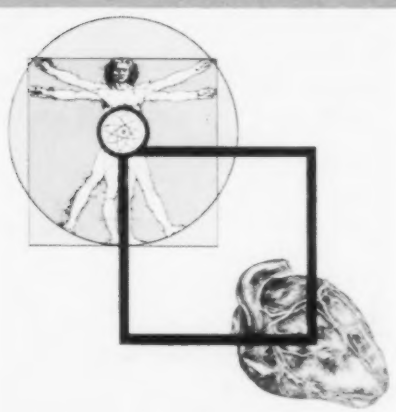

*Winter 1969-1970*

● VOLUME 7

● NUMBER 2

XUM

# Isotopes and Radiation Technology

is a Technical Progress Review prepared by the Isotopes Information Center, Oak Ridge National Laboratory, at the request of the Divisions of Technical Information and Isotopes Development, U. S. Atomic Energy Commission. This Review is intended to assist those interested in keeping abreast of significant developments in the fields of isotopes and radiation technology. It is not a comprehensive review of all literature published in this field during a given quarter; rather, it is a mechanism for presenting concise, selected reviews of information on subjects of prevailing Commission interest as it becomes available.

This Review attempts to relate the published results of research and development sponsored by the Division of Isotopes Development to significant developments in radioisotopes and radiation technology, as reported in the world literature. Coverage includes isotope production and development, isotope technology development, isotope applications technology, process radiation development, and radiation processing of food and medical supplies.

In addition to reviews of current literature and special review articles dealing with specific isotopes, facilities, and applications, this publication occasionally contains feature articles prepared by recognized experts on specific topics of current interest. Critical evaluations and interpretations presented are those of the editors and invited reviewers; therefore readers are encouraged to consult the original references in order to obtain all the background of the work reported and the interpretation of the results given by the original authors.

Insofar as feasible all references are checked by the editors, using the library facilities of Oak Ridge National Laboratory, Oak Ridge Associated Universities, and the University of Tennessee. Occasionally, however, the cited material is not available; such cases are identified by an asterisk (*).

The subject headings listed below have been adopted to help maintain continuity and order, from one issue to the next, in the material reviewed. All reviews, except Feature Articles, will be arranged under these headings; but any one issue will not necessarily contain all the headings.

*Isotope Production and Development*
*Isotope Technology Development*
*Food Irradiation*
*Process Radiation Development*
*Source Development*
*Isotopic Heat and Power Development*
*Applications in Life Sciences*
*Safety*
*Isotopes Around the World*
*Miscellaneous*

**P. S. Baker, Robert H. Lafferty, Jr., Martha Gerrard, R. E. Greene, F. E. McKinney, F. J. Miller, and D. N. Hess,** *Editors*
**A. F. Rupp,** *Adviser*

**OAK RIDGE NATIONAL LABORATORY**

Issued quarterly by the U. S. Atomic Energy Commission. Use of funds for printing this publication approved by the Director of the Bureau of the Budget on December 16, 1968.

XUM

# Isotopes and Radiation Technology

Vol. 7, No. 2 Winter 1969–1970


## Contents


I Isotopic Heat and Power Development

137 **Radioisotope-Powered Heart-Assist Devices**

138 **Factors Relating to the Application of Radioisotopes to Circulatory-Support Systems**

139 Power Supply

139 Radioisotope Fuels

142 Radiation Effects

144 Conclusions

145 **Development of a Simplified Stirling Engine To Power Circulatory-Assist Devices**

146 Engine Operation

151 Conceptual Design of a Radioisotope-Fueled Engine

155 Experimental Program

160 Conclusions

161 **A Radioisotope-Powered Stirling Engine for Circulatory Support**

161 Principles of Engine Operation

164 Description of Engine

169 Experimental Investigation

171 Conclusions

171 **Design of an Implantable, Rankine-Cycle Radioisotope Power Source**

172 Power-Source Design

173 Heat-Source Subsystem

174 Rankine-Cycle-Engine Subsystem

179 Hydraulic Subsystem

181 Reference Power-Source Specifications

181 Conclusions

182 **An Implantable Artificial-Heart Power Source**

182 Power-Source Concept

186 Conceptual Design of Power-Source Components

191 Conclusions

192 Acknowledgments

192 **Radioisotope-Powered Cardiac Pacemaker**

194 **British Radioisotope-Powered Cardiac Pacemaker**

194 Radioisotope-Powered Battery and Converter

194 Safety

196 Preliminary Performance Tests Under Simulated Body Conditions

197 **$^{238}$Pu for Biomedical Applications**

198 Experimental

201 Radiation and Dosimetry Measurements

206 Acknowledgments


XUM

207 **Promethium Technology: A Review**
208 Applications
209 Availability
209 Nuclear Properties
212 Shielding
213 Production
216 Chemistry of Promethium
218 Materials of Containment
218 Heat-Source Fabrication
222 **Study of $^{171}Tm$ as Power Source for Circulatory-Support System**
222 Reactor Production of $^{171}Tm$
227 Refinement of Product Radioisotopes
229 Comparison of Production Methods
231 Conclusions
231 **In-Phantom Dosimetry of $^{147}Pm_2O_3$ Heat Sources in Relation to Circulatory-Support Systems**
231 Procedure for Computing the Dose Rates Surrounding an Implanted Radioisotopic Heat Source
233 Procedure for Measuring the Dose Rates Surrounding an Implanted Radioisotopic Heat Source
233 Shielding and In-Phantom Dose Predictions
237 Shielding and In-Phantom Dose Measurements
240 Summary and Conclusions

II Isotopes Around the World

241 **French Radioisotope Use Increases in 1968**
241 **"Understanding the Atom" in German**
241 **Tritium Labeling of Biochemicals by Modified Wilzbach Technique**
242 **Skinpreg Process Enhances Wood Properties**

III Miscellaneous

243 **Availability of Isotopes and Services**
244 **AEC Activities**
246 **General**
247 **Publications by Isotopes Information Center**

Superintendent of Documents, U. S. Government Printing Office, Washington, D. C. 20402, $2.50 per year.

XUM

Section

I

Isotopes and Radiation Technology

# Isotopic Heat and Power Development

## Radioisotope-Powered Heart-Assist Devices*

For a number of years there has been considerable interest in the incorporation of radioisotopes into various types of heart-assist devices.[1-5] The National Heart Institute (NHI) has carried out a study to determine the need for a circulatory-support system, to identify key technological problems requiring solution, and to forecast the time and money required for the development of such devices. This study indicated that heart disease claimed about 700,000 American lives this year and that about 100,000 of these might have been helped if a circulatory-support system were available.

The NHI has undertaken a program to develop a series of devices beginning with a temporary-assist device such as the DeBakey left-ventricle-assist pump and ending with a totally implantable system to replace the biological heart.

The AEC selected four firms to conduct parallel conceptual-design studies of a radioisotope-powered engine to actuate blood pumps that would assist or replace a diseased or damaged heart.

At the present time, several contractors have completed early-phase development work, and it was felt that it would be appropriate to devote an issue of *Isotopes and Radiation Technology* to a consideration of these heart-assist devices. The total story includes descriptions of heart circulatory-assist devices, discussions of the preparation of candidate power fuels, a brief mention of the cardiac pacemaker, and a report on in-phantom dosimetry measurements.

Because of the complexities of the various systems involved, the editors have made no attempt to try to coordinate or correlate the individual papers, nor have they tried to delineate any apparent inconsistencies in the data. As a result, there is some duplication of background material and considerable difference in styles. However, we feel that each paper is more valuable as a unit. Any questions should be referred to the individual contractors. (PSB)

*Permission for the reproduction of the five papers on circulatory-assist systems has been kindly granted by the individual authors and by the Institute of Electrical and Electronics Engineers, Inc., at whose Intersociety Energy Conversion Engineering Conference in Boulder, Colo., they were presented on August 13–17, 1968. [Transactions were published in the March 1969 issue of *IEEE (Institute of Electrical and Electronics Engineers) Transactions on Aerospace and Electronic Systems.* The "Implantable Power Source" section is on pp. 723–778 of Volume I.]

### References


1. G. T. Seaborg, Mass Production and Practical Applications of Actinide Elements, *Isotop. Radiat. Technol.*, **6**(1): 6-9 (Fall 1968).
2. W. H. Pennington, D. W. Cole, and W. E. Mott, Radioisotopic Power Sources for Human Implantation, *Isotop. Radiat. Technol.*, **5**(4): 306-312 (Summer 1968).
3. D. L. Fleming, C. O. Brewer, D. L. Coffey, and P. L. Blue, Plutonium-238-Powered Cardiac Pacemaker, *Trans. Amer. Nucl. Soc.*, **11**: 89-90 (June 1968).
4. J. Greenborg and B. I. Griffin, Biological Dose Rate from an Implanted Isotope-Powered Circulatory Assist Device, *Trans. Amer. Nucl. Soc.*, **11**: 90-91 (June 1968).
5. R. K. Disney, Radiation Shielding Considerations of an Implanted $^{238}Pu$ Power Source for the Artificial Heart, *Trans. Amer. Nucl. Soc.*, **11**: 92-93 (June 1968).




XUM

# Factors Relating to the Application of Radioisotopes to Circulatory-Support Systems

By Donald W. Cole, William E. Mott, and Leonard A. Sagan*

**Abstract:** *The U. S. Atomic Energy Commission (AEC) in cooperation with the National Heart Institute (NHI) of the National Institutes of Health is developing radioisotope power supplies for devices to assist or totally replace the human heart. In a radioisotopically powered artificial heart, heat from the decay of radioisotopes would be used to provide power for the operation of a blood pump. Radioisotope power sources offer the advantages of being completely implantable and of having a relatively long life.*

*Initially, conceptual designs of radioisotope heat engines have been developed, candidate radioisotopes fuel forms evaluated, and the radiation doses to be expected from the various fuel forms studied. Conceptual-design studies indicate that a power supply capable of meeting the specifications of a circulatory-support system can be developed. The optimum fuel is $^{238}Pu$. Radiation damage does not appear to be a problem.*

More than 10 million Americans currently have some form of heart disease, and over one-half million die each year as a result of heart disease. Many of the victims could possibly have been helped by means of circulatory-assist devices. In recent years, externally powered blood pumps able to assist a failing heart have been used successfully on persons suffering from heart attacks or recovering from heart surgery. As the capability to pull people through heart attacks improves, there will be a need for completely implantable circulatory-support systems for long-term use in cases where severe heart damage has occurred. Radioisotope power holds great promise for such an application.

The AEC and the NHI recently sponsored a program to investigate the feasibility of developing an implantable radioisotopic power supply for a blood pump. The conceptual-design studies[1-4] of radioisotopically powered thermodynamic engines performed under this program are the subject of papers included in this issue.[5-8] Thermodynamic converters were selected for the studies because they offer higher conversion efficiencies than thermoelectric or thermionic converters. High efficiency reduces the amount of radioisotope required and hence the weight of the device and the waste heat to be dissipated.

As presently conceived, the components of a circulatory-support system would consist of a blood pump located in the region of the natural biologic heart, a power supply probably located in the abdominal cavity, some form of power transmission between the energy source and the blood pump, and a control system which would use physiological input signals to regulate the blood pumping rate.

The consensus of investigators working on blood pumps is that the pump output should be similar to that of the natural heart.[9] The collapsible bag or sac-type blood pump, with the repeated squeezings applied by hydraulic or pneumatic pressure, seems promising and nontraumatic to the blood if gentle, gradual pressures are applied.

With radioisotope power, the supply unit can be subdivided into a radioisotope heat source, a thermodynamic converter, and a heat sink. The radioisotopic fuel will be suitably encapsulated to contain the material under any foreseeable conditions. The thermodynamic converter will transform the thermal energy of the heat source into fluid energy to drive the blood pump. The amount of heat generated by the power supply to be rejected to the heat sink is comparable to that developed by other organs such as the liver, brain, or natural heart. The heat generated by these organs is normally removed by the blood and eventually dissipated from the body at the optimum rate to maintain and control body temperature. The blood also appears to be the optimum heat-sink medium for an implantable power source.[10] Some type of fluid coupling would have to be utilized to transmit the power between the power source and the blood pump. This would be particularly attractive if the blood pump were of the sac type that uses fluid power.

The final component of a circulatory-support system, the control mechanism, is the least defined part of the system since the ultimate requirements to satisfy bodily needs are not completely known at this time. A number of investigators have proposed that a circulatory-support system can be made sufficiently self-regulating by supplying a mechanical equivalent to Starling's law of the heart: the principle that the blood-pump output should be equal to, and regulated by, the venous input. This is a useful and necessary control principle, but it may not be sufficient, and additional controls may be required.

*U. S. Atomic Energy Commission.

This paper will discuss the general requirements that an implantable power supply must satisfy, the results of efforts to evaluate candidate radioisotopes as implantable heat sources, and estimates of the biological effects of an implanted source of radiation. It is intended as a companion paper to the four papers describing the work performed to date on nuclear power sources for circulatory-assist devices.[5-8]

## Power Supply

A circulatory-support system, whether it is an assist device or a total heart replacement, should:

1. Return a patient's circulation to such a level that he may resume useful activity.
2. Be sufficiently sensitive to changing activity and emotional levels so that the patient is not handicapped in a normal social environment.
3. Operate at such a level of reliability that both the patient and his associates can accept the fact of implantation without apprehension.

Further, it must be:

1. Available at a price that would allow those who could benefit from such a device to acquire one.
2. Biologically compatible with body tissues and fluids for an indefinite period of time.
3. Implantable with surgical risks no greater than those of current cardiac surgery.
4. Capable of widespread use without presenting a risk or nuisance to the general public as rehabilitated patients move about freely.

For the purpose of the conceptual-design studies, the following specific performance requirements were established:

1. Power output required is in the range of 1 to 7 watts to accommodate the varying activity level of the patient.
2. Heat rejection to the body is limited to a maximum of 50 watts. The bulk temperature rise in the blood heat exchanger is limited to 4°C, and the maximum temperature to which the blood is exposed should not exceed 43°C.
3. Weight and volume limits for an abdominal implant is limited to 3000 g anchored weight and 2 liters of volume.
4. Lifetime in the range of 7 to 10 years is required.

These specifications are not optimum, but are the limit cases. There is no question that the performance requirements will change in the future as the interface between the circulatory-support system and the body is better defined. Clearly, any future developmental program would be directed toward minimizing weight and volume.

## Radioisotope Fuels

The use of a radioisotopic heat source in an implantable power supply is very attractive because it is a highly reliable and predictable form of energy. The criterions for selecting radionuclides for implantation as heat sources place considerable emphasis on radiation, half-life, and power density. High power density and a minimum of penetrating radiation help to decrease the radiation dosage, the weight, and the volume of the unit. A reasonably long half-life is desirable to avoid the frequency of surgery to replace the power source. Plutonium-238, $^{147}$Pm, and $^{171}$Tm were initially selected as the principal candidates for implantable power sources.

### Plutonium-238

Neptunium-237, the precursor of $^{238}$Pu, is produced by irradiation of uranium in reactors by the following neutron reactions:

$$^{235}\mathrm{U}(n,\gamma)^{236}\mathrm{U}(n,\gamma)^{237}\mathrm{U} \xrightarrow{\beta^-} {}^{237}\mathrm{Np} \qquad (1)$$

$$^{238}\mathrm{U}(n,2n)^{237}\mathrm{U} \xrightarrow{\beta^-} {}^{237}\mathrm{Np} \qquad (2)$$

After being chemically separated from the uranium, the $^{237}$Np is further irradiated in a high-neutron-flux reactor to produce $^{238}$Np which beta decays with a 2-day half-life to $^{238}$Pu. Uranium-fueled power reactors are an excellent source of $^{237}$Np. Measurements of fuel from existing power reactors can be extrapolated to indicate that 100-kg quantities will be available from power reactors annually by 1980. Plutonium-238 combines a relatively high specific power output with a long half-life (87.5 years). This results in a useful lifetime of greater than 10 years. One gram of pure $^{238}$Pu produces approximately 0.56 watt of heat, primarily from alpha decay.

The shielding requirements for currently available $^{238}$Pu fuel are established principally by isotopic and elemental impurities in the product. The isotopic impurities in currently produced $^{238}$Pu fuel are shown in Table 1.

The isotopes of plutonium with atomic weights greater than that of $^{238}$Pu do not contribute significantly to the radiation flux. They act primarily as a diluent, reducing the energy density of the product. The important isotopic impurity is $^{236}$Pu that is present at a concentration level of about 1 ppm by weight. The decay chain of $^{236}$Pu has in it two important gamma-ray-emitting nuclides: $^{212}$Pb and



XUM

**Table 1 Composition of Currently Produced $^{238}$Pu Fuel**

| Isotope | Abundance, % |
|---|---|
| $^{238}$Pu | 81.0 |
| $^{239}$Pu | 15.0 |
| $^{240}$Pu | 2.9 |
| $^{241}$Pu | 0.8 |
| $^{242}$Pu | 0.1 |
| $^{236}$Pu | $1.2 \times 10^{-4}$ |

$^{208}$Tl (Fig. 1). As the $^{238}$Pu product ages from the purification date, its gamma activity increases as these two nuclides increase in abundance. For example, the calculated dose rate at 10 cm for a 10-year-old 30-watt source of the above composition having a total shielded weight of 2 lb is 37 mrems/hr, whereas that for an equivalent source of fresh $^{238}$Pu fuel is 17 mrems/hr (Ref. 11).

Elemental impurities in the $^{238}$Pu fuel as currently processed enhance the neutron flux from the material. The alpha particles that result from the natural decay

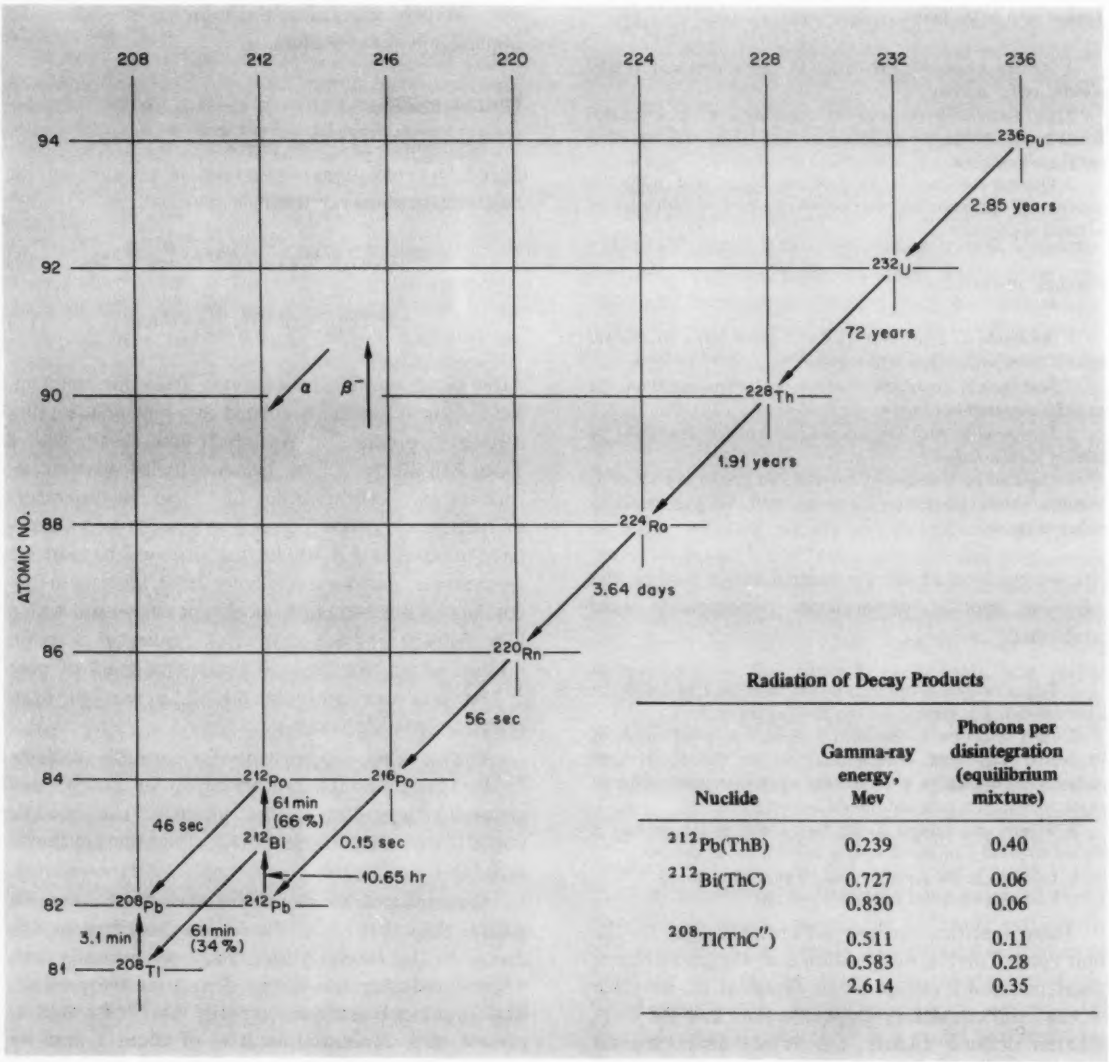


**Radiation of Decay Products**

| Nuclide | Gamma-ray energy, Mev | Photons per disintegration (equilibrium mixture) |
|---|---|---|
| $^{212}$Pb(ThB) | 0.239 | 0.40 |
| $^{212}$Bi(ThC) | 0.727 | 0.06 |
| | 0.830 | 0.06 |
| $^{208}$Tl(ThC″) | 0.511 | 0.11 |
| | 0.583 | 0.28 |
| | 2.614 | 0.35 |

**Fig. 1 Decay chain of $^{236}$Pu.**

of $^{238}Pu$ interact with the light-element impurities to produce an increase in neutrons. The total number of neutrons arising from these alpha–neutron reactions is directly proportional to the number of light-element impurity atoms present. In currently produced $^{238}Pu$ the impurity level is such as to cause an order of magnitude increase in the neutron flux over the irreducible minimum flux that results from the spontaneous fission of $^{238}Pu$ and $^{240}Pu$ (Ref. 12).

In an effort to reduce the radiation from $^{238}Pu$ fuel, the AEC has initiated programs to investigate the feasibility of reducing the isotopic and elemental impurity levels. The critical isotopic impurity, as mentioned before, is $^{236}Pu$. A lessening of this impurity from 1.2 ppm to 0.1 ppm would reduce this problem to one of negligible concern. A study to determine the feasibility and cost of producing large quantities of $^{238}Pu$ having a low $^{236}Pu$ content is now under way.

An electrorefining process, originally developed for purifying $^{239}Pu$, has been successfully adapted to decrease significantly the elemental impurities in $^{238}Pu$ (Ref. 13). The first batch of electrorefined $^{238}Pu$ was prepared by Los Alamos Scientific Laboratory during August 1967. Subsequent evaluation of electrorefined $^{238}Pu$ by Los Alamos has established the melting point as 639 ± 3°C. The specific neutron activity for several lots has ranged between 2420 and 2781 n/(sec)(g) [calculated rate for spontaneous fission is 2150 n/(sec)(g)].

In addition to $^{238}Pu$ metal, fuel compounds which have melting points higher than the metal are being evaluated. Initially, plutonium nitride appeared to be an attractive fuel, since it had a high melting point, good thermal conductivity and density, and satisfactory compatibility with container materials. For a check on the radiation from the nitride, a batch was prepared from electrorefined $^{238}Pu$ metal which had shown an average specific activity[14] of 2680 n/(sec)(g). After preparation, the nitride powders were encapsulated in two tantalum capsules with a wall thickness of 15 mils. There was no significant difference between the average neutron activity of the nitride and of the metal, which confirms the prediction of zero neutron yield from nitrogen in the presence of 5.5-Mev alpha particles, the thresholds for $(\alpha,n)$ reactions with $^{14}N$ and $^{15}N$ being 6.15 and 8.15 Mev, respectively. The average beta–gamma dose rate of 0.6 mrad/(hr)(g of Pu) at 10 cm distance, however, was approximately three times the average value of 0.2 mrad/(hr)(g of Pu) for metal samples. The increased dose rate is due to the $(\alpha,p)$ reaction on $^{14}N$ that leaves the product nuclide $^{17}O$ in the first excited state, the transition to the ground state producing a 0.869-Mev gamma ray. The $^{14}N(\alpha,p)^{17}O$ reaction has a low threshold of 1.54 Mev and is thus energetically possible with the 5.5-Mev alpha particles from $^{238}Pu$. The use of enriched $^{15}N$ in place of normal nitrogen would possibly materially reduce the abundance of the 0.869-Mev gammas. Nitrogen-15 has an $(\alpha,p)$ threshold of 5.05 Mev, and the first excited level in the product nucleus $^{18}O$ is at 1.98 Mev. Thus an alpha particle energy of at least 7.02 Mev is required to produce the 1.98-Mev gamma ray. However, since ordinary nitrogen contains 99.64% $^{14}N$ and only 0.34% $^{15}N$, the required high degree of enrichment may lessen the attractiveness of the enrichment approach.

The neutron and gamma emission rates of $^{238}Pu$ oxide are currently under investigation. The emission rates for a specimen prepared by converting pure $^{238}Pu$ nitride to pure $^{238}Pu$ oxide (natural oxygen) have been measured. The neutron emission rate of this oxide was 12,100 n/(sec)(g). For comparison, the emission rate from a sample of the production-grade oxide was 47,000 n/(sec)(g). A gamma dose rate of approximately 0.5 mrad/(hr)(g of Pu) at 10 cm was measured on the pure oxide after encapsulation in 30-mil tantalum. The neutron emission rate obtained for the pure oxide represents an increment of 9950 n/(sec)(g) above the spontaneous fission contribution of 2150 n/(sec)(g). The measured gamma dose rate from the pure oxide was 2.5 times that obtained for the pure metal. The increased neutron and gamma-ray dose rates can be attributed to the presence of $^{18}O$ and the resulting $(\alpha,n)$ reaction. Additional samples of pure $^{238}PuO_2$ are being prepared with natural and with depleted oxygen for further evaluation.

### Promethium-147

Promethium-147 is a fission product with a half-life of 2.62 years. About 2% of uranium and plutonium fissions yield $^{147}Nd$ that decays with an 11-day half-life to $^{147}Pm$. Power reactors produce about 3 curies per thermal megawatt-day (based on aging of the fuel for one half-life).

Promethium-147 metal has a specific power of 0.32 watt/g. Although the half-life of this nuclide is relatively short, its moderate radiation characteristics make it attractive for use in an implantable power source. The radiation associated with a promethium source is due to the $^{147}Pm$ beta emission and bremsstrahlung, the $^{148m}Pm$ gamma emission, and the $^{146}Pm$ gamma emission. The soft $^{147}Pm$ radiation is readily shielded



XUM

by as little as 0.050 in. of heavy metal. The penetrating radiation from $^{148m}$Pm requires heavy shielding. However, because of the short half-life (42 days) of $^{148m}$Pm, significant reduction can be achieved by allowing the material to decay for approximately 2 years following separation. Unfortunately, because of its long half-life (4.4 years), $^{146}$Pm cannot be handled in the same way. Separation of the promethium isotopes is possible by present technology but prohibitively expensive.

Consideration has been given to using the differences in neutron cross sections of $^{146}$Pm and $^{147}$Pm to achieve a reduction in $^{146}$Pm content by selective "burnout" in high-neutron-flux reactors. A program has been initiated at the Pacific Northwest Laboratory to evaluate the burnout of $^{146}$Pm. Promethium targets with 0.25 ppm by activity of $^{146}$Pm were irradiated during 1967 and are now in storage allowing the $^{148m}$Pm to decay to the point where measurements can be made. Preparations are under way to irradiate promethium from a power reactor (3.5 ppm $^{146}$Pm) under various thermal and resonance neutron-flux intensities and for various durations. At a $^{146}$Pm-to-$^{147}$Pm curie ratio of 0.01, the dose rate from a 60-watt promethium source would be roughly equivalent to that from a 30-watt $^{238}$Pu source for total shielded source weights of 2 lb [assuming a relative biological effectiveness (RBE) of 10 for $^{238}$Pu neutrons].

### Thulium-171

Thulium-171 has the shortest half-life (1.9 years) and the lowest specific power (0.2 watt/g) of the radionuclides under consideration for human implantation. Nevertheless, this nuclide has attracted attention for this application where minimal weight is a prime requirement because it would require less shielding than either $^{147}$Pm or $^{238}$Pu. It is a low-energy beta emitter (0.1 Mev) that produces photons (0.067 Mev) in only 2% of its disintegrations. The problem associated with the utilization of $^{171}$Tm is that of controlling the isotopic impurity level of $^{170}$Tm, which has more penetrating radiation associated with it. It emits 0.88- and 0.97-Mev beta rays and 0.084-Mev photons in 23% of the disintegrations. Thus, for a shielded $^{171}$Tm heat source to have reasonably low weight and external radiation, it can contain only about $10^{-5}$ curie of $^{170}$Tm per curie of $^{171}$Tm.

The method of producing $^{171}$Tm is reactor irradiation of isotopically enriched $^{170}$Er, natural erbium, or natural thulium. Reactor irradiation of enriched $^{170}$Er would produce the desired purity ratio with an economical use of the reactor, provided $^{170}$Er with a purity of 99.99% were available as feed material. At the present time, enriched $^{170}$Er can be produced only by electromagnetic separation. The initial capital costs and the annual operating expenses of an enrichment facility are extremely high. To make this method of producing $^{171}$Tm attractive, there would have to be a significant reduction in the cost of highly enriched $^{170}$Er.

The production of $^{171}$Tm from natural erbium requires neutron fluxes so high that the use of power reactors is prohibited. The ratio of $^{170}$Tm to $^{171}$Tm resulting from irradiation of natural erbium would be close to unity; therefore, after the thulium is separated from the erbium target, a final enrichment step would be required to produce a usable product. Three techniques exist for enrichment: (1) reirradiation to burn out $^{170}$Tm, (2) natural decay of $^{170}$Tm in storage, and (3) electromagnetic separation. Of the three enrichment techniques, none appears capable of producing an economically attractive product.

The irradiation of natural thulium to produce $^{171}$Tm also requires a high neutron flux—on the order of $10^{15}$ n/(cm$^2$)(sec). To achieve a ratio of $^{170}$Tm to $^{171}$Tm of $10^{-5}$, the irradiation would probably be performed in two cycles to permit an intermediate chemical processing step to reduce the volume of the irradiated target. For a given reactor the yield of $^{171}$Tm by this process would be approximately one-third that which could be achieved by the irradiation of natural erbium.

In conclusion, the prospect of producing large quantities of $^{171}$Tm fuel having a $^{170}$Tm/$^{171}$Tm activity ratio in the $10^{-4}$ to $10^{-5}$ range does not appear promising at this time.

## Radiation Effects

Radiation effects may be considered as either acute or chronic, the former occurring days or weeks following initial exposure and the latter occurring years later. The acute effects of radiation from an implanted source may be either local effects to surrounding tissues or general radiation sickness. The chronic effects of nonlethal radiation exposure are cancerous growth (carcinogenesis), leukemia, and life shortening.

For the purpose of this discussion, a 30-watt radioisotopic heat source is assumed to be the primary source of power. For a shielded $^{238}$Pu metal source typical of a fuel product currently available, the dose

rate at 10 cm is calculated to be about 25 mrems/hr (Ref. 11). The mean radiation dose to the abdominal contents is estimated to be about 0.5 rem/day. This estimation is admittedly based upon many assumptions concerning the quantity and radiation characteristics of the radioisotope fuel, the shielding, and the placement of the fuel within the body; it is intended here only as a model for discussion.

### Acute Effects

Evidence accumulated from radiotherapy experience suggests that, at relatively low dose rates, tissues are capable of repair and are therefore resistant to permanent damage.

A recent survey of the literature[15] indicates that, at dose rates of less than 1 rad/min, moist desquamation (which implies irreversible tissue destruction) is unlikely to occur at total doses of less than many thousand rads. This estimate is based on actual experience with radium therapy and covers the dose-rate range of 0.7 to 1.7 rads/min. Clinical information at lower dose rates is lacking; however, assuming that this slope can be extrapolated to lower dose rates, which would be a conservative assumption, a dose rate of 25 mrems/hr, or about 0.5 rem/day, would not produce necrosis within the lifetime of the patient.

The other acute effect to consider is the radiation syndrome—those symptoms of nausea, vomiting, diarrhea, and malaise that appear following exposure to a high dose of ionizing radiation. Although the mechanism of this response is not clearly understood, the acute radiation syndrome is most often produced by irradiation of the abdomen, whereas irradiation of the extremities alone does not produce this effect.

Estimates of the whole-body dose which will produce these symptoms are known for high dose rates;[16] very little is known about low dose rates, although they would be expected to be relatively ineffective.

Three kinds of human exposures provide some information. The first[17] of these was the accidental exposure of 82 Rongelap natives to nuclear weapon fallout in 1954. The calculated total absorbed dose to the epigastric region was about 175 rads. Although the dose rate changed over the 50-hr exposure period, the estimated average was 3 to 3.5 rads/hr. The observed incidence of vomiting was 10%.

Second, at the Medical Division of the Oak Ridge Associated Universities,[18] a series of patients have now received a course of radiation therapy totaling 100 to 200 rads, delivered at a dose rate of 1 rad/hr. Among these patients, under therapy for a variety of hematologic disorders, no symptoms of radiation toxicity have occurred.

Last, there is no history of radiation symptoms among radiologists who may have been receiving as much as 100 rads/hr. On the basis of these accidental, therapeutic, and occupational experiences, 25 mrems/hr would appear to be highly unlikely to produce symptoms.

### Chronic Effects

A wide range of experiments with animals and observations on man provide convincing evidence that ionizing radiations can cause cancer.[19] Many types have been produced, and the evidence is so extensive that the conclusion that all tissues—or very nearly all—are susceptible is reasonable.

To demonstrate whether low levels of radiation, of the magnitude considered here, are associated with an increased risk of cancer is particularly difficult. Three studies illustrate the difficulties involved.

The recent publication of studies among radium-dial painters[20] is of interest in that chronic exposure to localized organs is similar to the situation under discussion. No bone cancers were found in persons who have received up to 40 rems/year to the skeleton over a period of at least 30 years. Furthermore, there appears to be an inverse relationship between dose rates and latent period prior to the development of bone cancer, i.e., the lower the dose, the longer the latent period.

Recent studies[21] of 75 thousand women treated for carcinoma of the cervix with radium have demonstrated no excess incidence of leukemia, although they have received an average of 6000 rads to the pelvic organs.

Also recently studied[22] is a group of patients who have received radioiodine therapy for thyrotoxicosis. In comparison with expected rates, no excess in rate of incidence of leukemia was found. Estimated radiation to the thyroid gland is 6 to 10 krads, to the whole body 5 to 10 rads.

Although the conditions of exposure differ from those of an implanted isotope heat source, data gathered among survivors of the Japanese atomic bombings,[23] whose radiation exposure was acute and directed to the whole body, permit the most quantitative estimate of the risk of leukemia in man. Analysis of these data, compatible with a linear relationship between dose and effect, suggests the conclusion that 1 rad to the whole body will produce 1 to 2 cases per million people per year.[24] Thus at our 180 rems/year



XUM

dose (0.5 rem/day)—reduced to 90 rems/year because of the partial body exposure—induction of 248 cases of leukemia in a population of 50 thousand persons exposed over 10 years would be anticipated. This would be in addition to the 35 cases that would be expected due to spontaneous occurrence of this disease.

Such an estimate is very likely an overestimate of risk. The risk factor of 1 case per rad per million people is based first of all upon data derived from acute exposures, which are more biologically damaging than chronic exposures, and secondly upon uniform whole-body exposures.

Apart from inducing cancer, large doses of radiation also diminish the life-span by increasing mortality rates from other diseases. Such effects have been clearly demonstrated in mice by acute doses of over 200 rads, but there is conflict of opinion about whether these effects are produced with lower doses, given either acutely or spread out over many weeks. Moreover, whether the effect is due to an increase in some specified diseases or to a nonspecific process, such as a general acceleration of aging, is uncertain.

Several estimates have been made of life shortening for man, based on animal experimentation. Perhaps one of the best of these is by Failla and McClement[25] who estimated the life-shortening effect to be about 1 day/r for continuous exposures at dose rates not in excess of 0.5 r/day.

When relatively large masses of the body are exposed to radiation, the integral whole-body dose received can be prudently assumed to be a crude measure of the life-shortening risk. Alternatively the expectation of general delayed radiation injury, including life shortening, might be expressed in terms of mean marrow dose.

Assuming that an abdominal plutonium source would effectively irradiate half of the marrow and other organ systems, the integrated dose would be 0.25 rem/day, or about 90 rems/year. Over a 10-year period of irradiation, life shortening of 30 months might be incurred, on the average.

Delayed radiation effects in man are not manifested for a period of years following the exposure. This interval is often called the "latent period." In uranium miners,[26] exposed to radon and radon daughters in the mine environment, lung cancers appear after a mean latent period of 20 years. Therefore, considering that candidates for an artificial heart would be middle-aged persons, life shortening due to radiation exposure would not appear to present a problem because the anticipated long latent period would probably exceed the normal life expectancy of the recipient. The human data with which this may be compared are meager but are essentially in agreement with the animal data. Two studies of American radiologists[27,28] both indicate a life shortening of about 5 years. Although the average accumulated dose is not known, it has been estimated as more than 500 rads whole-body radiation.

Last to be considered is the radiation effect on those around the patient, e.g., medical personnel and family members. Radiation fluxes fall off so rapidly, however, that preliminary calculations imply that these exposures can be ignored.

In summary, based on present estimates of radiation from early designs of an isotope-powered engine for heart replacement, radiation is unlikely to produce significant problems due to early or late effects, either to the patient himself or to those around him.

## Conclusions

Although there has not been any experience with human implantation of radioisotope power sources, their use seems feasible. The results of the design studies on the four power-conversion concepts indicate the possibility of achieving suitable performance levels. The radioisotope fuels development efforts have resulted in the identification and characterization of a potential fuel, $^{238}Pu$. Finally, for radiation effects, a search of past experience has provided some gross estimates of the risk associated with various levels of exposure. Experimental evidence is needed to assess the risk, if any indeed exists, from the use of radioisotope power for circulatory-support systems.

(FJM)

## References

References marked with an asterisk have not been verified by the editors; for further explanation, see the Foreword.

1. K. E. Buck, Conceptual Design of an Implantable Radioisotope Power Source for Circulatory Support Systems, USAEC Report AGN-8258, Aerojet General Corp., Jan. 26, 1968.
2. R. B. Goranson, Application of the Radioisotope-Fueled Stirling Engine to Circulatory Support Systems, USAEC Report TID-24699, McDonnell Douglas Corp., June 1968.
3. Thermo Electron Corp., Study on an Implantable Power Source for Circulatory Support Devices, USAEC Report TE-3858-1, Nov. 1, 1968.
4. Westinghouse Astronuclear Laboratory, Study on an Implantable Power Source for Circulation Support Devices, USAEC Report WANL-3857-1, December 1968.
5. K. E. Buck, D. L. Forrest, and H. W. Tamai, A Radioisotope-Powered Stirling Engine for Circulatory Support, see pp. 161–171, this issue of *Isotop. Radiat. Technol.*

6. W. R. Martini, R. P. Johnston, R. B. Goranson, and M. A. White, Development of a Simplified Stirling Engine to Power Circulatory Assist Devices, see pp. 145–160, this issue of *Isotop. Radiat. Technol.*
7. F. N. Huffman, R. J. Harvey, and S. S. Kitrilakis, Design of an Implantable, Rankine-Cycle, Radioisotope Power Source, see pp. 171–181, this issue of *Isotop. Radiat. Technol.*
8. J. R. Lance and A. Selz, An Implantable Artificial Heart Power Source, see pp. 182–192, this issue of *Isotop. Radiat. Technol.*
9. Hittman Associates, Inc., Analytical Report on Six Studies Basic to Consideration of the Artificial Heart Program. Vol. II, Technology Survey for Artificial Heart Devices, Report PB-173051, July 26, 1966.
10. Battelle–Northwest, Pacific Northwest Laboratory, Twelve-Month Technical Progress Report, Study of the Effects of Additional Endogenous Heat, NHI Report PB-177328, Aug. 10, 1967 [U. S. Government Research and Development Reports, 68(9): 47 (May 10, 1968)].
11.*H. H. Van Tuyl, Pacific Northwest Laboratory, Battelle Memorial Institute, Richland, Wash., personal communications; see also pp. 207–221, this issue of *Isotop. Radiat. Technol.*
12. G. M. Matlack and C. F. Metz, Radiation Characteristics of Plutonium-238, USAEC Report LA-3696, Los Alamos Scientific Laboratory, September 1967.
13. L. J. Mullins and J. A. Leary, Refining of Plutonium-238 for Biomedical Applications, *Trans. Amer. Nucl. Soc.*, 11(1): 91-92 (June 10–13, 1968). (See pp. 197–207, this issue of *Isotop. Radiat. Technol.*)
14.*R. D. Baker, Los Alamos Scientific Laboratory, personal communications.
15. Wright H. Langham (Ed.), Radiobiological Factors in Manned Space Flight, National Academy of Sciences–National Research Council, Washington, 1967.
16. C. C. Lushbaugh and F. Comas, Clinical Studies of Radiation Effects in Man, *Radiat. Res., Suppl.*, **7**: 398-412 (1967).
17. E. P. Cronkite, V. P. Bond, and C. L. Dunham (Eds.), Some Effects of Ionizing Radiation on Human Beings, A Report on the Marshallese and Americans Accidentally Exposed to Radiation from Fallout and a Discussion of Radiation Injury in the Human Being, USAEC Report TID-5358, July 1956.
18.*C. Lushbaugh, Oak Ridge Associated Universities, personal communications.
19. Report of the United Nations Scientific Committee on the Effects of Atomic Radiation, General Assembly Official Records: Seventeenth Session, Suppl. No. 16(A/5216), United Nations, New York, 1962.
20. R. D. Evans, The Effect of Skeletally Deposited Alpha-Ray Emitters in Man, *Brit. J. Radiol.*, **39**: 881-895 (1966).
21. A. B. Brill, M. Tomonaga, and R. M. Heyssel, Leukemia in Man Following Exposure to Ionizing Radiation, *Ann. Intern. Med.*, **56**: 590-609 (1962).
22. International Commission on Radiological Protection, Committee I. The Evaluation of Risks from Radiation, *Health Phys.*, **12**: 239-302 (1966).
23. G. B. Hutchison, Leukemia in Patients with Cancer of the Cervix Uteri Treated with Radiation, A Report Covering the First 5 Years of an International Study, *J. Nat. Cancer Inst.*, **40**(5): 951-982 (May 1968).
24. E. Saenger, G. Thoma, and E. Tompkins, Incidence of Leukemia Following Treatment of Hyperthyroidism, *J. Amer. Med. Ass.*, **205**: 855-862 (Sept. 16, 1968).
25. G. Failla and P. McClement, The Shortening of Life by Chronic Whole Body Irradiation, *Amer. J. Roentgenol., Radium Ther. Nucl. Med.*, **78**: 946-954 (1957).
26. Federal Radiation Council, Guidance for the Control of Radiation Hazards in Uranium Mining, Staff Report No. 8, Revised, September 1967.
27. S. Warren, Longevity and Causes of Death from Irradiation in Physicians, *J. Amer. Med. Ass.*, **162**: 464-468 (1956).
28.*R. Seltzer and P. E. Sartwell, The Influence of Occupational Exposure to Radiation on the Mortality of American Radiologists and Other Medical Specialists, *Amer. J. Epidemiol.*, **81**: 2-22 (1965).

# Development of a Simplified Stirling Engine To Power Circulatory-Assist Devices*

By W. R. Martini, R. P. Johnston, R. B. Goranson, and M. A. White†

**Abstract:** The scope and present status of a research program at the Donald W. Douglas Laboratories to develop a Stirling engine power source for circulatory-support devices are presented. A simplified version of the Stirling engine, which can produce the required power output to drive a heart pump with high efficiency and reliability, is described. The predicted performance characteristics of the simplified Stirling and a conventional Stirling engine are compared.

The design is presented, and the results of a design analysis are discussed briefly. The status of an experimental program is reported. Basic design requirements are described along with presently achieved and projected performances for the laboratory prototypes. The major problems are outlined, and possible methods of solution are discussed.

*Sponsored by the U. S. Atomic Energy Commission and the National Heart Institute.

†Biomedical Applications, Donald W. Douglas Laboratories, Richland, Wash. 99352.



XUM

The Donald W. Douglas Laboratories has been engaged in developing a simplified Stirling engine for 2.5 years. The original goal was to achieve high reliability by simplifying the mechanical construction of a heat engine, without loss of efficiency. A number of concepts, based on the acceptance of heat from any source to produce electric energy, were evaluated. A preliminary model of a pressure pulse generator was tested. Tests of an electric generator in which the only moving part was a reciprocating armature resulted in a demonstrated 60% electrical efficiency. Using this simplified Stirling engine to power an artificial heart has certain distinct potential advantages: (1) high thermal efficiency, (2) reliable long-life operation, (3) pulsatile power directly for pumping, and (4) quiet, safe, and easily controllable operation.

The simplified Stirling engine will be compared to the better known conventional Stirling engine. The conceptual design developed for an isotope-fueled power source is described. Experimental work on preliminary models of test engines is also described, and the problems that must be solved to attain high efficiency and reliable operation will be identified.

## Engine Operation

### Comparison of Theoretical Cycles

Theoretical thermodynamic power cycles act to produce power by going through four phases: (1) compression, (2) heating, (3) expansion, and (4) cooling. In four common thermodynamic cycles involving a gaseous working fluid, these phases are completely separated. Figure 1 shows how the Brayton, Otto, Diesel, and Carnot cycles are defined; it also defines the Ericsson and Stirling cycles, in which some of the heating and cooling takes place during compression and expansion by specifying an isothermal compression and expansion. In an ideal regenerative thermal machine operating on either the Ericsson or Stirling cycle, the heat added to the gas on isothermal expansion is transferred from the heat source, and the heat removed from the gas on isothermal compression is transferred to the heat sink. The heat transfer needed to change the pressure of the gas at constant volume in the case of the Stirling cycle and to change the volume at constant pressure in the case of the Ericsson cycle is accomplished by a thermal regenerator inside the machine. That is, the gas is heated reversibly by passing it through a porous solid called a regenerator (Fig. 2). Gas is cooled reversibly by passing it back through the regenerator. Any machine using such a porous solid regenerator has come to be known as a Stirling engine, although it may not operate on the Stirling cycle.

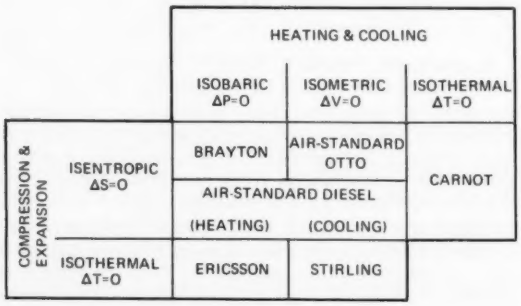


Fig. 1 Thermodynamic power cycles.

As shown in Fig. 2, this ideal thermal regenerator separates a gas space at the heat-source temperature from a gas space at the heat-sink temperature. In a confined space, pressure is increased and decreased without any heat transfer from the hot surface or to the cold surface, except for that resulting from conduction and regenerator inefficiency; no work is done. If work were done on the surroundings by allowing the boundaries of the gas space to move appropriately or by allowing gas to enter and leave the space in a proper manner, additional heat must be added to the gas from the hot surface and removed from the gas at the cold surface. Because, ideally, heat is always added at the heat-source temperature and is rejected at the heat-sink temperature and because the transition between heat-source and heat-sink temperatures is reversible through an ideal regenerator, any engine satisfying these requirements has an ideal efficiency equal to the Carnot cycle, no matter what cycle is followed.

### Conventional and Simplified Stirling Engines

Two regenerative thermal machines will now be compared. One was analyzed by Schmidt.[1] It is essentially the same machine built by the Reverend Robert Stirling in 1818, and it is the basis of most present-day Stirling engines. The conventional Stirling engine uses a crank and flywheel to cause regenerator motion to lead power-piston motion by 90°. The simplified Stirling engine uses some form of independent drive to move the regenerator. In Fig. 3 the simplified Stirling engine is acting as a pumping engine, and the conventional engine is following the Schmidt cycle. The regenerator drive mechanism has been omitted in each case for clarity.

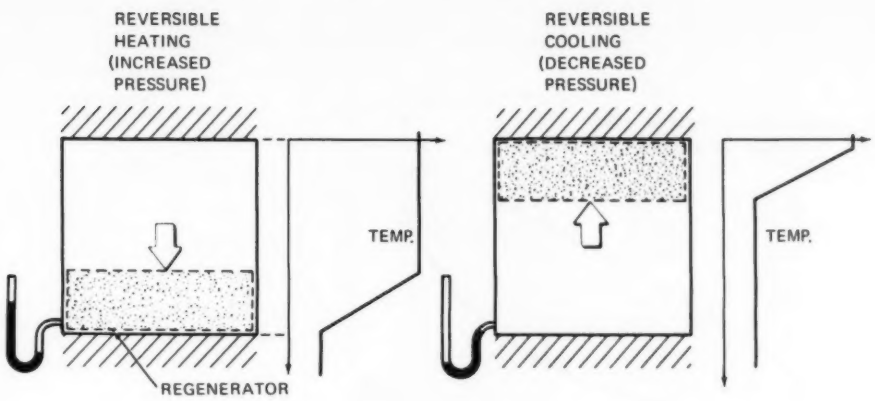


**Fig. 2 Reversible heating and cooling at constant volume.**

In the conventional Stirling engine, compression takes place with the gas generally in the cold portion of the engine (lower pressure) and expansion takes place with the gas generally in the hot portion of the engine (higher pressure). In this cycle, the four phases of the heat engine overlap and give a rounded indicator diagram.

In the simplified Stirling engine, the regenerator is moved independently by any of a number of means. The engine shown in Fig. 3 is a liquid pump. From position 1 to 2, the system is pressurized to the outlet pressure for the liquid pump. From position 2 to 3, the outlet valve is open, and liquid is forced out. From position 3 to 4, both valves are closed, and the pressure drops to the inlet pressure. From 4 to 1, the inlet valve is open, and new liquid is drawn in. The cycle then repeats.

Both engines shown in Fig. 3 operate on ideal thermodynamic cycles as well defined as those shown in Fig. 1. If attention is confined to thermodynamic cycles that alternate the processes of holding a particular measure of the gas constant, the matrix shown in Fig. 4 can be constructed.

Such a theoretically simple thermodynamic cycle as the simplified Stirling rectangle on a *PV* diagram must surely have been christened before now. The authors have found no reference to it, however.

One way of achieving self-operation of the regenerator is shown in Fig. 5. The pressure pulses generated by the oscillating regenerator serve to sustain its motion in a bootstrapping operation. A plug enters an orifice which momentarily separates the gas in the connecting line to the pump from that in the engine cylinder. Pressure on the pump side of the plug remains nearly constant, but pressure in the engine continues to change with regenerator and plug motion. The resultant pressure difference acts on the plug so that regenerator motion is reinforced. This reinforcement provides sufficient energy to overcome the windage and friction of the regenerator. Springs reverse the regenerator motion at the end of each stroke. Engine speed, and therefore power output, is controlled by a bypass valve that regulates the pressure difference appearing across the plug. A cutaway drawing of a conventional Stirling engine is included in Fig. 5 to show how the regenerator motion depicted in Fig. 3 is achieved in practice.

### Ideal Work Output

The ideal work outputs for the conventional Stirling engine and the simplified Stirling engine coupled to an ideal pump are given, respectively, by Eqs. 1 and 2. The essence of Eq. 1 was first derived by Schmidt[1] in 1871, and Eq. 2 results from a similar application of basic thermodynamics to the simplified cycle shown in Fig. 3.

Conventional:

$$W = mR\,T_C\,\frac{2\pi b V_P}{b^2 + c^2}\left[\frac{a}{(a^2 - b^2 - c^2)^{1/2}} - 1\right] \quad (1)$$

Simplified:

$$W = mR\,T_C\,\frac{4c\,(b - c)}{a^2 - (b - c)^2} \quad (2)$$

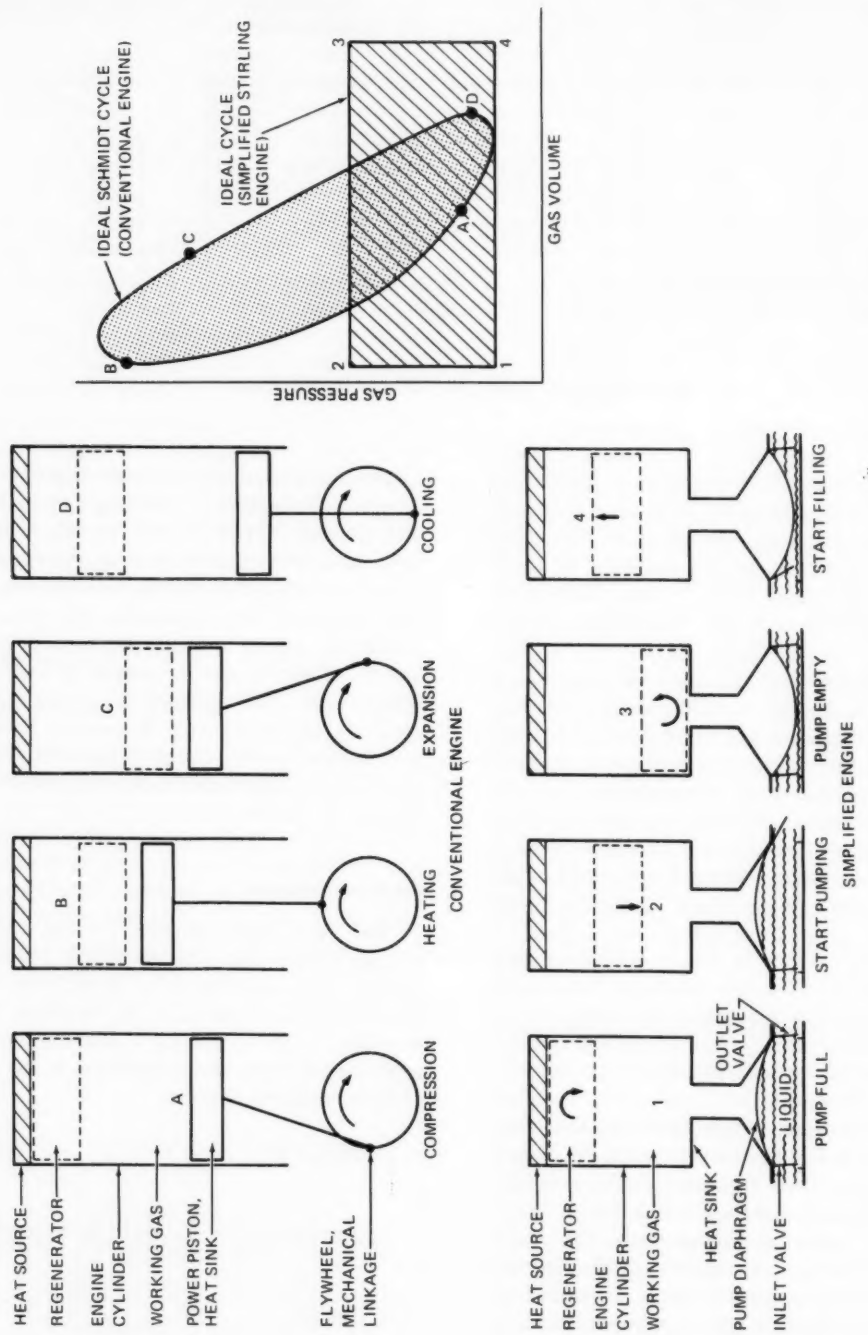


Fig. 3 Schematic comparison of conventional and simplified Stirling engines (regenerator drives not shown).

| | ISOTHERMAL ΔT=0 | ISOBARIC ΔP=0 | ISOMETRIC ΔV=0 |
|---|---|---|---|
| ISENTROPIC ΔS=0 | CARNOT | BRAYTON | OTTO |
| ISOMETRIC ΔV=0 | STIRLING | SIMPLIFIED STIRLING | |
| ISOBARIC ΔP=0 | ERICSSON | | |

Fig. 4 Matrix of theoretical thermodynamic cycles.

Fig. 5 Regenerator actuation methods.

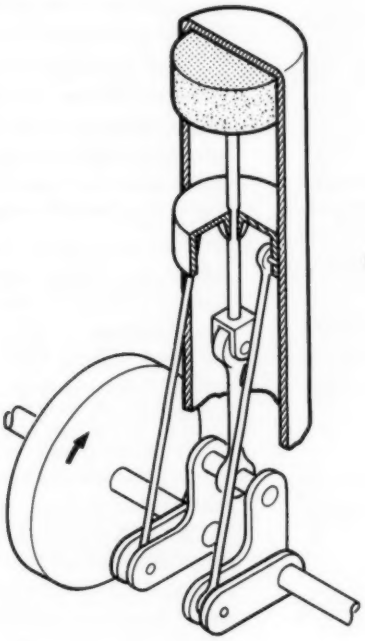

(A) CONVENTIONAL STIRLING ENGINE (MECHANICALLY PHASED REGENERATOR OPERATION)

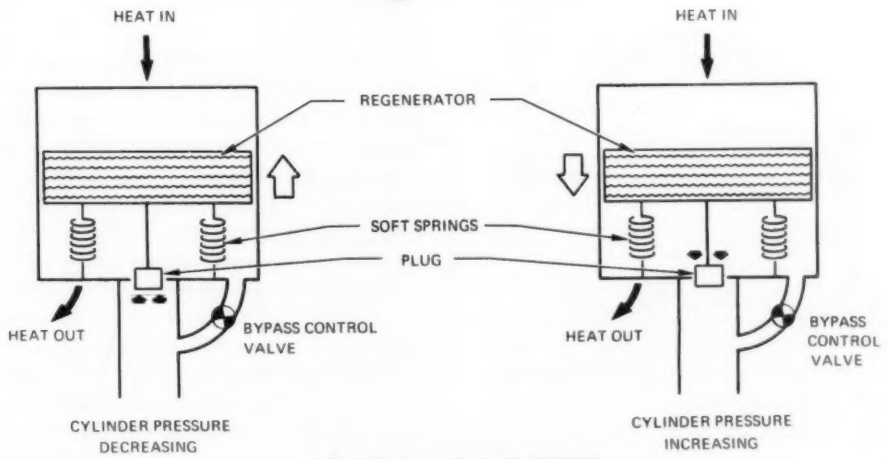


(B) SIMPLIFIED STIRLING ENGINE



XUM

where $W$ = ideal work output per cycle, joules
$m$ = amount of contained working fluid, gram moles
$R$ = gas constant [8.316 joules/(gram mole) (°K)]
$T_H$, $T_C$ = gas temperature, °K (hot, cold)
$a = V_{CO} + \tau V_{HO}$, cm$^3$

$b = V_R\,(1-\tau)$, cm$^3$
$c = V_P$, cm$^3$

These expressions for $b$ and $c$ are valid only for the conventional engine when the power piston lags the regenerator by 90°. For an arbitrary phase lag, $\phi$, $b = V_R\,(1-\tau)\sin\phi$ and $c = V_P - V_R\,(1-\tau)\cos\phi$.

$V_{CO}$ = volume between midpoint of regenerator travel and midpoint of power-piston or pump-diaphragm travel, cm$^3$
$V_{HO}$ = volume between hot surface and midpoint of regenerator travel, cm$^3$
$V_R$, $V_P$ = the volumes swept out by the regenerator and power piston or pump diaphragm as they move from the midposition to either extreme position, cm$^3$
$\tau = T_C/T_H$

A more useful form of Eq. 2, which specifies the operating pressures rather than the system gas charge, is given by Eq. 3:

$$W = \frac{\Delta P}{7500}\{[(a+b-c)/\psi] - (a-b-c)\} \qquad (3)$$

where $\Delta P = p_2 - p_1$ is the pump inlet to outlet pressure increase in torrs and $\psi$ is $p_2/p_1$. The volumes that define the two engines are shown in Fig. 6.

There are fundamental differences of operation in the two machines; for example, the conventional engine produces positive work for any power-piston phase lag between 0 and 180°, regardless of the relative values of $V_P$ and $V_R$. The simplified engine, however, produces positive work only if $(b-c) > 0$. In this case, phase lag is meaningless because the diaphragm is not moving during the isometric portions of the cycle. A direct general comparison of the performances of the two machines is therefore not possible, but a reasonable comparison is shown in Fig. 7.

Note that Eqs. 1 and 2 can be made nondimensional by dividing through by $mRT_C$. Figure 7 shows that (when the assumptions are made about the interrelationship of $V_{HO}$, $V_{CO}$, $V_R$, and $V_P$) the complicated functions of $a$, $b$, and $c$ in Eqs. 1 and 2 reduce to a function only of the temperature ratio $\tau$.

The assumptions for the conventional Stirling engine are: (1) The limiting case where there are no unswept volumes in the engine and the gas volume in the regenerator is negligible; (2) the engine is built in the usual manner with the volume displaced by the power piston equal to the volume displaced by the regenerator.

The assumptions for the simplified Stirling engine are: (1) The limiting case is the same as the one for the conventional Stirling engine; (2) the displacement of the power piston (or diaphragm) is adjusted to obtain maximum work output.

The ratio, $k = V_P/V_R$, that results in maximum work output is shown in Fig. 7 and is a function only

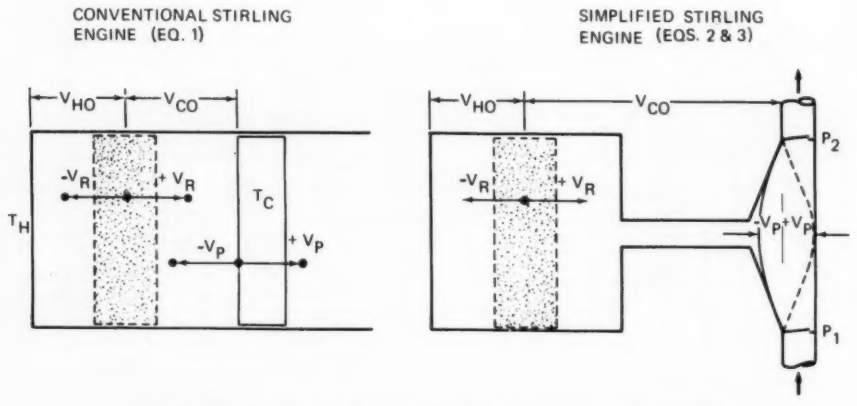


**Fig. 6 Basic dimensions for conventional and simplified Stirling engines.**

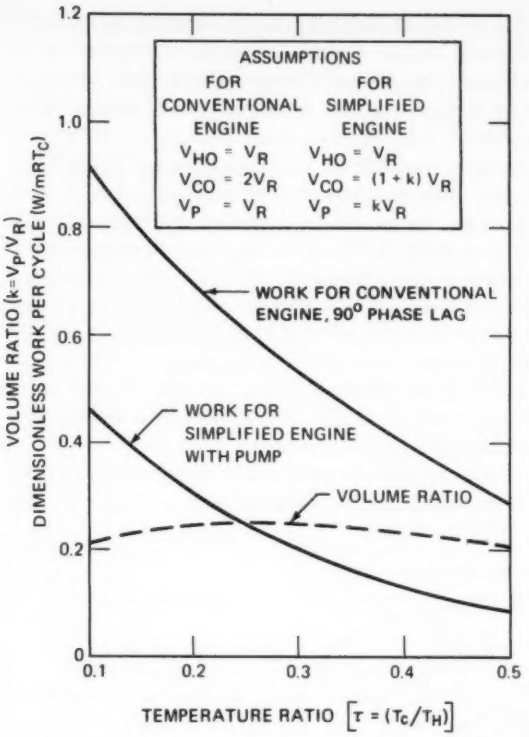


**Fig. 7 Dimensionless work output and $k = (V_P/V_R)$ as functions of temperature ratio for conventional and simplified engines.**

of $\tau$. Note that the work output for either machine may be determined from Fig. 7 by specifying the gas charge and operating temperatures. If other assumptions are made about the relationships of the engine volumes, other curves would result, but this relationship would still hold. Thus, theoretically, a large engine operating at low pressure is equivalent to a small engine operating at a high pressure if both have the same volume relationships and the same temperatures, hold the same moles of gas, and operate at the same speed.

For a conventional and a simplified Stirling engine to produce the same power and operate at the same frequency and average pressure, the working-gas volume of the simplified Stirling engine must be two to four times that of the conventional Stirling engine, depending upon the temperature ratio $\tau$. However, the conventional engine usually requires much more machinery outside the working-gas space than does the simplified engine. The simplified engine could well be smaller than the conventional engine, depending upon the specific mechanical design.

## Conceptual Design of a Radioisotope-Fueled Engine

A 6-month study conducted for the Atomic Energy Commission established the feasibility of a radioisotope-fueled engine, and a conceptual design of a promising configuration was prepared. By feasibility is meant that the conceptual design has met the design specifications set down in the contract.

The radioisotopes $^{238}Pu$, $^{147}Pm$, and $^{171}Tm$ were considered as possible heat sources for the engine. Table 1 compares these candidate fuels. At the presently available purity levels, $^{147}Pm$ and $^{171}Tm$ both require prohibitively heavy shields. In contrast, these isotopes, when absolutely pure, would not present a shielding problem, but they would always present a lifetime problem. A lifetime of at least 1 year is desirable, with the possibility of extending the lifetime up to the 7- to 10-year level without a major increase in technology. If enough isotope were loaded into the power source to last for 7 years, the power ratio from beginning to end of life would be 6.5 for $^{147}Pm$ and 12.9 for $^{171}Tm$. The amount of heat that would have to be rejected to the body would greatly exceed the present limit of 50 watts, and a very good power-flattening system would have to be worked out.

**Table 1 Comparison of Isotope Fuels for a 15-Watt(t) Heart Power Source**

**(Fuel At Presently Attained Purities)**

| | $^{147}Pm$ | $^{171}Tm$ | $^{238}PuO_2$ |
|---|---|---|---|
| Half-life, years | 2.6 | 1.9 | 86 |
| Time between refueling, years | 1 | 1 | 5 |
| Initial loading, watts(t) | 19.6 | 21.5 | 15.6 |
| Shield weight for 15 mrems/hr at surface of engine, g (see Fig. 8) | 2500 | 2500 | 200 |
| Required neutron attenuation distance, cm | | | 6.5 |

From a technical standpoint, $^{238}Pu$ is the only reasonable choice. There are no power-flattening problems, the shield weight is reasonable, and the 6.5 cm required between the fuel and any tissue is easily worked into the power-source design. The only reasons any other isotopes are considered are the great demand for and scarcity of $^{238}Pu$.



XUM

Figure 8 shows the conceptual design; Table 2 summarizes the basic characteristics of the reference design.

The fuel portion of the heat source is a shielded capsule containing a high-density sintered pellet of $^{238}PuO_2$. The capsule provides adequate containment of the fuel under any conceivable accident, efficient transfer of isotope decay heat, and containment of the helium produced by $^{238}Pu$ decay. The remaining portion of the integrated heat source consists of a thermal storage device that receives heat from the fuel capsule, stores the heat during low-patient-activity periods, and releases it for use by the engine during peak-demand periods. Heat is stored by using a salt that melts at engine operating temperatures. Thus thermal energy can be conveniently stored as latent heat of fusion and released during recrystallization. One problem associated with the development of the system will be the design and fabrication of a reliable thermal storage device. A thermal storage device of minimum weight and volume could be fabricated using LiH if the long-term containment and compatibility problems can be overcome. The experimental data presently available on the containment of LiH indicate severe hydrogen loss through most materials. Recent data on the permeation rate of hydrogen through arc-cast molybdenum have suggested the possibility of its use as a container for the LiH. Extensive experimental investigation will be necessary to fabricate and evaluate such a device. If LiH containment proves to be an insurmountable problem, the eutectic of LiF–NaF would be an alternate choice. It is heavier but has a volume similar to LiH. Preliminary containment tests on this salt have been favorable.

The engine cylinder wall is constructed of a low-thermal-conductivity material such as zirconia. The

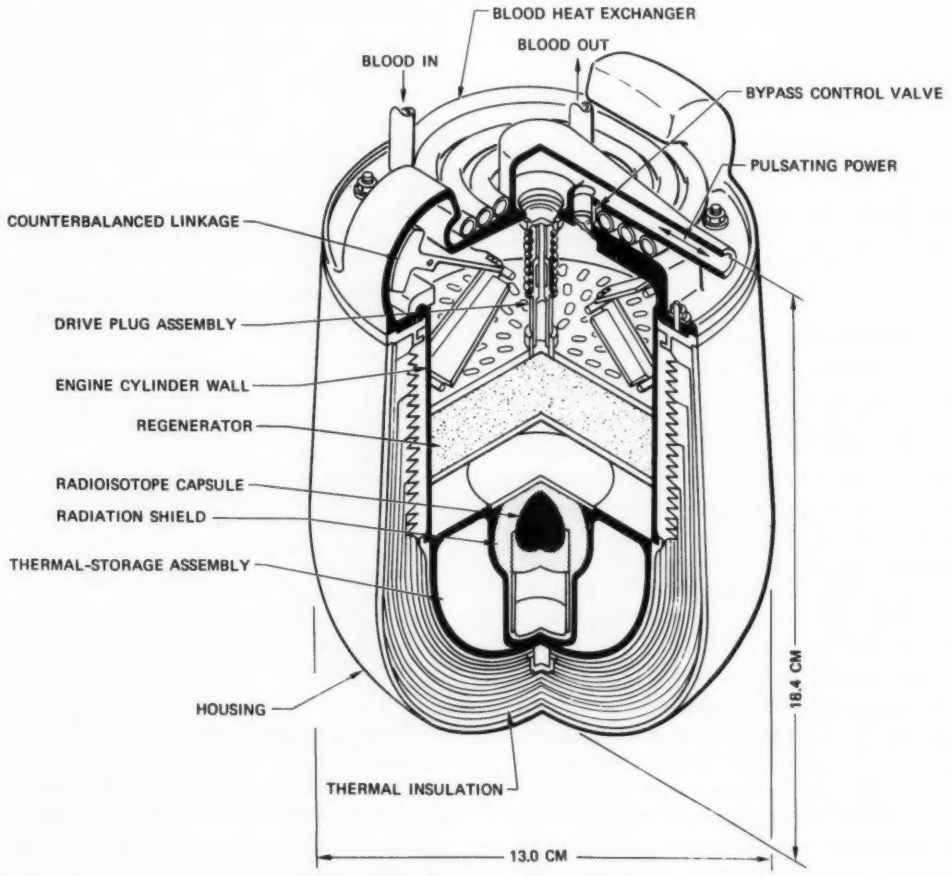


Fig. 8 Radioisotope-powered heat engine.

**Table 2 Summary of Reference-Design Characteristics**

| | |
|---|---|
| Thermodynamic cycle | Simplified Stirling |
| Fuel form | Sintered $^{238}PuO_2$ |
| Working fluid | Xenon |
| Maximum power output, watts mechanical | 7.0 |
| Type of output | Pneumatic pulses |
| Pressure range, torrs | 760 to 930 |
| Frequency, pulses/sec or Hz | 1.0 to 2.5 |
| Regenerator stroke, cm | 5.08 |
| Heat-source temperature, °C | 689 |
| Heat-sink temperature, °C | 38 |
| Efficiency (at 2.8 to 7 watts output) | 14 to 25% |
| Thermal storage materials | |
| Salt | LiH or NaF–LiF eutectic |
| Container | Arc-cast molybdenum or HS-25 |
| Radiation level at surface | 10 to 15 mrems/hr |
| Total weight, kg | 2.5 |
| Volume, $cm^3$ | |
| Engine cylinder (inside) | 441 |
| Fuel capsule | 3 |
| Thermal storage/ radiation shield | 260 |
| Composite cylinder wall | 202 |
| Heat exchanger | 32 |
| Linkage | 48 |
| Surrounding insulation | 598 |
| Housing and cold face structure | 212 |
| Total, $cm^3$ | 1796 |

wall is surrounded by a René 41 bellows that acts as a secondary containment vessel. The space between the wall and the bellows is filled with insulating material to minimize heat loss. Procedures for fabrication of the thin metal bellows will have to be developed since this is a critical element in the lifetime of the system. Sophisticated fabrication and assembly processes will also have to be developed to permit successful production of the cylinder wall–insulation–bellows assembly. High-quality insulation must be carefully packed in the assembly.

The regenerator in the reference design consists of 0.05 lb of 0.5-mil-diameter sintered gold wire with a packing density of 1%. This matrix is sandwiched between two orifice plates that are separated from the matrix by a spacer assembly. This design is required because of heat-transfer and fluid-flow considerations. The problem of mechanical strength of such a fragile oscillating structure has not been solved satisfactorily. Techniques must be developed for the fabrication of the regenerator matrix from a continuous length of wire, which is required to eliminate the "shedding" that has been a problem with experimental regenerators made from steel wool or felt metal. Commercial weaving and spinning processes are available and can be modified to produce a regenerator with the required specifications.

The regenerator is suspended from the cold face by a four-hinge Sarrut's linkage system that folds to a very small volume, thus minimizing engine size. Analysis of the loads on the bearings in the Sarrut's linkage showed a very long computed bearing life. This long life is dependent upon scrupulous exclusion of surface imperfection from the component parts and exclusion of foreign particles from the bearings during or after assembly.

The entire lower section of the engine is encased in Linde superinsulation, consisting of alternate layers of opaque metal foils and quartz fibers which are contained in an evacuated housing. This type of insulation provides the best protection against radiation and conduction heat losses. After application of the laminations to the cylinder, a housing is installed to protect the insulation. This housing must withstand external pressure without buckling and must be compatible with the body should body fluids penetrate the outer coating of polyether polyurethane and Silastic. A titanium alloy was chosen for use in the reference design. At the present time the manufacturing cost of the power source has not been estimated.

Figure 9 summarizes the calculated performance of the reference design. At the time-integrated average power output of 2.8 watts, the thermal-power consumption is 20 watts. Power-output variations are obtained by adjusting the regenerator drive-system

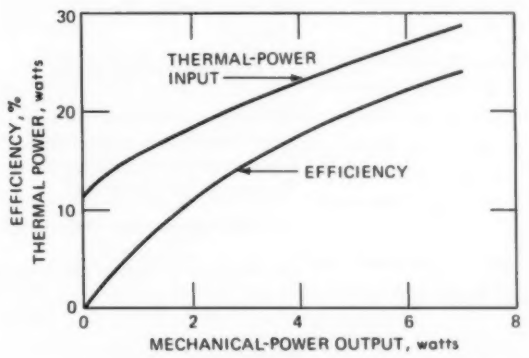


**Fig. 9 Reference-design performance.**



XUM

bypass control valve (Fig. 5). The bypass control-valve setting determines the regenerator stroke length and operating frequency. When the bypass control valve is full open, the machine is stopped. As the valve closes, the amplitude of oscillation increases to a maximum, and then the amplitude stays at the maximum while the frequency increases. The stiffness of the load pump also has an important effect on power-source operation. A controller is needed to determine whether more or less power is needed and to move the control valve accordingly.

The engine heat source can maintain an equilibrium temperature for 16 hr of bed rest by the patient. Following this period a gradual temperature increase will occur until the machine equilibrates. The machine has been designed to withstand these higher temperatures indefinitely with no deleterious effects on the overall system. Waste heat is rejected by a blood heat exchanger constructed in the cap of the unit. The waste heat rejected by a blood heat exchanger varies between 11 and 22 watts(t), depending on engine power output. The design specifications of the contract require that the heat-rejection rate be less than 50 watts. The main problem will be in developing a suitable means of getting the heat into the bloodstream. The blood heat exchanger previously described will depend on the availability of nonthrombogenic surfaces, which are currently under development.

Table 3 presents an engine performance summary at the maximum power output of 7 watts and at the

**Table 3 Detailed Performance Summary for Reference-Design Engine**

| | Peak power | Average power |
|---|---|---|
| Power output, watts | 7 | 2.8 |
| Frequency of operation, Hz | 2.5 | 1.0 |
| Average hot-plate temperature, °C | 689 | 689 |
| Average cold-plate temperature, °C | 38 | 38 |
| **Thermal-Power Input, watts** | | |
| Heat-source insulation | 2.2 | 2.2 |
| Engine insulation | 1.1 | 1.1 |
| Cylinder wall | 1.6 | 1.6 |
| Bellows | 0.9 | 0.9 |
| Bellows/sidewall fill | 0.1 | 0.1 |
| Tension rods | 0.8 | 0.8 |
| Total engine-cylinder heat leak | 6.7 | 6.7 |
| Regenerator solid conduction | 1.4 | 1.3 |
| Regenerator gas conduction | 1.3 | 1.2 |
| Radiation through regenerator | 0.7 | 0.7 |
| Radiation around regenerator[1]* | 1.3 | 1.3 |
| Regenerator/sidewall radiation short circuit[2] | 1.5 | 1.4 |
| Regenerator/sidewall gas-conduction short circuit[3] | 0.2 | 1.3 |
| Total regenerator heat leak | 6.4 | 7.2 |
| Main regenerator reheat loss[4] | 1.9 | 0.5 |
| Regenerator blow-by reheat loss[5] | 2.3 | 1.0 |
| Regenerator heat-capacity loss[6] | 0.1 | 0.0 |
| Regenerator gas-holdup loss[7] | 0.6 | 0.2 |
| Total regenerator reheat loss | 4.9 | 1.7 |
| Heat required for ideal (Carnot) engine | 11.0 | 4.4 |
| Total heat input | 29.0 | 20.0 |
| Efficiency, % | 24 | 14 |

*See Table 4 for explanation of superscripts 1–7.

**Table 4 Definitions of Parasitic Heat-Loss Terms**

**(1) Radiation around regenerator**
The moving regenerator acts as a shutter, alternately exposing the central portion of the engine sidewall to the engine hot and cold plates to produce an intermittent radiation short circuit.

**(2) Regenerator/sidewall radiation short circuit**
The periphery of moving regenerator is alternately exposed to hot and cold portions of the engine sidewall, resulting in a radiation short circuit across the regenerator.

**(3) Regenerator/sidewall gas-conduction short circuit**
Similar to (2), a thermal short circuit is produced through the gas layer in the clearance space between the regenerator and the engine sidewall.

**(4) Main regenerator reheat loss**
Because heat transfer between the working gas and the regenerator matrix is not perfect, the gas must be slightly reheated each cycle to maintain its temperature.

**(5) Regenerator blow-by reheat loss**
Ten percent of the gas flow is diverted through the clearance between the regenerator and the engine sidewall. This gas forms an insulating curtain between the regenerator and the sidewall to minimize the regenerator/sidewall gas-conduction short circuit (3). The thermal recovery of this gas is only 70%, requiring substantial reheating each cycle. The 10% and the 70% are used only as examples in this explanation and apply only to the case shown in Table 3.

**(6) Regenerator heat-capacity loss**
Because the heat capacity of the regenerator matrix is not infinite, the matrix temperature increases during gas cooling and decreases during gas heating, requiring an additional amount of gas reheating each cycle.

**(7) Regenerator gas-holdup loss**
More gas is entrained in the regenerator when it is near the cold plate than when it is near the hot plate because of the difference in working-gas pressure at the two regenerator positions. The entrained gas subsequently leaves the regenerator, which requires reheating not otherwise accounted for.

average power of 2.8 watts. Note that 20 watts are required at the average power, and 20 watts are supplied by the isotope heat source. At peak power, 29 watts are required. The 9 extra watts are supplied by the thermal storage device. At lower than average power, heat is supplied to the thermal storage device by the radioisotope. Note that at normal heartbeat frequencies and blood pressures the total engine-cylinder heat leak (which is constant with frequency) plus the total regenerator heat leak (which is almost constant) is more important than the total regenerator reheat loss (which is almost proportional to frequency). At higher engine frequencies, the total regenerator reheat loss would become much more important.

A simplified Stirling engine experimental program is described in the following section. The engines tested were similar to the reference engine design described above.

## Experimental Program

The purpose of this work was to determine the feasibility of the simplified Stirling engine for use in an implantable heart power source. The prototype development involved only the thermal engine. However, to measure engine performance, mockups of the heat source, surrounding insulation, mechanical power transfer, waste-heat rejection, and blood pump subsystems were required.

A demonstration model of the simplified Stirling engine was operated in March 1967. The engine powered a simple pump to circulate water. Fully instrumented engines have since been built, tested, and analyzed. Good progress has been made in solving the major engine design problems.

The test stand is shown in Fig. 10 and a schematic of the test apparatus in Fig. 11. The hot-plate temperature is maintained at approximately 1200°F (650°C) by an electric heater. The waste heat is removed by city water at 60°F (15°C), which is circulated through a cooling coil attached to the cold plate. Coolant at body temperature of 98.6°F (37°C) will be used when the engine is much closer to being developed. Engine speed and power output are regulated by the bypass control valve that controls the pressure across the drive piston. Pulsatile power is delivered to the load through a power transfer line. The engine operating pressures are determined by the pump inlet and outlet valve settings.

Figure 12 shows a typical engine operating record, including the pressure in various parts of the test apparatus and the pumped volume. Figure 13 shows a typical engine indicator diagram which provides a direct measure of engine power output. Other measurements include the thermal-power input and output and the temperatures at 24 locations.

The development model of the simplified Stirling engine is shown in Fig. 14. Two models have been tested, and a third model is being assembled.

The precision test models use readily available materials and fabrication techniques to avoid long-term component development efforts. The purpose of the



XUM

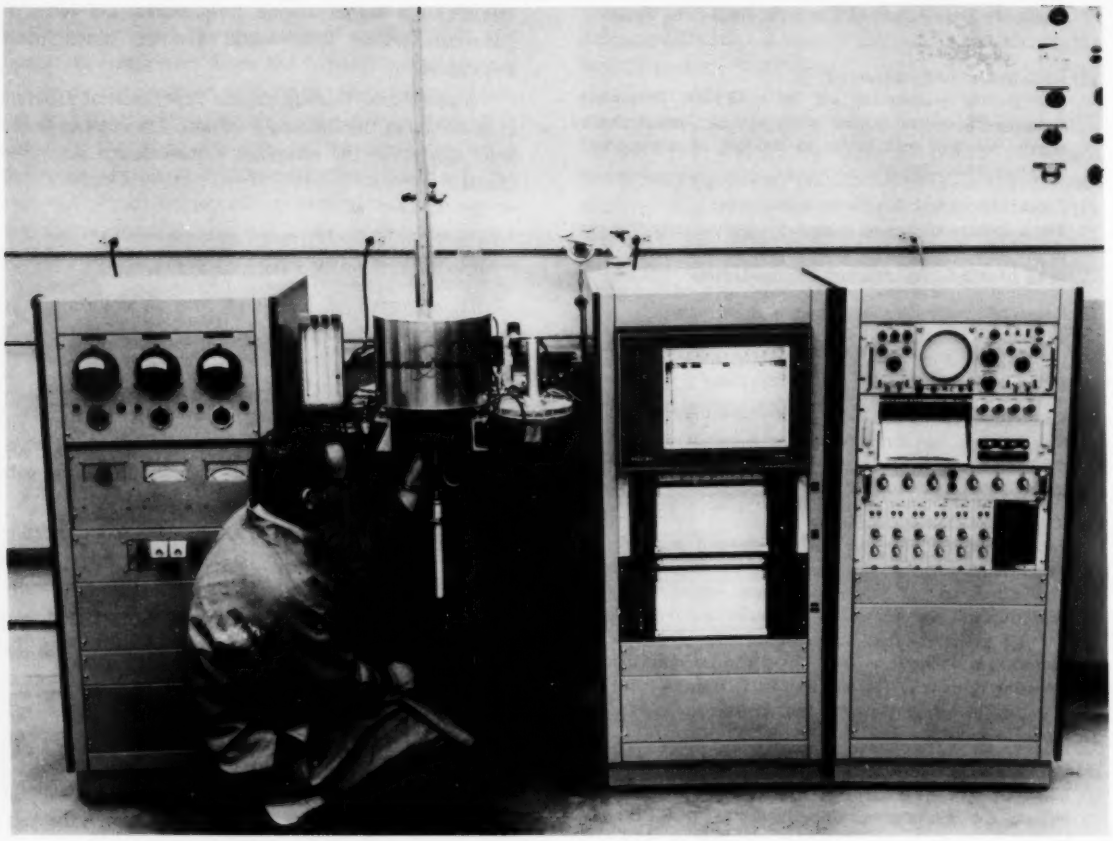

Fig. 10 Simplified Stirling engine test stand.

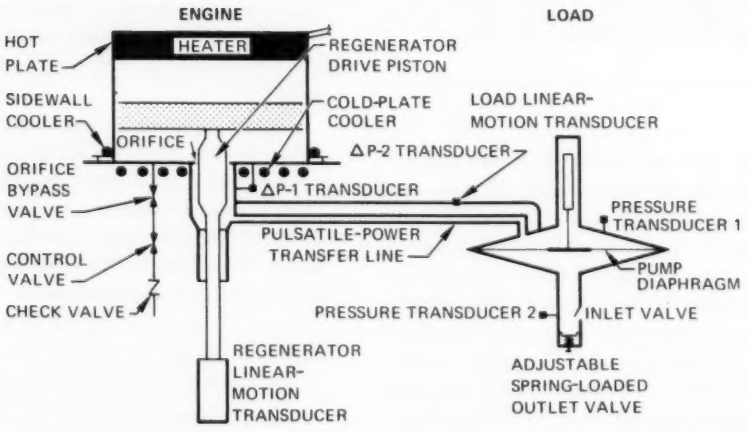


Fig. 11 Simplified Stirling engine test apparatus.

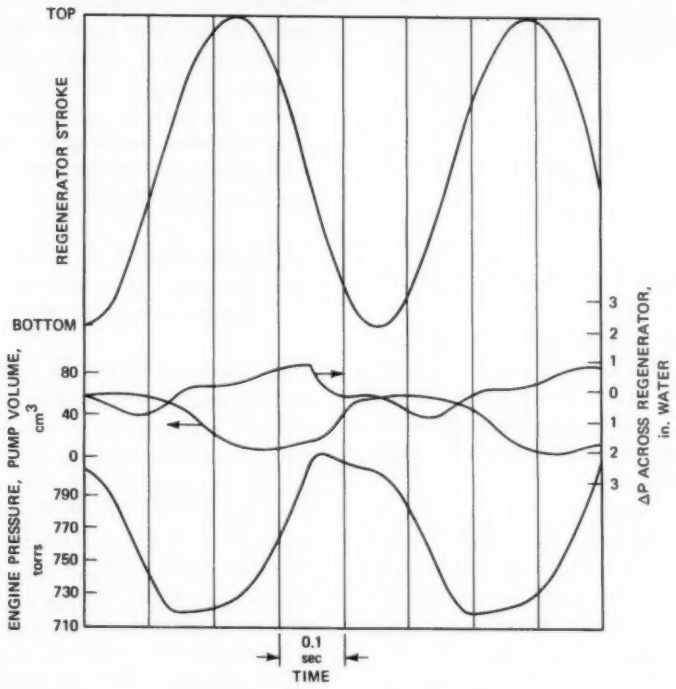


Fig. 12 Typical engine operating record.

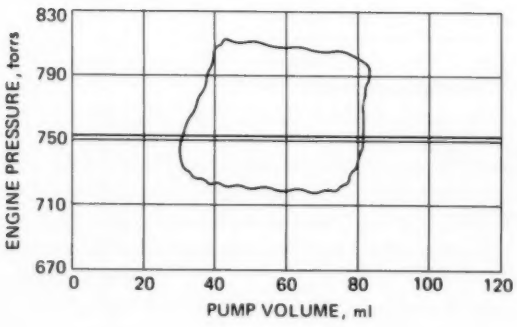


Fig. 13 Typical engine indicator diagram.

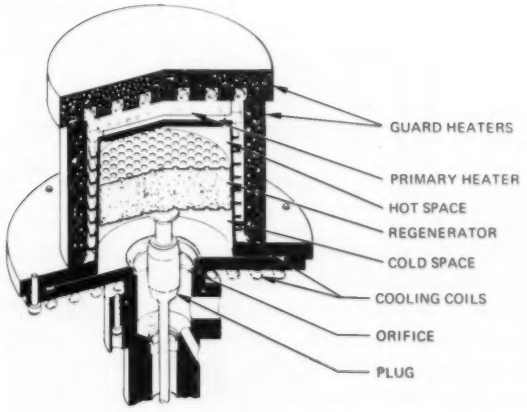


Fig. 14 Simplified Stirling engine development model.

**Table 5 Simplified Stirling Engine Performance**

| | Model 1 | Model 2 |
|---|---|---|
| Frequency, Hz | 4 | 4 |
| Hot-plate temperature, °C | 650 | 650 |
| Cold-plate temperature, °C | 15 | 15 |
| Power output, watts | 2 | 4 |
| Heat input, watts | 250 | 110 |
| Efficiency, % | 0.8 | 3.6 |

engine tests is to demonstrate engine performance and operation.

The performances of Models 1 and 2 are compared in Table 5 to illustrate the improvement with successive models. Figure 15 shows the performance of Model 2 over a range of operating frequencies. Substantial improvements must be incorporated to meet implantation requirements.

Table 6 provides a more detailed performance summary of Model 2, listing the breakdown of heat supplied to the engine. About 40% of the heat input is lost through the surrounding insulation and engine sidewall. In Model 3, evacuated Min-K 2000 will replace the commercial insulation used in Model 2. The stainless-steel engine cylinder will be retained in Model 3.

If the present insulation were replaced with the best vacuum insulation and if the cylinder wall were made by the best known design, the total engine-cylinder heat leak could be reduced below 10 watts. Assuming this loss to be 10 watts and all other losses to remain the same as shown in Table 5, the corrected efficiency shown in Fig. 15 was calculated. For instance, for twice the frequency, the efficiency would be calculated as follows:

Power output = 2(4.61) = 9.22 watts
Heat input = 10 + 46.8 + 2(17.6) = 92 watts
Overall efficiency = 10%

This corrected efficiency is based upon improvement of the engine performance in only one respect. Another improvement now under development that will substantially improve efficiency is a regenerator system that controls radiation heat loss and also has improved heat-transfer coefficients in the regenerator itself and on the hot and cold surfaces.

Much of the engine heat-input requirement is traced to losses in the regenerator. The regenerator used in Model 2 is shown in Fig. 16. The perforated plate produces gas jets to enhance heat transfer at the engine end plates. The regenerator matrix was made of a readily available commercial grade of sintered stain-

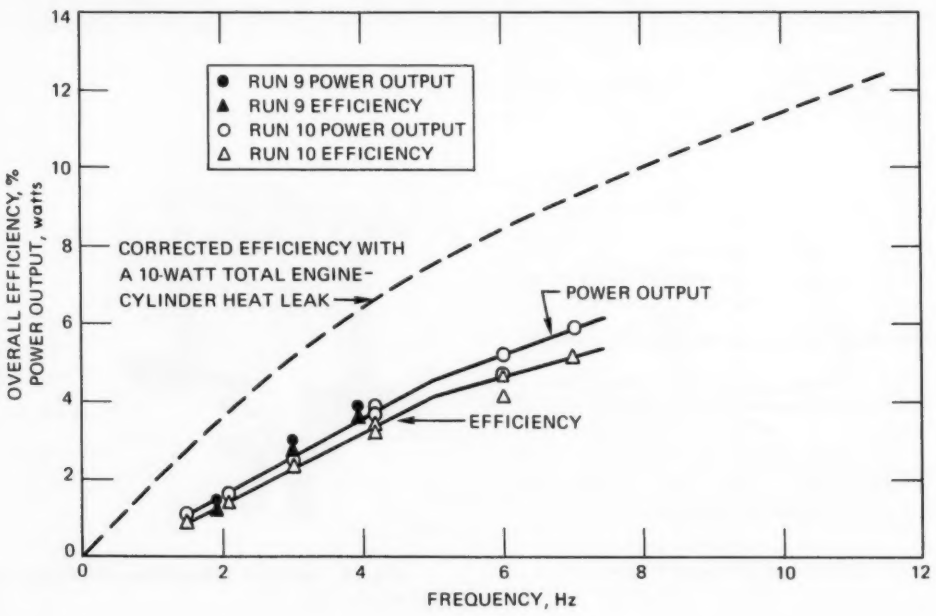


**Fig. 15 Performance summary for Model 2.**

**Table 6 Detailed Performance Summary for Model 2**

| | Measured | Calculated |
|---|---|---|
| Run number | 9 | |
| Data point | 10 | |
| Frequency of operation, Hz | 3.29 | |
| Average hot-plate temperature, °C | 646 | |
| Average cold-plate temperature, °C | 14 | |
| Maximum pressure, torrs | 857 | |
| Minimum pressure, torrs | 717 | |
| Theoretical maximum power output, watts | | 11.0 |
| Theoretical maximum power output at observed engine pressures, watts | | 8.95 |
| Engine power output, watts | 4.61 | |
| Power delivered to load, watts | 3.95 | |
| Heat input, watts | 110 | |
| Overall efficiency, % | 3.5 | |
| Working gas | Air | |
| **Heat Input, watts** | | |
| Surrounding insulation | | 39.2* |
| Sidewall | | 6.6* |
| Total engine-cylinder heat leak | 45.8 | |
| Regenerator solid conduction | | 2.8 |
| Regenerator gas conduction | | 6.0 |
| Radiation through regenerator | | 10.8 |
| Radiation around regenerator[1]† | | 5.3 |
| Regenerator/sidewall radiation short circuit[2] | | 1.3 |
| Regenerator/sidewall gas-conduction short circuit[3] | | 13.3 |
| Total regenerator heat leak | 46.8 | 39.6 |
| Main regenerator reheat loss[4] | | 10.8 |
| Regenerator blow-by reheat loss[5] | | 1.1 |
| Regenerator heat-capacity loss[6] | | 0.0 |
| Regenerator gas holdup loss[7] | | 2.4 |
| Total regenerator reheat loss | 17.6 | 14.3 |
| Heat required for ideal (Carnot) engine | | 9.2 |
| Total heat input | 110 | 109 |

*Calculated.

†See Table 4 for explanation of superscripts 1–7.

less-steel fibers. The packing density was about 5% and the wire diameter about 5 mils. Considerable variation in the packing density, wire shape, and wire diameter was present. A regenerator of improved design will be used in Model 3.

Increased power output will be attained largely through reduction of heat losses. Reduced regenerator heat loss will enable the hot- and cold-space gas temperatures to more nearly equal the engine hot- and cold-plate temperatures, thereby increasing power output.

Engine operation has proved to be very stable with the regenerator drive system. Also, the frequency of operation can be varied using the regenerator drive-piston bypass control valve. However, the Model 2 drive system produced rapid gas pulses in the power transfer line and load. Power-transfer-line losses resulted, which account for the difference in engine power output and the power delivered to the load indicated in Table 6. Other drive-system concepts are being investigated for Model 3 as well as a refined version of the Model 2 drive system.



XUM

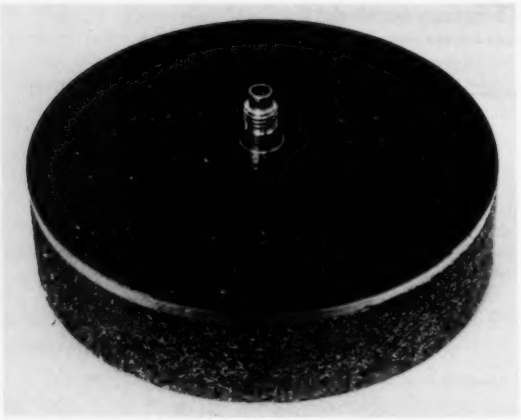

**Fig. 16 Model 2 regenerator.**

The experimental program has been successful in building and testing engines that begin to have the desired performance. However, the most important accomplishment is the consistent analysis—both experimental and analytical—of the losses experienced by these engines. This analysis shows where the most significant improvements can be made in power output and efficiency. Work on these improvements is now in progress.

## Conclusions

The simplified Stirling engine, as applied to a pumping application like that of a heart power source, is really a unique thermodynamic cycle with its own advantages and limitations. For the same regenerator displacement, the simplified engine has a lower power output than the conventional Stirling engine but requires less space devoted to keeping the regenerator and power piston moving properly. This simplified Stirling engine has as high a potential efficiency as any heat engine and has the advantage of coupling simply with most blood pumps so far developed.

The engine design predicts an efficiency of 24% at 2.5 Hz. The attainment of this high efficiency requires advances in the art of fabrication of thermal insulation, low thermal-conductivity engine sidewalls, and high-efficiency thermal regenerators. Auxiliary components, such as blood-cooled heat exchangers, and thermal-energy storage are also needed to make an implanted machine practical.

Design, construction, and testing of experimental engines have shown that the thermal losses and the power output can be predicted quite well, based on dimensions, material properties, and machine temperatures, pressures, and the frequency of operation. With this capability the task of increasing power output and decreasing heat input by design improvements has begun. To date an overall efficiency of 1.8% at 2.5 Hz has been observed. After a correction for the large heat loss through the insulation surrounding the experimental engine to a value attainable with high-quality vacuum insulation, an efficiency of 4.5% at 2.5 Hz is noted. Also, operation at higher frequencies for the engine greatly improves efficiency. At 8 Hz a corrected efficiency of 10% is noted. The regenerator and the engine walls are being modified to improve performance further. (FEM)

## Reference

Reference marked with an asterisk has not been verified by the editors; for further explanation, see the Foreword.

1.*G. Schmidt, Theory of Lehmann's Heat Machine, *J. Ger. Eng. Union*, **15**(1): (1871).

# A Radioisotope-Powered Stirling Engine for Circulatory Support*

By K. E. Buck, D. L. Forrest, and H. W. Tamai†

**Abstract:** *Aerojet-General has recently completed a conceptual design study of a radioisotope power source suitable for implantation in the human body. The output power from the device is to be used for circulatory support, either to assist a damaged heart or to drive an artificial heart. The design criterions are discussed in detail for a linear Stirling engine device. The compressor portion of the engine was tested, and its performance characteristics under experimental conditions are reported.*

Aerojet-General, under contract to the Atomic Energy Commission, recently completed a conceptual design study of an implantable radioisotope power source for circulatory support. The study included evaluation of various other engine configurations and component concepts. The basic objective of the study was to design and develop an engine with maximum efficiency and reliability and minimum size and weight. The performance of the engine was determined, and analytical models of the engine and key subsystems were developed. Major emphasis was placed on the power-conversion system.

## Principles of Engine Operation

### Requirements and Criteria

The general requirements for an implantable power supply are reliability, long operating life, high thermodynamic efficiency, minimum size, minimum weight, attitude insensitivity, and resistance to shock and vibration.

The standard Stirling engine has the highest thermodynamic efficiency of available closed-cycle engines and satisfies all these requirements except long operating life. If the operating life of Stirling engines can be improved, they will be well suited for many potential radioisotope applications and particularly for implantable power sources for circulatory support.

*Sponsored by the U. S. Atomic Energy Commission, Division of Isotopes Development. A more complete account of the work is given in USAEC Report AGN-8258, Conceptual Design of an Implantable Power Source for Circulatory Support Systems, Final Technical Report, Aerojet-General Corp., Jan. 26, 1968.

†Aerojet-General Corp., San Ramon, Calif. 94583.

In the Aerojet concept, the standard Stirling engine modifications primarily involve (1) elimination of engine bearings that would have to withstand high oscillating loads and (2) provision for direct coupling between the thermodynamic converter and the circulatory-support system. This is accomplished by using a free-piston assembly instead of the conventional piston and crank mechanism and by extracting power from the engine not as mechanical work but in the form of a pressurized gas that permits the use of a simple intermediate fluid and bellows arrangement to couple the engine output to the circulatory-support system.

### Modified Stirling Cycle

The Aerojet modified Stirling engine can be considered as one in which heat is converted to mechanical work by alternately heating and cooling a gas. In Fig. 1*a*, consider the enclosed volume of gas in the schematic diagram of the piston chamber and regenerator (regenerator cools hot gas flow and warms cool flow), temporarily disregarding the check valves. As the piston moves down, gas displaced from the cold chamber passes through the regenerator, where it is heated, and enters the hot chamber. The pressures in both hot and cold chambers are always virtually equal. However, the pressure level in the engine as a whole has increased since the average gas temperature in the enclosed volume has increased by the ratio $P_2/P_1 = T_2/T_1$, typical of a constant-volume process. The pressure profile corresponding to the respective piston positions, exclusive of the check valves, is shown in Fig. 1*b*.

Now consider the system with check valves. The exhaust check valve is connected to a gas reservoir at a pressure equal to the mean pressure in the previous situation. The intake check valve is connected to a reservoir at the minimum pressure. As the piston starts down, both valves are closed, and the pressure increases, as before, until it reaches the pressure of the high-pressure reservoir. At this point the exhaust check valve opens, and gas is forced into the high-pressure reservoir until the end of the stroke is reached. As the piston starts back up, the pressure in the engine starts to decrease (because the average temperature is de-



XUM

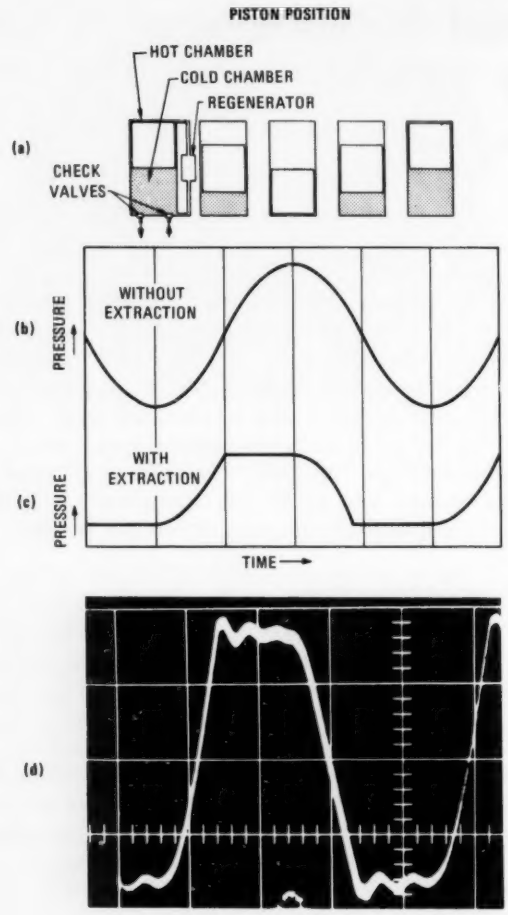


**Fig. 1 Modified Stirling-engine-compressor operation.**

creasing), and the check valve closes. The pressure continues to decrease until it equals that in the low-pressure reservoir, at which time the intake check valve opens, and gas is drawn into the engine. The pressure profile for this simplified model is shown in Fig. 1*c*. Figure 1*d* shows an actual pressure trace as measured on the Aerojet experimental engine. Thus, in a complete cycle, gas is pumped from the low- to the high-pressure reservoir. The system is a closed loop, through the pumping chamber, delivering work by expanding gas from a high to a low pressure. If the gas is expanded adiabatically, the ideal modified Stirling-cycle efficiency is within a few percent of the efficiency of the ideal Carnot cycle.

An important feature of the engine concept is elimination of the crank mechanism normally used in Stirling engines. The alternative drive mechanism for the displacer piston must accomplish two functions previously provided by the crank mechanism: (1) it must reverse the direction of motion as the piston reaches its end of stroke, and (2) it must provide a means for making up mechanical-energy losses due to fluid and mechanical friction.

Oscillating linear motion can be obtained in a number of ways. The spring-mass approach is particularly attractive because the kinetic energy of piston motion is conserved in such a concept. The spring can be mechanical, magnetic, or pneumatic. The pneumatic-spring system was selected because, to perform the function of energy addition, this was the simplest approach (Fig. 2). With such a pneumatic reversing piston, energy addition to the oscillating system occurs directly from the displacer piston as a result of the

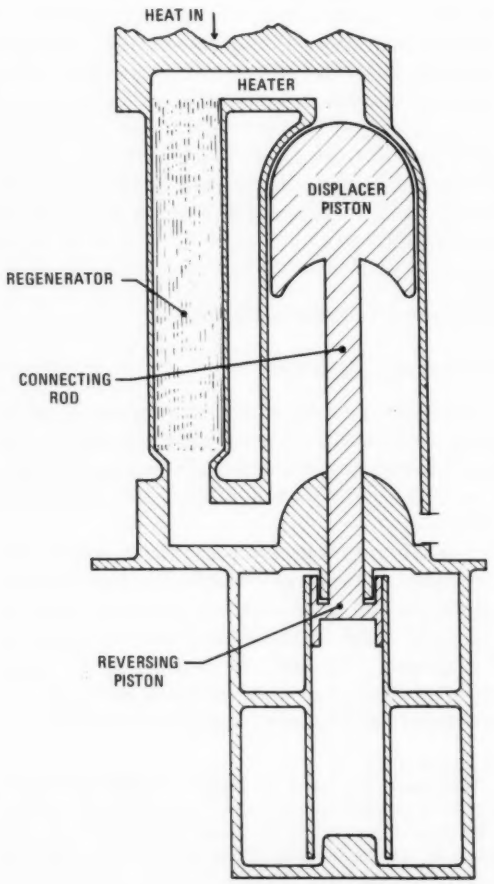


**Fig. 2 Linear Stirling-cycle-engine concept.**

nonsymmetrical nature of the pressure profile of the latter cylinder. The net effect is the addition of energy to the oscillating system.

### Application to Circulatory Support

The manner in which the modified Stirling engine can be used to provide power for a circulatory-support system is shown in Fig. 3. The interface between the engine and the circulatory-support pump is, primarily, the pumping chamber.

The configuration and operation of the pumping chamber are basically as follows. The chamber contains a movable plate to which three sets of bellows are attached. One set contains the pumping fluid that operates directly on the pumping membrane of the blood pump. The second set, located on the opposite side of the movable plate, contains a fluid at atmospheric pressure. The third set is located on both sides of the plate and contains the engine gas. By alternately valving high- and low-pressure gas to the two sides of the plate, pulsating power is delivered to the pumping fluid and, consequently, to the blood pump.

The fluid is kept at atmospheric pressure so that atrial pressure (i.e., pressure within an atrium of the heart) can be maintained essentially within a few mm Hg of atmospheric pressure. The fluid reservoir is a flexible sac located in the pleural cavity. The area ratio

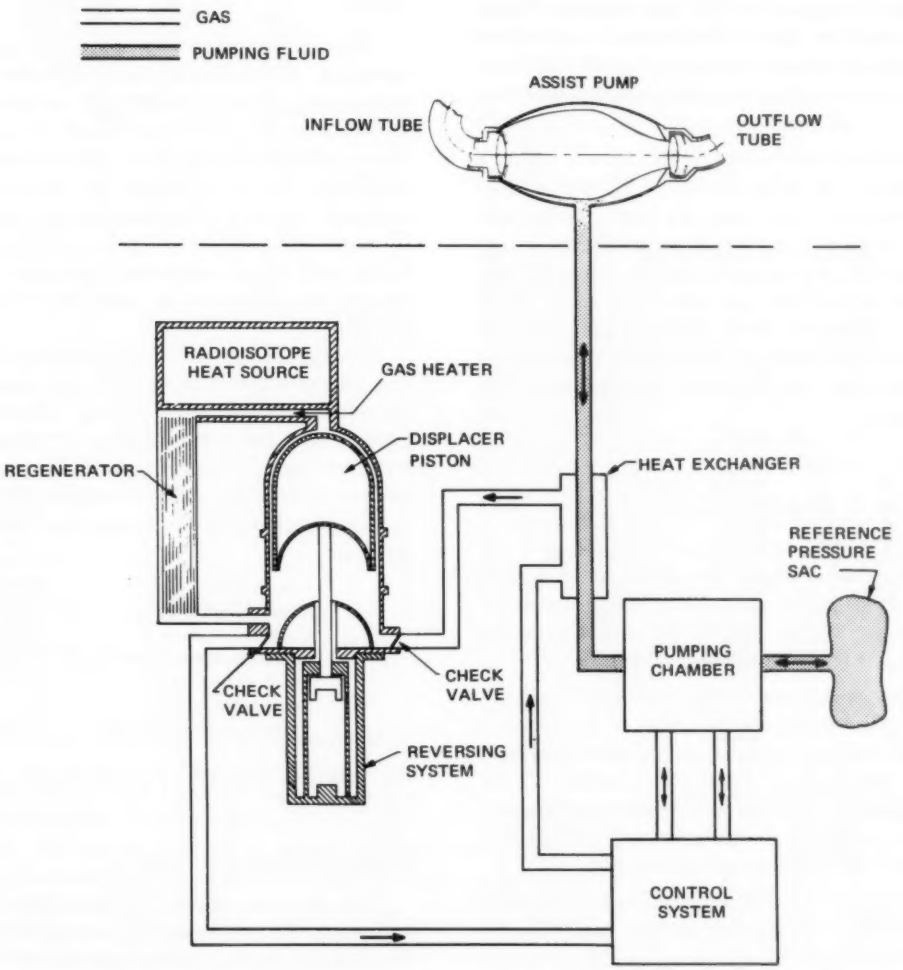


Fig. 3 Modified Stirling-cycle energy-conversion system. (Shown for one ventricle only.)



XUM

between the atmospheric-pressure bellows and the pumping-fluid bellows in the pumping chamber serving the left ventricle is selected so as to result in an equilibrium pressure in the pumping fluid of about 90 mm Hg. During systole the pressure in the gas bellows increases the pumping-fluid pressure to about 190 mm Hg, and during diastole the pressure is reduced to about atmospheric.

A system of the type shown in Fig. 3 offers several alternative methods of transferring waste heat from the engine to the blood. Waste heat can be extracted from the engine by cooling either the cold chamber or the low-pressure gas that is drawn into the cold chamber; the latter approach was selected for this design.

The low-pressure gas could be cooled directly in a blood heat exchanger, but the heat-exchanger design problems would be severe. The difference in temperature between inlet and outlet gas is >100°F (38°C), so that great care would be required to avoid overheating the blood.

A better technique is to first transfer the heat to a liquid, such as the pumping fluid or the atmospheric-pressure reference fluid. Since the heat capacities and mass flow rates of these liquids are much higher than those of the gas, a temperature rise of only a fraction of a degree results from the transfer of engine waste heat. If a pumping fluid is used, heat may be transferred to the blood in a separate heat exchanger without imposing any additional requirement on the blood pump.

## Description of Engine

Figure 4 shows how the major components of the power source are combined into an integrated system. The drawing shows all components except the waste-heat exchanger and the flexible sac that contains the fluid used as an atmospheric-pressure reference.

A linear arrangement of the heat source and the displacer and reversing system results in the simplest layout and minimizes the undesirable parasitic heat loss from the heat source. Since the location of the pumping chamber with respect to the other components is not critical, a configuration that resulted in a fairly regular external envelope was selected.

The major factors that affect efficiency are given in the tabulation at the top of the next column. The gross thermodynamic efficiency, including regenerator losses, is 41%. The overall efficiency of the modified engine is 20.7%.

| | Power, watts |
|---|---|
| **Output Power Required** | |
| Net output | 7.0 |
| To reversing piston | 0.9 |
| Control | 1.0 |
| Pumping chamber and line losses | 0.5 |
| Check-valve loss | 0.3 |
| Gross | 9.7 |
| **Thermal Power Required** | |
| Input to gas | 23.7 |
| Parasitic losses | 10.0 |
| Total | 33.7 |

### Heater

All the thermal power needed to sustain engine operation is transferred by conduction from the isotopic source to the heater, which subsequently heats the working gas. The transfer must be accomplished with a minimum temperature drop to minimize parasitic losses that would impair the system's efficiency and have adverse physiological implications. The pressure drop sustained by the gas in passing through the heater must also be minimized since power lost in this manner would have to be made up in the reversing system.

Finally, the heater and its connecting plenums are part of the unswept portion of the engine, and the amount of gas contained in these influences engine-pressure ratio and power density. Accordingly, a study was performed to optimize these aforementioned parameters to achieve a minimal configuration.

Specifications for the heater developed from this study are:

| | |
|---|---|
| Length, in. | 1.25 |
| Channel width, in. | 0.0645 |
| Channel height, in. | 0.1972 |
| Hydraulic diameter, in. | 0.0977 |
| Total volume, cu in. | 0.1275 |
| Heat transfer $\Delta T$, °F | 50 |
| Energy loss from $\Delta P$, watts | 0.047 |

The general configuration of the heater is shown in Fig. 5.

### Displacer Cylinder and Piston

The displacer cylinder is essentially a constant-volume chamber, one end being hot and the other cold. The function of the displacer piston is to transfer the engine working gas back and forth between the hot and cold ends through the regenerator and heater.

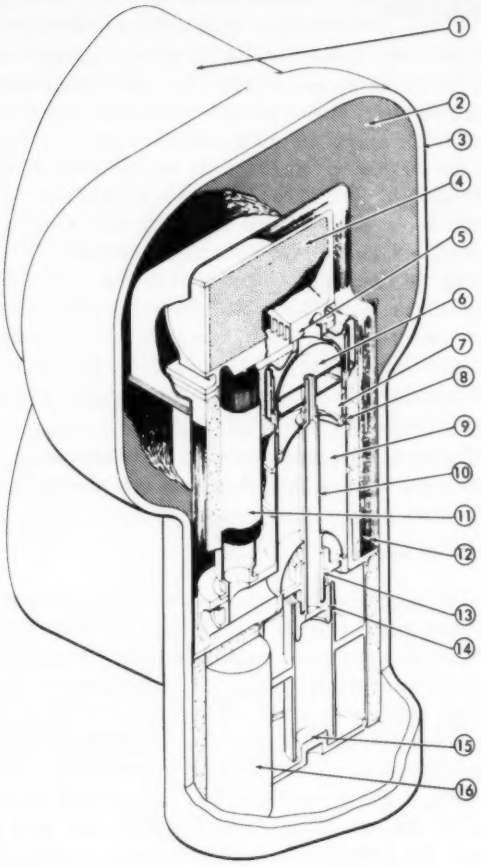

1. Pumping chamber
2. Polyethylene
3. Outer covering
4. Radioisotope heat source
5. Heater fins
6. Radiation baffle
7. Displacer piston
8. Displacer piston seal
9. Displacer cylinder
10. Connecting rod
11. Regenerator
12. Evacuated foil insulation
13. Seal
14. Reversing piston
15. Dashpot
16. Gas reservoir

**Fig. 4 Implantable power source.**

The major displacer-cylinder design criterion is that the parasitic heat loss from hot to cold end should be minimal. The piston and cylinder walls must be fabricated of light-gage, low-thermal-conductivity material to limit heat loss by conduction through these components. To further reduce conduction losses, the cylinder is made long and its diameter minimized. Thermal radiation through the piston is limited by radiation baffles. In addition to loss through thermal conduction, mechanical transport of heat by the moving piston contributes to axial heat loss. Heat is transferred from the hot portion of the cylinder to the piston during the upper portion of the stroke and is subsequently transferred to the low-temperature portion of the cylinder wall when the piston is in the lower portion of its stroke.

The displacer piston and cylinder are to be fabricated from Hastelloy alloy C, a solid-solution-strengthened nickel alloy. This material has good high-temperature strength, can be fabricated using most standard techniques, and has low thermal conductivity.

### Regenerator

The function of the regenerator is to maintain the temperature difference between the gas in the hot and cold chambers so as to lessen the need for addition of heat from an external source. This is accomplished by absorbing heat in the regenerator as the gas passes from the hot chamber to the cold chamber and subsequently reheating the gas when it returns to the hot chamber.

The volume of the regenerator should be small since it is a portion of the unswept volume of the

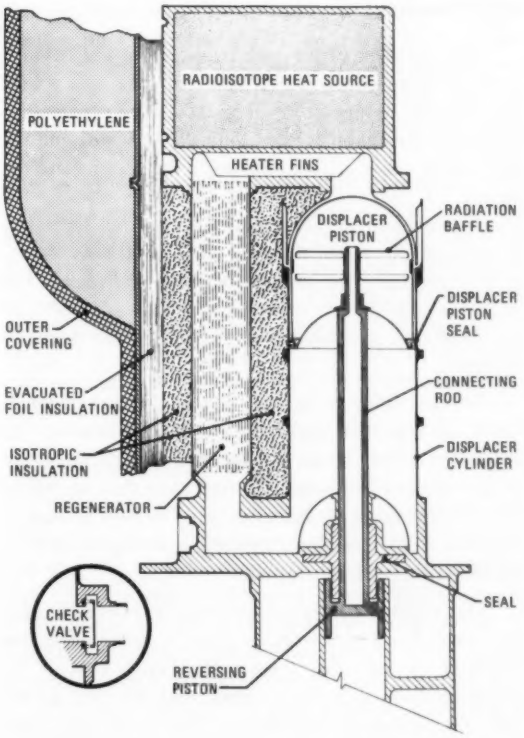


**Fig. 5 Engine design for implantable heart pump.**



XUM

engine. The effectiveness of the heat exchange between regenerator and gas must be maximum, which implies a large surface area and small hydraulic diameter. The pressure drop through the regenerator must be low; axial conduction must likewise be low since it contributes to parasitic heat losses. Since all these parameters are interrelated, the final configuration was selected on the basis of maximum overall engine efficiency.

The selected regenerator core geometry consists of many small hexagonal gas passages. Two-thirds of the metal webs that form the walls of the gas passages are 1 mil thick, with the remaining one-third being double that thickness. Other characteristics of the regenerator are as follows:

| | |
|---|---|
| Flow length, in. | 2.5 |
| Core diameter, in. | 0.508 |
| Hydraulic diameter, in. | 0.0216 |
| Effectiveness, % | 98 |
| Average pressure drop, psi | 0.056 |
| Energy loss due to $\Delta P$, watts | 0.4 |
| Axial heat loss, watts | 1.47 |

### High-Temperature Insulation

The function of the high-temperature insulation is to hold down parasitic heat loss from the heat source and the high-temperature portions of the engine. The insulation should be as close to both the engine and the heat source as possible to minimize the volume and the weight of the neutron shield (which is outside the thermal insulation). The insulation need not have high compressive or shear strength but should have insulation properties that do not degrade with time. The insulation should also contribute as little as possible to the axial heat loss down the regenerator and displacer cylinder.

Evacuated-foil insulation has the lowest conductivity of available insulating materials. However, its insulating properties are not isotropic, the conductivity within the foil being much greater than that normal to the foil. An isotropic insulator must be used at least in the area of the displacer cylinder and regenerator to avoid excessive axial heat loss.

The selected configuration was a layer of isotropic, flake-opacified fiber insulation directly surrounding the displacer piston and regenerator, with a layer of evacuated-foil insulation covering both the heat source and the isotropic insulation. The total heat loss through the high-temperature insulation is about 1.7 watts.

### Check Valves

The check valves regulate the flow of gas into and out of the displacer cylinder. The inlet check valve opens whenever engine pressure is less than that at the low-pressure inlet. The exhaust check valve opens when engine pressure is greater than the pressure in the high-pressure outlet line. The design criterions for the check valves include high reliability and minimum opening resistance, flow resistance, and backflow on closing. A simple disk valve appeared to meet these requirements very well. Movement of the disk is controlled automatically by gas pressure. By proper selection of geometry and dimensions, the pressure loss and backflow can be kept very low, and light springs are used to further reduce backflow.

Valves of this type were used in the experimental engine, and the anticipated performance was verified.

### Reversing System

The purpose of the gas chamber surrounding the reversing piston (Fig. 2) is to provide sufficient compression and expansion volume so that the pressure ratio in the reversing cylinder is about the same as that in the displacer cylinder. This results in a nearly continuous transfer of energy from the displacer to the reversing piston, although not at a constant rate. The amount of energy transferred is proportional to the area of the connecting shaft. The shaft area used is about 10% larger than needed; this tends to make the piston operate with a stroke slightly longer than design would indicate. Excess energy is dissipated by dashpots at the ends of the reversing cylinder.

### Seals and Bearings

A major advantage of the linear-engine concept is that all bearing loads are low. Bearing surfaces are required only for alignment and to sustain acceleration loads imposed by gravity and external movement. As a consequence, the surfaces provided for seals can also be used as bearings.

Three seals are required in the engine: one on the displacer piston, one on the reversing piston, and one between the displacer cylinder and the reversing cylinder. None of these need be an absolute seal, but leakage must be held to a small fraction of the gas volumes involved. The most stringent seal requirements are on the reversing piston. Both the piston and shaft seals must withstand the full engine-pressure ratio of about 1.25. The sealing requirement on the displacer

piston is much less severe because the pressure difference across the displacer piston is very low.

Since the operating temperature of the reversing piston is less than 250°F (120°C), a wide variety of materials is suitable for use as seals. The main selection criterions are low coefficient of friction and low wear rate. Requirements on the displacer piston seal are more severe since it may be exposed to a temperature of 600 to 800°F (315 to 400°C); several of the solid bearing materials based on molybdenum disulfide with binders or in porous metal matrices appear to have the properties required for this application.

### Pumping Chambers

The pumping chambers (Fig. 6) form the interface between the engine gas and the pumping fluid used to transmit power to the blood pump. These chambers convert the pressure level and pressure ratio most advantageous for engine operation to those required by the blood pump and also automatically adjust the output pressure for changes in atmospheric pressure. In the pumping chambers, neither leakage nor diffusion of the engine working gas into the pumping fluid can be tolerated. Therefore metallic, rather than plastic, seal material must be used. Other pumping-chamber requirements are maximum reliability and minimum volume.

Welded metal bellows are used because of their long cyclic life—this type of bellows has very good fatigue-life characteristics if the stress level is kept sufficiently low. The various bellows are arranged so that the pressures outside the bellows are always higher than those inside; this prevents bellows "squirm"—a mechanical instability analogous to column buckling.

The dimensions of a pumping chamber are fixed by the size of the stroke for the blood volume needed. Completely separate left and right pumping chambers are provided in the design; this permits synchronous pumping of left and right heart chambers and independent control of each side.

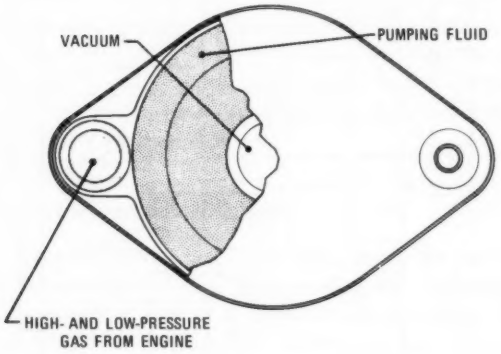


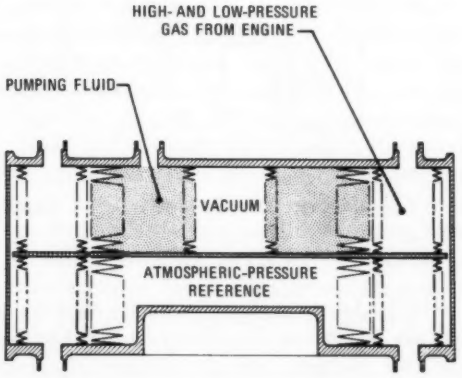


**Fig. 6 Pumping chamber of internal circulatory-support engine.**

### Heat Rejection

Waste heat is removed from the engine by cooling the extracted working gas before it is returned to the engine. Heat from the gas stream is transferred to the pumping fluid and, in turn, from the pumping fluid to the blood. Of a number of possible methods, the one chosen consisted in incorporating the heat exchanger into the abdominal aorta where it is close to the engine and where a suitably high blood flow is available. The heat exchanger is a simple tubular exchanger with the blood flowing in a central tube that is nearly identical to that in a normal artery. The pumping fluid flows in an annular chamber around the tube carrying the blood. An inner diameter of about 1 in. and a length of about 6 in. result in heat-transfer conditions which prevent damage to the blood (due to overheating), even at the lowest blood flow rates.

### Radioisotope Fuel and Shield

Plutonium-238 was selected as the thermal-power source for the implantable power system primarily because of its low shielding requirements and long half-life. The major problems associated with the use of $^{238}Pu$ are the neutrons emitted as a result of spontaneous fission and the possible release of helium resulting from alpha-particle emission.

Plutonium nitride was used because it is stable at temperatures much higher than those required in an implantable power source, and it has some advantages



XUM

over the oxide: a slightly higher plutonium density, a higher thermal conductivity, and complete absence of neutrons from $(\alpha,n)$ reactions (these can also be eliminated in the oxide by the use of oxygen enriched in $^{16}O$).

The fuel is pressed into cylindrical pellets and encapsulated in a W–Re alloy vessel. The wall thickness of the vessel is based on gamma-shielding requirements, since this thickness is greater than that required to withstand the helium pressure buildup. Although a W–Re alloy has the required strength, it is encapsulated in a thin can of Hastelloy alloy C for atmospheric-corrosion protection. To limit the neutron flux at the surface of the shield to 50 mrems/hr [based on a relative biological effectiveness (RBE) of 10], about 1 in. of polyethylene is mounted outside the thermal insulation.

### Pumping-Chamber Control

Largely because of autoregulatory regional circulatory controls, the heart (as a pump) fulfills its life-sustaining functions if it satisfies the following basic criterions:

1. It must maintain sufficient cardiac output (blood flow rate and systemic pressure) to satisfy all the needs of the body.
2. It must provide flow balance between the right and left heart circuits and between cardiac output and venous return.

These same must apply to an artificial heart pump which, to accommodate the dynamic changes in vascular impedance, additionally must have a stroke profile and a pulse rate similar to those of the natural heart.

Cardiac output is the product of stroke volume and heart rate. For a system in which systole and diastole are synchronized for both sides of the heart, flow balance can only be achieved by adjusting the stroke volume. Atrial pressure is the most sensitive control signal for flow-balance compensation. Until further clinical evaluations indicate otherwise, heart-pump operation should correspond closely to normal physiological behavior, i.e., pulsatile flow, variation in relative duration of systole and diastole, heart rate, and stroke volume.

A schematic diagram of the control system, designed to vary the implantable heart-pump operating parameters, is shown in Fig. 7. A load-sensitive, bistable fluidic amplifier (FA-1) is used as the primary switching element which directs the high-pressure gas stream to the right-ventricular pump during systole and diastole. Operation is based on the principle of "wall attachment"—the Coanda Effect. The fluidic device also provides pressure to actuate the spool valve (SV-1) that cyclically vents the opposite side of the right-ventricular pumping chamber. Additionally, it provides pressure to actuate the spool valve (SV-2) that directs the high-pressure supply stream to the left-ventricular pumping chamber and vents the opposite side of the chamber. The left ventricle is not directly driven by a bistable fluidic amplifier, since the output of such a device is only 40 to 50% of the supply pressure.

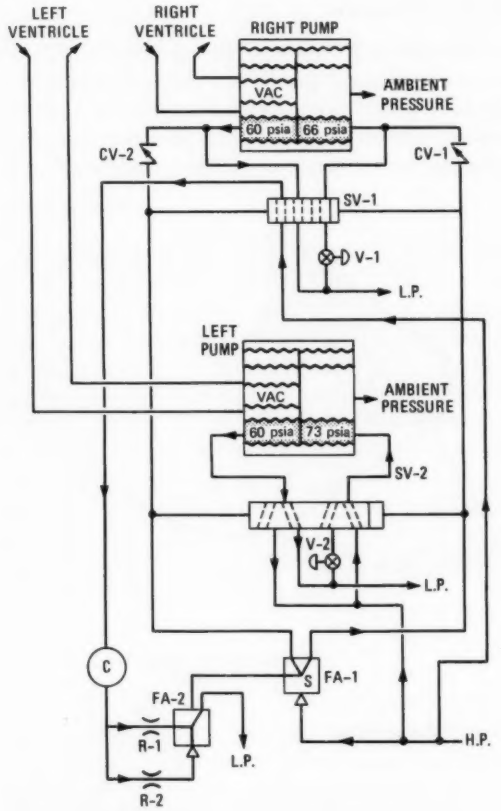


**Fig. 7 Control-system schematic diagram for implantable heart.**

The load-sensitive bistable fluidic amplifier automatically switches at the end of systole and diastole—when the pumping chamber reaches its maximum displacement. The pumping-chamber vent line is connected directly to the low-pressure reservoir during systole so that the full available pressure differential is

always applied for a firm systolic pulse. The duration of systole is therefore determined by the body autoregulatory mechanisms that control peripheral impedance. Control valve V-1, located in the right-ventricular pumping-chamber diastole vent line, determines the duration of diastole and the pulse rate. Control valve V-2, located in the left-ventricular diastole vent line, is required to adjust the left-ventricular stroke displacement and to maintain flow balance between the left and right ventricles. Two atrial-pressure sensors are required to provide the control signals for V-1 and V-2.

A timing circuit is provided to limit the pulse rate to a minimum permissible value consistent with normal physiological requirements of 60 to 65 beats per minute. During systole a capacitive element (C) is fully charged to line pressure by the actuation of spool valve SV-1. Restrictors (R-1, R-2) control a fixed-leakage flow rate to the fluidic amplifier device (FA-2). This leakage is normally vented to the low-pressure reservoir. If the pulse rate is too low (less than the minimum allowable rate of 60 to 65 beats per minute), the pressure in the capacitive element will be reduced by the controlled leakage to the point at which FA-2 will switch and direct an input signal to FA-1. This signal will automatically terminate the diastolic period and initiate systole.

## Experimental Investigation

Aerojet-General has undertaken work to verify certain features of the engine concept by evaluating experimentally several of the novel characteristics of the engine to support the analytical-design effort. These include (1) operation of the Stirling engine as a compressor, (2) the linear-engine concept with pneumatic reversing system, and (3) the direct coupling of a compressor and pumping chamber. Three separate tests were planned to investigate these three areas. The compressor-operation test is complete. Its purpose was to evaluate the operation of the regenerator, heater, check valves, and labyrinth seal, as well as the overall system performance. It is planned to complete the remaining tests within the next several months.

Figure 8 shows the test apparatus. No attempt was made to minimize the size of the drive mechanism or the reservoirs, since the experiment was designed to test only the functioning of the compressor. The assembly drawing of the engine is shown in Fig. 9, and the instrumentation used for data collection is shown in Fig. 10.

Dynamic response of the thermocouples used in this test was not adequate for detailed measurement of

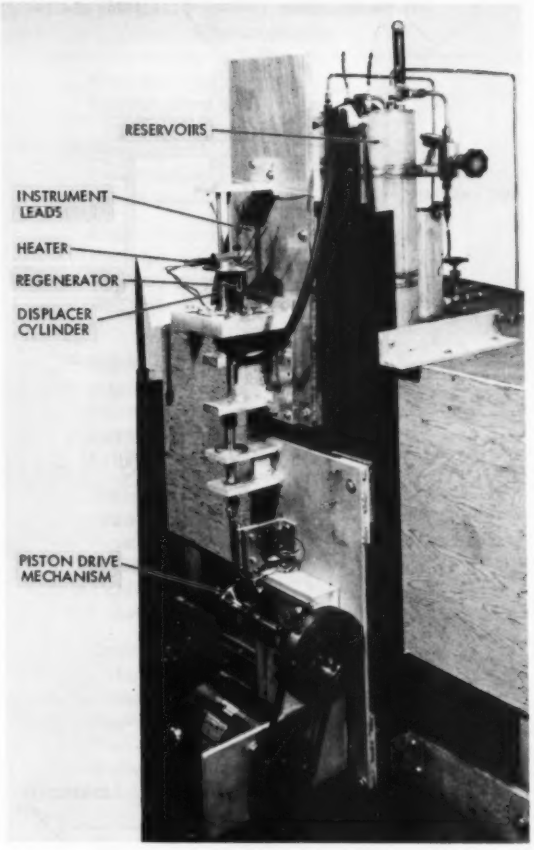


**Fig. 8 Stirling-engine-compressor test apparatus.**

the heater and regenerator performance. The general performance of these components was as anticipated, except that the initial regenerator-core geometry proved to be inadequate. The regenerator core consisted of a random packing of 1-mil Nichrome wire. The poor performance was apparently due to an insufficient amount of wire and to nonuniform packing and compaction of the wire. Subsequent runs with more densely packed wire in the regenerator yielded satisfactory results. Characteristics of the two regenerators tested are as follows:

| | Matrix 1 | Matrix 2 |
|---|---|---|
| Total wire length, ft | 800 | 2400 |
| Unswept volume, cu in. | 0.75 | 1.00 |
| Calculated effectiveness, % | 82 | 97 |



XUM

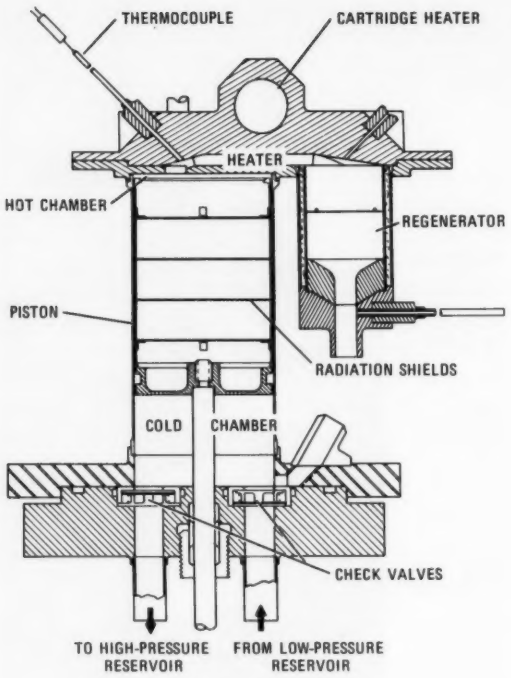


**Fig. 9 Stirling-engine assembly.**

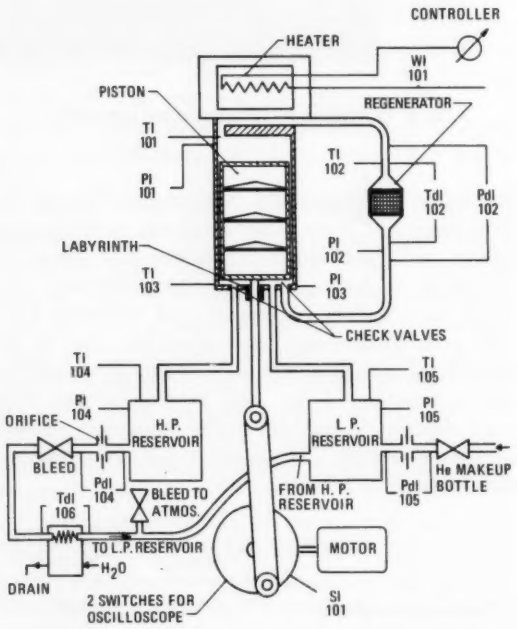


**Fig. 10 Stirling-engine test-apparatus diagram.**

The check valves and piston seal performed as expected. Leakage through the shaft seal was much higher than expected, however, due to an excessive amount of clearance that had been provided for differential thermal expansion. This loss can be easily eliminated in future engines; so the data reported here have been corrected for this seal leakage.

Figures 11*a* and 11*b* show measured and calculated values of engine output flow and gross power output, each as a function of pressure ratio for different engine speeds and maximum gas temperatures. Close correlation was observed between the engine-pressure profile predicted from theoretical analysis and that achieved in the test. The principal difference between the theoretical and observed profiles resulted from oscillations of the check-valve disks.

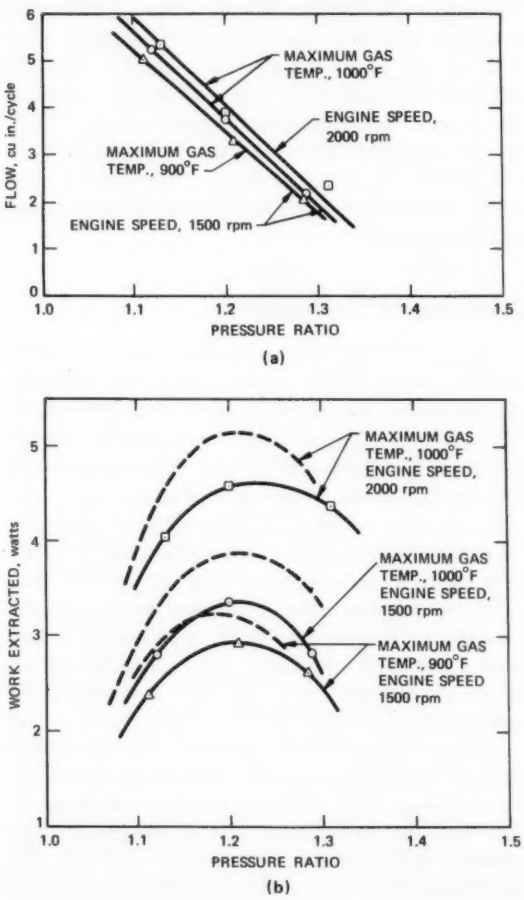
FLOW, cu in./cycle
MAXIMUM GAS TEMP., 1000°F
ENGINE SPEED, 2000 rpm
MAXIMUM GAS TEMP., 900°F
ENGINE SPEED, 1500 rpm
PRESSURE RATIO
(a)
WORK EXTRACTED, watts
MAXIMUM GAS TEMP., 1000°F ENGINE SPEED, 2000 rpm
MAXIMUM GAS TEMP., 1000°F ENGINE SPEED, 1500 rpm
MAXIMUM GAS TEMP., 900°F ENGINE SPEED 1500 rpm
PRESSURE RATIO
(b)

**Fig. 11 Data obtained on experimental Stirling-engine compressor. — — —, calculated. ———, measured.**

## Conclusions

The main advantage of the Stirling-cycle engine is high efficiency. The engine described herein can deliver 7 watts of output power from about 35 watts of thermal power, for an overall efficiency of about 20%.

It is proposed that the linear-engine concept is the most attractive way to utilize the Stirling cycle for circulatory-support systems. Long engine life is assured by the elimination of crank mechanisms, zero-leakage seals, and high bearing loads. Pneumatic transmission of energy to the artificial heart is simple and permits wide flexibility in the selection of techniques used to accomplish this.

Improvements must be made in several areas before a completely satisfactory system can be achieved, however. The total engine size, although within the estimated 2000-ml limit for an abdominal transplant, could hopefully be reduced. The major volume is the neutron shield for the radioisotopic heat source—a problem not related to engine type, but one that must nevertheless be solved before a practical system can be evolved. The pumping chambers are also quite large—a sizable reduction could be made if nonsynchronous pumping of left and right ventricles is acceptable.

A summary of the various important parameters involved in the radioisotope-powered Stirling engine for circulatory support is given in Table 1. (DNH)

**Table 1 Summary of Power-Source Characteristics**

| | |
|---|---|
| Net power output, watts | 7 |
| Thermal power input, watts (end of life) | 33.7 |
| Overall efficiency, % | 20.7 |
| Overall volume, cu in. | 110 |
| Overall weight, lb | 3.9 |
| Engine working gas | Helium |
| Maximum gas pressure, psia | 74 |
| Minimum gas pressure, psia | 60 |
| Maximum gas temperature, °F | 1200 |
| Minimum gas temperature, °F | 250 |
| Engine speed, cpm | 1000 |
| Engine displacement, sq in. | 1.32 |
| Stroke length, in. | 1.5 |
| Displacer cylinder diameter, in. | 1.08 |
| Cylinder wall thickness, in. | 0.010 |
| Piston wall thickness, in. | 0.005 |
| Regenerator volume, in. | 0.763 |
| Regenerator length, in. | 2.5 |
| Regenerator diameter, in. | 0.625 |
| Unswept volume in cold chamber, cu in. | 0.20 |
| Unswept volume in hot chamber (including heater volume), cu in. | 0.25 |
| Fuel | $^{238}Pu$ |
| Fuel form | PuN |
| Surface dose rate, mrems/hr | 50 |

# Design of an Implantable, Rankine-Cycle Radioisotope Power Source*

By F. N. Huffman, R. J. Harvey, and S. S. Kitrilakis†

**Abstract:** *An implantable power source, fueled with a radioisotope and using a miniature Rankine-cycle steam engine, has been designed to drive a circulatory-support system. The power-source design is based on parametric studies, system requirements, and experience in developing steam-engine power supplies. By coupling this 4-watt (mean hydraulic output) power source to circulatory-system-assist devices, a useful, implantable circulatory-support system is possible because of the efficiency (20%), size (1 liter), mass (2 kg), and high reliability.*

In the United States alone, 600 thousand deaths a year are caused by heart attacks. A significant fraction of these people could be helped and could continue useful employment if a permanent, totally implantable circulatory-support system were available. The objective of this design study is to characterize a radioisotope power supply for such a circulatory-support system.

Thermo Electron Corporation (TEC) has been actively engaged in the development of such a power source for over 4 years.[1,2] In conjunction with Chil-

*Includes work performed under U. S. Atomic Energy Commission, Division of Isotopes Development; edited and reprinted by permission of Thermo Electron Corp., 85 First Ave., Waltham, Mass. 02154.

†Thermo Electron Corp.



XUM

dren's Hospital Medical Center, studies of power requirements[3] and additional endogenous heat[4-6] have been performed under the sponsorship of the National Heart Institute (NHI).

The design of the power source which resulted from a recently completed AEC contract, "Studies on an Implantable Power Source for Circulatory Assist Devices" (Ref. 7), is described, and relevant data from the NHI-sponsored thermal-energy storage system are presented. A block diagram is used to illustrate system functions; then the major subsystems (heat-source, Rankine-cycle-engine, and hydraulic) are described. Next the system performance is summarized, and an evaluation of the limitations and advantages of the reference-design system is made.

## Power-Source Design

A simplified block diagram of a Rankine-cycle circulatory-support system is shown in Fig. 1. A radioisotope heat source provides the energy for the Rankine-cycle engine, which pressurizes a hydraulic reservoir (or accumulator). The blood pump and associated controls are powered from this hydraulic reservoir and are external to the power source.

The heat source consists of the radioisotope fuel with void volume, shielding, and encapsulation embedded in a thermal-energy storage material. The thermal-energy storage material reduces the fuel inventory (with its associated cost, heat, and radiation) and at the same time allows the power source to respond to peak loads.

The decay heat vaporizes the working fluid in the boiler. The vapor enters the expansion cylinder through the inlet valve and delivers work by expansion against the steam piston, which is directly coupled to the piston of the hydraulic pump.

The hydraulic pump and reservoir are located in the power source to permit use with either total-replacement or assist devices. Based on experience with

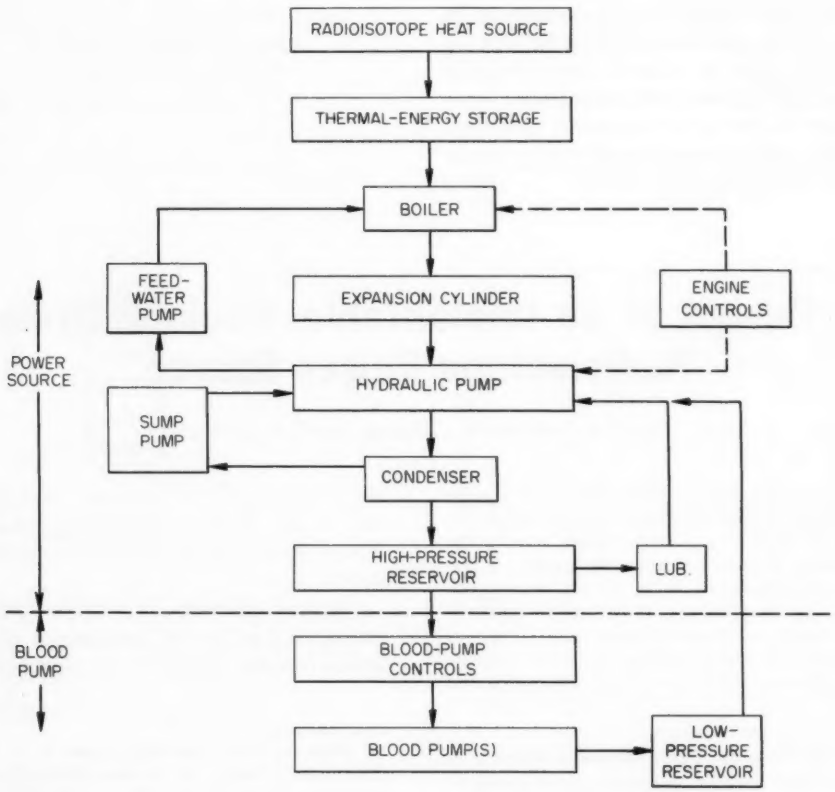


**Fig. 1 Block diagram of radioisotope-fueled circulatory-assist system.**

external assist-pump control systems, it does not seem realistic to expect the engine to synchronize directly with, and otherwise respond physiologically to, circulatory demands (variable heart rate, stroke volume, and systemic pressure) and still run efficiently. In addition, the hydraulic reservoir decouples the power source as far as possible, buffers the engine from responding to fast transients, provides the feedback for nondissipative engine control, and serves as part of the heat-transfer loop to carry the reject heat from the power source to the blood pump.

The reject heat is dumped through a condenser into the hydraulic system, where it is transferred to the blood pump. The functions of the blood pump are to (1) pump blood, (2) act as the physiological sensor for the blood-pump control system, and (3) exchange reject heat from the Rankine-cycle engine to the blood. The blood, in turn, rejects heat to the outside of the body by means of the usual physiological mechanisms of perspiration, radiation, and convection–conduction. Since blood must pass through the heat exchanger, either the heat exchanger should be located in an area of high blood flow or the prosthetic tubes must be relied upon to bring blood to the condenser. The most natural way to reject the heat in or adjacent to the blood pump or pumps of a circulatory-assist device is to use the artificial ventricle surface area as the heat-exchanger surface. This has the advantage of requiring no additional prosthesis or additional prosthetic surface in contact with the blood. It also simplifies the surgical implantation and reduces the maximum temperature rise of the blood. The temperature drop across the 30-mil polyurethane bladder of an assist pump is approximately 0.8°F/watt(t). The circulatory system is designed to have minimum weight and volume.

The feed pump is located between the high-pressure (80 psia) reservoir and the boiler (400 psia). The sump pump operates between the condenser (2.9 psia) and the low-pressure reservoir. Fluid for bearing lubrication is bled from either the high- or the low-pressure reservoir.

## Heat-Source Subsystem

### Fuel Capsule

In the power source shown in Fig. 2, the heat-source configuration is sized for 20 watts of $^{238}Pu$ as the oxide. Six millimeters (236 mils) of tantalum is used for shielding the $^{238}Pu$. For an initial impurity of 1 ppm $^{236}Pu$, the 6 mm of tantalum shielding is sufficient to keep the gamma dose rate equal to or less than the neutron dose rate for a period of 5 years. The fuel is encapsulated in 80 mils of Haynes 25 alloy. The void volume for helium buildup is equal to the fuel volume. A controlled leak releases the helium from the fuel volume to the void volume.

### Thermal-Energy Storage

The radioisotope fuel capsule is embedded in a cylinder of a thermal-energy-storage (TES) material—a eutectic composition of 30 mole % LiCl and 70 mole % LiF. This material has a high latent heat of fusion (362 cal/cm$^3$) and a convenient melting point (930°F). This material is stable, compatible with 304 stainless steel, and has no problem of hydrogen release (as with LiH).

Lithium hydride is an outstanding TES material from a weight standpoint. However, at its 1250°F melting point, it releases hydrogen, which escapes from the container at some small but finite rate. To prevent hydrogen from degrading the thermal insulation, either the lithium hydride must be sealed in heavy containers or the vacuum-foil insulation must be provided with a hydrogen "getter." Since neither alternative has yet been demonstrated, hydrogen diffusion associated with lithium hydride is still a serious drawback.

### Boiler

The boiler is a single tube wound around the TES capsule. This type of boiler has been used successfully on all of TEC's steam engines. The boiler is actually part of the engine subsystem, but it is cocooned within the thermal storage subsystem.

### Vacuum-Foil Insulation

Vacuum-foil thermal insulation is used around the heat source. These foils are located perpendicular to the direction of heat flow and form radiant-heat shields to reflect heat back to the heat source. The separator or thermal-conduction barrier between the metal foils is formed by a thin layer of oxide powder applied to each layer of the foil. Under AEC sponsorship TEC has investigated W, Ni, Ta, and Mo foils in combination with thoria and yttria powders. Experience has shown that the average spacing required per foil layer in the insulation is approximately 2 mils. Thermo Electron Corporation's data from these insulation systems, shown in Fig. 3, indicate a planar heat flux of less than $^{1}/_{1000}$ of a watt per square centimeter at the boiler temperature of 900°F. However, to realize this performance, the insulation must be packaged in a vacuum



XUM

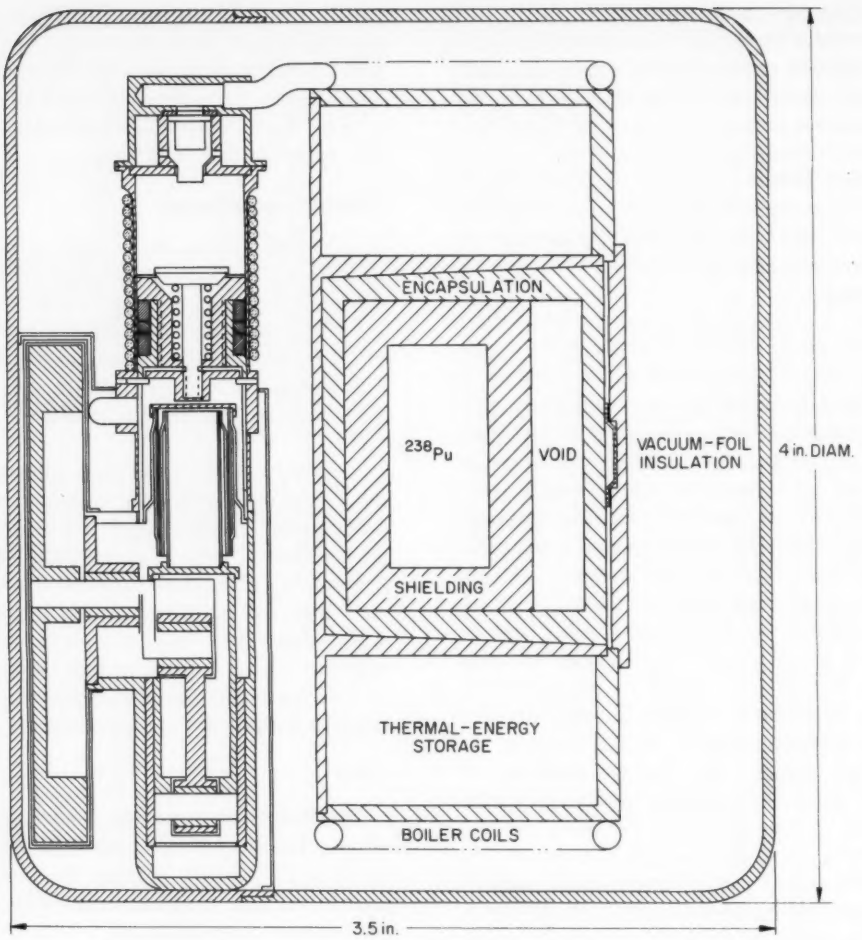


**Fig. 2 Layout drawing of radioisotope-fueled Rankine-cycle power source.**

environment to prevent conduction across the interfaces by gases.

The reference thermal storage assembly is similar to the TES prototype successfully demonstrated under NHI sponsorship. This unit has:

1. Demonstrated thermal-energy storage of 140 watt-hr using a LiCl/LiF eutectic mixture.
2. Shown the effectiveness of vacuum-foil thermal insulation (Fig. 3).
3. Confirmed that transient boiler temperatures are stable for good engine control.
4. Demonstrated the fabrication and containment of a LiCl/LiF eutectic mixture in 304 stainless steel.

The insulation loss of only 2.7 watts at the melting point (Fig. 3) is quite encouraging. This loss can be reduced further by use of a larger number of foils, refinement of "edge" configuration in the vacuum-foil package, use of foils of greater reflectivity, and reduction of heat-source surface area.

## Rankine-Cycle-Engine Subsystem

The concept of the power source is the conversion of heat from the source assembly to mechanical energy using a hydraulic accumulator and miniature steam engine directly coupled to a hydraulic pump.

The primary components of the Rankine-cycle engine are the working fluid, boiler, inlet valve, exhaust valve, cylinder, piston, flywheel, condenser, and feed pump.

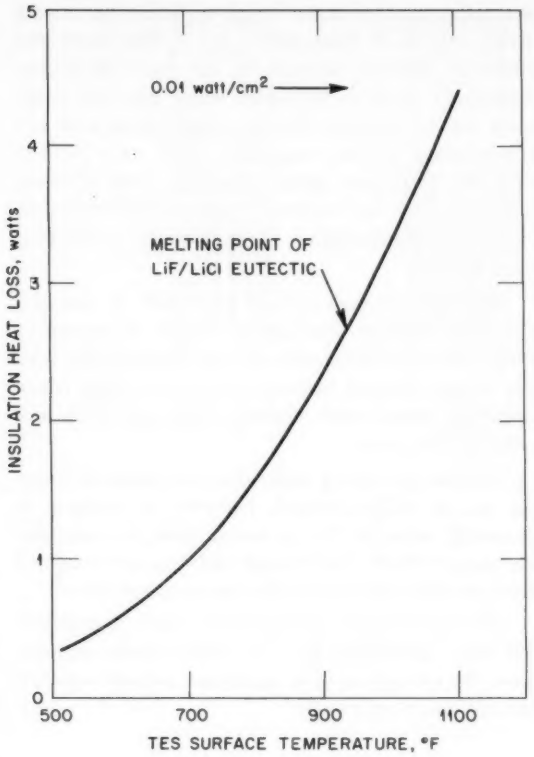


**Fig. 3 Heat loss through vacuum-foil insulation on prototype TES unit. Foil area = 68.2 sq in. Forty layers of nickel foil with zirconia. Pressure = $3 \times 10^{-5}$ mm Hg.**

The relationship of these components within a thermal storage Rankine-cycle circulatory-assist system is shown in Fig. 1.

### Working Fluid

The choice of the working fluid for a heat engine is of fundamental importance. Factors that influence this choice include cycle efficiency, thermal stability of the fluid, heat-source temperature, toxicity, and corrosiveness.

As part of a study on power sources for circulatory-assist devices, potential working fluids for low-power Rankine engines were surveyed. The most promising fluids were water and some organics—Freon E-1, Monsanto CP-34, and Monsanto CP-9. All the organic working fluids require regeneration.* The organic fluids are especially attractive because, up to their maximum working temperature, they give a cycle efficiency exceeding that of water. The working fluids were investigated as a function of inlet temperature, inlet pressure, cutoff pressure, condenser temperature, and mechanical efficiency. A typical data sample is shown in Fig. 4. Here the ideal efficiency of the Rankine cycle using a water working fluid is given as a function of inlet pressure, parametric in boiler temperature. The sensitivity of the steam-engine efficiency to release pressure is shown in Fig. 5.

The conclusion from this investigation was that, although the potential performance of organic working fluids is promising, water is the preferred working fluid. Water gives good cycle efficiency and has well-known thermodynamic properties; also, there is a wealth of practical experience involving its use in Rankine engines (i.e., "steam" engines). Unfortunately time comparable to the present life requirement are not available.

### Engine Configuration

A number of different engine configurations were evaluated. Review of older steam-engine designs showed that the popular double-acting design with

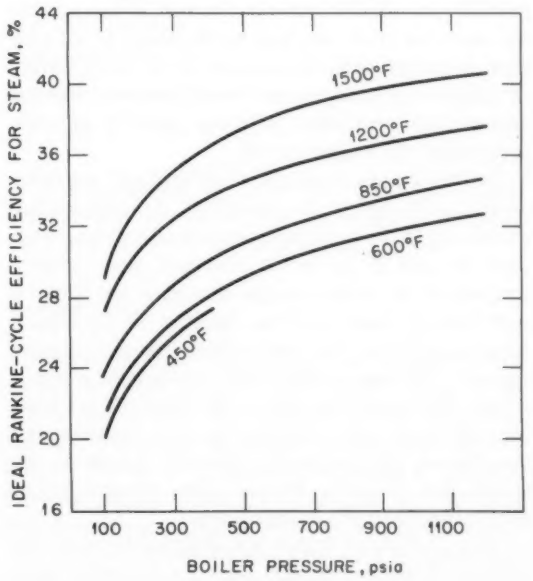


**Fig. 4 A typical family of curves for ideal Rankine-cycle efficiency, parametric in superheater temperature. Condenser temperature = 130°F. Condenser pressure = 2.22 psia. Release pressure = 10 psia.**

*Transfer of heat from engine-cylinder exhaust to boiler feedwater.



XUM

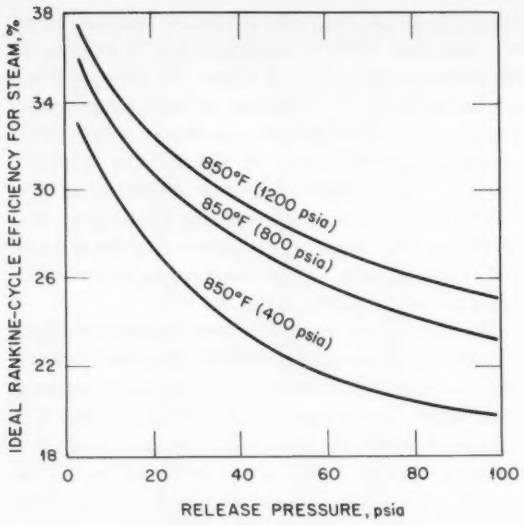


**Fig. 5 Steam-engine efficiency as a function of release pressure. Condenser temperature = 130°F. Condenser pressure = 2.22 psia.**

slide valve had a feature, in addition to high valve leakage, which was inevitably inefficient—steam was introduced and exhausted through the same port. Thus heat was transferred from the steam in its hot state to the wall and from the wall to the steam in its cold state. It follows that the enthalpy of the steam leaving the engine was greater than it would have been had the process been reversible; thus the quantity of work delivered by the engine was less.

This drawback is avoided in a "uniflow" engine by admitting the steam at one end of the cylinder and exhausting it through ports uncovered by the piston near the end of its stroke. However, more detailed analysis of the uniflow engine showed it was liable to high leakage losses and was sensitive to mechanical losses arising from the same problem found in Stirling engines—the compression work to return the piston is a large fraction of the total work. Since the net work obtained is the difference between two expansion and compression work terms of comparable magnitude, the output and efficiency become quite strongly dependent on frictional and leakage losses.

The TEC steam engine was designed to avoid this problem. A poppet exhaust valve on the piston stays open during the entire return stroke, and negligible compression work is done in the steam cylinder. A detail drawing of the steam-cylinder assembly is shown in Fig. 6. The valve position sequence, which has been successfully demonstrated in all of TEC's operational steam engines, is illustrated in Fig. 7. This figure also shows an indicator diagram for the cycle. Of course, feed-pump work to introduce water into the boiler must still be supplied, but this compression work is a few percent of the expansion work, even with a relatively inefficient pump. Thus this kind of steam engine is much less sensitive to irreversible losses than the conventional-uniflow, Rankine-cycle, or Stirling-cycle engines.

Basically the high ratio of expansion to compression work enables the Rankine engine to operate at higher practical efficiencies at lower temperatures than gas engines (Stirling, Brayton, or Ericsson). Also, lower operating temperatures minimize both conduction and radiation heat losses.

The use of a spring rather than a flywheel to return the piston was considered. However, an analysis of dynamics indicated that it was difficult to make the components both small enough and versatile enough to accommodate responses to changes in power level.

Multiple-cylinder arrangements were considered, but their advantages over the single-cylinder arrangement did not appear to be significant enough to justify the additional complexity.

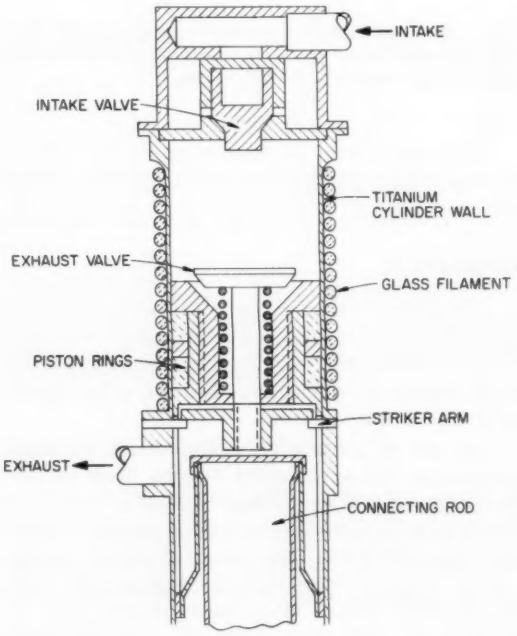


**Fig. 6 Steam-cylinder assembly.**

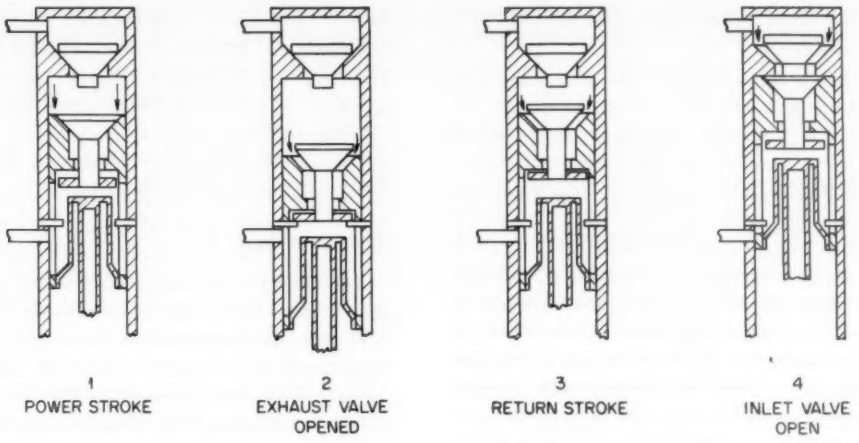


**Fig. 7 Valve position sequence and indicator diagram for TEC steam engine.**

A single-cylinder configuration with flywheel is used in the proposed design. Both the cylinder bore and the piston stroke are ½ in. The engine speed ranges from a minimum of 600 rpm, while the host is at rest, to a maximum of 1800 rpm, during periods of peak activity. These speeds correspond to output levels of 4 and 12 watts, respectively.

The boiler is a single tube wound around the TES material, a design which has been found satisfactory on small engines. Starting at the boiler, the steam enters the cylinder through the inlet valve, expands against the piston, exits through the exhaust valve in the piston, and is conducted through the exhaust line to the condenser located in the high-pressure system. This valving arrangement minimizes the work in returning the piston to top, dead center. Bearing loads are reduced by rigidly connecting the steam piston to the piston of the hydraulic pump. The flywheel is driven from the hydraulic piston. The bearings are water-lubricated graphite; they need only to be supplied with enough water to cool and wet the loaded surfaces, and this is provided from the low-pressure reservoir.

### Thermal Losses

One of the more difficult problems in scaling down a dynamic power supply is reducing the thermal losses through the structure and insulation. Direct losses from the heat source can be reduced to an acceptably low level by the use of vacuum-foil insulation. In addition, the hot engine must be connected to the main structure, which is close to body temperature, in such a way as to maintain its alignment and accommodate shock and vibration loads while minimizing thermal losses. In this design, titanium alloy is used for these functions and also for the cylinder, piston, and piping. It was chosen because of its high strength-to-weight ratio, low thermal conductivity, compatibility with



XUM

water, machinability, fabricability, and demonstrated reliability in engines.

Thermal-loss studies indicate that the overall efficiency of the engine at 900°F is approximately the same as that of a comparable engine operating at 1250°F. There is a reason for this apparent anomaly: although the higher inlet temperature increases the cycle efficiency by approximately 10%, it also increases thermal losses, and the structural materials needed at these temperatures have higher thermal conductivity than titanium and vitiate the increase in temperature. The higher temperature also introduces more difficult problems with materials, insulation, thermal-energy storage, and fuel containment. Comparable performance and efficiency can be realized more easily with a moderate-temperature system than with a high-temperature system.

The details of the steam cylinder, piston, intake valve, and exhaust valve are shown in Fig. 6. Graphite piston rings seal against the chrome-plated titanium cylinder wall. Side loads are minimized by extracting the bulk of the expansion-stroke work directly into the piston of the hydraulic pump. Glass filament is wound around the steam cylinder for reinforcement; this technique has been successfully applied to naval guns, steam boilers, and rocket cases. The filament is wound in such a way that the sides of individual loops do not contact. Because of the filament's low thermal conductivity and restricted contact area, the added conduction losses are negligible.

### Water Inventory

A common water inventory serves four functions in the system: (1) as the Rankine-cycle working fluid, (2) as the energy-transfer medium coupling the power source and blood pump, (3) as the agent for heat transfer from the condenser to the blood pump, and (4) as the lubricant for bearing surfaces. The entire power source–blood pump system is hermetically sealed so that no makeup water is required. Internal leakages from bearings and pistons are returned to the system via the sump pump. The condenser can be made to function in any orientation (lying, standing, etc.) by providing a tapered inlet to a small-bore condenser; this design has been used in space power systems to solve the analogous condenser-flow problem in zero gravity.

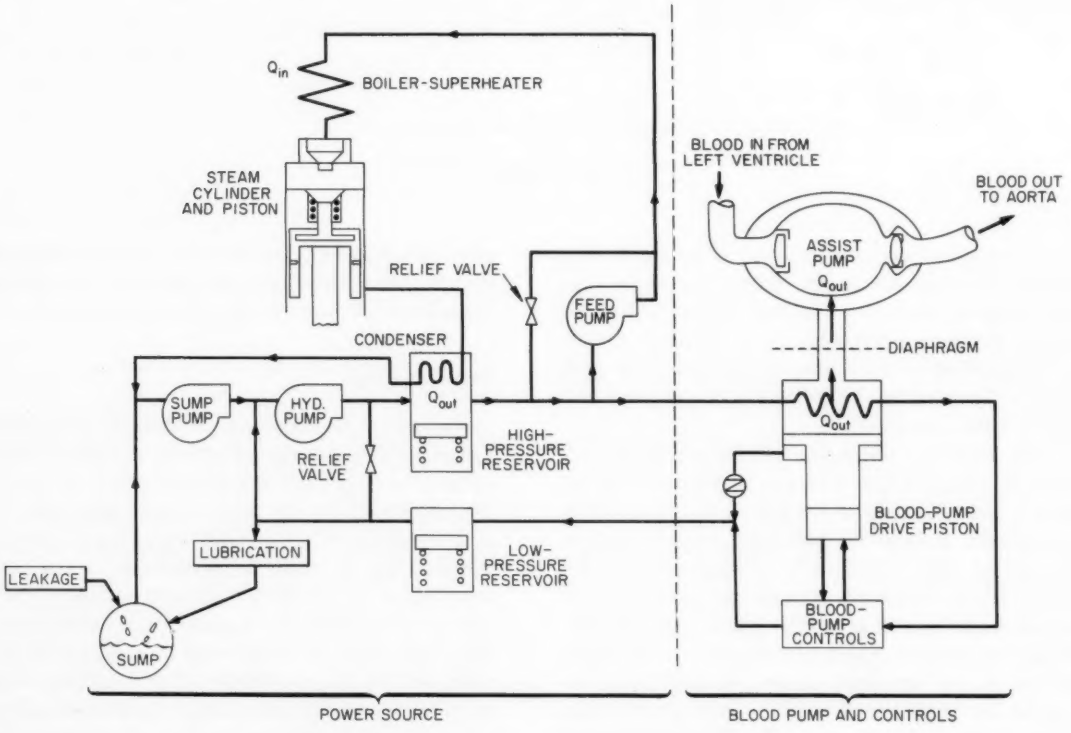


Fig. 8 Fluid-flow diagram for circulatory-support system.

### Engine Control

Primary control of the system is obtained by making the steam engine load-responsive but not responsive to dissipative controls. The engine speed is controlled by pressure variations in the high-pressure reservoir. Since the energy per expansion stroke is fixed, the engine must respond to fluctuations in power demand by changing its speed. Increased power demand by the blood pump drops the hydraulic reservoir pressure, which decreases the energy per stroke into the hydraulic pump. The difference between the energy of the expansion stroke and that absorbed by the hydraulic pump goes into speeding up the flywheel. Conversely, decreased power demand by the blood pump raises the hydraulic reservoir pressure and slows down the engine. A number of parameters are available for tailoring the response characteristics of the system. These include the flywheel inertia, the hydraulic-accumulator pressure differential, and the accumulator volume.

### Hydraulic Subsystem

The hydraulic pump and reservoir are designed as a part of the power source so that they can be coupled to either an assist pump or a total replacement pump.

The hydraulic subsystem is made up of the following major components: hydraulic pump, hydraulic accumulator (or high-pressure reservoir), low-pressure reservoir, hydraulic lines coupling the power source to the blood-pump controls, and sump pump.

A fluid-flow diagram of the proposed system is shown in Fig. 8. A section of the engine showing the sump and feedwater pumps is shown in Fig. 9. The

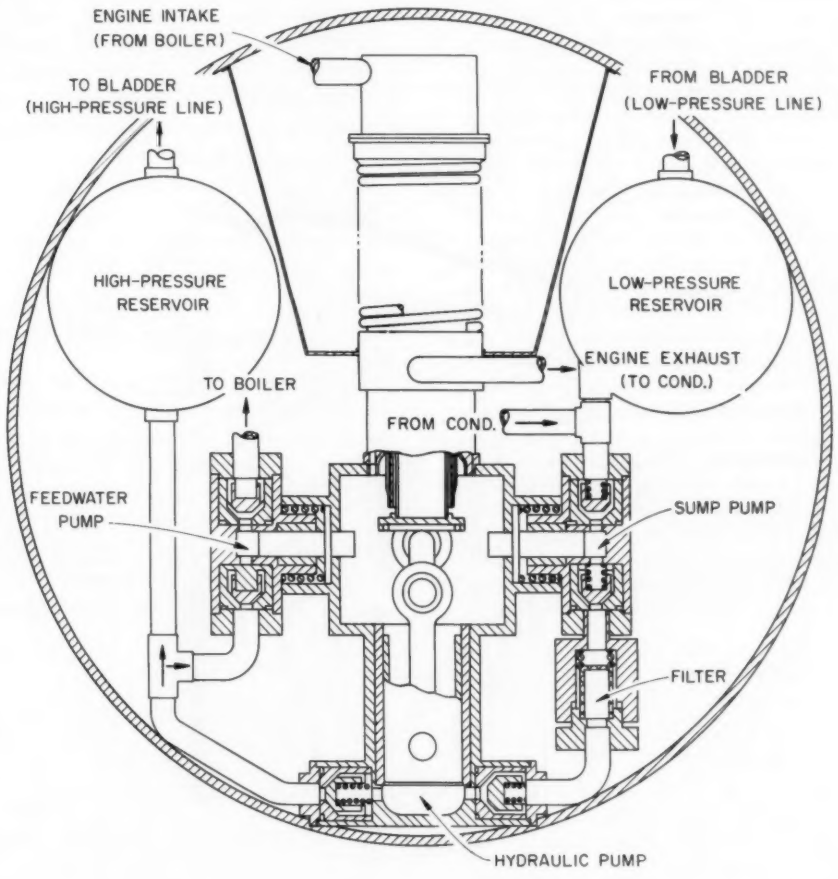


Fig. 9 Section of engine showing sump and feedwater pumps.



XUM

**Table 1 Specifications for Reference Implantable Power Source**

| | |
|---|---|
| Size | 4 in. in diameter by 4.5 in. long |
| Weight | 4.5 lb |
| Fuel | $^{238}Pu$ |
| Thermodynamic converter | Rankine cycle |
| Working fluid | Water |
| Boiler temperature | 900°F |
| Efficiencies | |
| Ideal Rankine | 32% |
| Practical Rankine | 24% |
| Shaft (thermal to engine shaft) | 20% |
| Thermal-energy storage | LiCl–LiF eutectic mixture |
| Temperatures | |
| Fuel-capsule surface | 935°F |
| Boiler | 850°F |
| Condenser | 140°F |
| Pressure levels | |
| Inlet | 400 psia |
| High-pressure reservoir | 80 psia |
| Low-pressure reservoir | 15 psia |
| Condenser | 2.9 psia |
| Power levels | |
| Isotope | 20 watts |
| Pump, resting | 4 watts |
| Pump, peak | 12 watts |

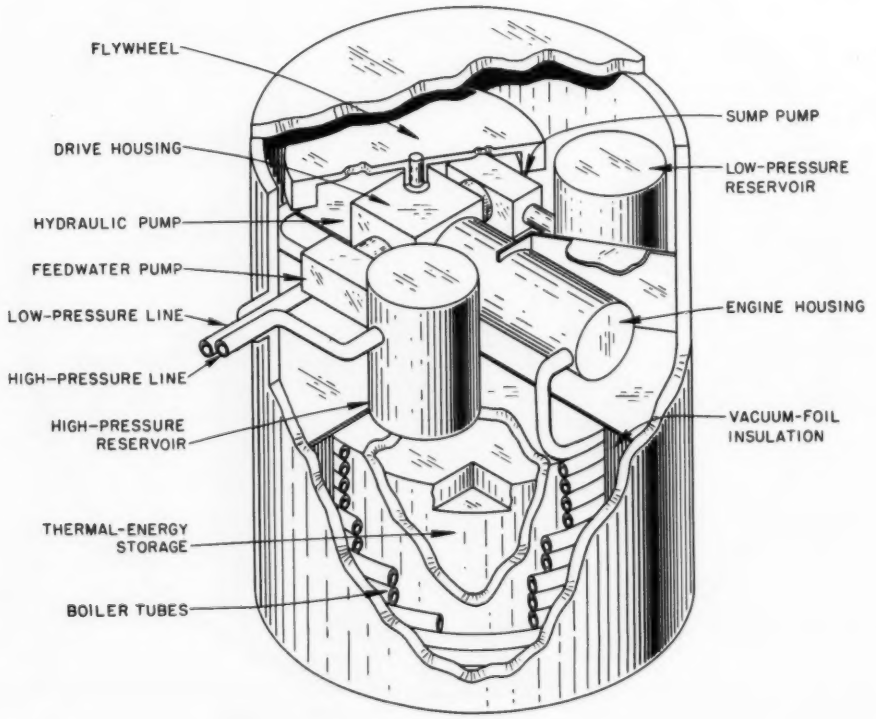


**Fig. 10 Implantable, Rankine-cycle radioisotope power source for circulatory-support devices.**

hydraulic pump is located at the bottom of the engine housing. The feedwater and sump pumps are located on the side of the housing and are driven by an eccentric off the flywheel drive. The high-pressure reservoir is located in the engine compartment above the heat source.

The high-pressure accumulator operates at a mean pressure of about 80 psia. This pressure represents a compromise among the following factors:

1. The size of the hydraulic lines coupling the power source with the blood pump.
2. The temperature rise of the hydraulic fluid in dumping the reject heat.
3. The size and weight of the system pressurizer.
4. The pressure-reservoir leakage.

The low-pressure reservoir operates at 15 psia. The condenser pressure at 140°F is 2.9 psia. The sump pump scavenges all leakage from pistons and bearings and pumps this water, along with the engine flow, up to the low-pressure reservoir. The hydraulic pump raises the fluid pressure from that in the low-pressure reservoir to that in the high-pressure reservoir, which supplies the blood pumps. This constitutes the primary flow in the system. The flow through the sump and feedwater pumps is very much less than that through the hydraulic pump (about 1 to 5000). The feedwater pump operates between the high-pressure reservoir and the boiler.

## Reference Power-Source Specifications

Specifications for the reference power source are given in Table 1. The average output power available at the hydraulic reservoir is 4 watts. A maximum of 12 watts can be obtained. The maximum dose rate on the surface of the power source at the beginning of life is 50 mrems/hr. A three-dimensional view of the implantable power source is shown in Fig. 10. Reference to Figs. 2 and 9 may be helpful in visualizing the component arrangement shown in Fig. 10.

## Conclusions

A power source with specifications tabulated in Table 1 is suitable for an implantable circulatory-support device. The heat-source design is quite similar to that demonstrated with the TES prototype. A large number of small engines have been operated with a 900°F steam inlet temperature, including a test run of over 2000 hr. The calculated thermal-to-shaft efficiency of 20% represents a modest improvement over measured efficiencies (17.6%) already achieved in engines of only twice the bore of the reference design. Therefore the design of the implantable Rankine-cycle radioisotope power source discussed here represents an attractive solution for driving a circulatory-assist device. (REG)

## References

1. R. J. Harvey, Nuclear Powered Mechanical Heart, U. S. Patent No. 3,379,191, Apr. 23, 1968 (filed Apr. 2, 1964).
2. R. J. Harvey, T. C. Robinson, E. J. Doyle, W. F. Bernhard, J. C. Norman, and C. G. La Farge, Evaluation of the Rankine Steam Cycle as a Power Source for an Implantable Artificial Heart, pp. 259-269, in *Progress in Biomedical Engineering*, L. J. Fogel and F. W. George (Eds.), Spartan Books, Washington, D. C., 1967 (*Biol. Abstr.*, 49: 125893).
3. T. C. Robinson, R. J. Harvey, L. van Someren, C. G. La Farge, W. F. Bernhard, and J. C. Norman, Determination of Blood Pumping Power Requirements for an Artificial Heart, pp. 243-257, in *Progress in Biomedical Engineering*, L. J. Fogel and F. W. George (Eds.), Spartan Books, Washington, D. C., 1967 (*Biol. Abstr.*, 49:, 125913).
4. J. C. Norman, C. G. LaFarge, R. J. Harvey, T. C. Robinson, L. O. van Someren, and W. F. Bernhard, Heat Dissipation: A Common Denominator of Implantable Power Sources for Cardiac Prostheses, *Surg. Forum*, 17: 162-164 (1966).
5. W. F. Bernhard, R. J. Harvey, G. LaFarge, J. C. Norman, T. Robinson, and L. van Someren, An Investigation of Induced Chronic Hyperthermia and In Vivo Heat Dissipation, *J. Thorac. Cardiovasc. Surg.*, 52: 611-617 (1966).
6. R. J. Harvey, M. A. Bankole, T. C. Robinson, and W. F. Bernhard, Studies Related to Development of an Implantable Power Source for Circulatory Assist Devices, *Amer. J. Surg.*, 114(1): 61-68 (July 1967).



XUM

# An Implantable Artificial-Heart Power Source*

By J. R. Lance† and A. Selz‡

**Abstract:** *The conceptual design of an implantable radioisotope power source for artificial-heart applications is described. The energy converter used is a novel rotary expansion steam engine, which converts the decay heat of $^{238}Pu$ to hydraulic power. A complete artificial-heart system would use the regulated hydraulic output to drive a biventricular blood pump. The power-source design meets currently defined physiologic constraints and requirements imposed by implantation within the human body. Six watts of peak blood pumping power is provided by the power source and is sufficient to extensively rehabilitate the average user. Total implantation of the power source frees the user from dependence on external power supplies and eliminates the problems associated with percutaneous leads. The design study indicates that only a modest extension of proved technology, without the necessity of engineering breakthroughs, is required to fully develop the described implantable power source.*

This paper describes the conceptual design of an implantable power source for artificial-heart applications. The power source consists of four major components: (1) a radioisotope heat source, (2) a Rankine-cycle rotary expansion steam engine which converts the decay heat of the isotope to shaft power, (3) a pump which converts the rotating shaft power to hydraulic power, and (4) a heat exchanger which rejects unused heat to the bloodstream. A complete artificial-heart system would use the pump hydraulic power, controlled in a suitable manner, to drive the left and right ventricles of an artificial blood pump.

Implantation within the human body imposes severe constraints and requirements on the power-source design. These include volume, weight, radiation-dose and heat-rejection limitations, long operating life with high reliability, and matching of power-source performance to the load line of the human vascular system. The design and performance characteristics of the power source that meet currently defined requirements and constraints are described.[1] The results of the study indicate that the weight and volume limits imposed by requirement for implantation within the human body can be met by using the rotary steam engine as the basic energy converter. With purified $^{238}Pu$ used as the radioisotope, a safe general public radiation level is achieved, and the user dose rate is within medical experience. Development of the power-source concept for actual human implant testing requires further development and testing of a miniaturized engine, solution of blood interface problems associated with the blood heat exchanger and blood pump, and the integration of the power source with a suitable blood pump and control system.

## Power-Source Concept

Figure 1 illustrates the installation of the implanted power source. The power source, placed in the abdominal cavity, drives the artificial blood pump located in the thoracic cavity. Water is used as the power transmission fluid in the tubing connecting the power source to the blood pump. The water also serves as a heat-transport medium to transfer the power-source rejected heat to the blood heat exchanger located in the abdominal aorta.

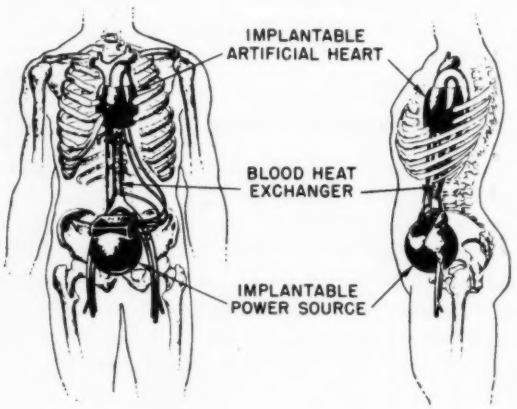


**Fig. 1 Installation of implantable power source for circulatory-support system.**

A suitable energy converter for converting the radioisotope decay heat must be selected within the given constraints and requirements. The desirable characteristics of the energy converter include:

1. *High Efficiency.* Radioisotope quantity required for a given blood hydraulic power level must be as low

*This study was funded by the Division of Isotopes Development, U. S. Atomic Energy Commission and the National Heart Institute.

†KPA Nuclear, Inc., Large, Pa. 15025.

‡Westinghouse Nuclear Energy Systems, Advanced Reactors Division, Pittsburgh, Pa. 15236.

as feasible. Minimizing the isotope quantity will minimize the radiation shielding required and, without increasing the total size of the unit, increase the volume available for thermal insulation. Not only must the energy converter have high efficiency, but also the output must be in a form that can be readily converted, again with high efficiency, to pulsatile blood hydraulic power.

2. *Low Temperature.* Extraneous heat-source losses will be proportional to the peak temperature for a given thermal-insulation material because of the volume limitation. For this reason, and to achieve the highest degree of reliability, the energy converter should operate at a peak cycle temperature as low as possible consistent with the requirement for high efficiency.

3. *Miniaturization.* The energy-converter concept must be capable of miniaturization to the power level and volume requirements of the implanted system while maintaining high efficiency.

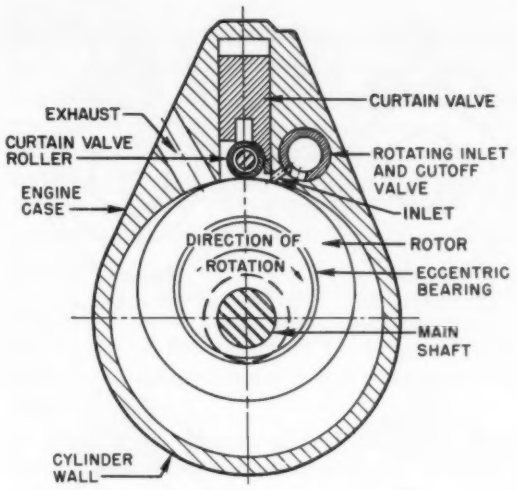


**Fig. 2 Engine configuration.**

## Rotary Expansion Engine

Consideration of the desired characteristics led to the selection of a rotary expansion engine, conceived by C. A. Meyer* for the implantable power-source application. Figure 2 is a schematic view of the engine, and the principle of operation is illustrated in Fig. 3. Fundamentally, the engine has a shallow cylinder with a shaft supporting a crank. A bearing surface on the eccentric allows a roller to roll on the cylindrical surface. A curtain valve equipped with a roller and roller seal rides on the surface of the main roller. The curtain valve oscillates about its hinge, and steam is admitted through the port and steam passages to the pressure side of the curtain valve. As the curtain valve follows the roller, it pulls the steam cutoff curtain, closing the inlet port and allowing the steam to expand. As the roller passes the exhaust port, the expanded steam at low pressure is exhausted. The action is that of a uniflow engine. Because of the disposition of the high-pressure inlet and exhaust port, the direction of rotation is fixed for any given configuration. In the actual engine, four cylinders spaced 90° apart are provided to assure continuous power output without large torque impulses.

The problem of destructive action of trapped vapor is eliminated because of the continuous unidirectional motion, the elastic response of the curtain valve, and the continuously open exhaust. For these reasons, the use of "wet" vapor in the system is permissible. The use of wet vapor, of less than 100% inlet quality, eliminates many of the disadvantages associated with reciprocating steam engines. For one, the expansion of vapor in the wet region represents an additional energy-recovery bonus in the form of latent heat as well as that due to sensible heat. Also, in the rotary engine, the heat rejection is in the final wet stage, and no part of the steam is recompressed and reevaporated due to work exerted on the vapor. The wet steam also seals the sidewalls of the cylinders and thus prevents pressure leakage.

Since there is no necessity of superheating the steam, temperature levels will remain low enough to permit the use of dry lubricants such as Teflon for the rubbing parts and bearings. The liquid condensate will provide additional lubrication and reduce friction losses. It should also be noted that each revolution of the piston is a power stroke which extends for almost 360°; hence a very high output for a given piston displacement is achieved. Mechanically, the steam engine is of low inertia, not requiring significant balance elements, because the only reciprocating parts are the light curtain valves which separate the high- and low-pressure sides of the cylinders. The extremely low inertia will also be advantageous from the overall system standpoint.

Considering the engine friction losses, one should note that the velocities are extremely low. The maximum velocity occurs at the surface of the eccentric bearing and is less than 1 ft/sec at an engine speed

*Westinghouse Astronuclear Laboratory.



XUM

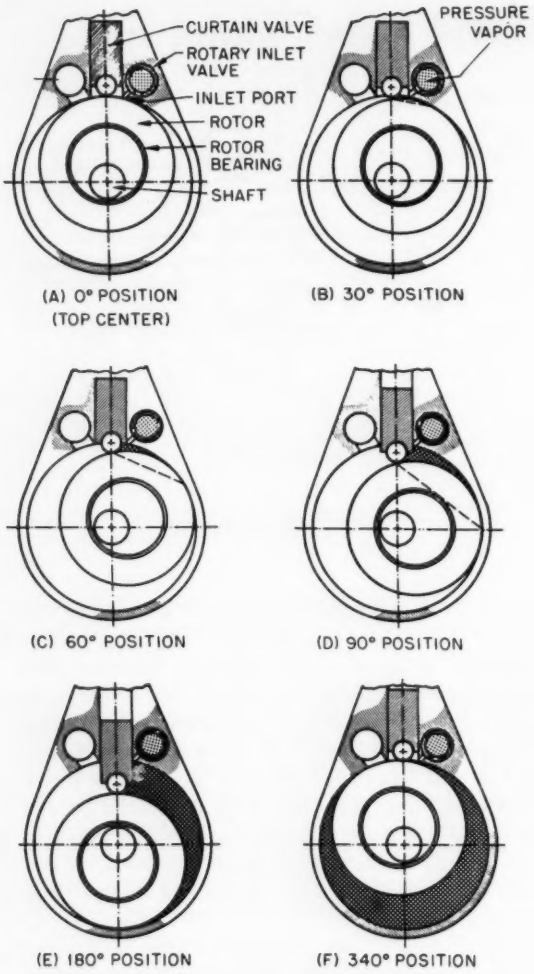


Fig. 3 Principles of rotary-engine operation.

of 363 rpm. At this speed the maximum piston speed is less than 0.4 ft/sec relative to the cylinder walls. The significant friction losses, indicated in Table 1, amount to 12.5% of the gross engine shaft output. The thermal-loss paths of the engine are illustrated in Fig. 4 and are tabulated in Table 2. The heat losses shown are for the initial design, and these losses probably can be reduced by a refined design and careful selection of materials with low thermal conductivities. The typical cycle operating diagram is shown in Fig. 5. Notice that, while the condensing temperature is 150°F (65°C), the condensate is pumped to a common water supply at 104°F (40°C), slightly below the 104.9°F (40.5°C) upper limit tolerable for blood and tissue. The com-

**Table 1 Engine Friction Losses**

| | Losses, % |
|---|---|
| Main journal bearings | 5.2 |
| Curtain valve bearings | 5.9 |
| Valve bearings | 0.5 |
| Valve operating mechanism | 0.9 |
| Rotor windage | Negligible |
| Side seals | Negligible |
| Curtain seals | Negligible |
| Rotor–cylinder wall friction | Negligible |
| Total | 12.5 |

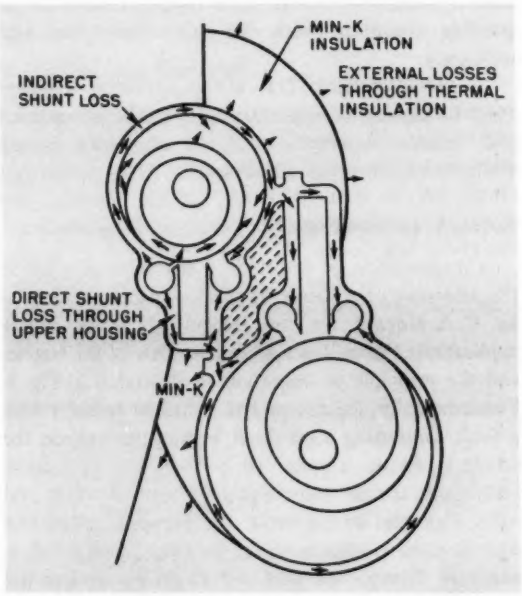


Fig. 4 Schematic diagram showing heat losses and heat-conduction paths.

**Table 2 Summary of Engine Thermal Losses**

| Source of losses | Losses, % |
|---|---|
| Direct shunt | |
| Upper housing | 0.7 |
| End plates | 0.4 |
| External | |
| Through external surface | 1.4 |
| Engine to pump | 0.2 |
| Indirect shunt | |
| Through steam casing | 1.9 |
| Total | 4.6 |
| Heat gain by steam | 0.9 |
| Net loss | 3.7 |

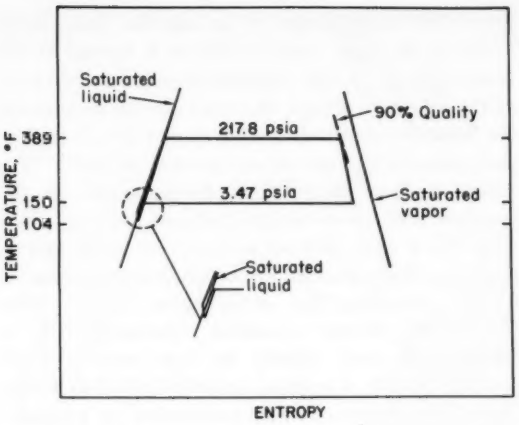


**Fig. 5 Nominal thermodynamic cycle (7-watt engine shaft output; end of use).**

bined effects of friction losses, thermal losses, and the power required for feed and scavenge pumps on engine efficiency are shown in Fig. 6.

### Philosophy of Design

Several factors influenced the design philosophy used. For one, the blood hydraulic power requirements vary considerably with exercise level from 1.7 watts during sleeping to short-duration peaks of 6.2 watts for stair climbing. This variable power demand indicates that some form of thermal-energy storage should be considered in the power-source design. Thermal storage can be achieved by using the heat of fusion of lithium hydride or a lithium fluoride/lithium chloride eutectic mixture. Unfortunately the melting points of these two materials are 1257°F (680°C) and 935°F (502°C). Therefore the use of lithium hydride or lithium fluoride/lithium chloride mixture requires a considerable increase in the peak heat-source temperature relative to the peak steam-engine cycle temperature of 500°F (260°C). For this reason, the design effort was directed into two phases: a standard design and an advanced design.

The standard design is a "no frills," low-temperature system without thermal storage that provides a steam-engine shaft power output of 7 watts. Since thermal-energy storage is not used, the maximum heat-source temperature is only slightly higher than the peak steam-cycle temperature, and a thermal-insulation material of known properties, such as Johns Manville Min-K 1999, can be used. With a shaft power output of 7 watts, the standard design provides the user with 3.7 watts of blood pumping power, which is sufficient to conduct the ordinary life functions. The standard design draws as little as possible on speculative technological developments and can be regarded as the base model upon which succeeding, improved power sources can be built through orderly development.

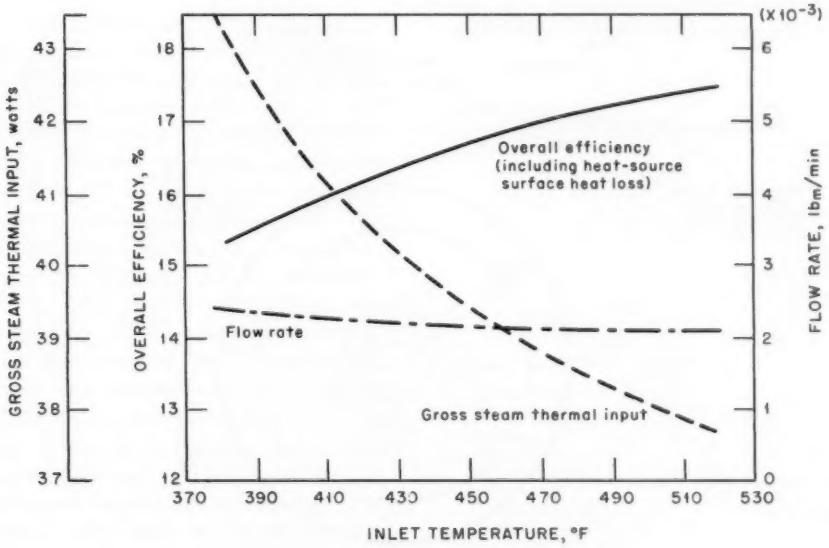


**Fig. 6 Synopsis of standard-engine parametric study (7-watt output).**



XUM

The advanced design can be regarded as the logical step to enhance the usefulness of the power source by providing peaking power capability. The concept is to store the excess thermal power available during sleep or other periods of light physical activity when it is not needed to meet power demands. In the advanced design the excess thermal power is stored as the heat of fusion of lithium hydride. During periods of peak activity, the reservoir of stored thermal power will provide the power-conversion system with amounts of heat substantially in excess of that available from the isotope source.

The advanced design uses lithium hydride for thermal storage; thus the resulting heat-source temperature of 1257°F (680°C) requires the use of a developmental high-performance thermal insulation, e.g., Linde super insulation.

## Conceptual Design of Power-Source Components

A number of alternative component designs for both the standard and advanced power sources were studied. The major components are discussed below.

### Heat Source

The standard- and advanced-design heat sources are illustrated in Figs. 7 and 8. Both are spherical and use the $^{238}Pu$ radioisotope in the metallic form. Since $^{238}Pu$ is an alpha emitter, helium is formed as the isotope decays. A void volume is provided at the center of the sphere to prevent excessive internal pressures as the helium concentration builds up. A porous tantalum shell provides internal support for the metallic $^{238}Pu$, which is then encapsulated by tantalum. In the standard heat-source design, tantalum and a uranium alloy (U–8 wt.% Mo) act as the heavy-metal gamma shielding. This is encased in a copper heat accumulator, which contains the steam-engine boiler tube. Min-K 1999 thermal insulation, encapsulated by a stainless-steel shell, reduces the heat losses to about 3 watts. Finally, a borated polyethylene (4 wt.% natural boron) neutron shield encapsulated by a silastic-covered stainless-steel shell completes the standard-design heat source.

In the advanced-design heat source (Fig. 8), lithium hydride serves as the thermal storage material and a gamma-radiation shield. This design requires Min-K 1999 thermal insulation between the LiH and the copper heat accumulator to maintain the LiH near its melting temperature of 1257°F (680°C) while passing 20 to 30 watts to the boiler operating between 250°F (121°C) and 500°F (260°C). Because the volume available for insulating is reduced, Linde super insulation is required around the copper accumulator to limit the loss to 3 watts. Borated polyethylene is

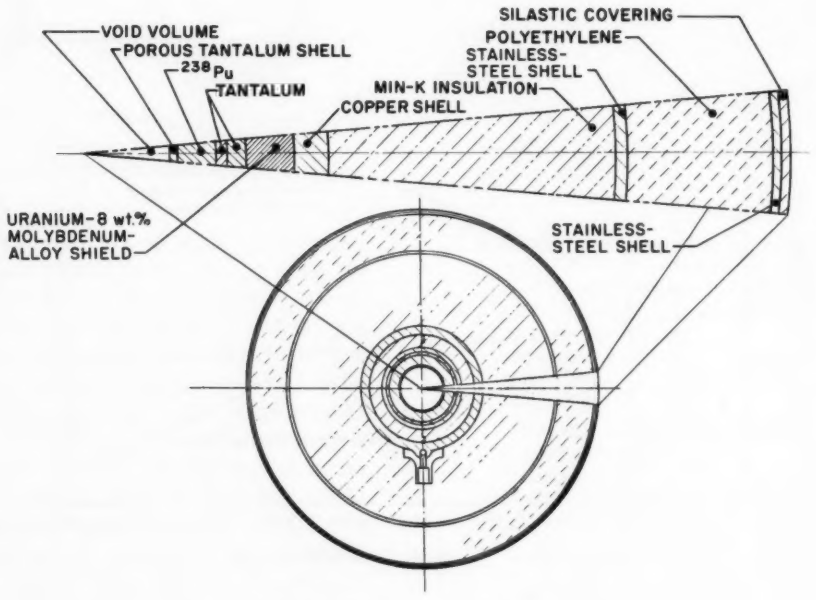


Fig. 7 Standard heat-source design.

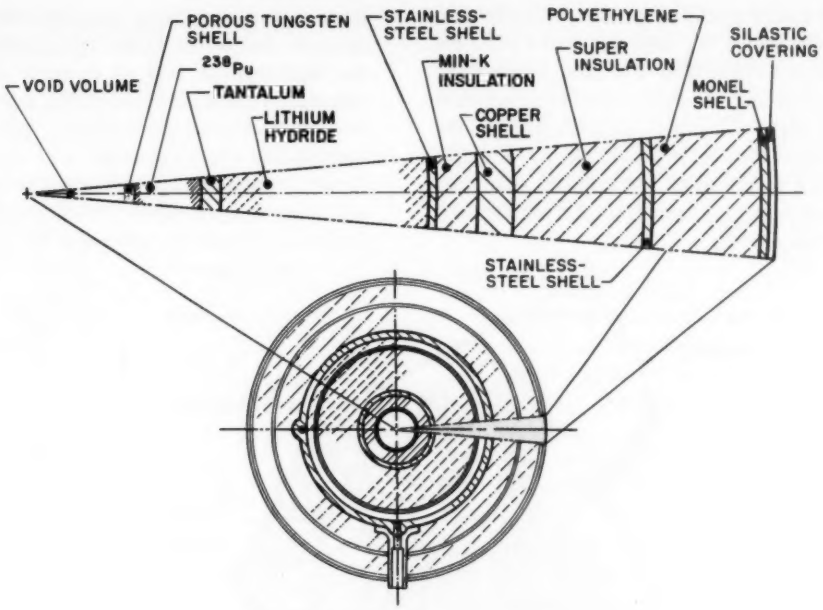


Fig. 8 Advanced heat-source design.

again used for neutron shielding, and the device is encapsulated with Monel and then with silastic to ensure compatibility with human tissue.

The study included analyses of the neutron and gamma-ray dose rates from the metallic $^{238}$Pu fuel.[2] The principal radioisotope impurity in $^{238}$Pu is $^{236}$Pu. The decay of this radioisotope, which results in a buildup of the gamma-emitting daughters, $^{208}$Tl and $^{212}$Bi, strongly influences the external dose rate. In addition to the $^{236}$Pu impurity, which can be controlled by proper $^{238}$Pu fuel preparation, the occurrence of low-atomic-number impurities in metallic $^{238}$Pu can give rise to neutron emissions from the alpha-particle interactions [i.e., $(\alpha,n)$ reactions]. The Division of Isotopes Development, AEC, has undertaken a fuel-purification program, and the production of metallic $^{238}$Pu with a neutron-emission rate approximately equivalent to the spontaneous-fission-emission rate has been achieved. The fuel for power-source application was assumed to be this purified metallic $^{238}$Pu. At a 0.3-ppm impurity level for $^{236}$Pu at the beginning of use, the heat-source surface dose rates are 542 rems/year and 472 rems/year for the standard and advanced designs. The neutron dose rates used in this study were based on Snyder–Neufeld energy-dependent relative biological effectiveness (RBE) conversion factors.

### Rotary Steam Engine and Hydraulic Pump

An assembly drawing of the rotary steam engine and the pump that converts the engine shaft output to hydraulic power is shown in Fig. 9. The positive-displacement hydraulic pump is similar in configuration and operation to the steam engine. However, a ball check valve is used to prevent backflow into the inlet

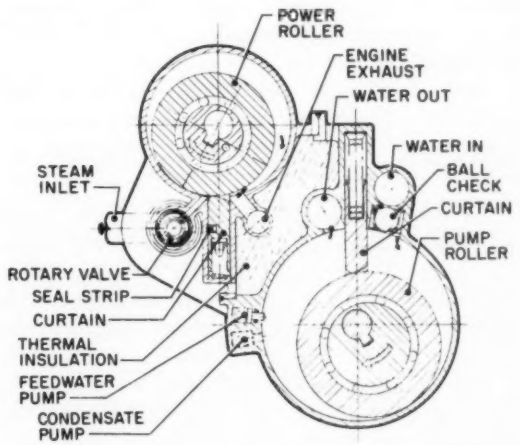


Fig. 9 Rotary steam-engine–pump assembly.



XUM

line when the rotary piston is between the inlet and outlet ports. Otherwise, the inlet and outlet ports are open at all times, eliminating the need for an inlet cutoff valve. There are four pump cylinders, 1.65 in. in diameter, and their rotors are staggered by 90° and driven at 1.5 times the engine speed to deliver water to the blood pump to compress the artificial ventricles. Figure 10 shows how the engine–pump combination is mated to the heat source.

strate a low-compliance ventricle-filling action analogous to that of the natural heart ventricles. Therefore the diaphragm- or sac-type ventricle blood pump was selected for the system model, although it is recognized that more detailed power-source studies and further analyses and experimentation with blood pumps may dictate another configuration for the blood pump at a later date. A hydraulic (water) rather than a pneumatic fluid was selected to compress the ventricles of the

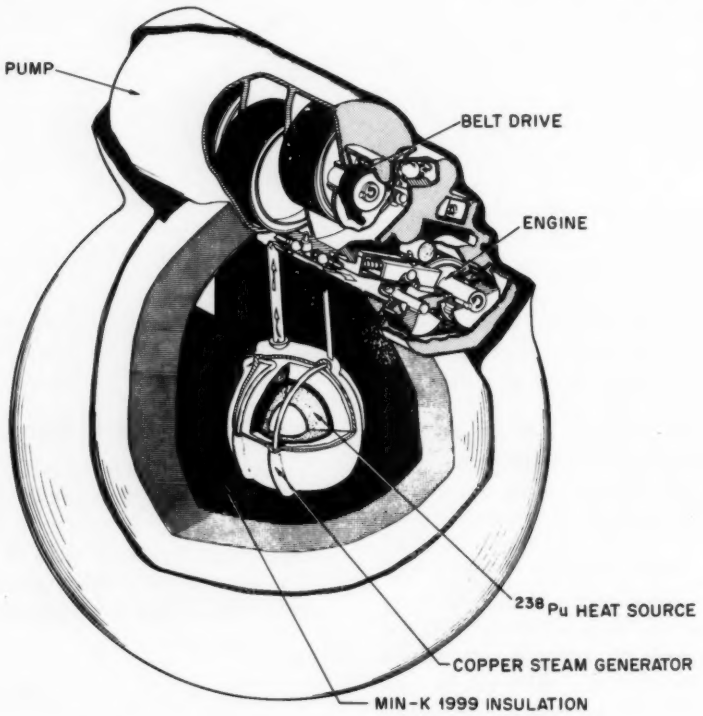


Fig. 10 Implantable power source.

### Hydraulic Power Transmission and Blood Pump

A detailed design study of the hydraulic power transmission and blood-pump components was beyond the scope of this study. However, models of these components were defined to permit an estimate of the total system performance and to relate engine output to blood hydraulic power and flow-rate requirements. A hydraulically actuated blood pump was selected for the system model for the following reasons. The diaphragm-type blood pumps utilizing silastic or polyurethane sacs for ventricles generally have the desirable characteristics of high pumping efficiency and demon-

blood pump to avoid the possibility of gas diffusion through the sac wall and into the bloodstream. The combination of a positive-displacement hydraulic pump and the incompressibility of water facilitates the monitoring of the ventricle blood volume, thereby simplifying the control system.

A schematic diagram of the hydraulic transmission and blood-pumping subsystem is shown in Fig. 11. The hydraulic transmission subsystem also provides the heat-rejection function. Liquid from the steam-engine condenser at 150°F (65°C) is pumped into the rotary-pump inlet line. The condensate temperature immediately drops to the hydraulic fluid temperature

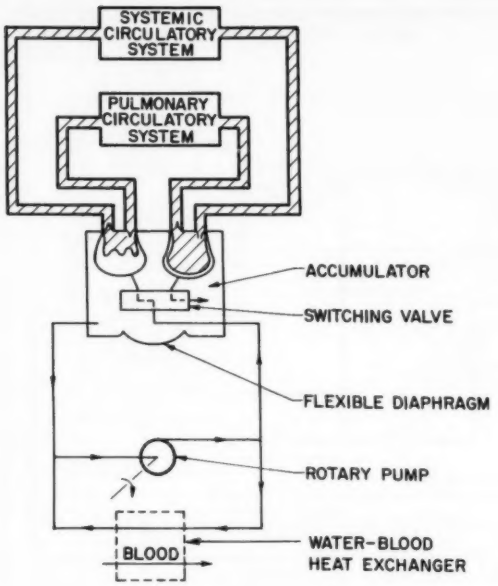


**Fig. 11 Direct hydraulic subsystem.**

of 104°F (40°C) because the flow rate in the hydraulic line is much larger than that of the condenser. Feedwater for the steam-engine boiler, also at 104°F (40°C), is extracted from the outlet side of the rotary pump. Three percent of the rotary-pump output is bypassed to the water-to-blood heat exchangers located in the abdominal aorta. While the steam-engine condensing temperature will vary over the engine power output range, the use of the main hydraulic system water as a buffer fluid prevents the blood interface temperature from exceeding 104.9°F (40.5°C). In addition, the relatively large volume of water in the hydraulic system serves as a reservoir, and the relatively small amount of water contained in the steam-engine loop will not be depleted over a period of time if a small amount of seal leakage occurs.

The rotary pump is located in the abdomen, and the hydraulic transmission tubes lead to the thoracic cavity where the blood pump is located. The blood pump is similar to a previously reported device.[3] A switching valve is used to provide sequential pumping of the left and right ventricles. Because the accumulator contains a flexible diaphragm, its volume is a function of the ventricle volume and the engine–pump speed. The control system monitors both the ventricle pressure and the accumulator volume. The ventricle pressure signal is then used to control the sequence of the switching valve. The control system, by monitoring and integrating the accumulator volume, compensates for unequal stroke discrepancies between left and right ventricles. The net result of the blood-pump control system is to regulate the cardiac output to the venous pressure. Therefore both the beat rate and stroke volume of the blood pump will vary in accordance with vascular-system demand.

### Complete System

Figure 12 is a schematic diagram of the complete power-source and blood-pumping system. The isotope heat source and power-conversion loop are located in the abdominal cavity, the blood pump in the thoracic cavity, and the water-to-blood heat exchangers in the abdominal aorta. Both the blood pump and the steam engine must be regulated in unison to meet biologic demands and follow the load line of the vascular system. Two separate control systems can be postulated. It is assumed that the primary control system controls the sequencing of the blood-pump switching valve to the venous return pressure. Then the steam engine must be regulated by a secondary control system which provides sufficient blood-pumping power at a given exercise level and which follows the blood-pump power demand as the user's exercise level changes. Now, for the artificial blood pump–power source system, consider a steady-state condition with a constant user-exercise level. The steam-engine power output is also constant at the appropriate steady-state value. If an increase in exercise level occurs, the blood-pump primary control system will increase the ventricle stroke volume and/or beat rate to supply the additional cardiac output demanded by the vascular system. However, the steam-engine output has not yet changed and is still at the power level required by the previous lower exercise level. But, the reduction in peripheral resistance of the vascular system brought on by the higher exercise level will also cause a related drop in the hydraulic transmission loop resistance seen by the rotary pump. A drop in the resistance seen by the rotary pump will result in an increase in engine–pump speed and a corresponding increase in rotary-pump flow rate. If a venturi is located in the output side of the rotary pump, the drop in venturi pressure caused by the increased flow rate can then be used to open the steam-engine throttle valve, increasing the engine power output until a new stable operating point at the higher exercise level is reached. The control system will react in a similar manner when a reduction in exercise level occurs, slaving the engine power



XUM

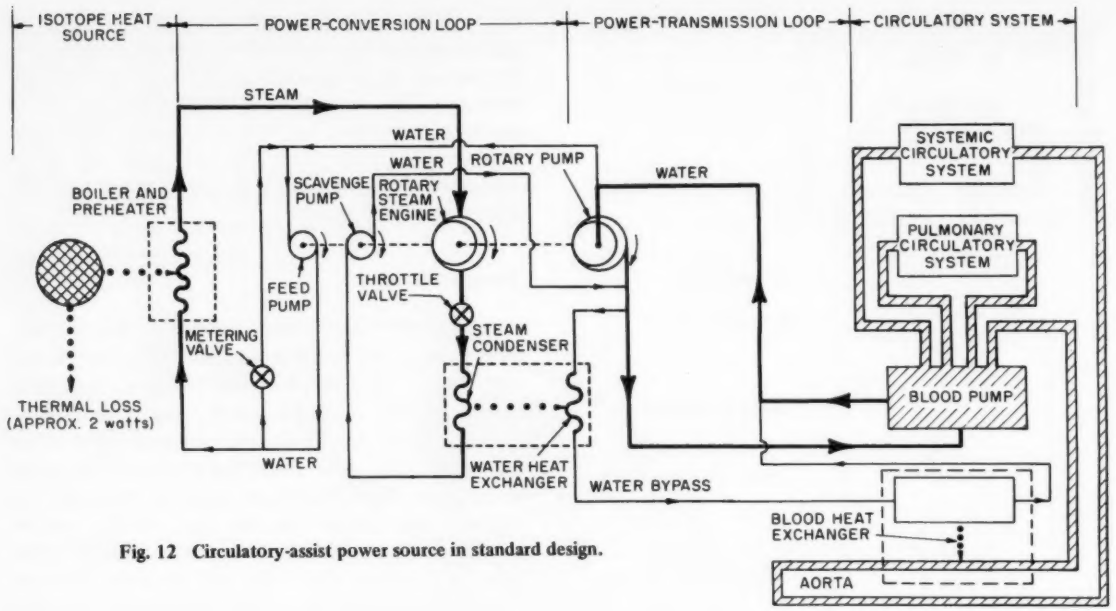


**Fig. 12 Circulatory-assist power source in standard design.**

output to the load line of the vascular system. This control concept is purely conceptual as yet, and a dynamic analog model of the entire system must be developed to completely determine the nature of the control system required. The low rotating mass of the rotary engine–pump combination indicates that the rotational speed of the engine and pump will closely follow the per cycle variations in the left and right ventricle pressures. Therefore the system transient response to rapid changes in cardiac output will not be limited by the engine–pump dynamic characteristics.

### Implantation

Some examination of the human anatomy was necessary to develop a preliminary concept because of the obvious problems in placement and anchoring of the implant in the abdominal cavity. Through the assistance of Dr. S. Bononi, some of the facilities of the Gross Anatomy Laboratory of the University of Pittsburgh School of Medicine were made available to the program. Examination of the skeletal structure revealed that the only region where structural support points appeared to be available was on the upper edge of the iliac fossa. This is the only portion of the superior pelvic structure not thickly covered with essential muscle and ligament tissue. The selected preliminary support configuration utilizes two relatively thin tubular members extending from the engine side of the power source to the upper edge of the iliac fossa where they are fastened to the bone. The support members, which are 0.375-in.-diameter Monel tubes encased in silastic sheaths, space the implant away from the spinal column and protect the descending aorta and the major veins from contact with the implant. The supports also space the implant away from the bladder and other soft organs of the genitourinary tract.

### Power-Source Performance and Data Summary

Figure 13 is an overall energy balance for a complete system using a standard-design heat source without thermal storage. At the end of a 5-year use period, the radioisotope thermal power is 45.2 watts. Four watts are lost through the thermal insulation and external engine–pump casting; the rest, 41.1 watts, are delivered to the steam-engine boiler. Then, with the engine operating at the maximum net output of 7 watts, 34 watts are rejected to the bloodstream via the water–blood heat exchangers, and a blood hydraulic power of 3.74 watts is available at the outlet of the blood pump. This pump output is high enough to permit partial rehabilitation of the user including such tasks as walking about, desk work, gardening, welding, and sheet metal work. Extensive rehabilitation would require the use of some form of thermal storage (i.e., the advanced design) to permit short-duration, high-

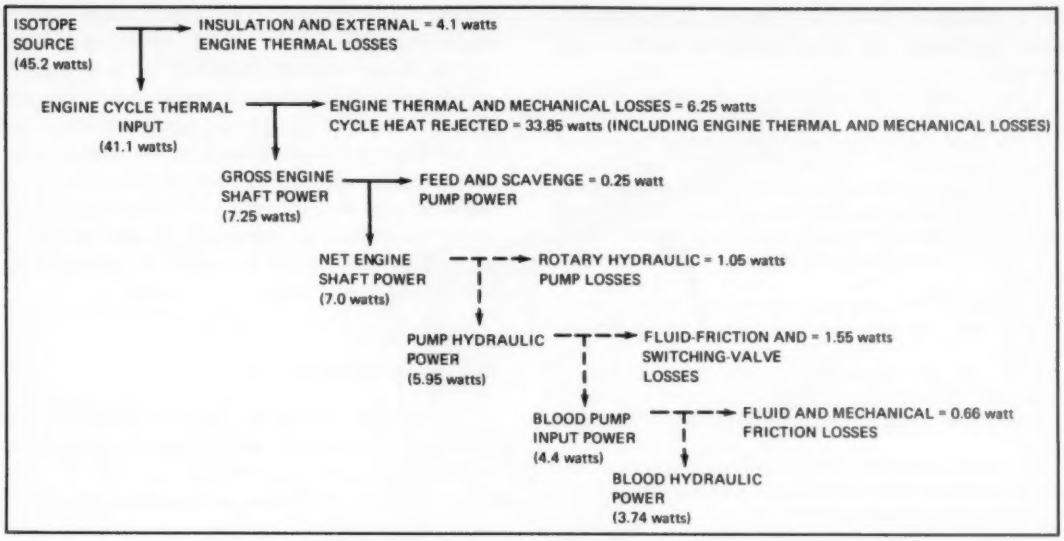
ISOTOPE SOURCE (45.2 watts)
INSULATION AND EXTERNAL = 4.1 watts ENGINE THERMAL LOSSES
ENGINE CYCLE THERMAL INPUT (41.1 watts)
ENGINE THERMAL AND MECHANICAL LOSSES = 6.25 watts
CYCLE HEAT REJECTED = 33.85 watts (INCLUDING ENGINE THERMAL AND MECHANICAL LOSSES)
GROSS ENGINE SHAFT POWER (7.25 watts)
FEED AND SCAVENGE = 0.25 watt PUMP POWER
NET ENGINE SHAFT POWER (7.0 watts)
ROTARY HYDRAULIC = 1.05 watts PUMP LOSSES
PUMP HYDRAULIC POWER (5.95 watts)
FLUID-FRICTION AND = 1.55 watts SWITCHING-VALVE LOSSES
BLOOD PUMP INPUT POWER (4.4 watts)
FLUID AND MECHANICAL = 0.66 watt FRICTION LOSSES
BLOOD HYDRAULIC POWER (3.74 watts)

**Fig. 13 Circulatory-assist power source showing overall system energy balance for standard design having overall system efficiency of 8.3%.**

power-level tasks such as rapid climbing of stairs. Table 3 gives a comparison of the performance of the standard and advanced designs at the end of a 5-year service-life period. When the engine operates at a higher boiler temperature and contains lithium hydride for thermal storage, a peak blood hydraulic power of 6 watts is available while still maintaining the 50-watt heat-rejection limit. Table 4 gives the volume, weight, and radiation dosage characteristics of the standard and advanced power-source designs. For the standard design the volume and weight are below the 2000-$cm^3$ and 3000-g limits for an abdominal implant, and the bystander dose rate is within accepted practice. The advanced design, because of the reduced quantity of isotope required, is much lower in volume, weight, and bystander dose rate.

**Table 3 Standard and Advanced Power-Source Performance, $^{238}$Pu Isotope, 5-Year Service Life**

| | Standard | Advanced |
|---|---|---|
| Maximum power, watts | 7.0 | 13.3 |
| Maximum continuous engine output at end of use, watts | 7.0 | 4.7 |
| Isotope thermal power at beginning of use, watts | 47.0 | 20.4 |
| Boiler temperature, °F | 389.0 | 450.0 |
| Maximum blood heat-exchanger heat rejection, watts | 45.3 | 50.0 |
| Power-source efficiency at end of use, % (engine shaft power ÷ thermal-source power) | 15.5 | 23.9 |
| Blood hydraulic power (maximum) at end of use, watts | 3.7 | 6.0 |
| Overall system efficiency at end of use, % (blood hydraulic power ÷ thermal-source power) | 8.0 | 13.0 |

**Table 4 Standard and Advanced Power-Source Data Summary, $^{238}$Pu Isotope, 5-Year Service Life**

| | Standard | Advanced |
|---|---|---|
| Power-source outside diameter, cm | 13.6 | 12.3 |
| Power-source volume, $cm^3$ | 1716 | 1384 |
| Power-source weight, kg | 2.465 | 1.663 |
| Power-source specific gravity | 1.44 | 1.2 |
| Bystander dose rate, rems/year at 36 cm, 8 hr/day | 5.0 | 3.6 |
| Power-source surface dose rate, rems/year | 542 | 472 |

## Conclusions

The primary conclusion of this conceptual-design study is that the implantable radioisotope power-



XUM

source concept is technically feasible. The attractive design features of the rotary-engine concept are the following:

1. The energy converter is a low-temperature dynamic system of high efficiency.
2. The low temperature minimizes thermal losses and insulation problems.
3. The engine is self-lubricated by the cycle working fluid.
4. Water is used as the cycle working fluid and as a thermal buffer fluid to prevent blood and tissue overtemperature.
5. The low temperature permits flexibility in the choice of materials.
6. Purified $^{238}Pu$ does not exceed a safe general public radiation level, and the user dose rate is within medical experience.
7. The size and weight are acceptable for an abdominal implant, and neutral buoyancy appears attainable.
8. The power source has advanced developmental capability.
9. A modest extension of proven technology, without the necessity of engineering breakthroughs, is all that is required to fully develop the power source.

The major technical problem areas or items requiring further study are:

1. Integration with a suitable blood pump and development of the control system.
2. Ensuring minimal wear and high reliability.
3. Two-phase fluid stability.
4. Control of corrosion, corrosion-product formation and deposition, and materials compatibility.
5. Blood heat-exchanger materials and design standards.
6. Implantation design standards.
7. Radiation-dose-level design standards and public safety.

The proposed development plan for the implantable power source has been divided into four phases: (1) an engineering-information-acquisition and engine-evaluation phase which has already begun, (2) the design and development of a miniaturized engine and power source, (3) integration of the power source with the artificial blood pump and development of the control system, and (4) in vivo animal tests of the complete system. If this development plan is followed and the assumption is made that a suitable blood pump can be developed in the interim, the complete system could be ready for human implant tests within several years.

## Acknowledgments

A study of this nature reflects the work of many individuals. The authors acknowledge the contributions of Project Manager W. D. Pouchot and of P. O. Tauson, R. K. Disney, J. W. H. Chi, L. Van Bibber, S. J. Orban, and J. A. Kyslinger. (RHL)

## References

1. Westinghouse Electric Corp., Astronuclear Laboratory, Study on Implantable Power Source for Circulatory Support Devices, USAEC Report WANL-3857-1, December 1968.
2. R. K. Disney, Radiation Shielding Considerations of an Implanted $^{238}Pu$ Power Source for the Artificial Heart, *Trans. Amer. Nucl. Soc.*, 11: 92-93 (1968).
3. W. H. Burns, R. Loubier, and R. Bergstedt, The Development of an Electrohydraulic Implantable Artificial Heart, Vol. XI, pp. 265-270, *Trans. Amer. Soc. Artif. Intern. Organs*, 1965.

# Radioisotope-Powered Cardiac Pacemaker

There is a high degree of automatism about the beating of the heart. And one important stimulus is the inherent rhythmic contraction characteristic of cardiac tissue. The wave of contraction that spreads over the heart originates in a small area of specialized tissue, the pacemaker, in the wall of the upper-right quadrant. A relatively common cardiac disease, heart block, involves blocking of impulse conduction to the lower quadrants, the ventricles, i.e., there is interruption of the normal stimulus to the heart.

Approximately 10 thousand persons with heart block have been helped by the implantation of battery-powered pacemakers, which stimulate the heart by providing electrical shocks at a nominal rate of about 70 per minute through leads to the left ventricle of the heart. These battery-powered devices require replacement approximately every 2 years. With the objective of reducing the frequency of implantation surgery, consideration has been given to the use of a radioisotope-powered battery.[1] Nuclear Materials & Equipment Corp. (NUMEC), a subsidiary of the Atlantic Richfield Company, Apollo, Pa., is carrying out research under the sponsorship of the AEC Division of Reactor Development and Technology and the National Heart Institute on a radioisotope-powered pacemaker with a minimum life of 10 years.

The approximately 97-g pacemaker will be powered by a small (~0.2 g) $^{238}Pu$ source, which will

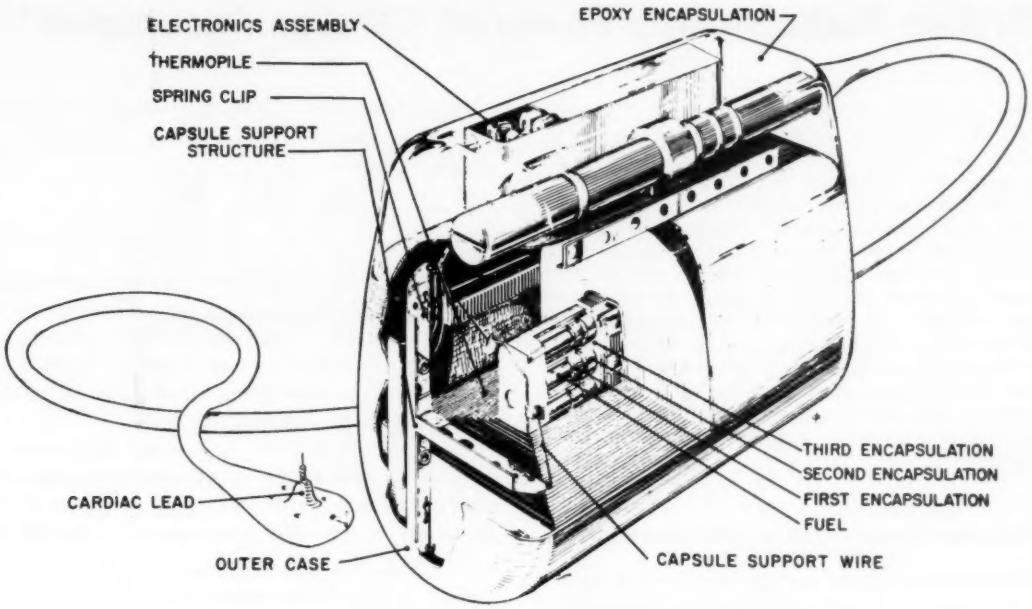


**Fig. 1 Radioisotope-powered cardiac pacemaker.**

supply 160 $\mu$w of electric power by a thermoelectric conversion system.

The primary design objectives for the nuclear battery were established as follows:[2]

| | |
|---|---|
| System size: | ~6 x 5 x 2.8 cm |
| System weight: | 100 g |
| Design life: | 10-year minimum plus 1-year shelf life |
| Reliability: | 0.95 at 0.90 confidence |
| External radiation: | 0.3 mrad/hr at 5 cm and 5 mrads at the surface |
| Sterilization: | Capable of sterilization under hospital conditions |
| Radioisotope thermoelectric generator: | Based on series–parallel wire thermocouples woven into tapes |
| Nuclear battery output: | 160 $\mu$w (end of design life) |
| Fuel: | $^{238}$Pu (0.5 g) |
| Pacemaker electronics: | Cordis Model Ventricor or equivalent |
| Electrode: | Monopolar |
| Shock: | Capable of withstanding a 3-ft drop on a graphite surface with the unit encased in 2-mm Silastic for test purposes. |

A cutaway view of an operational radioisotope-powered cardiac pacemaker is shown in Fig. 1. The nuclear battery and the electronics assembly are self-contained within separate, but integral, hermetically sealed titanium enclosures. A covering of epoxy serves the dual purpose of mechanically locating the cardiac lead termination while producing a rounded outer shape suitable for implantation.

As of February 1969, two complete pacemakers and four complete nuclear batteries had accumulated a total of 24,860 hr without degradation, with the first sealed unit achieving 9184 hr. The electrical output of the early radioisotope-powered cardiac pacemakers is lower than the specification requirement, but these units produce sufficient power to obtain satisfactory cardiac stimulation. The latest complete nuclear battery achieved the power-output requirements and has been operated successfully with a pacemaker electronics package.

In June 1969, one of these units was successfully implanted in a dog at the National Heart Institute, National Institutes of Health, Bethesda, Md. The National Heart Institute's program calls for implantation of the devices in several additional healthy dogs within the next 8 months. (RHL)

## References

1. J. E. Carden, Medical Pacemakers and Controls, *Isotop. Radiat. Technol.*, 4(2): 180 (Winter 1966–1967).
2. Nuclear Materials & Equipment Corp., Radioisotope-Powered Pacemaker, USAEC Report NUMEC-3731-13, Apr. 19, 1968.



XUM

# British Radioisotope-Powered Cardiac Pacemaker*

**Abstract:** *The British demonstration model of a battery powered with a long-lived radioisotope—$^{238}Pu$—has operated since June 7, 1968, with a dc–dc converter to drive a cardiac pacemaker. The battery is being developed at the British Atomic Energy Research Establishment (AERE), Harwell, and the commercially designed pacemaker circuit was constructed at the Atomic Weapons Research Establishment, Aldermaston. Tests are being made with the unit for the Department of Health and Social Security to determine the long-term reliability of implantable radioisotope-powered cardiac pacemakers. Possible improvements in the protection of the electronics by encapsulation are also being investigated, with the idea of eventual implantation, and plans for future development include studies aimed at decreasing the $^{238}Pu$ inventory and ensuring that the lifetime of more than 10 years can be guaranteed.*

## Radioisotope-Powered Battery and Converter

The radioisotope-powered battery (Fig. 1) is a heat engine that converts the spontaneous heat generated by the $^{238}Pu$ to electricity, using a thermopile. It has no moving parts. Heat losses are minimized because the source and thermopile are inside a primary capsule, which is surrounded by thermal insulation and this, in turn, enclosed in an outer capsule.

Thermopiles can, in principle, be built to generate any value up to several volts, but the output in such a small device is limited in practice to less than 1 volt. To obtain a useful voltage—somewhat greater than 4 volts—the battery is matched to a pacemaker circuit (Fig. 2) by a dc–dc converter, which can be designed for use with any circuit. The converter now in use is a three-stage electronic circuit:

1. A multivibrator (with germanium power transistors to decrease the internal voltage loss), which converts the dc to ac.
2. A transformer to increase the ac to a higher voltage.
3. A rectifier and stabilizer of the ac.

Converters of this type can be made more than 60% efficient with 0.25-volt input if care is taken to match them to the battery.

The ultimate lifetime of the $^{238}Pu$ battery is limited by the decay of the isotope, but, with $^{238}Pu$ (half-life 86.4 years), lifetimes of greater than 10 years are feasible. The decrease in output power due to decay of $^{238}Pu$ in a 30-year period is shown in Fig. 3.

The characteristics of the demonstration model and of proposed future units of cardiac pacemakers are shown in Table 1.

## Safety

Plutonium-238 is primarily an alpha emitter, and, with reliable encapsulation, an ultrasafe source can be produced. It will neither emit harmful radiation nor constitute a hazard to the general public. Provided that the containment of the plutonium is maintained intact, no risk is involved in its use.

In the British battery, the primary containment is designed to ensure that it will not burst under any conditions likely to be met either in use or if the pacemaker is lost. The major potential hazards are

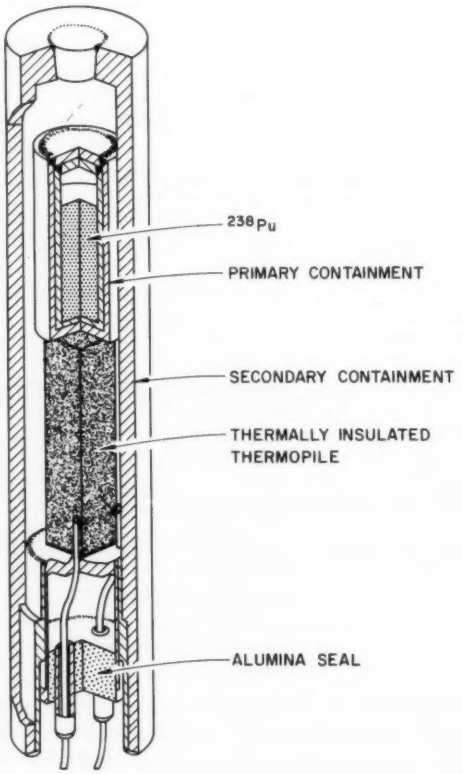


**Fig. 1 Radioisotope-powered battery; size approximately 4.5 by 1.5 cm.**

*Adapted from *Atom*, No. 150, pp. 100-106 (April 1969).

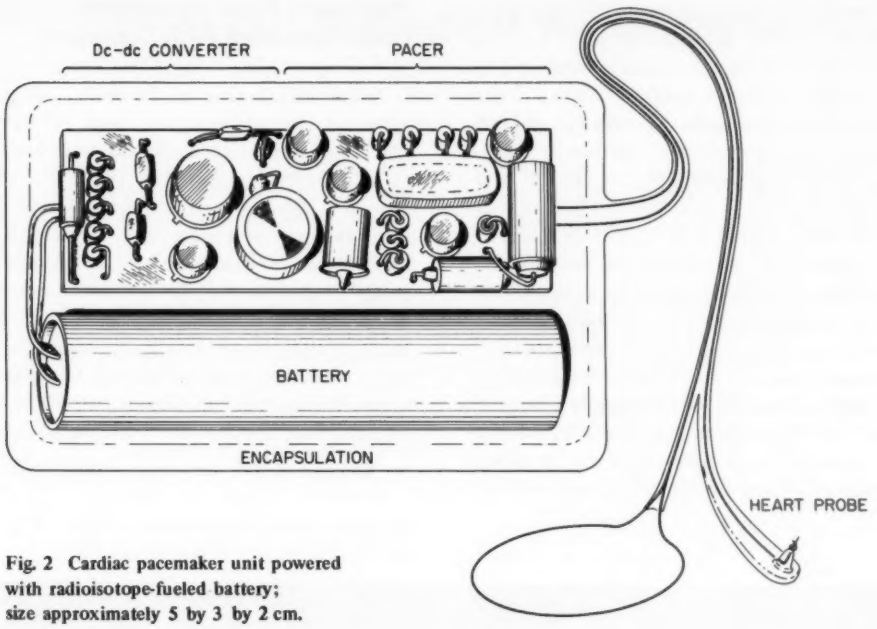


Fig. 2 Cardiac pacemaker unit powered with radioisotope-fueled battery; size approximately 5 by 3 by 2 cm.

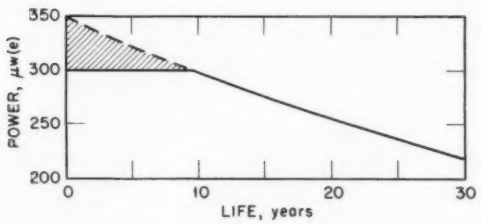


Fig. 3 Electric-power change due to $^{238}Pu$ decay. The hatched-line region shows the excess power required to enable the rated power to be generated for a full 10-year life. Longer lifetimes can be obtained by either adding more fuel or accepting a lower rated power.

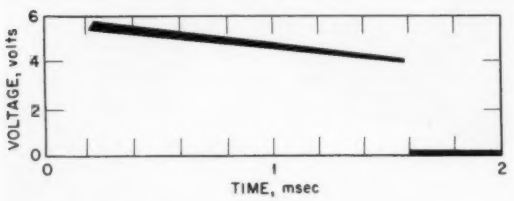


Fig. 4 Output pulse from demonstration pacemaker (load 330 ohms, rate 78 pulses/min).

**Table 1 Characteristics of Demonstration Model and of Proposed Future Units of Cardiac Pacemakers**

| | Demonstration model | Fully developed unit |
|---|---|---|
| Source | | |
| Fuel | $^{238}Pu$ oxide | $^{238}Pu$ metal |
| Can | Inconel, 1-mm-thick wall | Hastelloy, 1.5-mm-thick wall |
| Shield | None | Heavy alloy, <0.5 mm thick |
| Radiation at 2 cm | 5 mr/hr | 1 mr/hr |
| Thermopile, optimum output at 38°C | 0.175 volt, 3.7 ma, 650 μw | 0.5 volt, 0.6 ma, 300 μw |
| Dc–dc converter output | 5.5 volts, 55 ma 302 μw | 4.5 volts,* 45 ma,* 200 μw* |
| Pacer output | | See Fig. 4 |
| Battery weight | 20 g | <140 g |
| Battery life | >0.5 year | >10 years |
| Max. battery temp. | 120°C | 150°C |

*Sample values; can be altered to suit a particular requirement.



XUM

mechanical crushing, internal pressure buildup, and heating to 850°C for 0.5 hr (cremation).

The inner can is made of stainless steel and is hermetically sealed. In initial crushing tests, a 2-ton crushing load between steel jaws distorted but did not burst the cans. Internal pressure buildup is easily withstood under normal operating conditions, and calculations have shown that a can of one of the Hastelloy steels will not burst even when held at 850°C for several hours with an internal pressure of 10 thousand psi. Since 120 years would be required for pressures of this magnitude to build up under ordinary conditions, no danger from this factor is envisaged.

The thermopile may be damaged by temperatures greater than 150°C. However, this temperature is more than sufficient for sterilization, and it means that the temperature to which the complete unit can be raised without damage is limited by the electronics and not by the battery.

## Preliminary Performance Tests Under Simulated Body Conditions

When functioning in the body, the pacemaker is subjected to an electrical load of approximately 300 ohms, to continuous contact with body fluids, and to a constant temperature of 37°C, which is appreciably higher than the normal laboratory temperature. Twenty-five pacemakers of six different manufacturers, both British and other countries', are now under observation in the laboratory under simulated body conditions. The pacemakers are immersed in Ringer's solution in a constant-temperature bath at 37°C, with the leads connected to a standard resistance. The units are monitored daily on an oscilloscope for pulse height, pulse width, and pulse frequency.

The size of the pacemaker is indicated in Fig. 5.

(MG)

Fig. 5 Close-up view of radioisotope-powered cardiac pacemaker.

# $^{238}$Pu for Biomedical Applications*

By L. J. Mullins and J. A. Leary†

**Abstract:** *The successful utilization of $^{238}$Pu as a biomedical radioisotopic power source requires that the external radiation of $^{238}$Pu be understood quantitatively and kept to a minimum. To achieve these objectives, $^{238}$Pu metal (80 at.% $^{238}$Pu) of high chemical purity has been prepared and characterized. An electrorefining process was developed to prepare the metal on a 1-cm$^3$ scale. The neutron-emission rate of three lots of electrorefined metal was 2446 (±30) n/(sec)(g of Pu). Correcting this measured rate for chemical impurities and fast fission gives a spontaneous fission rate of 2234 n/(sec) (g of Pu), or 2800 n/(sec)(g of $^{238}$Pu). Neutron and gamma dose rates were also measured. Plutonium-238–gallium alloy, $^{238}PuO_2$, and $^{238}$PuN were prepared and evaluated as radioisotopic heat sources.*

Utilization of $^{238}$Pu as a radioisotopic heat source for life-support applications depends on attaining low external radiation levels. Penetrating radiation from conventional $^{238}$Pu metal derives primarily from the following sources:

1. Spontaneous fission neutrons.
2. Neutrons produced by $(\alpha,n)$ reactions in impurities of low atomic number.
3. Fast fission neutrons.
4. Photons from the decay of $^{238}$Pu.
5. Photons from other plutonium isotopes and their daughters.
6. Photons that result from alpha-particle reactions with light-element impurities.

An irreducible neutron-emission rate results from the spontaneous fission of $^{238}$Pu and $^{240}$Pu. However, this rate is not known accurately. The most recent literature value for $^{238}$Pu is 2586 (±398) n/(sec) (g of $^{238}$Pu), obtained from the measured values of the number of neutrons emitted per fission and the spontaneous fission half-life. The average number of neutrons per spontaneous fission is[1] 2.33 ± 0.08, and the reported half-life is[2] $(5.0 \pm 0.6) \times 10^{10}$ years. The neutron-emission rate of $^{240}$Pu is $1.02 \times 10^3$ n/(sec) (g of $^{240}$Pu). Thus, for a metal containing 80 at.% $^{238}$Pu and 2.9 at.% $^{240}$Pu, the spontaneous fission rate should be 2100 ± 320 n/(sec) (g of Pu). (The basis of calculation for all numbers presented in this paper, unless stated otherwise, *is 1 g of total plutonium isotopes of isotopic composition shown in Table 1.*)

**Table 1 Isotopic Analysis of Electrorefined $^{238}$Pu Metal**

(Typical Lot LA-2)

| Isotope | Abundance, at.% |
|---|---|
| $^{238}$Pu | 79.7 |
| $^{239}$Pu | 17.0 |
| $^{240}$Pu | 2.9 |
| $^{241}$Pu | 0.3 |
| $^{242}$Pu | 0.1 |
| $^{236}$Pu | $1.2 \times 10^{-4}$ |

The neutrons resulting from $(\alpha,n)$ reactions obviously depend on the particular elements present and on their concentrations. The important elements in this respect are Li, Be, B, C, O, F, Na, Mg, Al, and Si. The $(\alpha,n)$ contribution in $^{238}$Pu metal[3] can be as large as $30 \times 10^4$ n/(sec)(g of Pu).

The neutrons from spontaneous fission and $(\alpha,n)$ reactions cause additional fission of the plutonium isotopes, which, in turn, produce excess neutrons. Thus there is a self-multiplication of the neutron rate. The magnitude of this multiplication will depend upon the mass, density, and geometry of the plutonium as well as on the neutron flux. Gamma rays accompany the alpha decay of the plutonium isotopes and account for most of the gamma radiation observed from chemically pure 80%-enriched $^{238}$Pu. As the material ages, more gamma rays appear from daughter products of $^{236}$Pu and $^{241}$Pu. Gamma rays also arise from $(\alpha,n)$ or $(\alpha,p)$ reactions induced by alpha-particle bombardment of impurity nuclides. This is particularly evident if the impurities are nitrogen or fluorine.

For biomedical applications, it is imperative that the radiation emitted by the power source be understood quantitatively and that it be kept to a minimum. Therefore research was initiated to accomplish the following objectives:

1. To prepare and evaluate $^{238}$Pu metal of high chemical purity.

*The Editors wish to acknowledge the kind permission of the American Nuclear Society to reprint an edited version of an article from *Nuclear Applications*, 6(4): 287-297 (1969).

†Los Alamos Scientific Laboratory, Los Alamos, N. M. 87544.



XUM

2. To provide a chemically pure material for synthesizing $^{238}Pu$ compounds and alloys.

3. To provide a standard to which other fuel forms could be compared.

4. To improve the accuracy of the spontaneous-fission rate of $^{238}Pu$.

Two general methods of preparing pure plutonium metal are available: bomb reduction and electrorefining. Meticulous quality control of the bomb-reduction process can produce $^{239}Pu$ varying in purity from 99.8 to 99.96%. To obtain metal of this quality, chemically pure $PuF_4$, Ca, and $I_2$ must be used since little or no purification of plutonium is obtained in the bomb-reduction process. The product from the electrorefining process, on the other hand, is relatively insensitive to the purity of the feed metal. Plutonium-239 of purity >99.98% is obtained routinely by electrorefining impure $^{239}Pu$ (~99.8% Pu) and Pu alloys (Pu–2.5 wt.% Fe and Pu–1 wt.% Ga). Electrorefining procedures have been developed to prepare this high-purity metal on the 0.5- and 3-kg scales.[4,5] A plant with a capacity of 10 kg of Pu/week has been in operation at the Los Alamos Scientific Laboratory for the past 4 years. Some of this high-purity metal is distributed by the National Bureau of Standards as a primary chemical plutonium standard. Because of the superior chemical purity of the product and the assured quality control, electrorefining procedures were adapted to the present $^{238}Pu$ work.

## Experimental

### Process Flow Sheet for Preparing Pure $^{238}Pu$ Metal from $^{238}PuO_2$

The processing flow sheet is given in Fig. 1. The general procedure consisted of the following steps:

1. Dissolution of ~33 g of as-received $^{238}PuO_2$ in 350 ml of 15.6*M* $HNO_3$–0.05*M* HF.
2. Precipitation of plutonium peroxide.
3. Conversion of the peroxide to $PuF_4$.
4. Bomb reduction of $PuF_4$ to plutonium metal by calcium, using $I_2$ booster.
5. Casting of the bomb-reduced metal into an anode.
6. Electrorefining of the bomb-reduced metal.
7. Casting of the electrorefined metal.

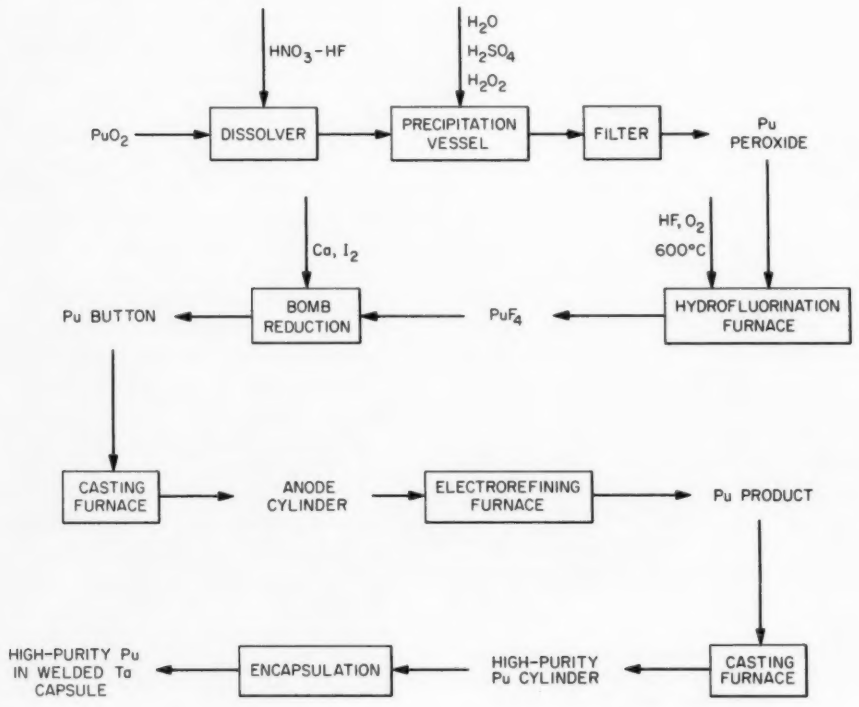


**Fig. 1 Process flow sheet for converting $^{238}PuO_2$ to encapsulated $^{238}Pu$ metal.**

### Conversion of $^{238}PuO_2$ to Metal

The technology and equipment used for the preparation of bomb-reduced $^{238}Pu$ metal were developed at Los Alamos in 1959 and have been described.[6]

### Electrorefining

The first phase of the experimental program consisted of developing an electrorefining process for producing ~15- to 20-g batches of high-purity metal. Since the technology for large batches of $^{239}Pu$ was well established, much of this technology was transferred directly to the small-scale process.

Figure 2 shows the equipment and feed materials for the small-scale electrorefining process. The bomb-reduced metal was placed in the anode leg (the tapered leg) of the $MgO–Y_2O_3$ crucible. A cylinder of equimolar NaCl–KCl was also placed in the crucible. The entire assembly was then loaded into a commercial resistance-heated furnace and brought to an operating temperature of 740°C. The slotted tantalum stirrer, which also served as the anode lead, and the cathode rod were lowered into position, and direct current was passed at 1 amp through the cell to generate $PuCl_3$ and sodium metal. During this phase of the operation, the cell reaction was:

$$\underset{\text{(anode)}}{Pu(l)} + \underset{\text{(molten salt)}}{3NaCl(l)} \rightarrow \underset{\text{(molten salt)}}{PuCl_3(l)} + \underset{\text{(cathode)}}{3Na(l)}$$

The back electromotive force (emf) of the cell was monitored periodically during this operation to ensure that the above reaction was taking place. Upon completion of the $PuCl_3$ generation, the stirrer was activated, and a brief preelectrolysis at 0.5 amp was conducted. The cathode rod was then raised, and a second tungsten cathode rod was lowered into the cathode leg of the crucible. The normal electrorefining process was then conducted at 0.8 amp. The cell reaction during electrorefining was:

$$\underset{\text{(anode)}}{\text{Impure } Pu(l)} \rightarrow \underset{\text{(molten salt)}}{Pu^{3+}} \rightarrow \underset{\text{(cathode)}}{\text{Pure } Pu(l)}$$

The refining process also was monitored by back-emf measurements and the electrorefining discontinued when these measurements indicated serious anode polarization or when ~85% of the Pu had been

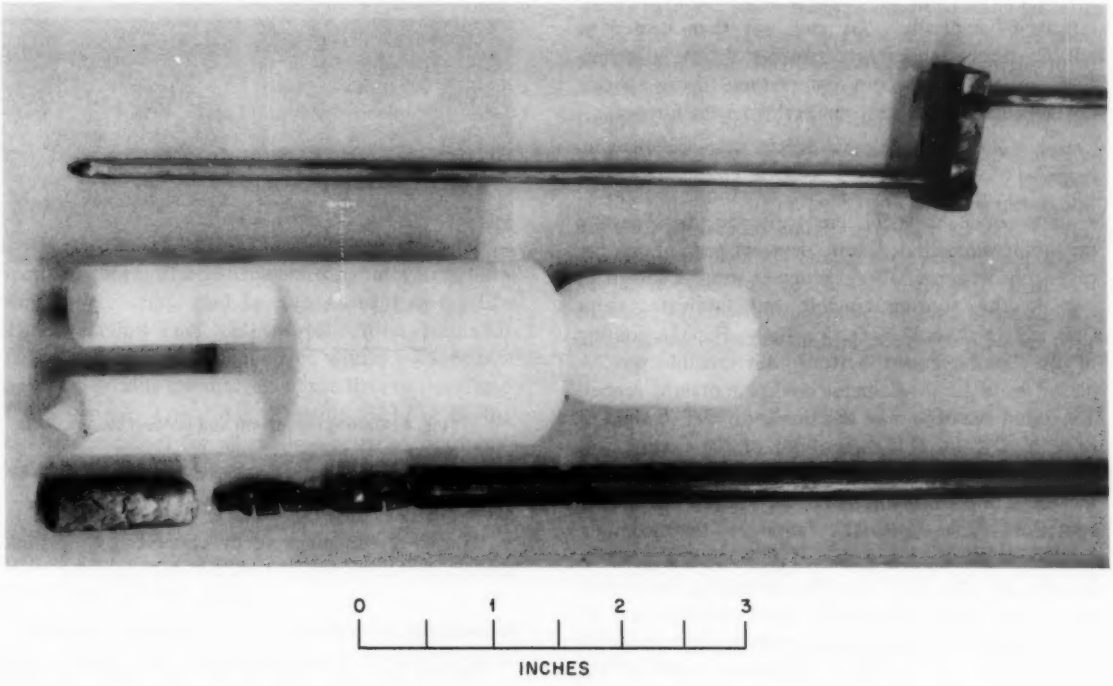


**Fig. 2 Small-scale electrorefining components.**



XUM

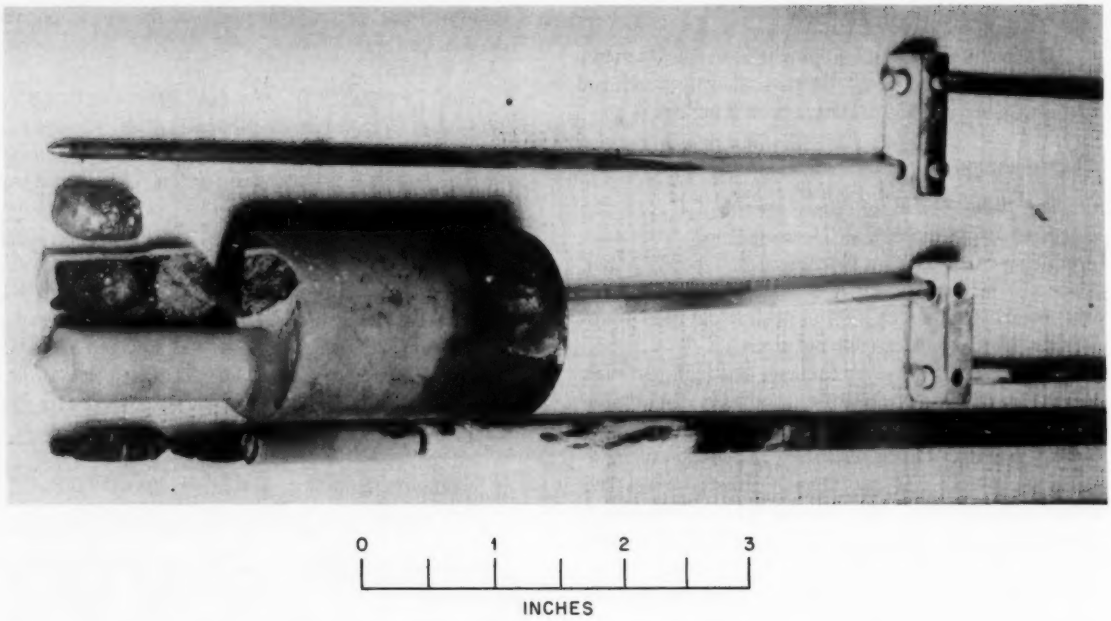


Fig. 3 Small-scale electrorefining components after removal from electrorefining furnace.

dissolved anodically. The cell was then heated to 850°C, vibrated briefly to improve the metal collection, and cooled to room temperature. Figure 3 shows the cell components after removal from the furnace.

### Casting

The small scale (1 $cm^3$) of the metal-casting operation necessitated the development of special casting procedures. The equipment used is shown in Fig. 4. The pouring crucible was fabricated from $CaF_2$, MgO–3 wt.% $Y_2O_3$, or $ThO_2$. For the pouring of the bomb-reduced buttons, this crucible was replaced by a 1.5-in.-diameter conical tantalum funnel. The mold crucible was also made of $CaF_2$, MgO–3 wt.% $Y_2O_3$, or $ThO_2$. The end of the casting was broken off to provide a sample. The melting point of the metal was normally determined during the remelt operation. The $\frac{1}{8}$-in.-OD tantalum thermocouple sheath shown in Fig. 4 passed through the pouring crucible into the mold crucible containing the molten metal. The melt was cooled at a constant rate to ~500°C and then heated at a constant rate to ~750°C to determine the melting and freezing points of the metal. The metal was usually cast in the form of a cylinder having a diameter of 0.95 cm.

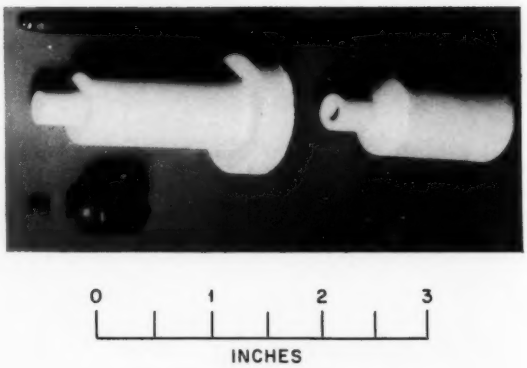


Fig. 4 Casting equipment and product casting.

### Preparation of $^{238}Pu$–1 wt.% Ga Alloy

The alloy was prepared by co-melting $^{238}Pu$ and gallium in a stirred MgO–3 wt.% $Y_2O_3$ crucible.

### Preparation of $^{238}PuO_2$

Several lots of $^{238}PuO_2$ were prepared for characterization. These were prepared by conventional methods such as heating the nitride and peroxide in air

to constant weight at 900°C. Some of the as-received $^{238}PuO_2$ also was evaluated for comparison.

### Preparation of $^{238}$PuN

The procedure normally used to convert $^{239}$Pu metal to $^{239}$PuN was used[7] to prepare $^{238}$PuN. In this process the metal is hydrided and dehydrided twice to form metal powder. The powder is reacted with $N_2$ to form PuN.

### Encapsulation

Tantalum capsules were used for encapsulation. The initial loading operation was conducted in an unshielded pure argon-filled glove box. The $^{238}$Pu metal, alloy, or compound was placed in a 0.5-in.-OD crucible that was 1.5 in. long and 0.015 in. in wall thickness. A tapered tantalum plug was then pressed into place using a small vise. This "inner capsule" was then transferred to a welding box where it was placed in a 0.625-in.-OD by 0.015-in.-wall "outer crucible." The lid of the latter container was then welded to provide a container that was not contaminated on the outside surface.

## Radiation and Dosimetry Measurements

### Neutron-Emission Rates

The neutron counter used in these measurements was a water-moderated $BF_3$ detector arranged in a well-type geometry that afforded a fixed and reproducible geometry for all samples. The neutron counter was calibrated with two sources. The first was a Pu–Be source, and the second was 10.64 g of electrorefined $^{238}$Pu metal sealed in a container as described above. The neutron-emission rates from both sources were established by measurement in the Los Alamos Graphite Pile[8] and gave calibration factors for the neutron counter which agreed within 1.2%. Subsequently it became the practice to use the electrorefined $^{238}$Pu source, Lot LA-2 (Capsule 823-6), as the reference standard for all neutron-activity determinations for $^{238}$Pu samples.

**Neutron Dosimetry.** Lithium-6 fluoride thermoluminescent detectors (TLD) were placed in a 10-in.-diameter polyethylene sphere with the neutron source exterior to the sphere.

**Gamma Dosimetry.** Lithium-7 fluoride TLD's were used for gamma measurements that were made in air at distances of 0.8, 2.0, 4.0, 6.0, 8.0, 10.0, 14.0, and 18.0 cm from the center of the source.

### Electrorefined $^{238}$Pu Metal

The material balance for a typical electrorefining experiment is given in Table 2. Although no study has been made to optimize this small-scale process, unintentional losses are low, e.g., 1.05 g.

**Table 2 Typical Electrorefining Material Balance**

Lots LA-9 and LA-8

| | Weight of Pu, g |
|---|---|
| Pu feed to cell | 28.32 |
| Electrorefined ingot | 20.97 |
| Anode metal | 4.45 |
| $PuCl_3$ generated in salt | 1.20 |
| Pu adhered to cathode | 0.65 |
| Loss as slag and shot (by difference) | 1.05 |

The neutron-emission rates for three lots of electrorefined metal are shown in Table 3. A different casting material was used in each case. In this study, $CaF_2$, MgO, and $ThO_2$ were used because they have all proved to be satisfactory materials for molten high-purity $^{239}$Pu metal. In each case the metal was cast in the form of a cylinder having a height-to-diameter ratio of 1. The third column in Table 3 gives the measured neutron-emission rate. The average value for the three metals was 2446 ± 30 n/(sec)(g of Pu). In the last column the measured rate is corrected for the analyzed impurities present in the metal by using the reported $(\alpha,n)$ yields.[3] In principle, this number should be equal to the sum of the spontaneous-fission and fast-fission rates for plutonium metal containing 80 at.% $^{238}$Pu. The self-multiplication rate of the electrorefined metal has been calculated to be 158 n/(sec)(g). This contribution varies with the geometry, weight, and density of the source. The self-multiplication for cylinders with

**Table 3 Neutron-Emission Rate of Electrorefined $^{238}$Pu Metals**

| Lot | Casting ware | Neutron-emission rate, n/(sec) (g of Pu) | |
|---|---|---|---|
| | | Measured | Corrected for impurities |
| LA-2 | $CaF_2$ | 2450 | 2415 |
| LAR-3 | MgO | 2400 | 2325 |
| LA-8 + LA-9 | $ThO_2$ | 2487 | 2437 |
| Average value | | 2446 ± 30 | 2392 ± 45 |



XUM

equal ratio of length to diameter is shown[10] in Fig. 5. The measured neutron-emission rate is compared with the spontaneous-fission rate in Table 4. The published value of the spontaneous-fission rate is 2100 ± 320 n/(sec)(g of Pu). The value calculated for electrorefined metal is 2234 n/(sec) (g of Pu).

Other properties that have been measured are shown in Table 5. The published[9] melting points of conventional $^{238}$Pu metal vary from 575 to 615°C. The value of 639°C obtained with electrorefined $^{238}$Pu is essentially identical to that which is accepted for $^{239}$Pu, namely, 640 ± 2°C. The neutron dose rate in air at 10 cm through 0.030 in. of tantalum was 0.24 mrem/(hr)(g of Pu). This number was calculated from the neutron-emission rate and confirmed by TLD dosimetry. The gamma dose rate in air at 10 cm for the refined metal is 0.20 mr/(hr)(g of Pu) for a cylinder having a diameter and height of 0.95 cm. The gamma TLD measurements were made as a function of distance. Typical results, plotted in Fig. 6, indicated

**Table 4 Comparison of Neutron-Emission Rate of Electrorefined Metal with $^{238}$Pu Spontaneous-Fission Rate**

| | n/(sec) (g of Pu) |
|---|---|
| Electrorefined metal (measured rate) | 2446 ± 30 |
| Correction for impurities | 54 |
| Correction for fast fission[10] | 158 |
| Spontaneous-fission rate (by difference) | 2234 |
| Spontaneous-fission rate (literature value[1,2]) | 2100 ± 320 |

**Table 5 Properties of Electrorefined $^{238}$Pu Metal**

| | |
|---|---|
| Melting point, °C | 639 (±3) |
| Neutron-emission rate, n/(sec) (g of Pu) | 2446 |
| Dose rates at 10 cm* | |
| *Neutron, mrem/(hr)(g of Pu)* | |
| Calculated from emission rate | 0.24 |
| Thermoluminescent dosimetry | 0.24 |
| *Gamma, mr/(hr)(g of Pu)* | |
| Thermoluminescent dosimetry | 0.20 |
| Specific power, watt/g of Pu† | 0.456 |

*Dose rates in air through 0.030 in. of tantalum.

†The specific power was measured more precisely. However, $^{234}$U grows in at the rate of 525 ppm/month, and there normally is about 500 ppm of $^{237}$Np present. Therefore the specific power has been rounded off to a less precise value.

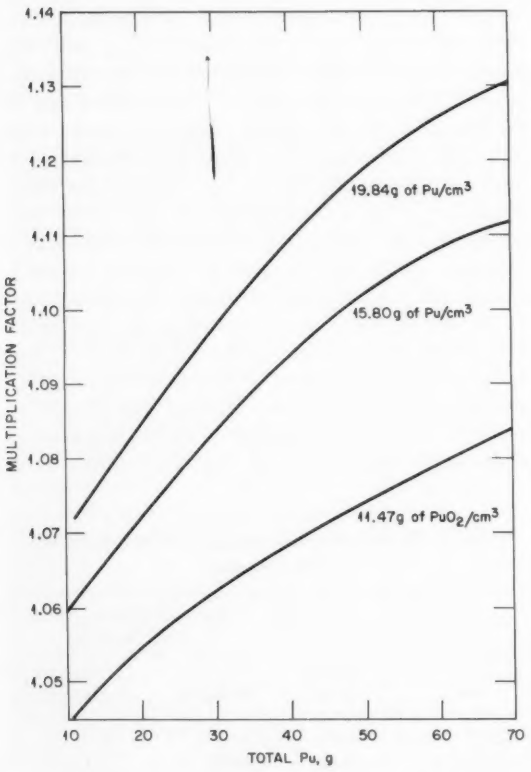


Fig. 5 Neutron self-multiplication factors for plutonium cylinders. $L = D$; 80 at.% $^{238}$Pu.

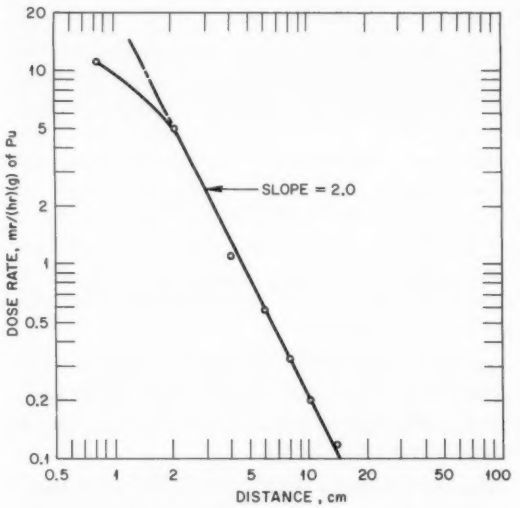


Fig. 6 Gamma dose rate of electrorefined metal (measurements made through 0.030 in. of tantalum).

that the data fit an inverse square law between 2 and 14 cm. The specific power (determined calorimetrically) is essentially the same as the literature value.[9]

Chemical purity of the three lots of electrorefined metal is compared to the bomb-reduced metal in Table 6. Except for the high neptunium concentration, the purity of the $^{238}Pu$ metal is similar to that obtained with $^{239}Pu$. About 80% of the neptunium and all of the uranium were removed from the plutonium in the electrorefining. The rapid growth of

**Table 6 Chemical Purity of Electrorefined and Bomb-Reduced Metals**

| | Impurity concentration, ppm by weight | | | | |
|---|---|---|---|---|---|
| | LA-2 | LAR-3 | | LA-9, LA-8 | |
| Element | Electro-refined | Bomb-reduced | Electro-refined | Bomb-reduced | Electro-refined |
| Li | <0.02 | <0.01 | <0.005 | 0.1 | 0.8 |
| Be | <0.001 | <0.002 | <0.001 | <0.002 | <0.002 |
| B | <0.3 | NA | 0.5 | <0.3 | <0.3 |
| Na | 1 | <2 | 1 | 30 | <6 |
| Mg | 5 | 5 | 20 | 9 | <4 |
| Al | 2 | 35 | 2 | 25 | 2 |
| Si | 15 | NA | 10 | 73 | 20 |
| K | 0.5 | <1 | <0.5 | 0.6 | 2 |
| Ca | 6 | 19 | 3 | 155 | <6 |
| Ti | 0.4 | 0.4 | 0.5 | 4 | <0.6 |
| V | <0.5 | <1 | <0.5 | <1 | <1 |
| Cr | 0.5 | <2 | 1 | <1 | <1 |
| Mn | 0.6 | 5 | 0.7 | 4 | 0.8 |
| Fe | <35 | 120 | <35 | 68 | <40 |
| Co | <0.5 | <1 | <0.5 | <1 | <1 |
| Ni | 3 | 70 | <8 | 47 | 5 |
| Cu | 0.5 | 7 | 4 | 2 | 1 |
| Zn | <5 | <5 | <5 | 5 | <5 |
| Rb | <0.5 | <1 | <0.5 | <1 | <1 |
| Sr | <0.1 | <0.2 | <0.1 | <0.2 | <0.2 |
| Y | <0.1 | <0.2 | <0.1 | <0.2 | <0.2 |
| Zr | <0.1 | 2 | <0.1 | 3 | <0.2 |
| Mo | <0.5 | 3 | 2 | 2 | 1 |
| Cd | <0.5 | <1 | <0.5 | <1 | <1 |
| Sn | 2 | <1 | <0.5 | 2 | 2 |
| Cs | <2 | <3 | <2 | 3 | <4 |
| Ba | <0.1 | <0.2 | 0.5 | 0.1 | <0.2 |
| La | <1 | <1 | <0.5 | <1 | <1 |
| Hf | <0.5 | <1 | <0.5 | <1 | <1 |
| Re | <0.5 | <1 | <0.5 | <1 | <1 |
| Pb | 2 | <1 | <0.5 | <1 | 2 |
| Bi | <0.5 | NA | <0.5 | <0.15 | <0.5 |
| $^{241}Am$* | 4 | 13 | 2 | 13 | 0 |
| $^{237}Np$ | NA† | 2800 | 537 | 4180 | 865 |
| $^{232}U$ | NA | 0.016 | NA | 0.02 | NA |
| $^{234}U$* | NA | 870 | 0 | 870 | 0 |
| F | NA | NA‡ | <2§ | NA‡ | <2§ |

*$^{241}Am$ and $^{234}U$ values corrected to date of electrorefining.
†NA, no analysis.
‡Fluorine reaction gammas very strong.
§Analysis of top and bottom samples of ingot.



XUM

$^{234}U$ in the product, ~525 ppm/month, does not warrant additional chemical processing to remove the neptunium.

### Bomb-Reduced $^{238}Pu$ Metal

Table 7 shows the results of neutron measurements with bomb-reduced metals. The average measured rate of 2928 n/(sec)(g of Pu) is 482 neutrons higher for bomb-reduced metals than for the refined metal, and the average of the rates corrected for light-element impurities is 405 neutrons higher. In the case of the bomb-reduced metals, no corrections have been made for fluorine, which has been detected in all these metals either by chemical analysis or gamma spectrometry. However, the distribution is so heterogeneous that no meaningful correction can be made. For example, Lot LA-9 was cast in tantalum. Two top and two bottom samples of the ingot were cut for fluorine analysis. The analyses for the top were 90 and 10 ppm by weight. The analyses of the bottom samples were 8 and 4 ppm. The average value for the ingot is 28 ppm with an uncertainty of 26 ppm. Thus the calculated neutron correction is 504 ± 468. The electrorefined metals did not present the fluorine segregation problem since fluorine could not be detected in either top or bottom samples. Thus it would be impossible to estimate the spontaneous-fission rate of bomb-reduced metal with any reasonable accuracy.

**Table 7 Neutron-Emission Rate of LASL Bomb-Reduced $^{238}Pu$ Metals**

| Lot | Neutron-emission rate, n/(sec) (g of Pu) | |
|---|---|---|
| | Measured | Corrected for impurities* |
| LAR-1 | 4027 | 3957 |
| LAR-3 | 3119 | 3000 |
| LA-4 | 2622 | 2482 |
| LA-5 | 3006 | 2731 |
| LA-6 | 2663 | 2568 |
| LA-7 | 2665 | 2545 |
| LA-8 | 2815 | 2666 |
| LA-9 | 2510 | 2425 |
| Average | 2928 ± 342 | 2797 ± 341 |

*No correction for fluorine.

Other properties of the LASL bomb-reduced metals are given in Table 8. The melting point of 636°C is slightly lower than that for the electrorefined metal. The measured neutron dose rate of 0.27 mrem/(hr)(g of Pu) is 0.03 mrem higher. The gamma dose rates were identical for both metals.

**Table 8 Properties of LASL Bomb-Reduced $^{238}Pu$ Metal**

| | |
|---|---|
| Melting point, °C | 636 ± 3 |
| Neutron-emission rate, n/(sec)(g of Pu) | 2928 |
| Dose rates at 10 cm* | |
| *Neutron, mrem/(hr)(g of Pu)* | |
| Calculated from emission rate | 0.29 |
| Thermoluminescent dosimetry | 0.27 |
| *Gamma, mr/(hr)(g of Pu)* | |
| Thermoluminescent dosimetry | 0.20 |

*Dose rates in air through 0.030 in. of tantalum.

### $^{238}PuO_2$ (Natural Oxygen)

As part of this study, the radiation properties of as-received oxide powders were evaluated. These properties are summarized in Table 9. The calculated neutron activity of 80%-enriched $^{238}PuO_2$ is $1.34 \times 10^4$ n/(sec)(g of Pu), based on the spontaneous-fission rate and the neutron yield from the bombardment of oxygen with 5.5-Mev alpha particles. Most oxide lots received at LASL showed activities of around $4.5 \times 10^4$ n/(sec)(g of Pu), with one lot as high as $10.3 \times 10^4$, as shown in Table 9. It was concluded that the increase over the calculated value was caused by $(\alpha,n)$ reactions arising from the presence of low-$Z$ impurity elements. This was confirmed by high-resolution gamma spectrometry which showed characteristic gamma rays resulting from the $(\alpha,n)$ reaction involving fluorine, in addition to those caused by oxygen.

A few oxides were prepared in this laboratory. The properties of these powders are summarized in Table 10. The first oxide was prepared by igniting as-received Lot LA-6 $PuO_2$ to constant weight and constant neutron activity. The neutron-emission rate was reduced from 4.7 to $1.3 \times 10^4$. Elimination of fluorine by ignition was mainly responsible for this decrease in neutron activity. The second oxide was prepared by igniting the peroxide precipitate from a solution of Lot LA-8, and its neutron-emission rate is similar to that of the pure $PuO_2$ prepared by the reaction of high-purity PuN with air. This latter oxide is the purest oxide prepared to date. The gamma dose rate of 0.35 mr/(hr)(g of Pu) for oxide powders prepared in this laboratory was ~30% less than that of

as-received oxide. However, the comparison of gamma dose rates for these powders is only qualitative since the self-absorption of gamma rays by plutonium will depend upon the density and geometry of the system.

The increase in neutron-emission rate in going from $^{238}Pu$ metal to $^{238}PuO_2$ is due principally to $^{17}O$ and $^{18}O$ in natural oxygen.[11-13] It is possible to synthesize $^{238}PuO_2$ that is depleted in $^{18}O$ by a factor of at least 100. This would result in an oxide having an emission rate that is about one-fifth that of the oxide made from natural oxygen or about 100 n/(sec)(g) greater than the electrorefined metal. Experiments now in progress will evaluate the dependence of neutron and gamma dose rates on the oxygen isotopic composition.

**Table 9 Radiation Properties of As-Received $^{238}PuO_2$ (Natural Oxygen)**

| Lot | Neutron-emission rate, n/(sec)(g of Pu) | Dose Rates at 10 cm*: Neutrons, mrems/(hr)(g) Calculated | Neutrons, mrems/(hr)(g) Thermoluminescent dosimetry | Photons, mr/(hr)(g) Thermoluminescent dosimetry |
|---|---|---|---|---|
| LA-5 | $4.1 \times 10^4$ | 4.07 | 4.13 | 0.48 |
| LA-6 | $4.7 \times 10^4$ | 4.68 | | |
| LA-9 | $4.4 \times 10^4$ | 4.38 | 4.59 | 0.51 |
| LA-10 | $4.1 \times 10^4$ | 4.08 | | |
| LA-11 | $10.3 \times 10^4$ | 10.3 | | |

*Dose rates in air through 0.030 in. of tantalum.

**Table 10 Radiation Properties of LASL $^{238}PuO_2$ (Natural Oxygen)**

| Method of preparation | Neutron-emission rate, n/(sec)(g of Pu) | Dose Rates at 10 cm*: Neutrons, mrems/(hr)(g) Calculated | Neutrons, mrems/(hr)(g) Thermoluminescent dosimetry | Photons, mr/(hr)(g) Thermoluminescent dosimetry |
|---|---|---|---|---|
| Ignition of as-received $PuO_2$, Lot LA-6 | $1.30 \times 10^4$ | 1.29 | | |
| Ignition of Pu peroxide, Lot LA-8 | $1.25 \times 10^4$ | 1.24 | 1.61 | 0.34 |
| Reaction of PuN with air | $1.21 \times 10^4$ | 1.20 | 1.42 | 0.35 |

*Dose rates in air through 0.030 in. of tantalum.

### $^{238}Pu$–1 Wt.% Ga Alloy

The physical properties of plutonium metal are complex, due to the fact that the metal exists in six allotropic modifications between room temperature and its melting point, 639°C. Thus the linear expansion functions are discontinuous. For example, the linear expansion coefficients vary from $58 \times 10^{-6}$/°C for the alpha phase to $-118 \times 10^{-6}$/°C for the delta-prime phase. Large expansions and contractions also accompany some of the solid-state transitions. These transitions are summarized in Table 11.

However, the metal can be stabilized in the delta phase by the addition of small amounts of alloying agents. For example, a 1 wt.% Ga–Pu alloy is stable in the delta phase from room temperature to ~500°C. From 500 to 525°C, delta + epsilon phases exist, and from 525 to 645°C the epsilon phase is stable. The coefficients of linear expansion of the delta and epsilon phases are $-16 \times 10^6$ and $27 \times 10^6$/°C. Thus, if a metallic $^{238}Pu$ fuel is required, it would be most advantageous to stabilize the plutonium in the delta phase.



XUM

Ten grams of $^{238}$Pu–1 wt.% Ga was prepared from bomb-reduced $^{238}$Pu Lot LA-7. The plutonium and gallium were melted in the MgO–3 wt.% $Y_2O_3$ electrorefining crucible, and the molten metal was stirred with a tantalum stirrer to ensure homogeneity. As shown in Table 12, the radiation properties of the metal and the alloy were essentially the same.

### $^{238}$Pu Nitride (Natural Nitrogen)

Thirty-four grams of $^{238}$PuN have been prepared in two lots from $^{238}$Pu metal. Portions were separated in two different zones in a quartz reaction tube, Zone A and Zone B. Natural $N_2$ gas was passed over the metal in Zone A before it contacted the metal in Zone B. After reaction, the nitride powders were sampled and encapsulated in the standard tantalum capsules.

As anticipated,[3] the neutron-emission rate of the PuN product was approximately equal to the emission rate of the metal feed. The emission rates were 2600 n/(sec) (g of Pu) for the PuN from Zone A and 2613 n/(sec)(g) for the PuN from Zone B. The corresponding rates for the metal before reaction were 2702 and 2663, respectively. The gamma dose rates of the nitride powders, however, were higher than those of the metal by a factor of 2.7 and higher than those of chemically pure oxide powders by a factor of 1.6. The increased gamma activity is primarily due to the $^{14}N(\alpha,p)^{17}O$ reaction. The radiation properties of the nitride from Zone B are compared to those of the metal in Table 13.

**Table 11 Volume Changes Accompanying Unalloyed-Plutonium Phase Transitions[14]**

| Phase transition | Transition temp., °C | Volume change, % |
|---|---|---|
| Alpha → beta | 110 | 9.62 |
| Beta → gamma | 190 | 2.67 |
| Gamma → delta | 310 | 6.90 |
| Delta → delta prime | 452 | −0.36 |
| Delta prime → epsilon | 480 | −2.16 |
| Epsilon → liquid | 639 | −0.82 |

**Table 12 Comparison of the Radiation Properties of $^{238}$Pu Metal and $^{238}$Pu–1 Wt.% Ga Alloy**

| | $^{238}$Pu metal | $^{238}$Pu–Ga |
|---|---|---|
| Neutron-emission rate, n/(sec)(g of Pu) | 2665 | 2728 |
| Dose rates at 10 cm* | | |
| *Neutron, mrem/(hr)(g of Pu)* | | |
| Calculated from emission rate | 0.27 | 0.27 |
| Thermoluminescent dosimetry | 0.24 | 0.26 |
| *Gamma, mr/(hr)(g of Pu)* | | |
| Thermoluminescent dosimetry | 0.21 | 0.20 |

*Dose rates in air through 0.030 in. of tantalum.

**Table 13 Comparison of the Radiation Properties of $^{238}$Pu and $^{238}$PuN (Zone B Portion)**

| | $^{238}$Pu metal | $^{238}$PuN |
|---|---|---|
| Neutron-emission rate, n/(sec) (g of Pu) | 2663 | 2613 |
| Dose rates at 10 cm* | | |
| *Neutron, mrem/(hr) (g of Pu)* | | |
| Calculated from emission rate | 0.26 | 0.26 |
| Thermoluminescent dosimetry | 0.24 | 0.20 |
| *Gamma, mr/(hr) (g of Pu)* | | |
| Thermoluminescent dosimetry | 0.21 | 0.56 |

*Dose rates in air through 0.030 in. of tantalum.

## Acknowledgments

We are indebted to the following LASL personnel for the assistance indicated: G. M. Matlack, gamma spectrometry work and measurement of neutron-emission rates; A. M. Valentine, dosimetry measurements; A. N. Morgan, preparation of bomb-reduced metals; R. L. Nance, preparation of $^{238}$PuN; L. H. Treiman, calorimetric measurements; and A. J. Beaumont, assistance in electrorefining, casting, and encapsulation. This work was presented at the American Nuclear Society meeting, Toronto, Canada, June 10–13, 1968, and sponsored by the USAEC Division of Isotopes Development. (PSB)

## References

Reference marked with an asterisk has not been verified by the editors; for further explanation, see the Foreword.

1. D. A. Hicks, J. Ise, Jr., and R. V. Pyle, Probabilities of Prompt-Neutron Emission from Spontaneous Fission, *Phys. Rev.*, **101**: 1016-1020 (1956).
2. V. A. Druin, V. P. Perelygin, and G. I. Khlebnikov, Spontaneous Fission Periods of $^{237}$Np, $^{238}$Pu, and

$^{242}$Pu, *Sov. Phys. JETP (Engl. Transl.)*, 13(5): 913-914 (1961).
3. G. M. Matlack and C. F. Metz, Radiation Characteristics of Plutonium-238, USAEC Report LA-3696, Los Alamos Scientific Laboratory, October 1967.
4. L. J. Mullins and J. A. Leary, Fused Salt Electrorefining of Molten Plutonium and Its Alloys by the Lamex Process, *Ind. Eng. Chem., Process Design Develop.*, 4: 394-400 (1965).
5. J. A. Leary and L. J. Mullins, Preparation of Ultra High Purity Plutonium, USAEC Report LA-3356-MS, Los Alamos Scientific Laboratory, August 1965.
6. A. N. Morgan, J. L. Green, J. A. Leary, and W. J. Maraman, Preparation of Plutonium-238 Metal, USAEC Report LA-2411, Los Alamos Scientific Laboratory, July 1960.
7. J. A. Leary, W. C. Pritchard, R. L. Nance, and M. W. Shupe, Refractory Plutonium Fuel Materials, in *Plutonium 1965*, Proceedings of the Third International Conference on Plutonium, London, 1965, A. E. Kay and M. B. Waldron (Eds.), pp. 639-653, Chapman & Hall, London, 1967.
8. A. C. Graves, R. L. Walker, R. F. Taschek, A. O. Hanson, J. H.Williams, and H. M. Agnew, Neutron Sources, Chap. 2 in *Miscellaneous Physical and Chemical Techniques of the Los Alamos Project*, Division V, Volume 3, pp. 47-161, National Nuclear Energy Series, A. C. Graves and D. K. Froman, (Eds.), McGraw-Hill Book Company, Inc., New York, 1952.
9. Plutonium-238 and Polonium-210 Data Sheets, USAEC Report MLM-1441, Monsanto Research Corp., November 1967.
10. *G. E. Hansen, Group N-2, LASL, personal communication.
11. V. Keshishian and K. M. Broom, Jr., Use of Oxygen-16 with Plutonium-238 To Reduce Neutron Yield, *Trans. Amer. Nucl. Soc.*, 9: 102-103 (1966).
12. W. M. Rutherford, G. N. Huffman, and D. L. Coffey, Preparation and Neutron Counting of $^{238}PuO_2$ Depleted in $^{18}O$, *Nucl. Appl.*, 3: 366-371 (1967).
13. D. L. Plymale, The Exchange of Isotopically Enriched Oxygen with $^{238}PuO_2$, *J. Inorg. Nucl. Chem.*, 30: 886-890 (1968).
14. *Plutonium Handbook*, Vol. 1, p. 37, Gordon and Breach Science Publishers, New York, 1967.

# Promethium Technology: A Review

By H. T. Fullam* and H. H. Van Tuyl*

**Abstract:** *The technology that has been developed for using promethium as lightly shielded heat and radiation sources is described. A summary of available information is given about applications, nuclear properties, production in USAEC and commercial power reactors, chemical purification, chemical and physical properties of candidate fuel forms, compatibility, and source-fabrication technology.*

Promethium does not occur in nature except as a fission product from the minute amounts of natural fission. Its existence was predicted in 1914 by Moseley[1] when X-ray work showed clearly that an element should exist between neodymium and samarium. The first observation of radioactivity from promethium was reported by Pool and Quill[2] in 1938, and a chemical separation of promethium from other rare earths was reported in 1945 by Marinsky and Glendenin.[3] Now, only 25 years after its first separation, promethium is available in kilogram quantities and has been well characterized for use in a variety of applications.

*Pacific Northwest Laboratory (PNL), Richland, Wash. 99352, operated by Battelle Memorial Institute for the USAEC.

The principal source of promethium is fission of uranium and of plutonium in nuclear reactors, but it can also be made by neutron irradiation of neodymium. Either method yields mostly $^{147}$Pm, with only trace amounts of other promethium isotopes. The $^{147}$Pm decays primarily by beta emission (0.225 Mev maximum) with a half-life of 2.62 years, giving a specific power of 0.333 watt per gram of promethium. The disintegration rate of pure $^{147}$Pm is 928 curies/g.

Promethium is the only fission product that has potential application as a lightly shielded radioisotope power source.[4] Most fission products emit penetrating gamma radiation, which requires massive shielding. A few, e.g., $^{90}$Sr—$^{90}$Y, are pure beta emitters, but the beta energies are high enough to produce large amounts of moderate- to high-energy bremsstrahlung. For sources as small as a few watts, the shielding required for high-energy beta emitters is comparable to that required for the gamma emitters.[5]

The betas from $^{147}$Pm have sufficiently low energy to yield only soft bremsstrahlung, which is easily shielded by moderately high-atomic-number absorbers.[6] Associated with the $^{147}$Pm are smaller amounts of $^{146}$Pm and $^{148m}$Pm, which yield pene-



XUM

trating gamma radiation. In a properly designed heat source, only the penetrating radiations of the $^{146}Pm$ and the $^{148m}Pm$ contribute significantly to personnel exposure.

Promethium is currently available in multi-megacurie amounts as aged material suitable for use in radioisotope power sources.[7] Much larger amounts will be potentially available from power reactors in the next 5 to 10 years.

For several years, a program on promethium production, evaluation, and property measurement was sponsored by the USAEC and conducted, prior to 1965, by the Hanford Atomic Products Operation and, since then, by its successors, the Pacific Northwest Laboratory (PNL) and the Atlantic Richfield Hanford Co. (ARHCO). The program has resulted in a technology for producing large amounts of highly purified promethium, measurement of its chemical and nuclear properties, and fabrication of prototype sources.

## Applications

The use of promethium and its compounds in industrial applications has been very limited, the two major uses being as beta sources in instruments and batteries and as isotopic heat sources. Applications that utilize the beta-emission properties of promethium include:

Promethium-activated phosphor light sources[8]
Thickness gages[9]
X-ray spectroanalysis[10]
Betavoltaic electric-power sources[11]
Photoelectric batteries[12]

Heat-source applications represent by far the largest market potential for promethium. The desired fuel form in most future applications will probably be $Pm_2O_3$ and possibly promethium metal. Promethium should find its greatest use in sources designed for moderate-duration missions (1 to 5 years), where weight considerations are critical. In addition, promethium is still under consideration as the fuel for heart-pump and heart-pacemaker applications.

To date, only a limited number of promethium-fueled heat sources have been fabricated (one has been approved for aircraft use, but none has been submitted for space qualification). They include:

1. A compact radioisotopic heater[13] called a "Thermopac," produced and sold by Atomics International, a division of North American Aviation, Inc. Various isotopes, including $^{147}Pm$, can be used as fuel, depending on the application. Sizes from 0.1 to 100 watts(t) are available.

2. A small heater[14] developed by McDonnell Douglas Aircraft Co., through its Donald W. Douglas Laboratory. The fuel is made from $^{147}Pm_2O_3$ microspheres coated with tungsten, and the output is approximately 2 watts(t).

Three types of promethium sources, using $Pm_2O_3$, have been developed at PNL:

1. A 60-watt(t) source to power a radioisojet (RIJ) developed by the NASA–Goddard Space Flight Center and the General Electric Company.[15] The RIJ was designed to develop a thrust of 0.020 lb, using an ammonia propellant, and was intended for attitude control and station keeping in spacecraft. The RIJ and its heat source were successfully ground tested in 1966.

2. A 60-watt(t) source (Fig. 1) for use as a heater in the guidance systems of aircraft of the U. S. Air Force. The source has been successfully tested by Sandia Corp. and the Air Force.[16,17]

3. Several 15-watt(t) sources for use in dosimetry studies at PNL.

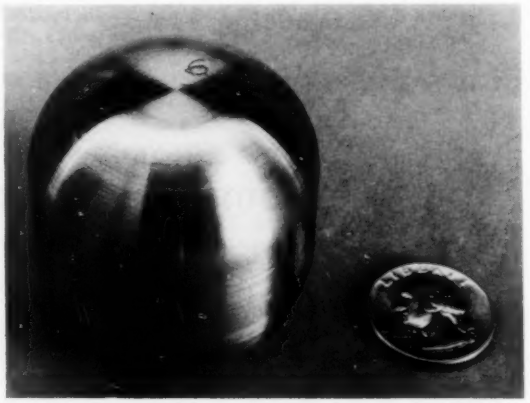

**Fig. 1 A 60-watt promethium oxide heat source.**

The principal isotopes considered for heat sources that have low dose rates are $^{147}Pm$, $^{210}Po$, and $^{238}Pu$. The isotope $^{171}Tm$ has many desirable properties, but the possibility of production on a significant scale has not yet been demonstrated. Promethium is the least hazardous of the available nuclides, since a relatively large amount is permissible in the environment (Table 1). Its half-life is sufficiently long to yield uniform power for missions of short to moderate duration and sufficiently short to permit decay to negligible levels in a reasonable length of time. Containment of some nuclides, e.g., $^{238}Pu$ and $^{90}Sr$, would be required for several centuries.

Isotope selection is sometimes determined by mission-lifetime requirements, but other factors can be more important if two or more isotopes have acceptable half-lives. Integrity of the source for several

half-lives is usually required, and the probability of significant environmental contamination must be acceptably low. Promethium is superior to the alpha emitters because of both its lower biological hazard and the absence of the helium buildup that necessarily accompanies alpha decay. Since promethium decays to a daughter with very similar chemical properties, the source will retain essentially the same chemical properties throughout its lifetime. Alpha emitters, on the other hand, produce helium, which builds up pressure in the source, and their daughters are not chemically similar to the parents.

**Table 1 Properties of Radioisotopes Useful as Heat Sources**

| Isotope | Half-life, years | Specific power, watts/g | Type of decay | Permissible concentration in air | |
|---|---|---|---|---|---|
| | | | | $\mu c/cm^3$ | $\mu w/cm^3$ |
| $^{90}Sr$ | 28 | 0.96 | $\beta$ | $1 \times 10^{-10}$ | $6.8 \times 10^{-13}$ |
| $^{147}Pm$ | 2.62 | 0.33 | $\beta$ | $2 \times 10^{-8}$ | $7.2 \times 10^{-12}$ |
| $^{171}Tm$ | 1.9 | 0.2 | $\beta$ | $4 \times 10^{-8}$ | $7 \times 10^{-12}$ |
| $^{210}Po$ | 0.38 | 144 | $\alpha$ | $7 \times 10^{-11}$ | $2.2 \times 10^{-12}$ |
| $^{238}Pu$ | 87.4 | 0.56 | $\alpha$ | $7 \times 10^{-13}$ | $2.3 \times 10^{-14}$ |

## Availability

Current and potential availability of promethium is adequate to supply many mission requirements. Several megacuries of aged promethium are on hand at PNL in varying degrees of purity and can be fully purified as required. (The need for using aged promethium is discussed below.) The exact amount available from Hanford production reactors has not been published, but, in the Hanford Isotopes Plant study,[7] the availability was assumed to be 30 Mc (i.e., about 10 kw) per year. Additional promethium can be isolated from the Savannah River production reactors, but the amount potentially available has not been published.

Promethium is potentially available in very large amounts from power reactors[18] (Fig. 2). The net yield of $^{147}Pm$ depends on the accumulated exposure of spent fuel and is expected to average between 7 and 11 curies for each megawatt-day of reactor operation. However, the aging required to reduce the gamma-emitting contaminant, $^{148m}Pm$, to negligible proportions (page 211) will reduce the $^{147}Pm$ available from spent-fuel-reprocessing plants by 50% of the amount in the discharged spent fuel.

Promethium can also be made by irradiation of neodymium.[19] Because of the high neutron-capture cross sections of some neodymium isotopes below 146, several neutrons are captured for each atom of $^{147}Pm$ produced. Promethium produced in this manner is likely to be more expensive than fission-product promethium unless a low-cost method for separation of neodymium isotopes can be developed.

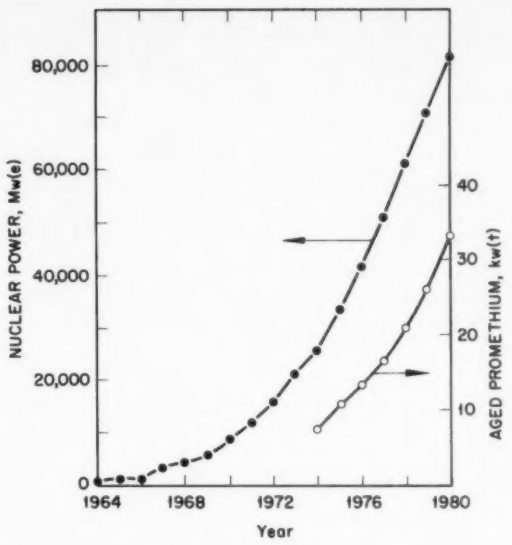


**Fig. 2 Estimated availability of promethium from power reactors, based on estimated growth of nuclear power in the United States (end-of-year basis); developed from data in table in "15th Annual Forecast," *Electrical World* (Sept. 21, 1964, p. 135). The promethium will be available 3.5 years from date power is on line (assuming 33⅓% thermal to electrical conversion, 80% time efficiency, and 90% yield).**

Cost is an important factor in all applications. Promethium is currently available at about $560 per watt, and the cost could be halved by large-scale recovery from power-reactor fuels in a few years if demands were sufficiently great.

## Nuclear Properties

Some of the principal nuclear properties of an aged-promethium radioisotope heat source are summarized in Table 2. The heat generated[20] by $^{147}Pm$ and the half-lives[21,22] of $^{147}Pm$ and $^{146}Pm$ are probably the most important properties since an aged source is principally $^{147}Pm$. The heat generated by other isotopes is negligible, and the isotopic composition is affected by the half-lives. The isotopes $^{146}Pm$ and $^{148m}Pm$ are important, however, since they contribute an appreciable amount of penetrating gamma radiation, while $^{147}Pm$ does not yield any high-energy radiation (Figs. 3 to 5). A source of pure



XUM

$^{147}$Pm would be ideal, but satisfactory promethium isotopic purity for most purposes can be achieved by controlling the reactor conditions and the storage time after discharge from the reactor.

The principal nuclear reactions that form the promethium isotopes of practical interest are shown in Fig. 6. Neutron reactions form the two undesired promethium isotopes from $^{147}$Pm. The most important neutron cross sections are listed in Table 3. Because of the high cross sections of $^{146}$Pm and the $^{148}$Pm isomers, equilibrium among the promethium isotopes is achieved in a few months in most power reactors. Equilibrium ratios depend on the neutron-flux and -energy distribution.

The isotopes $^{146}$Nd, $^{147}$Nd, and $^{148}$Nd are formed in fission either as direct fission products or as a result of decay of short-lived parents. The $^{147}$Nd then decays to $^{147}$Pm. The 147 chain is formed in about 2.1% of the fissions, depending somewhat on the fissioning nuclide.[23] Most of the 146 and 148 chains result in stable neodymium isotopes. Some $^{146}$Pm is also formed as a direct fission product in about $10^{-6}$% of the fissions.[24] Fission yields of the $^{148}$Pm isomers are negligible compared to the amount formed from

**Table 2 Selected Nuclear Properties of Aged Promethium Metal**

| Isotope | Half-life | Specific activity, curies/g | Heat generation |
|---|---|---|---|
| $^{147}$Pm | 2.6234 ± 0.0004 years | 928.4 ± 1.7 | 0.3330 ± 0.0005 watt/g<br>0.3587 ± 0.0006 watt/kc<br>2788 ± 8 curies/watt<br>3.003 ± 0.005 g/watt |
| $^{146}$Pm | 5.53 ± 0.05 years | 0.00023 | |
| $^{148m}$Pm | 43 days | <0.00002 | |
| $^{148}$Pm | 5.4 days | | |

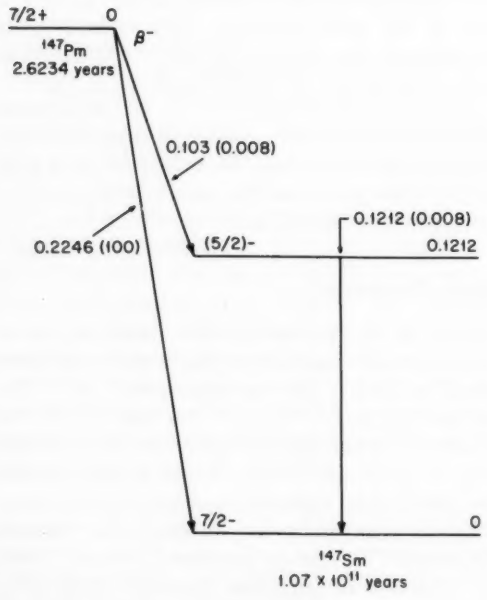


Fig. 3 Decay scheme of $^{147}$Pm.

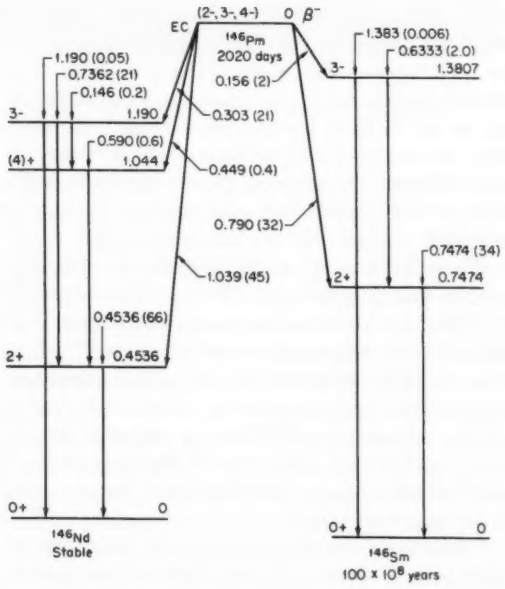


Fig. 4 Decay scheme of $^{146}$Pm.

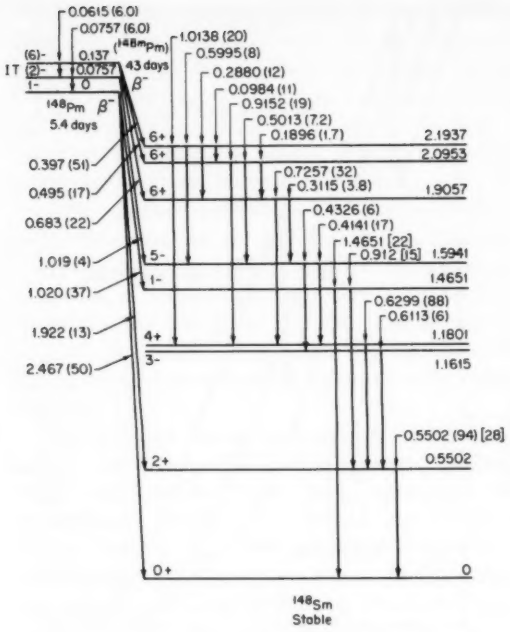


Fig. 5 Decay schemes of $^{148m}$Pm and $^{148}$Pm.

$^{147}$Pm by neutron capture. The $(n,2n)$ reaction with $^{147}$Pm is the most important source of $^{146}$Pm. This reaction requires high-energy neutrons—greater than 7.8 Mev—and therefore the production of $^{146}$Pm is dependent on the neutron spectrum in which the promethium is formed. Under favorable conditions, as in the well-moderated Hanford reactors, the amount of $^{146}$Pm in $^{147}$Pm is about 0.25 ppm on a curie basis.

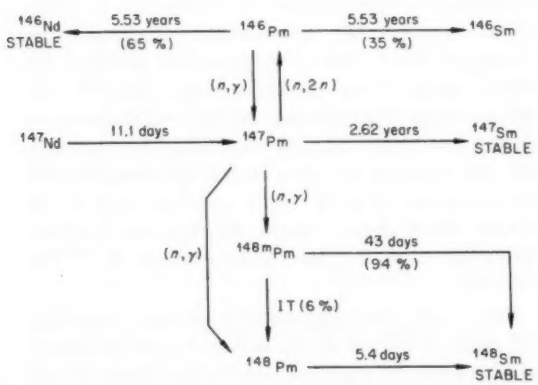


Fig. 6 Methods of formation of promethium isotopes.

Table 3 Neutron Cross Sections of Promethium Isotopes

| Isotope | Cross section, barns | | | |
|---|---|---|---|---|
| | Thermal | Resonance integral | Reactor* | Fission spectrum |
| $^{147}$Pm | 154 | 2,300 | 315 | 0.0059 |
| $^{146}$Pm | | | 8,400 | |
| $^{148m}$Pm | 22,000 | 32,000 | 24,000 | |

*Well-moderated reactor, $r = 0.07$.

As much $^{146}$Pm as 4 ppm has been observed in power-reactor promethium.[25]

At the time the fuel elements are discharged, the penetrating radiation from promethium is essentially all $^{148m}$Pm and $^{148}$Pm. After the fuel has cooled for about one half-life of $^{147}$Pm (2.62 years), the $^{146}$Pm radiation is 10 times that of the $^{148m}$Pm, since the shorter half-life of $^{148m}$Pm (43 days) has permitted most of it to decay (Fig. 7). At even shorter cooling times, the $^{148}$Pm (half-life 5.4 days) has decayed to a negligible value, although a small amount is continually

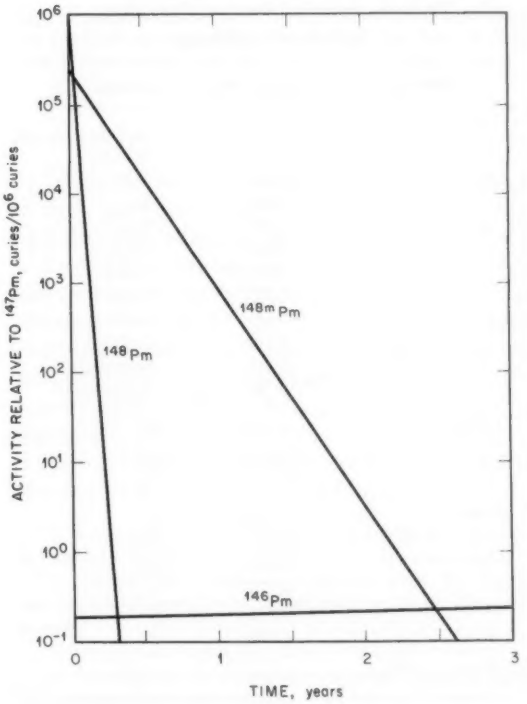


Fig. 7 Relative decay rates of promethium isotopes.



XUM

being formed by decay of $^{148m}$Pm. Promethium for use in radioisotopic power sources must be well aged to minimize radiation from $^{148m}$Pm.

## Shielding

The principal gamma[26] radiations and bremsstrahlung from promethium isotopes are listed in Table 4. The $^{147}$Pm bremsstrahlung is actually a continuum rather than discrete energies as listed, but division into discrete groups is convenient for shielding calculations. The $^{147}$Pm energies are all less than 1 Mev, and the attenuation of $^{147}$Pm radiation is quite dependent on both the atomic number and the mass of the absorber.[6] A plot of the gamma mass-attenuation coefficients for iron, molybdenum, and tantalum[27] vs. photon energy (Fig. 8) shows that at energies above 1 Mev the coefficients are essentially equal for the three absorbers; however, at somewhat lower energies the photoelectric effect becomes important, with higher-atomic-number absorbers having higher mass-attenuation coefficients. At X-ray absorption edges, the photoelectric absorption coefficient changes discontinuously, with the discontinuity corresponding to the minimum energy required to ionize an electron from a particular shell of the absorber atom. The location of these absorption edges depends on the atomic number of the absorber.

**Table 4 Principal Gamma Radiations and Bremsstrahlung**

| Nuclide | Energy, Mev | Abundance, % |
|---|---|---|
| $^{147}$Pm | 0.121 | 0.004 |
| | 0.040* | 0.0034 |
| | 0.02† | 0.74 |
| | 0.04† | 0.17 |
| | 0.06† | 0.064 |
| | 0.08† | 0.026 |
| | 0.10† | 0.011 |
| | 0.12† | 0.0041 |
| | 0.14† | 0.0015 |
| | 0.16† | 0.00042 |
| | 0.18† | 0.000089 |
| | 0.20† | 0.0000091 |
| $^{146}$Pm | 0.454 | 65 |
| | 0.736 | 21 |
| | 0.747 | 34 |
| $^{148m}$Pm | 0.414 | 17 |
| | 0.550 | 93 |
| | 0.630 | 87 |
| | 0.726 | 32 |
| | 0.915 | 19 |
| | 1.014 | 20 |
| $^{148m}$Pm ($^{148}$Pm) | 1.465 | 1.3 |

*Characteristic X ray.
†Bremsstrahlung.

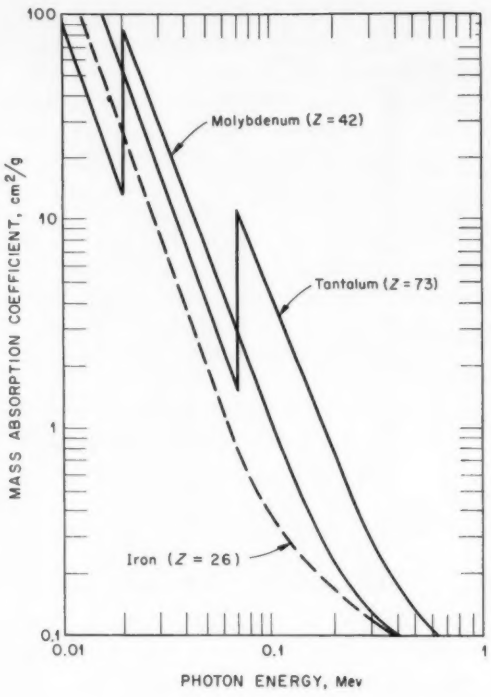


**Fig. 8 Gamma mass-absorption coefficients for molybdenum, tantalum, and iron, plotted on the basis of equal shielding weights.**

The optimum atomic number for shielding promethium bremsstrahlung is about 75; at lower atomic numbers the photoelectric absorption coefficient is lower, and at higher atomic numbers the highest energy X-ray absorption edge occurs at too high an energy, thus allowing radiation to penetrate at energies just below the absorption edge. For example, lead and tantalum are about equal in attenuating the bremsstrahlung (Fig. 9), while stainless steel is far inferior. Below about 2 mr/hr, the dose rate is almost exclusively from the penetrating gammas of $^{146}$Pm (Fig. 10).

Dose rates from promethium sources containing 0.25 ppm $^{146}$Pm are shown in Fig. 11 as a function of uranium-shield thickness and source size. About 0.2 cm of uranium is sufficient to shield out virtually all the $^{147}$Pm radiations, while each 10-fold attenuation of

$^{146}$Pm radiation requires about 1.3 cm of uranium. Since the dose rate due to $^{146}$Pm is directly proportional to its concentration, an increase in the $^{146}$Pm content from 0.25 to 4 ppm will cause the dose rate with a uranium shield more than 0.2 cm thick to be about 16 times that shown in Fig. 11. With less shielding, $^{147}$Pm radiations are controlling.

The neutron-capture cross sections of the promethium isotopes are such that selective decrease in $^{146}$Pm content might be possible by reirradiation of promethium. Experiments are now in progress to determine the extent of $^{146}$Pm burnout and the equilibrium amount that might be expected. Preliminary results show that reduction below 0.15 ppm is possible.

As described below, chemical processing is sufficiently well developed to prevent excessive amounts of other radionuclides from being associated with promethium. Of particular interest are $^{144}$Ce and $^{154}$Eu because of their chemical similarity to promethium and the large amount of highly penetrating radiation associated with them. Their contribution to the total dose rate can be held to less than 1%.

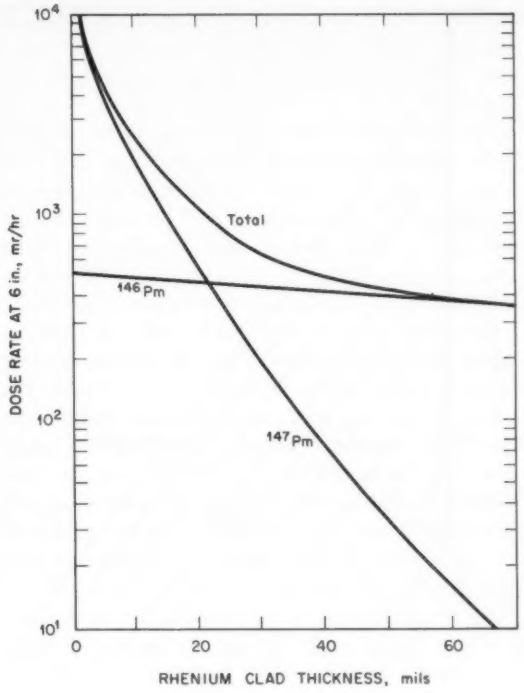


**Fig. 10 Expected dose rates at 6 in. from a 60-watt rhenium-clad promethium source 1 in. in diameter by 2.56 in. long inside.**

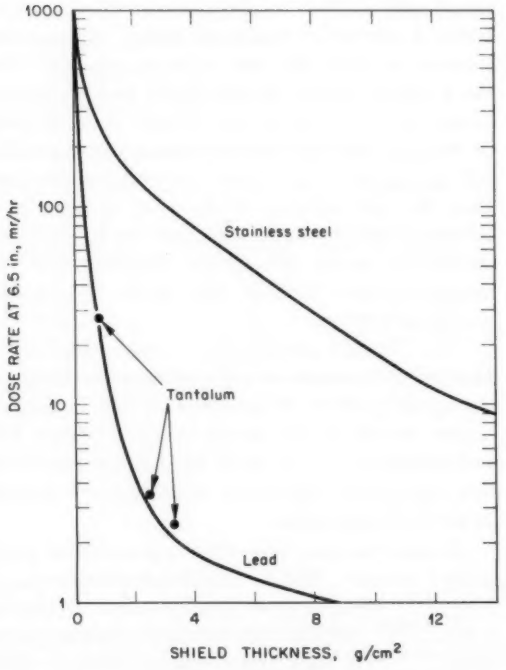


**Fig. 9 Measured dose rates at 6.5 in. from 730 curies of $^{147}$Pm containing 0.25 ppm $^{146}$Pm measured through stainless steel, tantalum, and lead shielding.**

## Production

All the promethium produced in the United States, to date, has been obtained from spent reactor fuels. Recovery, separation, and purification of promethium at the Hanford facilities during the past several years have isolated about 20 Mc of aged promethium as a rare-earth fraction. Of this amount, 3 Mc has been purified and converted to the oxide. Current plans call for purification of approximately 10 Mc during 1969. Approximately 100 g of the purified promethium has been converted to the metal.

The promethium-production process at Hanford may be broken down into five basic operations:

1. Separation of fission products, as a high-activity waste stream, from the plutonium and uranium in the spent fuels.
2. Recovery of a rare-earth fraction from the fission-product waste stream by a precipitation or solvent extraction process.
3. Separation of the cerium from the other rare earths.
4. Separation of the promethium from the other rare earths by chromatographic ion exchange.
5. Conversion of the purified promethium, from the ion-exchange columns, to the sesquioxide ($Pm_2O_3$).



XUM

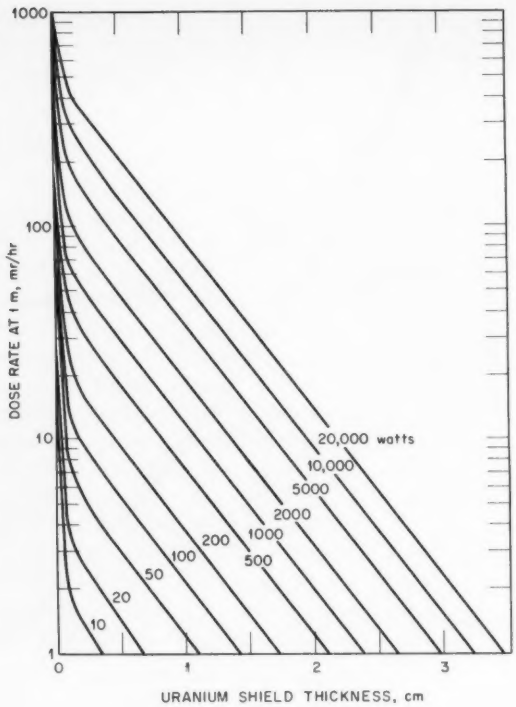


**Fig. 11 Expected dose rates at 1 m from uranium-shielded promethium source containing 0.25 ppm $^{146}$Pm.**

The first three steps of the process are carried out in facilities operated for the AEC by ARHCO, and the last two by PNL.

The Purex flow sheet[28] is used at Hanford in processing spent reactor fuels. The fission-product promethium leaves the process in the high-activity acid waste, from which it can be recovered as a rare-earth fraction. The process used to isolate the 20 Mc that has been recovered at Hanford is a carrier precipitation process developed at Hanford several years ago.[29,30] In this process, strontium coprecipitates with the rare earths and is separated from them by converting the precipitates to acid-soluble salts by carbonate metathesis, dissolving them in acid, and precipitating the rare earths as oxalates. Another method that could be used is solvent extraction.[31,32] A solvent of di-2-ethylhexyl phosphoric acid (D2EHPA), tributyl phosphate (TBP), and a hydrocarbon diluent extracts the rare earths and strontium from the Purex waste, and the strontium is separated from the rare earths by selective stripping of the organic phase. This is the process that will be used under the current waste-management program at Hanford to separate strontium (and rare earths) from Purex acid waste.

Two processes for separating cerium from the other rare earths have been developed in the laboratory and successfully used in the plant.[33-35] In one, a sparingly soluble compound—Ce(IV) peroxyacetate—is precipitated. In the other, cerium is oxidized with silver-catalyzed persulfate and extracted with D2EHPA, using the same solvent–diluent combination that is used in the strontium-recovery process. The solvent extraction process is currently being used at Hanford, but considerable effort has been expended to develop a different oxidation technique. Electrolytic oxidation and various chemical methods have been investigated on a laboratory scale and show promise.[36,37]

After removal of the cerium, the rare-earth fraction is normally stored for at least 2 years prior to the promethium purification. The aged promethium is separated from the other rare earths by chromatographic ion exchange,[38,39] using a process based on the earlier, large-scale Ames[40-43] process for separation of nonradioactive rare earths. The promethium-containing feed is loaded on the first of a series of cation-exchange columns (typically Dowex 50) and eluted sequentially through successive columns with a buffered solution of a selected eluant. The successive columns are preloaded with a cation, e.g., $Zn^{2+}$, that has a higher affinity for the eluant than do the rare earths. Use of the barrier ion restrains the leading edge of the band and prevents the bands from "spreading out" as they do in most other ion-exchange processes. Thus the full capacity of the resin is at all times saturated with the rare earths, and the bands do not increase in length but simply become purer with increased elution distance. This results in a compact and efficient process.

The Hanford contribution consists primarily in adapting the process to highly radioactive feeds and solving the problem of radiolysis of resin, eluant, and barrier. Several eluant–barrier ion combinations have been evaluated,[39,44-46] all of which can be used in the same equipment. The choice of which to use depends on the feed composition.

Eluants that have been used in promethium purification include EDTA (ethylenediaminetetraacetic acid),[44,45] HEDTA (hydroxyethylenediaminetriacetic acid),[44,45] DTPA (diethylenetriaminepentaacetic acid),[39-45] and NTA (nitrilotriacetic acid).[46] NTA, which is currently used at Hanford, with $Zn^{2+}$ as a barrier ion, has a number of advantages over other eluants. In the normal DTPA elution sequence, for-

merly used at Hanford, yttrium is eluted between samarium and neodymium,[47] the sequence being $Zn^{2+}$, $Am^{3+}$, $Gd^{3+}$, $Eu^{3+}$, $Sm^{3+}$, $Y^{3+}$, $Pm^{3+}$, $Nd^{3+}$, $Pr^{3+}$, $Ce^{3+}$, $La^{3+}$. The Y–Pm separation coefficient is significantly smaller than those of Sm–Pm or Pm–Nd. With NTA, yttrium is eluted ahead of the gadolinium, the sequence being $Y^{3+}$, $Gd^{3+}$, $Eu^{3+}$, $Sm^{3+}$, $Pm^{3+}$, $Nd^{3+}$. This shift removes the yttrium from the critical Sm–Pm–Nd zone and results in a larger yield of high-purity promethium.[46]

The NTA process has certain cost advantages over the DTPA process. For one thing, NTA costs about half as much as DTPA. For another, the improved reaction kinetics allows a 100% increase in the rate of band advance while maintaining the necessary separation efficiency. The process cycle time is thus cut in two, with the attendant cost savings. Also, because of the shorter purification cycle, the resin can be used for more purification cycles before radiolytic damage necessitates replacing it.

As shown in the ion-exchange flow sheet currently used at PNL for promethium purification (Fig. 12), 300 g of promethium can be processed in each cycle. Promethium of 99.99% chemical purity can be produced,[45] but, since $^{147}Pm$ decays to stable $^{147}Sm$ at a rate of 2.2% per month, there is little practical advantage in preparing promethium of extremely high chemical purity with respect to neodymium and samarium. Even promethium with a chemical purity of only 99% at the time of purification has very little radiochemical impurity, i.e., $<5 \times 10^{-10}$ curie of total $\alpha$, and $10^{-11}$ curie of $^{154}Eu$, per curie of $^{147}Pm$, with no other detectable activities except other promethium isotopes.[45]

A very recent advance has been the development of a two-cycle flow sheet. Here the promethium is partially purified by ion exchange, as outlined above, and stored; it is finally purified only when a promethium demand arises. This procedure permits higher throughputs in existing equipment and lower operating costs and makes purified promethium available on demand. Several megacuries per run of partially purified promethium [about 1 kw(t)] can be given the final purification in existing small-scale equipment.

The purified promethium from the ion-exchange columns is converted to oxide by addition of oxalic acid to precipitate promethium oxalate, which is subsequently calcined at 1100°C in air or oxygen.

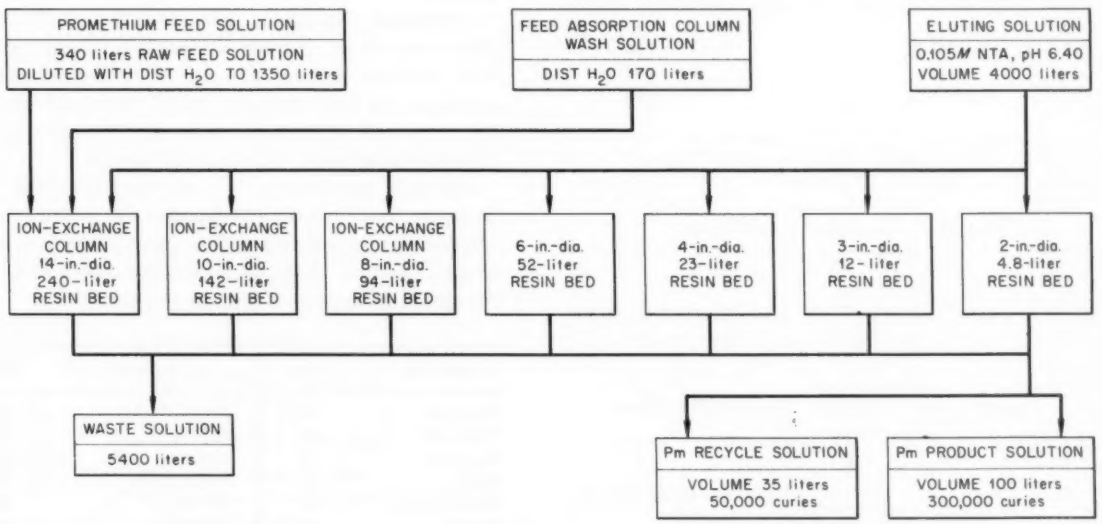


**Run Conditions**

Elution temperature, 60 to 65°C
Feed- and wash-solution flow rates, 3.8 ml/(min)($cm^2$)
Elution-cycle flow rate, 8 ml/(min)($cm^2$)
Rate of band advance, 35 cm/hr
Absorption and wash cycle, 7.5 hr
Elution cycle, 60 hr
Turnaround time, 48 hr

**Fig. 12 Promethium-purification flow sheet.**



XUM

A typical analysis of oxide prepared in this manner is

Chemical purity, >99%
$^{146}Pm$, $2.2 \times 10^{-7}$ curie/curie $^{147}Pm$
$^{148m}Pm$, $7 \times 10^{-9}$ curie/curie $^{147}Pm$
$^{154}Eu$, $2.5 \times 10^{-11}$ curie/curie $^{147}Pm$
Crystal structure, 100% monoclinic

High-purity (>99%) promethium metal has been prepared[47] in multikilocurie quantities at PNL by calcium (+ iodine) reduction of promethium trichloride (Fig. 13). The procedure used is similar to that used for preparation[28] of plutonium metal by bomb reduction of plutonium fluoride.

The promethium metal produced by bomb reduction contains several percent calcium and magnesium impurities. These impurities are removed by melting the promethium in a tantalum crucible under an argon atmosphere and then applying a vacuum to distill off the calcium and magnesium. The purified promethium metal is subsequently cast into a cylinder in a MgO crucible. This gives promethium that is >99% pure. The overall yield is approximately 80%, with most of the promethium "loss" occurring in the vacuum distillation and casting operations. This "lost" promethium is recovered by leaching the slag and crucibles and the process equipment in nitric acid and precipitating the promethium from the leach liquor as the oxalate.

All steps in the preparation of oxide and metal are carried out in a lightly shielded gloved box.

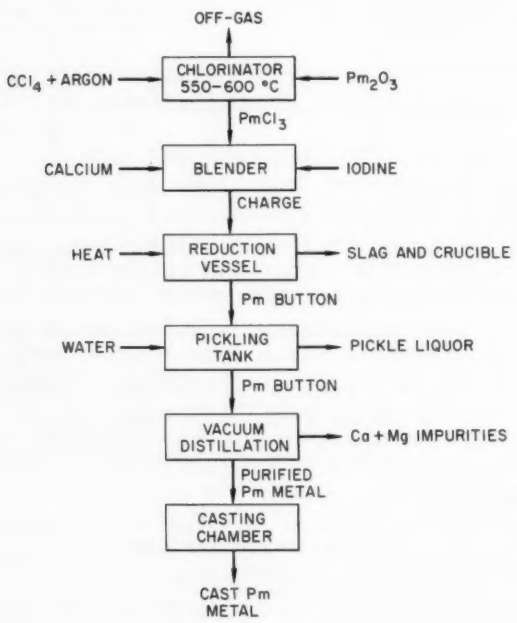


**Fig. 13 Flow sheet for promethium-metal preparation.**

## Chemistry of Promethium

Compared to the other rare earths, only a very limited amount of experimental work has been devoted to the chemistry of promethium and its compounds. Most of the work that has been done has been limited to the recovery and purification of promethium from other fission products. Only the chemistry of the metal and the sesquioxide has been studied in any detail.

The chemical properties of the individual rare-earth elements depend primarily on the electronic configurations of the outer shells which are almost identical for all the rare earths.[48] Because of this similarity in configuration, the rare-earth elements and their compounds should have similar chemical properties, and the data reported in the literature demonstrate this similarity very clearly. We would therefore expect the chemical properties of promethium and its compounds to be quite similar to those of the other rare earths, especially its nearest neighbors—neodymium and samarium.

Published data show that promethium, like the other rare earths, exhibits a tripositive valency, with little evidence of any divalent or tetravalent characteristics. As with other rare earths, we would expect the compounds of promethium to exhibit a high degree of ionic character and little or no covalency.

Weigel[49] and Scherer[50,51] and their coworkers in Germany have prepared a number of promethium compounds and determined their crystal structures and lattice constants. Some of the compounds that have been prepared by various investigators are:

| Compound | Ref. | Compound | Ref. |
|---|---|---|---|
| $Pm_2O_3$-A | 49 | $Pm_2(C_2O_4)_3$ | 53 |
| $Pm_2O_3$-B | 49 | $PmPO_4$ | 49 |
| $Pm_2O_3$-C | 54 | $PmAsO_4$ | 49 |
| $PmCl_3$ | 52 | $Pm_2(CrO_4)_3$ | 50 |
| $PmCl_3 \cdot xH_2O$ | 53 | $PmVO_4$ | 50 |
| PmOCl | 50 | $PmCrO_3$ | 49 |
| $PmBr_3$ | 50 | $PmBO_3$ | 50 |
| PmOBr | 50 | $PmScO_3$ | 50 |
| $PmF_3$ | 49 | $PmInO_3$ | 50 |
| PmOF | 49 | $Pm_2(MoO_4)_3$ | 49 |
| PmOI | 50 | $Pm_2(WO_4)_3$ | 49 |
| $Pm(IO_3)_3$ | 50 | $Pm(HCOO)_3$ | 50 |
| $Pm(NO_3)_3$ | 53 | $Pm(CCl_3COO)_3$ | 50 |
| $Pm(OH)_3$ | 49 | $Pm_2(CO_3)_3 \cdot 2H_2O$ | 50 |

Promethium sesquioxide has been studied in more detail than any other promethium compound because, to date, $Pm_2O_3$ has been the preferred fuel form for promethium heat sources. The properties of $Pm_2O_3$ that have been measured experimentally are summarized in Table 5. Estimated values for a number of chemical, mechanical, and physical properties that have not been measured are summarized in Ref. 64. An extensive program is under way at PNL to measure various properties of the oxide.

Promethium sesquioxide may exist in three different crystal modifications: a cubic phase (C form) stable to about 750°C (Ref. 56); a monoclinic phase[49,57] (B form) stable to above 1600°C; and a hexagonal phase[49,57] (A form), which forms at temperatures above 1600°C. The phase transitions appear to be irreversible. Extensive high-temperature studies at PNL have indicated the possible coexistence of a hexagonal and a monoclinic phase in samples of oxide heated to 1800 and 2350°C (Ref. 56).

Experimental measurements have shown that the dissolution rate of $Pm_2O_3$ in fresh or saline water is quite slow, and the solubility quite low (Table 5). However, when a compacted shape of $Pm_2O_3$ is exposed to water, the shape disintegrates in a few days, apparently due to hydrolysis of the oxide.[61] A cold-pressed and sintered (1400°C) pellet cracked and disintegrated after 5 days' exposure to fresh water at 40°C, and a hot-pressed (1590°C) pellet tested under similar conditions began to disintegrate after a 50-hr exposure. Potential users of the oxide as a heat source should therefore realize that containment of the oxide

**Table 5 Properties of Promethium Sesquioxide**

(Unless Otherwise Noted, the Values Listed Are for the Monoclinic Form of $Pm_2O_3$)

| Property | Value | Ref. |
|---|---|---|
| Crystallography | | |
| C form, bcc | $a = 10.99$ | 54 |
| B form, monoclinic | $a = 14.15$; $b = 3.69$; $c = 8.78$ | 50 |
| A form, hcp | $a = 3.806$; $c = 5.954$ | 50 |
| Density, g/cm$^3$ (obtained from X-ray data) | | |
| C form | 6.84 | 55 |
| B form | 7.43 | 55 |
| A form | 7.62 | 55 |
| Phase-transition temperature, °C | | |
| C → B | 750–800 | 56 |
| B → A | >1600 | 49, 57 |
| Melting point, °C | 2320 | 57 |
| Thermal conductivity, cal/(sec)(cm)(°C) (+ 10% B form $Sm_2O_3$) | 0.006 | 58 |
| Thermal diffusivity, cm$^2$/sec (+ 10% B form $Sm_2O_3$) | 0.0075 @ 75°C<br>0.0040 @ 1600°C | 59<br>59 |
| Thermal expansion, in./(in.)(°C) (+ 12% B form $Sm_2O_3$) | $9.4 \times 10^{-6}$ (70–1000°C) | 60 |
| Solubility in distilled water, g/liter | 0.003 | 59 |
| Dissolution rates, μg/(cm$^2$)(hr) | | |
| $Pm_2O_3$ pellets sintered at 1400°C and 80% of theoretical density | | |
| Seawater | 0.04 | 61 |
| Distilled water | 3.80 | 61 |
| $Pm_2O_3$ powder calcined at 850°C, distilled water | ≥8 | 61 |
| Electrical resistivity, ohm-cm (+ 10% B form $Sm_2O_3$) | $3 \times 10^8$ @ 41°C | 62 |
| Power density, watts/cm$^3$ (at theoretical density) | 2.12 | 20 |



XUM

must be ensured by adequate encapsulation. If the cladding is breached or water contacts the oxide, the oxide shape will disintegrate and the compound will hydrolyze, the hydrolyzed oxide being dispersed into the aqueous medium as discrete particles. Tests with an encapsulated samarium oxide source have shown that a minute water leak causes the $Sm_2O_3$ to hydrolyze and swell, generating tremendous pressures that can rupture the containment vessel. Figure 14 shows a Hastelloy

**Fig. 14 Hastelloy C capsule containing $Sm_2O_3$ after exposure to water.**

capsule ($\frac{1}{8}$ in. wall thickness) containing sintered $Sm_2O_3$ pellets. A $\frac{1}{32}$-in.-diameter hole was drilled in one end of the capsule, which was then placed in water. After a 72-hr exposure, the capsule had swelled and ruptured, as shown, due to hydrolysis of the oxide. One would expect $Pm_2O_3$ to react similarly, and tests are under way at PNL to verify this assumption.

Promethium metal has been studied to a much lesser degree than the oxide. The metal, however, does possess certain properties that make it attractive as a source fuel. These include a higher power density than the oxide and the fact that it can be cast or machined into complex shapes. Properties of the metal that have been determined experimentally are:

| Property | Value | Ref. |
|---|---|---|
| Crystallography: double hexagonal | $a$ = 3.68 A | 63 |
| | $b$ = 11.75 A | |
| Melting point, °C | 1168 ± 6 | 47 |
| Density, g/cm$^3$ (by weight) | 7.22 + 0.02 | 47 |
| (by X ray) | 7.31 | |
| Hardness (Knoop, 500 g) | 63 | 62 |
| Power density, watts/cm$^3$ | 2.40 | |

Estimated values for other properties of the metal are summarized in Ref. 64. Work is now under way at PNL to determine some properties of the metal not previously measured.

## Containment Materials

The use of promethium as a heat source requires an adequate knowledge of the compatibility of the fuel form with containment materials at elevated temperatures. Since the sesquioxide is currently the preferred fuel form, extensive programs are under way at PNL and at private laboratories to determine the compatibility of $Pm_2O_3$ with various materials at temperatures up to 2400°C. Unfortunately the data obtained at PNL are classified and available only to those persons having the necessary access permits. The data developed at private organizations are, for the most part, proprietary, and only a limited amount has been published.[65]

It can be stated, however, that, by the proper selection of a containment material and by using specially purified oxide, $Pm_2O_3$ can be safely used in heat sources up to 1100°C for periods of at least one half-life, and probably much longer. It appears likely that work now under way will extend the useful temperature range of $Pm_2O_3$ sources to temperatures approaching 2000°C. The oxide purification treatment consists in calcining the oxide in oxygen at 1100°C, followed by prolonged heating in hydrogen at 1100°C. This treatment removes impurities such as C, CO, $CO_2$, and $H_2O$, which accelerate oxide–clad interaction. Rhenium appears to be the most satisfactory cladding material over the temperature ranges under investigation.[66]

A program is also under way at PNL to evaluate the compatibility of promethium metal with containment materials. Samarium metal is being used as a stand-in for promethium in the study.

## Heat-Source Fabrication

Although the designs and specifications for the $Pm_2O_3$ heat sources fabricated at PNL have differed markedly, the general fabrication technique outlined below was used for most sources.[15] Specially purified $Pm_2O_3$ was cold pressed into pellets, and the pellets were sintered at 1450°C to increase the density to approximately 90% of theoretical. The pellets were then loaded into a metal capsule (Fig. 15), and a thin layer of foil of the same material as the capsule was pressed into place on top of the pellets. (Aluminum

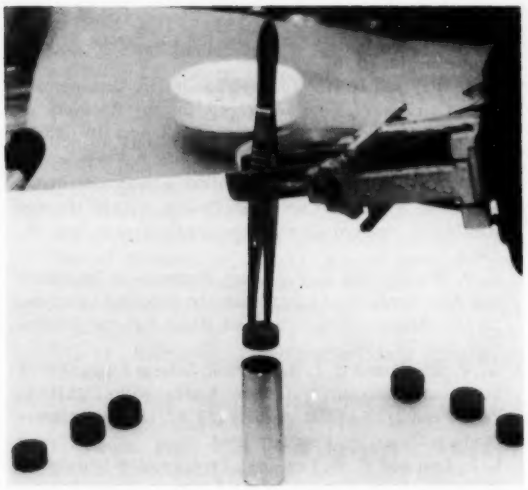

**Fig. 15 $Pm_2O_3$ pellets being loaded into capsule in hot cell.**

foil was wrapped around the capsule during loading to decrease decontamination problems.) The capsule was transferred to a decontamination facility and cleaned, and a lid was pressed into place. The capsule was then transferred to a welding box and closed by electron-beam welding. Weld integrity was checked by various nondestructive test methods. This capsule was placed in a second capsule, which was also sealed by electron-beam welding. Decontamination decreased the smearable contamination on the external surface of both capsules to a nondetectable level. The pellet-pressing and capsule-loading operations were carried out in hot cells as well as in shielded glove boxes, and all welding was done in a glove box or in the working chamber of an electron-beam welder.

The procedure described above has also been used to fabricate a large number of capsules for use in the $Pm_2O_3$ compatibility program at PNL.

Details of the fabrication techniques used at private companies are not available.

Although cold-pressed and sintered pellets of $Pm_2O_3$ have been used in fueling most of the promethium heat sources fabricated at PNL, other methods of fabricating the oxide into useful shapes have been evaluated, including pneumatic impaction,[67] step pressing,[68] plasma spheroidization,[14,69] hot pressing,[70] slip casting,[71] cold pressing of Al–$Pm_2O_3$ composites,[72] and sol–gel spheroidization. Each method has certain advantages and disadvantages. Selection of which procedure to use in compacting the oxide will depend on source specifications, e.g., density, size, and dimensional tolerances.

Promethium metal has a major advantage over the oxide as the fuel form in heat-source applications: The metal can be fusion-cast into the desired shape in magnesia crucibles or it can be machined into shapes not obtainable by casting.[47] Close dimensional tolerances can be maintained in both operations. However, both casting and machining of the metal must be carried out in a vacuum or inert atmosphere to prevent oxidation.

Promethium feed material is available for fabrication of additional sources as needs arise. Technology for producing heat sources has been demonstrated with promethium using cold-pressed and sintered pellets as well as with promethium in a metal matrix. Other fabrication technology has been demonstrated in making compatibility capsules for promethium, or by using samarium or neodymium stand-ins. Promethium properties are characterized well enough to permit a wide variety of applications that take advantage of its favorable biological and half-life aspects. (MG)

## References

References marked with an asterisk have not been verified by the editors; for further explanation, see the Foreword.


1. H. G. J. Moseley, The High-Frequency Spectra of the Elements, *Phil. Mag. (Ser. VI)*, **27**: 703-713 (1914).
2. M. L. Pool and L. L. Quill, Radioactivity Induced in the Rare Earth Elements by Fast Neutrons, *Phys. Rev.*, **53**: 437-446 (1938).
3. Earlier work described by J. A. Marinsky, L. E. Glendenin, and C. D. Coryell, The Chemical Identification of Radioisotopes of Neodymium and of Element 61, *J. Amer. Chem. Soc.*, **69**: 2781-2785 (1947).
4. C. A. Rohrmann, *Radioisotopic Heat Sources* and *Supplementary Data*, USAEC Reports HW-76323 and 78180, Hanford Atomic Products Operation, 1963.
5. E. D. Arnold, Handbook of Shielding Requirements and Radiation Characteristics of Isotopic Power Sources for Terrestrial, Marine, and Space Application, USAEC Report ORNL-3576, Oak Ridge National Laboratory, April 1964; summarized in *Isotop. Radiat. Technol.*, **2**(1): 72-81 (Fall 1964).
6. H. H. Van Tuyl, F. P. Roberts, and E. J. Wheelwright, Shielding Requirements for Promethium Sources, USAEC Report HW-77375, Hanford Atomic Products Operation, April 1963.
7. C. A. Rohrmann, Hanford Isotopes Plant, *Isotop. Radiat. Technol.*, **2**(2): 99-123 (Winter 1964–1965).
8. A. Bradley, Observations on Packaged $^{147}_{61}$Pm-Activated Phosphor Light Sources, *Int. J. Appl. Radiat. Isotop.*, **13**: 15-18 (1962).
9. L. Mandel, The $\beta$-Ray Absorption Spectrum of $^{147}$Pm and




XUM

Its Application to Thickness Measurement, *Brit. J. Appl. Phys.*, **5**: 287-289 (1954).

10.*S. Enomoto and T. Tanemura, at Symposium on Radiochemical Methods of Analysis, Salzburg, October 1964 (Paper SM-68/5). (Not in proceedings.)

11. R. H. Barnes, R. L. Ritzman, J. F. Kircher, and D. N. Sunderman, Fabrication Studies on $^{147}$Pm Betavoltaic Batteries, USAEC Report BMI-1709, Battelle Memorial Institute, Jan. 25, 1965.

12. A. Scharman, A Photoelectric Radionuclide Battery and Its Limits, in *Industrial Applications for Isotopic Power Generators*, pp. 645-653, UKAEA–ENEA Symposium Proceedings, Harwell, 1966, European Nuclear Energy Agency, OECD, Paris.

13. Compact and Versatile Radioisotope Heaters, Atomics International, Canoga Park, Calif., brochure [summarized in *Isotop. Radiat. Technol.*, **5**(2): 154 (Winter 1967–1968)].

14. R. S. Cooper, R. A. Andelin, and R. K. Robinson, Development of High-Temperature Isotope Heat Sources—$^{147}$Pm, *Trans. Amer. Nucl. Soc.*, **10**: 453-454 (1967).

15.**Radioisojet Program Summary Report*, X-734-67-475, Goddard Space Flight Center, Greenbelt, Md., September 1967.

16.*N. C. Davis and D. W. Brite, Promethium-147 Radioisotope Application Program, AMSA Heat Source, Final Report, USAEC Report BNWL-994, Pacific Northwest Laboratory, March 1969.

17. W. J. Dalby, AMSA Fuel Capsule Impact Tests, USAEC Report SC-DR-67-718, Sandia Corp., August 1967.

18. C. A. Rohrmann, Values in Spent Fuel from Power Reactors, *Isotop. Radiat. Technol.*, **6**(1): 19-41 (Fall 1968).

19. R. W. McKee, An Evaluation of the Prospects for Large-Scale Production of $^{147}$Pm, USAEC Report BNWL-310, Pacific Northwest Laboratory, August 1966.

20. E. J. Wheelwright, D. M. Fleming, and F. P. Roberts, Calorimetric Determination of the Mean Beta Energy and Half-Life of $^{147}$Pm, *J. Phys. Chem.*, **69**: 1220-1223 (1965).

21. Mound Laboratory Progress Report for Chemistry: October–December 1966, USAEC Report MLM-1399, Dec. 30, 1966.

22. L. R. Bunney and E. M. Scadden, Decay Characteristics of $^{146}$Pm, Report USNRDL-TR-1109, U. S. Naval Radiological Defense Laboratory, Nov. 7, 1966.

23. S. Katcoff, Fission Product Yields from Neutron-Induced Fission, *Nucleonics*, **18**(11): 201-208 (1960).

24. F. P. Roberts, E. J. Wheelwright, and H. H. Van Tuyl, Detection of $^{146}$Pm Among the Products of Uranium Fission, *J. Inorg. Nucl. Chem.*, **25**: 1298-1300 (1963).

25. F. P. Roberts and H. H. Van Tuyl, Promethium-146, Fission Product, and Transuranium Isotope Content of Power Reactor Fuels. Comprehensive Chemical Analysis, USAEC Report BNWL-45, Pacific Northwest Laboratory, March 1965.

26. *Nucl. Data, Sect. B*, **2**(4): 1-120 (December 1967).

27. J. H. Hubbell and M. J. Berger, Photon Attenuation and Energy Transfer Coefficients. Tabulations and Discussion, Report NBS-8681, National Bureau of Standards, May 10, 1965.

28. J. M. Cleveland, in *Plutonium Handbook, Vol. II*, Chapters 14, 15, O. J. Wick (Ed.), Gordon and Breach, Science Publishers, Inc., 1967.

29. L. A. Bray and H. H. Van Tuyl, Laboratory Development of a Carrier–Precipitation Process for the Recovery of Strontium from Purex Wastes, USAEC Report HW-69534, Hanford Atomic Products Operation, May 9, 1961.

30. H. H. Van Tuyl, Report of Invention—Improvements of Strontium Sulfate Precipitation Process, USAEC Report HW-74036, Hanford Atomic Products Operation, June 18, 1962.

31. R. P. Wischow and D. E. Horner, Recovery of Strontium and Rare Earths from Purex Wastes by Solvent Extraction, USAEC Report ORNL-3204, Oak Ridge National Laboratory, Jan. 29, 1962.

32. W. W. Schulz and G. L. Richardson, Solvent Extraction of Strontium, Cesium, and Rare Earths with D2EHPA, Parts 1 and 2, USAEC Report HW-79762, Hanford Atomic Products Operation, February 1964.

33. L. F. Lust and H. H. Van Tuyl, Peroxyacetate Separation of Ce(IV) from Trivalent Rare Earths in Purex Process Solutions, USAEC Report HW-73135, Hanford Atomic Products Operation, Mar. 26, 1962.

34. E. J. Wheelwright and N. C. Howard, The Separation of Cerium from the Trivalent Rare Earths Using Hydrogen Peroxide and Sodium Acetate, USAEC Report HW-62505, Hanford Atomic Products Operation, Aug. 15, 1960.

35. L. A. Bray and F. P. Roberts, Hanford Atomic Products Operation, unpublished data, October 1963.

36. R. E. McHenry, Separation of $^{144}$Ce from Other Rare Earths by Electrolytic Oxidation and Differential Extraction, USAEC Report ORNL-TM-657, Oak Ridge National Laboratory, February 1965.

37. R. E. Lerch, Oxidation of Ce(III) by Ozone and by Electrolysis, USAEC Report BNWL-805, Pacific Northwest Laboratory, August 1968.

38. E. J. Wheelwright and F. P. Roberts, Development and Demonstration of an Ion-Exchange Process for Kilogram-Scale Production of High-Purity Promethium, USAEC Report HW-78651(Rev.), Hanford Atomic Products Operation, October 1963.

39. P. B. Orr, Ion-Exchange Purification of $^{147}$Pm and Its Separation from $^{241}$Am with Diethylenetriaminepentaacetic Acid as the Eluant, USAEC Report ORNL-3271, Oak Ridge National Laboratory, July 6, 1962.

40. E. J. Wheelwright, F. H. Spedding, and G. Schwarzenbach, The Stability of the Rare Earth Complexes with Ethylenediaminetetraacetic Acid, *J. Amer. Chem. Soc.*, **75**: 4196-4201 (1953).

41. F. H. Spedding, J. E. Powell, and E. J. Wheelwright, The Use of Copper as the Retaining Ion in the Elution of Rare Earths with Ammonium Ethylenediaminetetraacetate Solutions, *J. Amer. Chem. Soc.*, **76**: 2557-2561 (1954).

42. J. E. Powell and F. H. Spedding, The Separation of Rare Earths by Ion Exchange, *Trans. Met. Soc. AIME*, **215**: 457-463 (1959).

43. J. E. Powell and F. H. Spedding, Basic Principles Involved in the Macroseparation of Adjacent Rare Earths from Each Other by Means of Ion Exchange, in Adsorption, Dialysis, and Ion Exchange, *Chem. Eng. Progr., Symp. Ser.*, **55**(24): 101-112 (1959).

44. E. J. Wheelwright and T. R. Myers, Parametric Evaluation

of DTPA, EDTA, and HEDTA for Ion-Exchange Purification of Promethium, USAEC Report BNWL-69, Pacific Northwest Laboratory, September 1965.

45. E. J. Wheelwright, F. P. Roberts, U. L. Upson, L. J. Kirby, T. R. Myers, and H. H. Van Tuyl, Ion-Exchange Separation of Kilocurie Quantities of High-Purity Promethium, USAEC Report BNWL-318, Pacific Northwest Laboratory, December 1966.
46. E. J. Wheelwright and T. R. Myers, Investigation of NTA as a Replacement for DTPA in the Ion-Exchange Purification of Promethium, USAEC Report BNWL-SA-1493, Pacific Northwest Laboratory, Mar. 8, 1968.
47. E. J. Wheelwright, Preparation of $^{147}Pm$ Metal and Determination of the Density and Melting Point, USAEC Report BNWL-959, Pacific Northwest Laboratory, January, 1969.
48. F. H. Spedding and A. H. Daane, *The Rare Earths*, John Wiley & Sons, Inc., New York, 1961.
49. *F. Weigel, *Fifth Rare Earth Research Conference—Book 3*, Iowa State University, Ames, Iowa, 1965.
50. V. Scherer, Chemistry of Promethium (in German), USAEC file No. NP-16254, Munich University, 1966.
51. V. Scherer, Research on Binary and Ternary Oxides of Promethium, Thesis (in German), USAEC file No. NP-15339, Munich University, 1965.
52. J. G. Conway and J. B. Gruber, Luminescence Spectrum of $PmCl_3$, *J. Chem. Phys.*, **32**: 1586-1587 (1960).
53. G. W. Parker and P. M. Lantz, The Separation of Milligram Quantities of Element 61 from Fission, USAEC Report AECD-1996, Oak Ridge National Laboratory, 1948.
54. A. S. Wilson, F. P. Roberts, and E. J. Wheelwright, Promethium Oxide Structure, *Nature*, **198**: 580 (1963).
55. F. Weigel and V. Scherer, Chemistry of Promethium. II. Polymorphism of Pm(III) Oxide (in German), *Radiochim. Acta*, **4**: 197-203 (1965).
56. T. D. Chikalla and F. P. Roberts, Pacific Northwest Laboratory, unpublished data, 1967.†
57. C. E. McNeilly, P. G. Pallmer, and C. M. Cadwell, Pacific Northwest Laboratory, unpublished data, 1968.†
58. R. L. Gibby, Pacific Northwest Laboratory, unpublished data, 1967.†
59. R. L. Moore (Ed.), Pacific Northwest Laboratory, Division of Isotopes Development Programs Quarterly Report, October–December 1967, USAEC Report BNWL-680, January 1968.
60. R. P. Nelson and T. D. Chikalla, Pacific Northwest Laboratory, unpublished data, 1968.†
61. H. T. Fullam and F. P. Roberts, Pacific Northwest Laboratory, unpublished data, 1968.†
62. T. D. Chikalla, Pacific Northwest Laboratory, unpublished data, 1967.†
63. P. G. Pallmer and T. D. Chikalla, Pacific Northwest Laboratory, unpublished data, 1968.†
64. H. T. Fullam and H. H. Van Tuyl, Promethium Isotopic Power Data Sheets, USAEC Report BNWL-363, Pacific Northwest Laboratory, February 1967.
65. R. A. Andelin, J. D. Watrous, and W. E. Ferguson, High-Temperature Compatibility Testing of Radioisotope Fuel-Container Systems, *Trans. Amer. Nucl. Soc.*, **10**: 430-431 (1967).
66. United States Atomic Energy Commission Annual Report, 1966, pp. 209-210.
67. E. J. Wheelwright and V. L. Hammond, The Densification and Encapsulation of Isotopic Fuels by High Energy Pneumatic Impaction, USAEC Report HW-81332, Hanford Atomic Products Operation, Oct. 26, 1964.
68. H. T. Fullam and L. J. Kirby, Cold Pressing and Sintering of Rare Earth Oxides, USAEC Report BNWL-386, Pacific Northwest Laboratory, April 1967.
69. *E. A. Snajdr and D. W. Brite, Processing $Pm_2O_3$ and $Sm_2O_3$ by RF Induction Plasma Heating To Produce High Density Microspheres, American Ceramic Society Annual Meeting, Chicago, Ill., April 1968.
70. H. T. Fullam and C. J. Mitchell, Hot Pressing of Rare Earth Oxides, USAEC Report BNWL-448, Pacific Northwest Laboratory, June 1967.
71. *H. T. Fullam, Slip Casting of Rare Earth Oxides, USAEC Report BNWL-437, Pacific Northwest Laboratory, June 1967.
72. *H. T. Fullam, Cold Pressing of Aluminum–$Pm_2O_3$ Composites, USAEC Report BNWL-1014, Pacific Northwest Laboratory, 1969.

†Data are available in classified AEC reports. Access permit holders can obtain report numbers by contacting appropriate authors at BNWL.



XUM

# Study of $^{171}$Tm as Power Source for Circulatory-Support System*

By J. K. Poggenburg†

**Abstract:** *A study of production methods for and properties of $^{171}$Tm indicated that the limited production capacities and extremely high estimated cost—more than $30 thousand per watt—make it impracticable as a power source for a circulatory-support system. The technical and economic factors were considered for targets of natural erbium, enriched $^{170}$Er, and natural thulium.*

Thulium-171 is one of the power-source candidates for an implantable circulatory-support system. The light shielding required and the small size in which the ultimate devices might be manufactured make it worthy of consideration. However, cost must also be considered in designing such a system, and the power source chosen will be dictated by several factors.

The properties of $^{171}$Tm pertinent to the proposed use are:

| | |
|---|---|
| Half-life, years | 1.9 |
| Beta emission ($E_{max}$), Mev | 0.97 (98%); 0.030 (2%) |
| Photon emission, Mev | Bremsstrahlung; 0.067 gamma (0.2%); X rays |
| Specific power, watt/g | |
| Pure nuclide | 0.2 |
| $^{171}Tm_2O_3$ | 0.175 |

A suitable fuel form ($Tm_2O_3$) exists, which has a very low biological toxicity.[1] The oxide is stable, melts at 2380°C, and, by analogy with other rare-earth oxides, should be compatible with a number of source-container materials. The decay product, ytterbium, is a rare earth and is chemically similar to the parent.

A study was therefore made of $^{171}$Tm production and properties to evaluate the feasibility of the use of this nuclide in a circulatory-support system. The properties of $^{238}$Pu, the nuclide most likely to be used, served as the criterions for radiation exposure, shield weight, and total heat-source weight.

## Reactor Production of $^{171}$Tm

Thulium-171 can be produced in a nuclear reactor by irradiation of $^{170}$Er, either natural (14.88% abundance) or isotopically enriched:

$$^{170}\mathrm{Er} \xrightarrow{(n,\gamma)} {}^{171}\mathrm{Er} \xrightarrow[7.5\ \mathrm{hr}]{\beta^-} {}^{171}\mathrm{Tm}$$

or of $^{169}$Tm (100% natural abundance):

$$^{169}\mathrm{Tm} \xrightarrow{(n,\gamma)} {}^{170}\mathrm{Tm} \xrightarrow{(n,\gamma)} {}^{171}\mathrm{Tm}$$

The $^{171}$Tm product of any of these irradiations is contaminated by $^{170}$Tm (Fig. 1). In the erbium irradiation the $^{168}$Er (27.07% natural abundance) is first converted to $^{169}$Tm,

$$^{168}\mathrm{Er}(n,\gamma)^{169}\mathrm{Er} \xrightarrow[9.4\ \mathrm{days}]{\beta^-} {}^{169}\mathrm{Tm}\ (\mathrm{stable})$$

which follows the same course as the natural thulium. In the $^{169}$Tm irradiation, of course, the $^{170}$Tm intermediate is not completely converted to $^{171}$Tm.

The $^{170}$Tm contaminant is a significant factor in determining the suitability of $^{171}$Tm as an implantable source. It has a half-life of 128.5 days and decays by a 0.97-Mev beta emission, which produces an energetic and intense bremsstrahlung. There is 23% branching to an excited state at 0.084 Mev, and, although the 0.084-Mev gamma transition is highly converted, photon emission occurs in 3% of the disintegrations. Because of the effect of these radiations on dose rates, even though the $^{170}$Tm disintegration rate is only $10^{-5}$ to $10^{-6}$ of the $^{171}$Tm, the $^{170}$Tm determines the shielding needed for a $^{171}$Tm source. Further, the amount of $^{170}$Tm that can be tolerated in a source determines the cost and capabilities of producing a suitable $^{171}$Tm product. A practical basis for setting the $^{170}$Tm limit is the stipulation that a $^{171}$Tm power source should not yield a dose rate greatly exceeding that of $^{238}$Pu having the same total source and shield weight.

Satisfactory rates of production of $^{171}$Tm from either erbium or thulium require a neutron flux of at least $10^{15}$ n/(cm$^2$)(sec). Since such a high flux is not obtained in commercial power reactors, special reactors are necessary. The production capacities and costs for a hypothetical 1000-Mw reactor were used for calculating $^{171}$Tm production rates in the study reported here.

*Based on Report ORNL-4283, which gives many more details.

†Isotopes Development Center, Oak Ridge National Laboratory, Oak Ridge, Tenn. 37830.

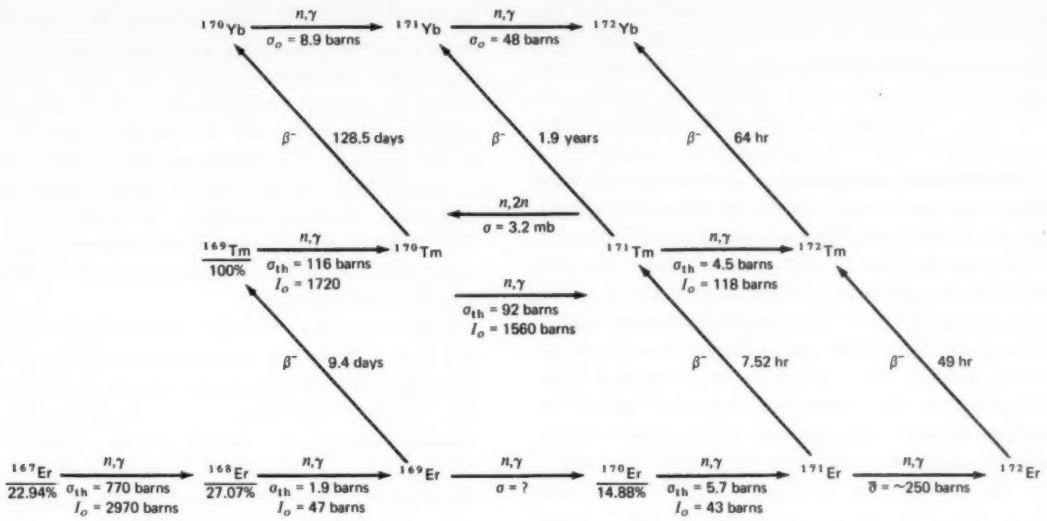


**Fig. 1 Nuclear reactions involved in production of $^{171}$Tm from erbium or thulium. The underscoring indicates stable nuclides and the percentages, natural abundances.**

Capital costs for such a reactor have been projected at about $100 million, and annual operating costs at about $15 million.[2] A 1000-Mw reactor burns about 1 kg of $^{235}$U per day, at a cost of $4.5 million per year. Since the fuel cost is about a third of the total cost and the ratio of neutrons released per neutron absorbed by $^{235}$U is 2.08, the cost for 1 g of neutrons is about $7 thousand. More than half these neutrons will either be absorbed by the structural components of the reactor or leak out. Thus the cost per gram of productive neutrons will be from $15 thousand to $20 thousand.

The power output of a reactor is proportional to the fission rate of the fuel, and the maximum is fixed by the reactor design. The fission rate is directly proportional to both the neutron flux and the quantity of fuel present. In order to increase the flux within the design power limitation, the fuel density must be decreased—a scheme that naturally results in shorter fuel cycles and increased operating expenses. With lighter fuel loading, the reactor becomes even more susceptible to flux depression resulting from neutron consumption in a target, and the problem becomes one of counterbalancing the conflicting requirements of high-flux operation against efficient isotope production.

Some general conclusions can be drawn on how first-order effects of neutron absorption act to limit the target capacity of a reactor. Of the 2.08 neutrons released per neutron absorbed in $^{235}$U, 1.08 are in excess of the number required to sustain the fission rate, and only half of these are available for productive absorption in the target. If a flux is to be maintained at a given level, the approximate neutron-absorption rate in the target (product of flux and cross section) must not exceed the rate at which neutrons are made available for that purpose. For a flux of $10^{15}$ n/(cm$^2$)(sec), the absorption rate in a target of $\sigma$ (barns) cross section is about $\sigma A \times 10^{-4}$ n/day per mole of target,* where $A$ is $6.02 \times 10^{23}$. A 1000-Mw reactor with a fission rate of about 1 kg of $^{235}$U per day makes available about $2A$ n/day for target consumption. The target loading capacity of the reactor is therefore about $(2/\sigma) \times 10^4$ moles. Thus the loading capacity of the reactor varies inversely with both the target cross section and the operating flux.

### Natural Erbium

The production of $^{171}$Tm from natural erbium (Table 1) proceeds by two reaction routes:

$$^{170}\text{Er (stable)} \xrightarrow{(n,\gamma)} {}^{171}\text{Er} \xrightarrow{\beta^-} {}^{171}\text{Tm}$$

*Using the approximation 1 day = $10^5$ sec, the daily consumption at $10^{15}$ n/(cm$^2$)(sec) is $10^{-4}$ $\sigma$ n/atom of target, or $\sigma A \times 10^{-4}$ n/(day)(mole).



XUM

and

$$^{167}\text{Er (stable)} \xrightarrow{(n,\gamma)} {}^{168}\text{Er (stable)} \xrightarrow{(n,\gamma)} {}^{169}\text{Er}$$

$$\xrightarrow{\beta^-} {}^{169}\text{Tm (stable)} \xrightarrow{(n,\gamma)} {}^{170}\text{Tm} \xrightarrow{(n,\gamma)} {}^{171}\text{Tm}$$

The first route predominates at short exposures. With longer irradiation times the second route is significant because of the larger natural abundances of $^{167}$Er and $^{168}$Er and because of the relatively large neutron-capture cross sections of $^{169}$Tm and $^{170}$Tm. The very large cross section of $^{167}$Er also makes it significant in the second route and places severe restrictions on reactor loading. The second route produces $^{170}$Tm contamination and causes the large $^{170}$Tm/$^{171}$Tm activity ratio in the product, which makes radio-isotopic refinement necessary.

**Table 1 Isotopic Composition of Natural Erbium**

| Mass No. | Amount, % | Mass No. | Amount, % |
|---|---|---|---|
| 162 | 0.136 | 167 | 22.94 |
| 164 | 1.56 | 168 | 27.07 |
| 166 | 33.41 | 170 | 14.88 |

The advantage of using natural erbium as a target material is its current availability in large amounts at comparatively low cost. The price for the oxide is about $180 per kilogram. Chemical separation of $^{171}$Tm from the erbium target and ytterbium decay products would be required, probably by ion exchange, for which capital costs would be about $3 million and annual operating costs, about $0.5 million.

Calculation of the production of $^{171}$Tm from natural erbium after a 1-year irradiation in a flux of greater than $10^{15}$ n/(cm$^2$)(sec) ($10^{15}$ thermal plus 10% resonance-energy neutron contribution) indicates that 10.6 n are captured for every atom of $^{171}$Tm obtained. The cost of $^{171}$Tm calculated by using the estimate of $15 thousand to $20 thousand per gram of neutrons thus ranges from $4700 to $6200 per watt.

Estimation of the target loading capacity of the reactor [$(2/\sigma) \times 10^4$ moles] gives 20 kg for natural erbium with a cross section of 160 barns. Figure 2 shows a $^{171}$Tm yield of 7% after a 1-year exposure at $10^{15}$ n/(cm$^2$)(sec), and the annual output of $^{171}$Tm is therefore only about 0.3 kw for a 1000-Mw reactor, at a cost of $50 thousand per watt. It would be advantageous to expose the natural erbium to a preliminary lower flux [about $5 \times 10^{14}$ n/(cm$^2$)(sec)] to burn out $^{167}$Er and decrease the target cross section, thereby increasing the loading capacity of the higher-flux production reactor. By this scheme it would be possible to approach a production-reactor output of 2 kw annually at a product cost of about $7500 per watt. The product would, however, have a $^{170}$Tm/$^{171}$Tm activity ratio of about 1, and further refinement would be necessary. To reach the $10^{-4}$ to $10^{-5}$ range of activity ratio, three calutron refinement stages would be required, at a cost of $35 thousand to $45 thousand per watt.

The variation of $^{171}$Tm yield as a function of time and flux is shown for natural-erbium targets in Fig. 2. This figure gives the atomic percentage of $^{171}$Tm and the $^{170}$Tm/$^{171}$Tm activity ratio resulting from continuous irradiation of a natural-erbium target at fluxes of $2 \times 10^{14}$ and $1 \times 10^{15}$ n/(cm$^2$)(sec). A 10% contribution from resonance-energy neutron absorption is assumed. The abundance of thulium isotopes in the target after a 1-year irradiation is:

| Flux, n/(cm$^2$)(sec) | $2 \times 10^{14}$ | $1 \times 10^{15}$ |
|---|---|---|
| Thulium isotope abundance in target, at. % | | |
| $^{169}$Tm | 0.91 | 1.15 |
| $^{170}$Tm | 0.37 | 1.07 |
| $^{171}$Tm | 0.935 | 7.03 |
| Activity ratio, $^{170}$Tm/$^{171}$Tm | 2.1 | 0.8 |
| Atomic ratio, $^{169}$Tm/$^{171}$Tm | 0.97 | 0.16 |

If the thulium product from the $10^{15}$-n/(cm$^2$)(sec) flux is chemically separated from the erbium target and inserted again in the same flux, it would take about 1.5 years to attain a product with a $^{170}$Tm/$^{171}$Tm activity ratio of $10^{-4}$ to $10^{-5}$. The $^{171}$Tm yield would then be down to a third of its initial value. For the reactor refinement method to be effective, the erbium content must be decreased to 0.01%. The separated erbium could then be blended with natural erbium and recycled as feed that would be low in $^{167}$Er and not require the suggested first-cycle low-flux irradiation. Eventually the $^{170}$Er content would be decreased to the point that further recycling would be impractical. It appears feasible that, by using at least two 1000-Mw reactors and this recycled-target process, $^{171}$Tm of requisite quality could be produced at a rate of 1 kw/year. Capital costs would thus be about $200 million for reactors, plus $3 million for a chemical separation plant. Annual operating costs would be $30 million for reactors and about $0.5 million for the chemical separation plant. The cost of a suitable $^{171}$Tm product would range from $30 thousand to $40 thousand per watt.

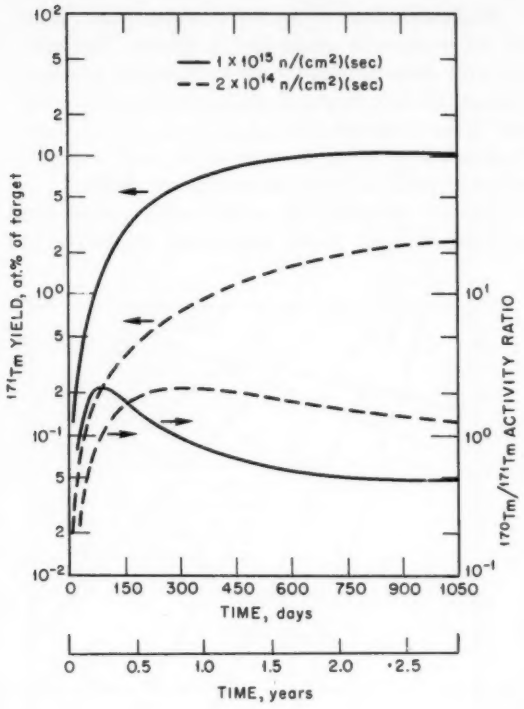


**Fig. 2 Yield and activity ratio as a function of irradiation time for natural erbium.**

There is a possible variation on the production of $^{171}$Tm from natural erbium. Since $^{170}$Tm contamination results from the capture of a second neutron by the $^{169}$Tm formed in decay of $^{169}$Er, it is obvious that for short irradiations [e.g., 0.5 day at a flux of $10^{14}$ n/(cm$^2$)(sec)] the $^{170}$Tm contamination is extremely low. In principle, then, it is possible to irradiate natural erbium briefly at low flux and separate chemically a $^{171}$Tm product having $10^{-5}$ part of $^{170}$Tm activity. However, $^{171}$Tm would constitute less than $10^{-3}$% of the natural-erbium target. Because erbium and thulium are practically indistinguishable chemically, the recovery of low concentrations of $^{171}$Tm from the erbium target would require a multistage separation facility based on advanced technology, the cost of which would be prohibitive.

### Enriched $^{170}$Er Targets

Production of $^{171}$Er from enriched $^{170}$Er is potentially the most economical and productive method if the present limitations and costs of highly enriched target material can be substantially altered by technological breakthroughs in isotopic separations. While the prospect for such a development is not immediate, it offers the most promising means of substantially decreasing costs and increasing production capacity.

To obtain a product with a $^{170}$Tm/$^{171}$Tm activity ratio of $10^{-4}$ to $10^{-5}$, the target enrichment must be greater than 99.99% $^{170}$Er. The best enrichment currently obtainable is only 96% from a single calutron pass, with a reasonable prospect for 99% enrichment. A two-stage calutron enrichment would be required with current technology. The requisite $^{170}$Er target is not currently available and is, in fact, the prime bottleneck in this production scheme.

A study of neutron economy in the production of $^{171}$Tm from $^{170}$Er shows that the number of neutrons required for each atom of $^{171}$Tm formed ranges from slightly more than the theoretical minimum of 1 to about 2, the number depending on the length of the irradiation cycle before chemical separation. This number yields a cost estimate of $450 to $600 per watt for irradiation costs, based on neutron costs. The favorable neutron economy means that the target payload is highest for $^{170}$Er. With a 5.6-barn cross section, the loading capacity of the reactor is about 600 kg at $10^{15}$ n/(cm$^2$)(sec). With 90-day cycles the annual output from one reactor would be about 18 kw of $^{171}$Tm of product quality, which leads to an irradiation cost estimate of $830 per watt, based on assumed operating costs of $15 million per year. This is the largest reactor output among the three modes of production. Another advantage is that much lower fluxes can be tolerated—5 x $10^{14}$ n/(cm$^2$)(sec), for example—but volume limitation rather than flux depression is the limiting factor in reactor capacity.

With highly enriched $^{170}$Er, no further radioisotopic refinement is necessary, but chemical separation to recover the valuable target material is required. This production scheme would require the largest chemical separation facility, probably using ion exchange, and capital costs might run to more than $5 million, with annual operation costing about $1 million. With an 18-kw annual production, however, the unit chemical processing cost is about $55 per watt.

The annual $^{170}$Er target requirements of a single 1000-Mw reactor will be about 110 kg, assuming about 10% processing loss in irradiation. Such requirements cannot reasonably be met with existing facilities for isotopic separations. With a two-stage enrichment using calutrons operating with two arcs at 10 to 15% process efficiency, 85% retention, and 30 ma total ion current,



XUM

each machine will produce 0.58 g of $^{170}$Er per day in the first refinement stage. For second-stage refinement, single-arc operation has been found to result in better mass separation than with two arcs; each machine will produce about 1.92 g of $^{170}$Er per day. Thus the need for about 110 kg/year implies the need for some 160 machines for the second-stage refinement and some 760 for the first-stage. Since they would operate ~80% of the time, the number of machines required will be ~1150. No such capacity is available, and a rough estimate of capital costs for such a plant is $\$1 \times 10^9$. A reasonable estimate for operating costs of a new facility is \$600 per machine per day. If 25% of the $^{170}$Er is lost during second-stage enrichment, the target material would cost \$1600 per gram or \$8100 per watt of $^{171}$Tm product.

The total $^{171}$Tm product cost, per watt, resulting from irradiation of enriched $^{170}$Er would be ~\$9000:

| | |
|---|---|
| Enriched target | \$8100 |
| Chemical separation | 55 |
| Reactor irradiation | 830 |
| | \$8985 |

There is no advantage in using $^{170}$Er of single-stage enrichment. The $^{171}$Tm product would have to be refined further by being irradiated for 1.4 years at a flux of greater than $1.5 \times 10^{15}$ n/(cm$^2$)(sec), and the cost would be \$14 thousand per watt.

The above statements are based on an optimized system for large-scale production. The capacity for such production is nonexistent, and capital costs seem prohibitive if the interim role of radioisotopic power in the heart program is acknowledged. Production on a smaller scale would increase the unit cost, probably by a factor of 2 or 3. Any method of increasing isotopic enrichment of $^{170}$Er which may be lower in capital and operating costs could substantially improve the outlook for this method of production. At present there are no known compounds of erbium that are volatile, except under vacuum and at elevated temperatures, which might afford a practical basis for isotope separation.

### Natural-Thulium Targets

The main problems with the double neutron-capture reaction to produce $^{171}$Tm from natural ($^{169}$Tm) thulium are the need for long-term irradiations to deplete the $^{169}$Tm and $^{170}$Tm intermediate and the high flux that must be used to minimize loss through decay of $^{170}$Tm during irradiation.

Thulium is one of the less abundant rare earths, and its commercial availability is limited. The latter drawback does not appear to be a serious problem, however, because potential production capacity could meet future demands. The current price of \$3000 per kilogram of oxide may be expected to drop eventually to about \$1600 per kilogram upon greater demand.

Figure 3 illustrates the activity ratio attained as a function of time under continuous irradiation at

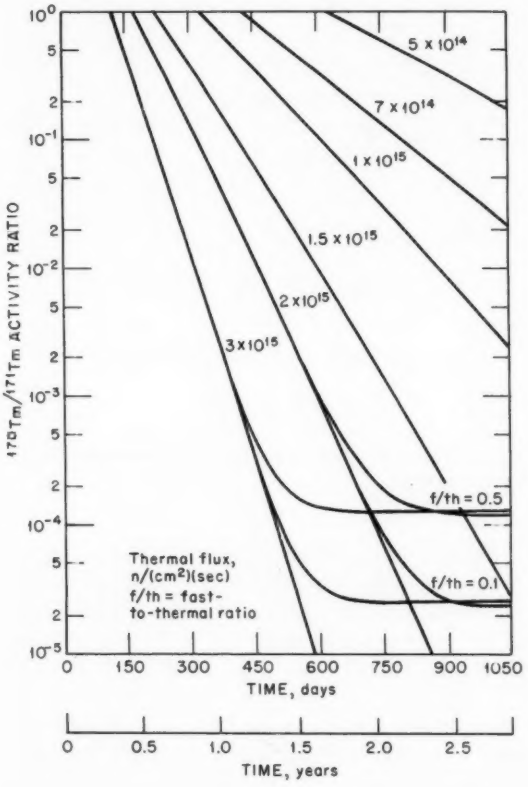


**Fig. 3 Activity ratio as a function of irradiation time and flux for natural $^{169}$Tm.**

various effective fluxes (i.e., under the assumption of no flux depression or self-shielding of the target). These corrections to the nominal flux will, in fact, be significant. Also shown in Fig. 3 is the limiting effect that a fast-flux component has on the attainable activity ratio. The effect of resonance-neutron capture in decreasing the irradiation time required and increasing the yield is shown in Fig. 4. The activity ratio and corresponding percentage yield of $^{171}$Tm from the

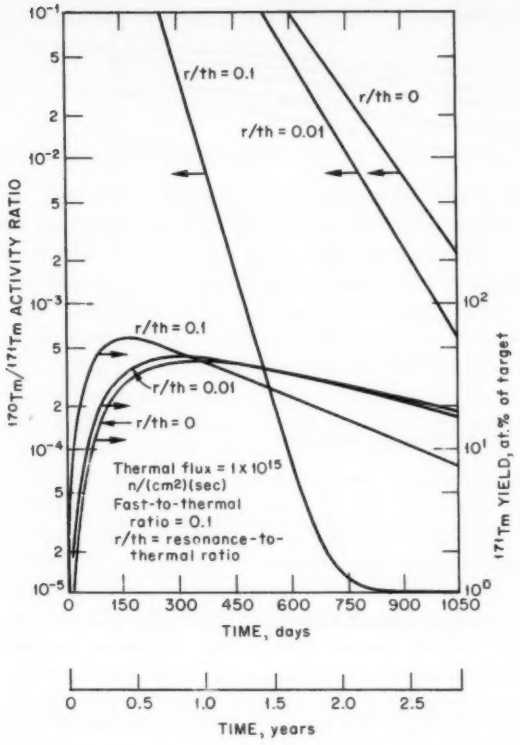


**Fig. 4 Yield and activity ratio as a function of irradiation time for natural $^{169}$Tm.**

target are plotted as a function of time for continuous irradiation at an effective thermal flux of $10^{15}$ n/(cm$^2$)(sec), with assumed effective resonance-flux components of 0, 1, and 10%. Because of the large resonance integrals of $^{169}$Tm and $^{170}$Tm, a high resonance-energy flux is desirable. The self-shielding effect is also severe for the same reason, and target dilution is required to achieve a large effective contribution from the resonance flux and to minimize flux depression. The relation of the $^{171}$Tm yield from the target to the desired activity ratio and to the effective flux at which it is produced is shown in Fig. 5.

The irradiated targets will require chemical processing to separate the thulium from the ytterbium-decay products, probably by electrolytic reduction with sodium amalgam. Such a technique has been tested and found to be effective in rapidly removing ytterbium from thulium. This process would be considerably cheaper than ion exchange, and processing costs would be negligible compared with irradiation costs.

The reactor capacity for the initial natural-thulium target (116 barns cross section) is about 30 kg of thulium. The average cross section will decrease as $^{169}$Tm and $^{170}$Tm are converted to $^{171}$Tm, but the output based on the 30-kg loading at an effective flux of $10^{15}$ n/(cm$^2$)(sec) with about 10% yield in 3.5 years is about 0.2 kw annually. If the flux is doubled, the loading capacity is halved but the yield will be 20% for an irradiation time of 1.75 years, and the $^{171}$Tm output will increase to about 0.3 kw annually. Higher flux favors higher outputs, but this advantage is offset by shorter fuel cycles and increased costs. After substantial fractions of $^{169}$Tm and $^{170}$Tm are burned out, the loading capacity is increased, but this gain must also be traded off against costs of target processing and fabrication. An annual output of 0.25 kw of product $^{171}$Tm from a single reactor operating at $2 \times 10^{15}$ n/(cm$^2$)(sec) appears to be feasible, with a price range of $50 thousand to $75 thousand per watt, based on annual operating expenses of $15 million for the reactor.

## Refinement of Product Radioisotopes

The optimum rate for $^{171}$Tm production in a 1000-Mw reactor by irradiation of any of the three targets does not necessarily result in a product with a $^{170}$Tm/$^{171}$Tm activity ratio of $10^{-4}$ to $10^{-5}$. The methods that can change this ratio by a factor of 50—the factor expected for a single pass in a calutron—are natural decay, reactor irradiation, and electromagnetic separation. The processing costs, which must, of course, be included in total product costs, are calculated from the relation

$$U_o\$_o = U_i\$_i + P_oU_o$$

(i.e., the total processing cost is the cost of the initial product being processed plus the processing costs)

where $U_i$ = units in
$U_o$ = units out
$\$_i$ = cost per unit in
$\$_o$ = cost per unit out
$P_o$ = process cost per unit out

The cost per unit of product is:

$$\$_o = \$_i(U_i/U_o) + P_o$$

where $U_i/U_o$ is the reciprocal of the process yield. In comparisons involving a very large initial unit cost, the process yield can be much more important than the process cost per unit out.



XUM

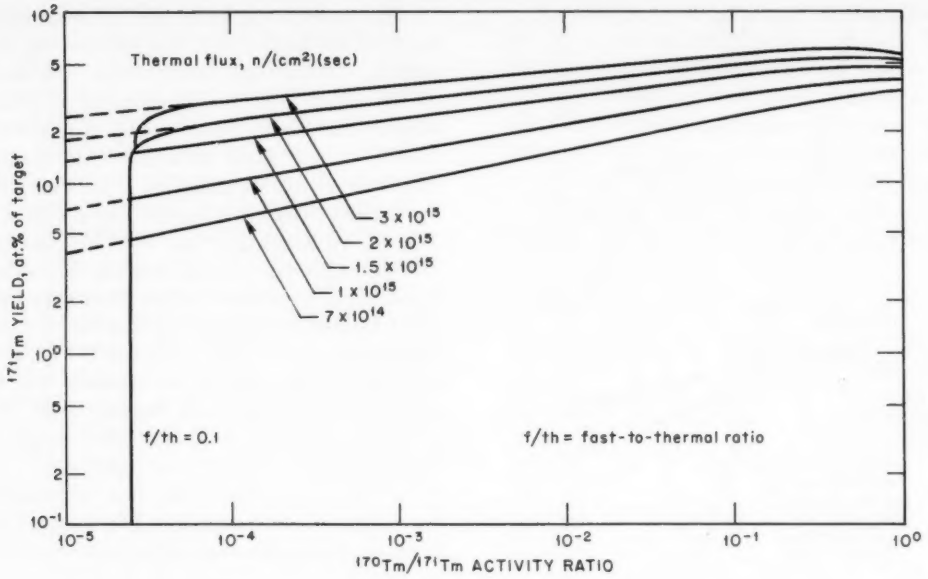


**Fig. 5 Yield from natural $^{169}$Tm as a function of activity ratio at various thermal fluxes and a fixed fast-to-thermal flux ratio of 0.1.**

### Natural Decay

Since $^{170}$Tm has a shorter half-life than $^{171}$Tm, the $^{170}$Tm content of the product can be decreased by aging. In 1 year $^{170}$Tm decays to 0.140 of its original value, but, at the same time, $^{171}$Tm decreases to 0.694 of its initial value; the $^{170}$Tm/$^{171}$Tm ratio thus changes by a factor of 5. The cost of refining $^{171}$Tm by this method, if storage costs are negligible, increases the unit cost as a result of decay according to the expression $(1.44)^x$, where $x$ is the number of years. The cost per watt of product for decreasing the $^{170}$Tm/$^{171}$Tm activity ratio by a factor of 5 is

$$\$_o = 1.44\$_i$$

### Reactor Irradiation

The $^{170}$Tm/$^{171}$Tm ratio can be decreased by neutron irradiation in a reactor since the neutron-capture cross section of $^{170}$Tm is 24 times that of $^{171}$Tm. To obtain significant advantage over natural decay, the neutron flux must be greater than $5 \times 10^{14}$ n/(cm$^2$)(sec). Furthermore, the effectiveness of reactor irradiation is decreased if $^{169}$Tm is a substantial fraction of the product. Thus reactor irradiation is most advantageous for refining a $^{171}$Tm product that has been chemically separated from an enriched $^{170}$Er starting target. On the other hand, the product from irradiation of natural erbium contains comparable amounts of $^{169}$Tm and $^{170}$Tm from neutron capture of the lower erbium isotopes and decay of $^{169}$Er. Any production of $^{171}$Tm from $^{169}$Tm is equivalent to prolonging the production irradiation.

The limitations on reactor refinement due to the fast-neutron reaction $^{171}$Tm$(n,2n)^{170}$Tm must be considered for any practical application. The cross section for this reaction imposes the limit:

$$\text{Activity ratio of } ^{170}\text{Tm}/^{171}\text{Tm} \approx 2 \times 10^{-4}\ (\phi_f/\phi_{th})$$

where $\phi_f/\phi_{th}$ is the ratio of the fission-spectrum average flux to the thermal-neutron flux. This ratio could be as high as 0.5 for an exceptionally hard neutron spectrum, but a value of about 0.1 is more typical of reactor spectrums. A hard spectrum is clearly undesirable for this refinement.

Irradiation in a flux of $1.5 \times 10^{15}$ n/(cm$^2$)(sec) for 1 year changes the $^{170}$Tm/$^{171}$Tm activity ratio by a factor of about 500, while the $^{171}$Tm is decreased to about half its initial value. The cost of the 1-year irradiation results in a factor-of-2 increase in the unit cost, plus an incremental irradiation and processing cost of \$750 ± \$150 per watt. The cost per watt of

product for decreasing the $^{170}Tm/^{171}Tm$ activity ratio by this factor of 500 is

$$\$_o = 2\$_i + 750$$

### Electromagnetic Separation

The cost of electromagnetic separation is difficult to estimate because no large-scale calutron refinement experience is available with shielded facilities and radioactive operations. Tentative extrapolations can be made from Oak Ridge National Laboratory calutron separations of a few radioisotopes at the curie level. The amount of shielding required depends greatly on the anticipated $^{170}Tm$ contamination, and the length of a separation cycle might well be determined solely by considerations of radiation safety. Calutron operating experience has shown that about 15% collection efficiency can be anticipated for each cycle. Overall recovery, after processing and decay losses, is estimated to be 65%. The separation factor for adjacent-mass rare earths is about 50, so that the $^{170}Tm/^{171}Tm$ ratio will be altered by a factor of about 50 with each pass. Since isotope separators are current-limited devices, the collection rate for $^{171}Tm$ product is a linear function of its atom concentration in the charge. Thus the lower the $^{171}Tm$ content, the higher the operating cost allocation per unit of product because $^{171}Tm$ must carry the full cost.

An estimate of the operating cost for a shielded calutron based on two-arc ion-source operation with 30 ma total ion current is \$2500 (±20%) per day. This type of operation, although not common, appears to be feasible. Since 1 ma-day is required to collect approximately 1 mmole of material, some 2.5 g would be collected per day of operation if 50% operating time is assumed. If $f$ is the weight fraction of $^{171}Tm$ in the feed, then the separation cost per product unit is $\$1000/f$ per gram, or $\$5000/f$ per watt. The unit cost of the charge material is multiplied by a factor of 1.5 to account for an assumed process loss of 35%. Refinement by electromagnetic separation would be limited to starting materials with a low $^{170}Tm/^{171}Tm$ ratio where $f$ is near unity. The cost per watt of product for decreasing the $^{170}Tm/^{171}Tm$ activity ratio by a factor of 50 is

$$\$_o = 1.5\$_i + 5000/f$$

### Comparison of Processing Costs

The processing costs for the three methods discussed are:

| Method | Process cost per watt of product ($P_o$) | Yield factor ($U_o/U_i$) | Process time |
|---|---|---|---|
| Natural decay | Assumed negligible | 0.41 | 2.44 years |
| Reactor irradiation | ~\$500 | 0.69 | 0.62 year |
| Electromagnetic separation | ~\$5500 | ~0.65 | ~0.5 watt/day per calutron |

## Comparison of Production Methods

The three production methods are summarized and compared in Table 2. The method currently offering the best reactor yield and price is that of recycling natural erbium. The price range for a product with a $^{170}Tm/^{171}Tm$ activity ratio of $10^{-4}$ to $10^{-5}$ is \$30 thousand to \$40 thousand per watt. The use of enriched $^{170}Er$ target holds the greatest promise for increased production capacity and prices less than \$10 thousand per watt. A major advance in technology for separating erbium isotopes could reduce the cost to a few thousand dollars per watt.

The use of one 1000-Mw reactor was chosen as the basis of comparison, except for the natural-erbium method, which requires at least two such reactors. These results are necessarily broad-range estimates. In order to narrow the range, more detailed study is required, with consideration of the characteristics of particular reactors, but the present study defines the obvious problems for large-scale production.

The annual requirement for $^{171}Tm$ was set at 600 kw. This is based on studies[2] sponsored by the National Heart Institute, which indicated that 2 to 5 watts of power will provide for normal patient activity. If a 15% conversion efficiency is assumed, the thermal source[3] must supply ~30 watts. The projection[4] for annual patient load is of the order of 10,000, which implies the need for a total annual power of ~300 $kw_{th}$. For a short-lived isotope like $^{171}Tm$, the annual requirement would be 600 $kw_{th}$ to allow for radioactive decay losses. Even the most productive method covered in this report would require more than thirty 1000-Mw reactors and a capital outlay of \$30 billion to meet this requirement. The production of $^{171}Tm$ from recycled natural erbium is technically feasible at present with a 1000-Mw production reactor, but the 600-kw objective would require 600 such reactors.



XUM

**Table 2 Comparison of $^{171}$Tm Production Methods**

| | Natural erbium | Natural $^{169}$Tm | Enriched $^{170}$Er |
|---|---|---|---|
| | **Reactor Production** | | |
| Minimum facilities | At least two 1000-Mw reactors | One 1000-Mw reactor | One 1000-Mw reactor |
| Procedures | Preliminary low flux to remove $^{167}$Er or blending of recycled Er remaining after chemical separation of Tm | Irradiation at a flux of $>10^{15}$ n/(cm$^2$)(sec) for ~2.5 years; probable chemical processing and compaction of targets for final refinement stage | Flux of $<10^{15}$ n/(cm$^2$)(sec) (very high flux not required) |
| | Irradiation at a flux of $>10^{15}$ n/(cm$^2$)(sec) for ~1 year to produce $^{171}$Tm | | |
| | Chemical separation of Tm and recycle of Er target in first step | | |
| | Reirradiation of Tm at a flux of $>10^{15}$ n/(cm$^2$)(sec) to remove $^{170}$Tm | | |
| | **Target Material** | | |
| Requirements | ~180 kg/year | ~8 kg/year | ~110 kg/year of 99.99% enrichment |
| Availability | Unlimited commercial oxide | Potentially unlimited commercial oxide | Not available; separation plant required |
| | **Chemical Processing** | | |
| Method | Ion-exchange separation of Er, Tm, and Yb | Sodium-amalgam extraction of Yb from Tm | Ion-exchange separation of $^{170}$Er, Tm, and Yb |
| | **$^{171}$Tm Product** | | |
| $^{170}$Tm/$^{171}$Tm ratio | $10^{-4}$ to $10^{-5}$ | $10^{-4}$ to $10^{-5}$ | $10^{-4}$ to $10^{-5}$ |
| Production capacity, kw/1000 Mw-year | ~1 | ~0.25 | ~18 |
| Cost range per watt | $30,000–40,000 | $50,000–75,000 | ~$9,000–10,000 |
| | **Capital Costs,* Millions** | | |
| Reactors | $200 | $100 | $ 100 |
| Chemical processing | 3 | 2 | 5 |
| Isotopic separations | | | 1000 |
| Total capital | $203 | $102 | $1105 |
| | **Annual Operating Costs,* Millions** | | |
| Reactor | $ 30 | $ 15 | $ 15 |
| Target materials | 0.03 | 0.01 | 165 |
| Chemical processing | 0.5 | 0.4 | 1 |
| Total operating | $ 30.53 | $ 15.41 | $ 181 |

*Costs are approximate.

## Conclusions

The present capacity for producing $^{171}Tm$ is severely limited by the fact that special reactors capable of fluxes in excess of $10^{15}$ n/(cm$^2$)(sec) must be used. In order to realize the low dose rates desired for the circulatory-support system, the $^{170}Tm$ contamination in a heat source must be extremely low. The $^{170}Tm/^{171}Tm$ activity ratio must be in the range $10^{-4}$ to $10^{-5}$ so that dose rates equivalent to those expected from a $^{238}Pu$ source will not be exceeded. The lowest cost range for a suitable $^{171}Tm$ product within present reach is $30 thousand to $40 thousand per watt using a recycled natural-erbium target. Increased productive capacity and a price substantially less than $10 thousand per watt could be attained if a significant breakthrough were made in producing highly enriched $^{170}Er$ cheaply. Even if this should be achieved, the cost would greatly exceed current estimates of ~$500 per watt for $^{238}Pu$. Because of both the limited capacity to produce a heat-source product meeting stringent dose-rate limitations and the high cost estimate of such a product, it is not practical to consider $^{171}Tm$ for large-scale use in the artificial heart program. (MG)

## References


1. R. J. Everett, Radiological Health Aspects of $^{170,171}Tm$ Oxide, USAEC Report SC-RR-66-2679, Sandia Corp., February 1967.
2. B. I. Spinrad, Limitations of Steady State, High Flux Reactors, Current and Future, in Intense Neutron Sources, Proceedings of a U. S. Atomic Energy Commission–European Nuclear Energy Agency Seminar on Intense Sources, September 19–23, 1966, Santa Fe, N. Mex., USAEC Report CONF-660925, p. 316.
3. Hittman Associates, Inc., Final Summary Report on Six Studies Basic to the Consideration of the Artificial Heart Program, Report PB-173-483.
4. D. W. Cole, W. E. Mott, and L. A. Sagan, Factors Relating to the Application of Radioisotopes to Circulatory Support Systems, Intersociety Energy Conversion Engineering Conference, Boulder, Colo., August 13–16, 1968 (see pp. 138-145, this issue of *Isotop. Radiat. Technol.*).


# In-Phantom Dosimetry of $^{147}Pm_2O_3$ Heat Sources in Relation to Circulatory-Support Systems*

By F. T. Cross† and J. C. Sheppard‡

The overall objective of the in-phantom dosimetry program at the Pacific Northwest Laboratory is to develop the dosimetry of suitable implantable radioisotopes for circulatory-support systems. The approach is a combination of experimentation and computation. The experimentation provides a measure of the dose rates surrounding an implanted radioisotopic heat source, while the latter is concerned with the development of a computational code that can predict the measurements. The computational code allows dose-rate values to be generated for directions and locations in tissue that are not readily or easily measured. It is also useful for predicting dose rates obtainable from other source–shield types and geometries, especially when prototypes cannot be measured.

The dosimetry of cold-pressed and sintered $Pm_2O_3$ sources of nominal 15-watt (t) rating, containing about 44.1 kilocuries of $^{147}Pm$ and small quantities of $^{146}Pm$ impurity, is reported herein. Various protocols in the predictions and measurements on implantable sources are included. They are expected to be generally applicable, the procedures changing only in minor respects, depending on the type of radiations to be measured.

*This is a modified version of Report BNWL-1018, published by Battelle Memorial Institute, Pacific Northwest Laboratory, Richland, Wash. 99352, June 1969. Available from CFSTI.

†Radiological Sciences Department, Environmental and Radiological Sciences Division, Battelle–Northwest.

‡Chemical Technology Department, Chemistry and Metallurgy Division, Battelle–Northwest.

## Procedure for Computing the Dose Rates Surrounding an Implanted Radioisotopic Heat Source

The approach for characterizing the dose rates surrounding an implanted isotopic power source was to borrow the procedures used in radiology. Ground rules



XUM

such as the Paterson–Parker[1] and Quimby[2] systems are available for developing the dosimetry for planar and volume implants when a larger number of needles are used. Recently, to save time, computer codes such as the M. D. Anderson[3] method have been developed which utilize the coordinates of the individual needles as determined by stereoroentgenograms to calculate the dose at various points on a superimposed three-dimensional grid system. The dose within any organ of interest would be determined by averaging the appropriate grid points. The development of computer codes was a necessary extension of the earlier work, mainly because of an increased patient load which increased the dosimetry effort and to free the radiologist from the geometry restrictions or ground rules referred to above. Although an attempt is usually made to place the individual sources in the configurations necessary for referral to tabulated doses, the sources are very often skewed from the intended positions.

Because only one source is used in the artificial heart system, there was no compelling reason to complicate the in-phantom dose-rate predictions by developing a computer code that treats all the parameters needed to characterize the dose rates from distributed sources. Therefore a computer code was sought that would characterize the dose rates surrounding a source placed in an "infinite" homogeneous tissuelike medium in order to predict the physical measurements on a source placed "centrally" in a phantom. The perturbations from placement near the phantom surface or near other density organs such as the lung or bone are handled by correcting the dose rates predicted or measured for a homogeneous medium. The characterization consists of dose-rate tabulations or profiles as a function of source configuration and distance from the surface or geometric center of the source.

The methods are in keeping with the dose-rate tabulations and profiles presently used by radiologists and radiation physicists. If the source configuration and orientation are known from roentgenograms, the distances to the various points or organs of interest can be scaled, and, by consulting the tabulations or profiles, the dose rates can be determined.

The perturbations of the dose-rate fields arising from interposed bone or lower-density cavities such as the lung are accounted for by estimating the water (used to represent tissue) centimeter-equivalents of bone and lung tissue. For the 0.6-Mev average photon energy from $^{146}$Pm, these are obtained from the relative electron densities of water and those of the perturbing medium. Thus, from an absorption viewpoint, 1 cm of bone is equivalent to 1.66 cm of water; 1 cm of air is equivalent to 0.0012 cm of water; and 1 cm of lung tissue is equivalent to about 0.30 cm of water. If there is no reduction in dose due to the inverse-square effect, the correction to the depth dose (as estimated from the tumor–air ratios by Johns[4]) per centimeter of tissue bolus is 6.4% at the $^{146}$Pm energies. Thus 1 cm of bone should reduce the depth dose by $(1.66 - 1)6.4 = 4.2\%$; 1 cm of air should increase it by $(1 - 0.0012)6.4 = 6.4\%$; and 1 cm of lung tissue should increase the depth dose by $(1 - 0.30)6.4 = 4.5\%$. These estimates are based upon data for sources outside the body at an "infinite" source–skin distance and for a radiation-field size of 100 cm$^2$. When applied to an implantable heat source, it might be expected that the values would be appropriate to large source–dosimeter distances since the corrections depend on this parameter and the field size. Since the corrections are approximations, and rather small values at that, the choices might be –4%, +4%, and +6% per centimeter for bone, lung, and air, respectively.

The interpretation for bone is as follows: All depth-dose values beyond the interposed bone are reduced by about 4% per centimeter of bone from the value that would be found at the same depth in tissue. Inside the bone the dose will be altered by the ratio of $\overline{f}$ (bone) to $\overline{f}$ (tissue), or 0.963, interpolated from values listed[5] in NBS Handbook 85. An example of the use of these data follows: Suppose the depth-dose rate at 5 cm into tissue is 10% of that at the source surface and 2 cm of bone is interposed at 3 cm. The actual depth-dose rate at 5 cm is 0.92 x 10%, or 9.2%. Inside the bone the dose is altered by 0.963$d$ (tissue). The dose rate just inside the bone at about 5 cm, therefore, is 0.963 x 9.2%, or 8.8% of the source-surface dose rate. In view of the overall uncertainty in the depth-dose rates, these small corrections can probably be neglected except when the interposed bone thickness amounts to a few centimeters. The same may be said for air cavities. The entire lung would significantly perturb the dose-rate fields, and, if dose-rate values for the cranium are desired, the values determined for the homogeneous medium should be increased about 4% for each centimeter of interposed lung tissue. However, the cranium dose-rate values should be negligible for a source placement near the pelvic girdle.

In summary, the dose rates in a nonhomogeneous phantom such as the human body can be determined by applying the corrections –4%, 4%, and 6% per centimeter of interposed bone, lung, and air, respectively, to the dose-rate values determined for a homo-

geneous tissuelike phantom. It is recognized that these corrections apply to points located far enough from the source that inverse-square effects are minimal, but these corrections are sufficiently accurate in view of (1) the small percentages; (2) the fact that the source might eventually be "buried" within a blood-pump subsystem and thus be located "sufficiently far" from any interposed perturbing materials in the body; and (3) the relatively large overall uncertainty in the true dose-rate values. If the perturbing medium is smaller than a few centimeters thick, the correction factor can be neglected altogether.

Finally, to aid in estimating the integrated dose rate within the body, the dose rate can be averaged for various tissue volumes surrounding the source. For a centrally placed source in the abdominal cavity, for example, most of the energy will be deposited in the gastrointestinal system or any one organ or organ system that may lie closest to the source. For this reason it is necessary to know the eventual placement of the source. Otherwise the average dose rates within the surrounding volumes may be overestimated if some of the energies are lost to the body and absorbed by the surrounding air. That amount not lost to the surrounding air is estimated from the solid angle subtended by the source in the body.

## Procedure for Measuring the Dose Rates Surrounding an Implanted Radioisotopic Heat Source

A number of tissue-equivalent (to radiation) phantoms were utilized to accommodate the various dosimeters used in the measurements program. These were a nonhomogeneous Remab or man-simulating phantom, which contains an actual skeleton, and two homogeneous (water and polystyrene) phantoms. The former phantom is used for estimating the effect on the tissue dose rates from interposed bone or lower-density cavities such as the lung. It also provides a grasp of the dose rates that would be found at various locations in the body of an individual of similar size and contour, this being the U. S. Air Force 50th percentile male. The latter two phantoms are used for accurate scaling of source–dosimeter distances and, therefore, allow more accurate measurements of dose rate vs. thickness of interposed tissue. The polystyrene phantom, in particular, is most useful for measurements with dosimeters that are adversely affected by moisture.

The dosimeters found most useful for the promethium source measurements were small thermoluminescent (TLD) blocks 0.125 in. square by 0.035 in. thick; various pencil-type ionization chambers; and an extrapolation–ionization chamber. The most accurate measurements were made by placing the TLD and the extrapolation–ionization chamber on a thin platform of polystyrene, which was in turn placed upon the water surface in the water phantom. The back plate of the extrapolation–ionization chamber was thick enough to provide adequate backscatter for simulating a dosimeter that is "buried" within tissue. The TLD blocks and pencil-type chambers also were backed with adequate thicknesses of tissuelike material. Accurate scaling of source–dosimeter distance was accomplished by adjusting the height of the polystyrene platform by attached nylon threaded rods. The water level was continually adjusted to eliminate any air gaps. Figures 1 to 4 portray some of the dosimeters and phantoms that were used in the measurements. In order to cool the promethium heat source, a heat exchanger of aluminum, coated with Fiberfrax and Silastic insulation, was fabricated. Water coolant was passed through a portion of the heat exchanger which was not in contact with the source. The source, some shields, and the heat exchanger are also portrayed in the figures.

Since one of the purposes of the promethium program was to develop a suitable computational code that could predict the measurements, little thought needs to be given to the proper choice of materials for the source shields and heat exchanger. Whatever the choice, it was still to be demonstrated that the dose rates measured in the phantom could be predicted with sufficient accuracy. Thus a combination of materials was utilized, and their efficacy in removing the radiations while keeping the overall weight of the source at a minimum was determined.

## Shielding and In-Phantom Dose Predictions

### Description of Codes

Two computer codes (Isoshld-II, a PNL code,[6,7] and QAD-P5A, a LASL code[8,9]) were adapted for use in the prediction program. The PNL code has the advantage in determining the contribution to the dose rate from the $^{147}$Pm bremsstrahlung radiations. If the bremsstrahlung spectrum is known, QAD can also compute this contribution; but, in any event, this contribution becomes negligibly small ($<\frac{1}{2}\%$) after interposition of about $\frac{1}{4}$ cm of high-atomic-number shielding material. A heat source–blood pump subsystem will most likely contain this amount. The remainder of the dose is from the $^{146}$Pm radiations of about



XUM

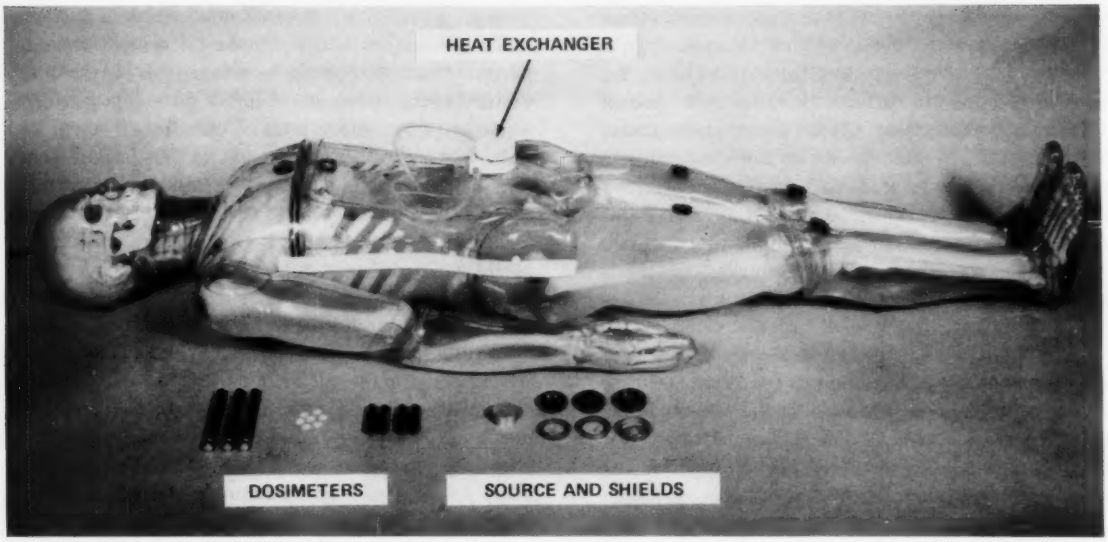


Fig. 1 Remab or man-equivalent phantom and various ancillary equipment used in the in-phantom dosimetry circulatory-support program. The dosimeters (left to right) are pencil ionization chambers (one is projecting out of the cranium); thermoluminescent dosimeters, or TLD's (some are taped to the surface of the phantom); and tissue-equivalent, or TE, ionization chambers for measuring total absorbed dose in mixed radiation fields.

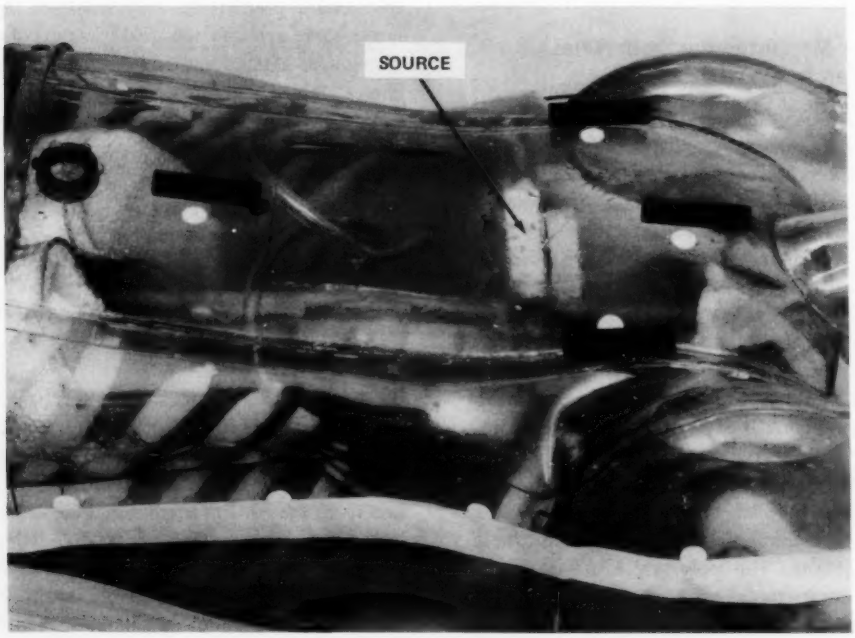


Fig. 2 Close-up of Remab phantom with the source positioned on the inside surface of the left ilium. Various dosimeters are placed on the surface of the phantom.

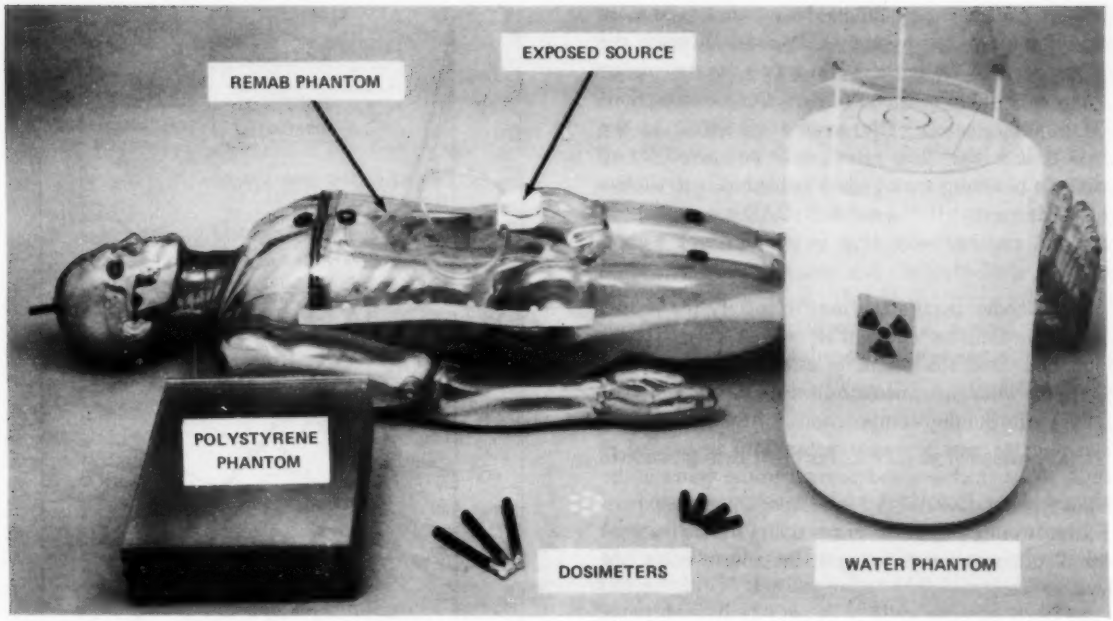


**Fig. 3** Tissue-equivalent phantoms and various dosimeters used in the in-phantom dosimetry circulatory-support program. The Remab phantom contains an actual skeleton and tissue-equivalent (to radiation) fluid. Dosimeters are placed within and around the phantoms. The heat exchanger, in which the radioisotopic heat source is placed, is shown out of the body.

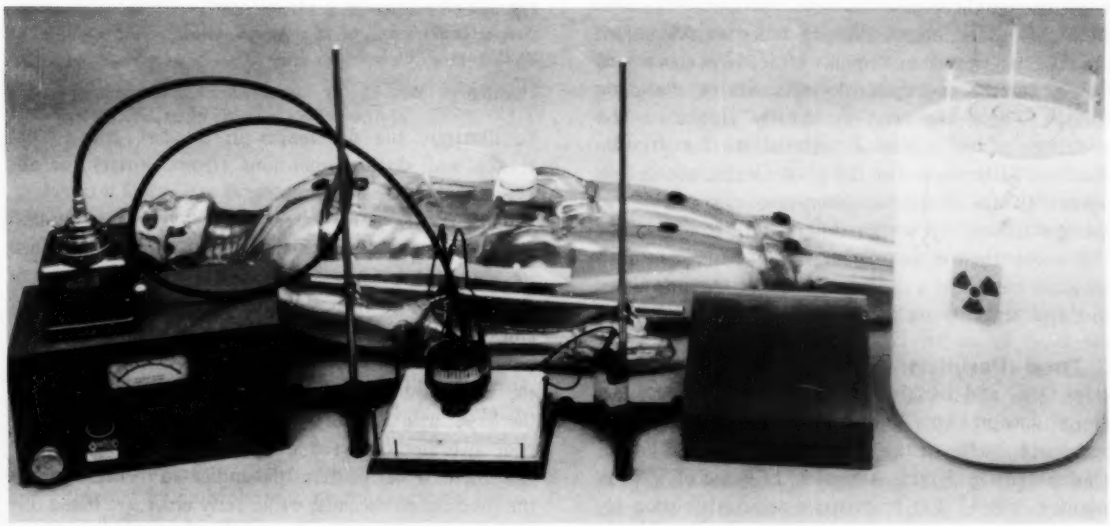

**Fig. 4** Various tissue-equivalent phantoms and the extrapolation–ionization chamber used in the in-phantom dosimetry circulatory-support program. The extrapolation–ionization chamber is a standard for measuring surface dose values after interposing various kinds and thicknesses of material between the source and detector.



XUM

0.6 Mev average energy and has been found to be more accurately predicted by the QAD code, although the differences may be more attributed to the parameters in the code libraries such as interaction cross sections and buildup factors. The greatest advantage to the QAD code is that dose rates can be computed for all points in phantom space, whereas Isoshld is restrictive to certain geometries. In addition, QAD is a more rapid code but requires more time in programming a given situation.

Both codes require the user to specify the proper buildup medium to represent all media between source point and dosimeter point. In essence, the user must determine which intermediate-atomic-number materials to use in the buildup computations for the surface dose rates and the first few centimeters into tissue and at which tissue thickness and beyond to use water in the buildup computations (this is because a photon experiences scattering within the promethium source material and all other materials between the source point and the dosimeter).

### Computations

**Shielding Computations.** The shielding effectiveness of uranium, tungsten, and iron, for $^{147}Pm$–$^{146}Pm$ heat sources, was studied using the computational code Isoshld-II. As expected, the higher $Z$ (atomic number) materials were much more effective in removing the bremsstrahlung radiations. Uranium and tungsten were about equally effective in this regard (based on the absorption coefficients in the code library). These computations merely emphasize the usefulness of the higher $Z$ materials as the primary cladding, particularly for the photoelectric-absorption region. In the Compton-absorption region ($^{146}Pm$ energies fall mainly within this region), iron is about 15% better than uranium, tantalum, or tungsten on a per-gram basis. On a centimeter basis, uranium, tantalum, and tungsten are about twice as effective as iron.

**Tissue Dose-Rate Computations.** The computer codes QAD and Isoshld-II were used to compute the photon dose in tissue from a 15-watt $^{147}Pm_2O_3$ heat source and shields of the same dimensions used in the measurements program. Assuming 11.9 mc of $^{146}Pm$ impurity, the $^{147}Pm$ bremsstrahlung contribution to the dose is less than 2%; the remainder of the dose is due to the higher photon energies from $^{146}Pm$. Figure 5 compares some of the predicted dose rates of the two codes. Many other phantom points were calculated, but these values along the source axis serve

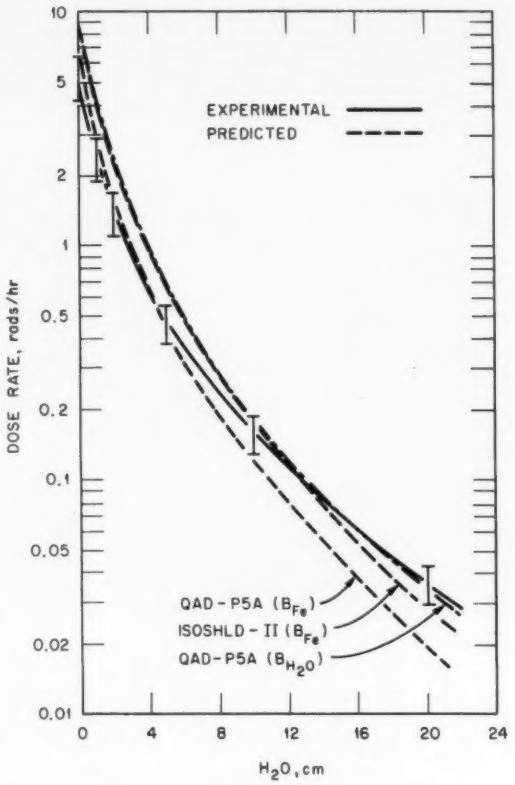


**Fig. 5 Comparison of predicted and measured in-phantom dose rates along axis of 15-watt cylindrical $^{147}Pm_2O_3$ source (0.25 ppm $^{146}Pm$).**

to illustrate the differences in the two codes. The source and shield dimensions (from center) for all reported data are shown in Fig. 6.

The QAD code agrees more closely with the measurements. Selecting iron as the dose buildup medium, a divergence from the measurements starts at about 8 cm into tissue. Beyond 8 cm, water is a better and certainly a more logical choice for the dose buildup medium. Throughout the distances measured, the QAD code predicted the measurements to within the experimental errors (±20%), whereas the Isoshld-II code overpredicted the dose-rate values. In fact, the agreement is better than that indicated in Fig. 5 since the predictions, because of an early error, are based on 11.9 mc of $^{146}Pm$ rather than the actual amount measured (11.0 mc). At 8 cm tissue thickness, the dose rates are only about 5% of the surface values; thus the departures of the predictions and measurements beyond 8 cm become less significant.

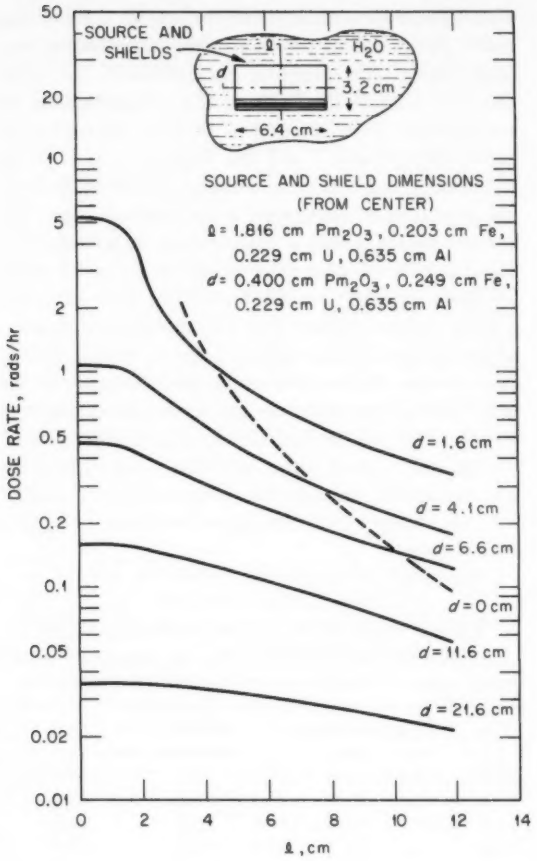
SOURCE AND SHIELDS
$H_2O$
3.2 cm
6.4 cm
SOURCE AND SHIELD DIMENSIONS (FROM CENTER)
ℓ = 1.816 cm $Pm_2O_3$, 0.203 cm Fe, 0.229 cm U, 0.635 cm Al
d = 0.400 cm $Pm_2O_3$, 0.249 cm Fe, 0.229 cm U, 0.635 cm Al
d = 1.6 cm
d = 4.1 cm
d = 6.6 cm
d = 0 cm
d = 11.6 cm
d = 21.6 cm
DOSE RATE, rads/hr
ℓ, cm

**Fig. 6 In-phantom measurements on 15-watt cylindrical $^{147}Pm_2O_3$ source (0.25 ppm $^{146}Pm$ impurity).**

**Integral Dose-Rate Computation.** The integral dose rate of a spherical 15-watt $^{147}Pm_2O_3$ source, containing 0.25 ppm $^{146}Pm$ and shielded similarly to the sources measured, was approximated using the equation

$$\Sigma = \rho \sum_{1} V_i \overline{D}_i$$

where $\rho$, the tissue density, is unity. If the source is placed centrally in a 30-cm-diameter sphere of tissue, $\Sigma \approx 2600$ (g)(rads)/hr. For a source not placed centrally in a similar-size body, the integral dose rate is approximated by multiplying $\Sigma$ by the fractional tissue volume subtended by the source.

### Corrections for Dose Buildup

An attempt was made to develop a correcting equation as a function of atomic number which would be general (i.e., apply to any source–shield configuration) and correct all phantom predictions that were based on, say, iron as the buildup medium. No single satisfactory equation was developed, and, in retrospect, it appears that the rule of thumb utilizing iron for the first 8 cm and water for the rest would yield satisfactory agreement with the promethium measurements. Of course, for the particular source and shields studied, precise buildup factors, as determined by the ratio of the experimental and the unbuildup dose-rate values, could be used. This is the more satisfactory approach if closer agreement is desired and also emphasizes the usefulness of measurements on the prototypic heat source–blood pump subsystems.

## Shielding and In-Phantom Dose Measurements

The measurements were performed on two cylindrical (height-to-diameter ratio approximately 1 : 4) 58-g $^{147}Pm_2O_3$ sources, each of nominal 15-watt rating, with $^{146}Pm$ impurities of 0.25 and 3.5 ppm, or about 11 and 154 mc of $^{146}Pm$, respectively. Photon spectrum analysis revealed no other radioisotopic impurities were present in significant amounts. The dosimetry measurements included: (1) surface dose rates on stainless-steel-clad surfaces, the first source covering, and on the surfaces of various combinations of tantalum, uranium, and aluminum shields; (2) tissue dose rates in the homogeneous phantoms along the source axis and at right angles or in the radial direction; and (3) tissue dose rates in the Remab phantom (source location on inside surface of left ilium) for both sources with minimal or no shielding other than the stainless-steel cladding and an aluminum heat exchanger. (The latter measurements were made before the full complement of shields was fabricated and were mainly for the purposes of intercomparing the various dosimeters that might be used in the measurements program.)

The surface dose rates are presented in Table 1. They were taken at about $\frac{1}{16}$ in. in air from the source–shield end surfaces and through a tissue thickness of 7 mg/cm$^2$ (about 0.007 cm); this depth represents the front-window thickness of the extrapolation–ionization chamber. The "true" surface dose rates are estimated to be within 10% of these tabulations for either source having four or more shields and a minimum of 30 to 40% larger than these tabulations for two or fewer shields. It is experimentally difficult to determine window-correction factors for mixed radiation containing low-energy bremsstrahlung and photoelectrons which come from the metal surfaces.



XUM

**Table 1 Extrapolation–Ionization Chamber Measurements on $^{147}Pm_2O_3$ Source–Shield Ends**

| Shields (thickness and total source and shield weight) | Dose rate, rads/hr ± 20% | |
|---|---|---|
| | Source 1* | Source 2† |
| Stainless steel (S.S.), 0.249 cm, 131 g | 422 | 658 |
| S.S. + 1 uranium (U), 0.076 cm, 211 g | 84.6 | 299 |
| S.S. + 2 U, 0.152 cm, 291 g | 21.9 | 206 |
| S.S. + 3 U, 0.229 cm, 371 g | 13.0 | 148 |
| S.S. + 3 U + aluminum (Al) heat exchanger, 0.635 cm, 540 g | 3.66 | 50.7 |
| S.S. + 1 tantalum (Ta), 0.076 cm, 201 g | 60.2 | 321 |
| S.S. + 2 Ta, 0.152 cm, 271 g | 18.1 | 218 |
| S. S. + 3 Ta, 0.229 cm, 341 g | 14.6 | 164 |
| S.S. + 3 Ta + Al, 0.635 cm, 510 g | 4.52 | 61.0 |

*Source 1, nominal 15-watt source with 0.25 ppm $^{146}Pm$.

†Source 2, nominal 15-watt source with 3.5 ppm $^{146}Pm$ (percent decay per day: 0.0343% $^{146}Pm$, 0.0724% $^{147}Pm$).

To a good first approximation, the measurements in tissue can be interpolated from these tabulations and those in Tables 2 to 5, which represent dose rates at various depths in tissue for one source–shield configuration. In order to ascertain the effect of the total source–shield weight on the dose rates, the mass values are also included in Table 1. It should be kept in mind, however, that the dose rates tabulated are those occurring from the end surfaces of a 4-to-1 cylinder (height, 0.800 cm; diameter, 3.632 cm) and thus are higher than those which would be found for a 1-to-1 cylinder or those measured out the radial direction of a 4-to-1 cylinder. It is estimated that the dose rates found for the latter two cases would be reduced by a factor of 2.

Most of the tissue dose rates were taken with TLD's of size 0.125 in. by 0.125 in. by 0.035 in., which were distributed on planes throughout a homogeneous water phantom and exposed to the source containing 0.25 ppm $^{146}Pm$. The exposure conditions simulated full buildup and are comparable to a centrally placed source in a torso with the dosimeters completely surrounded by tissue. Tables 3, 4, and 5 present data in planes perpendicular to the source axis, in the bisecting radial plane, and in planes parallel to the source axis, respectively. The phantom measurements for other shielding configurations or $^{146}Pm$ impurities can be interpolated from the ratios of the surface values presented in Table 1 and the impurity ratios. As an example, if part of the uranium shielding and the aluminum heat exchanger were omitted from the present source, giving a total source–shield weight of about 0.5 lb, all dose rates would be increased about 20 times. It might be noted that the TLD values are slightly higher than the extrapolation–ionization chamber values presented in Tables 1 and 2. This is because the TLD values more closely represent the dose rates at a point in the phantom. The diameter of the chamber is 3 cm, and thus its measurements are an average over a much larger area. When the TLD values are averaged to represent the area seen by the chamber, the two measuring systems agree to within the experimental errors.

**Table 2 Central-Axis Tissue Depth-Dose Rates from End Surface of $^{147}Pm_2O_3$ Source 1***

| Tissue thickness, cm | Dose rate, rads/hr ± 15% (estimated error) |
|---|---|
| 0 | 4.0 |
| 0.5 | 2.5 |
| 1 | 1.9 |
| 2 | 1.2 |
| 3 | 0.82 |
| 4 | 0.60 |
| 5 | 0.46 |
| 6 | 0.35 |
| 7 | 0.28 |
| 8 | 0.22 |
| 9 | 0.18 |
| 10 | 0.15 |
| 11 | 0.12 |
| 12 | 0.10 |
| 13 | 0.086 |
| 14 | 0.070 |
| 15 | 0.062 |
| 20 | 0.027 |

*The tabulations are interpolated from a plot of dose rate vs. depth in a water phantom since the actual thicknesses measured do not always correspond to the indicated values. (The interpolated surface value agrees within the experimental errors with the value listed in Table 1.) The source shields are 0.249 cm of S.S. (Fe), 0.299 cm of U, and 0.635 cm of Al. The measurements were taken with an extrapolation–ionization chamber.

**Table 3 Dose-Rate Measurements (rads/hr) in Planes Perpendicular to the Source Axis***

| Tissue depth ($d$), cm | Lateral displacement ($l$) | | | | |
|---|---|---|---|---|---|
| | 0 cm | 1 cm | 2 cm | 5 cm | 10 cm |
| 0.475 | 3.4 | 3.3 | 2.5 | 0.75 | 0.34 |
| 1.11 | 2.1 | 2.2 | 1.8 | 0.64 | 0.29 |
| 1.74 | 1.5 | 1.5 | 1.3 | 0.53 | 0.24 |
| 2.38 | 1.1 | 1.1 | 0.90 | 0.44 | 0.22 |
| 3.65 | 0.65 | 0.65 | 0.57 | 0.36 | 0.17 |
| 4.92 | 0.46 | 0.44 | 0.40 | 0.27 | 0.14 |
| 7.46 | 0.26 | 0.25 | 0.23 | 0.17 | 0.095 |
| 12.54 | 0.10 | 0.10 | 0.092 | 0.080 | 0.049 |
| 21.43 | 0.028 | 0.028 | 0.027 | 0.029 | 0.020 |

*Source dimensions are the same as in Fig. 6. The estimated accuracy of the dose-rate values is ± 20%.

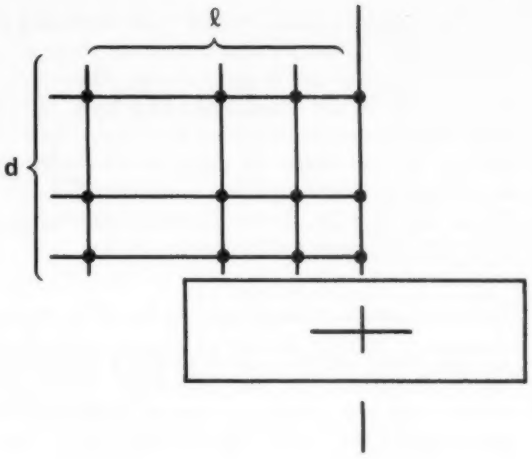


**Table 4 Dose-Rate Measurements (rads/hr) in Bisecting Radial Plane***

| Tissue depth ($d$), cm | Lateral displacement ($l$) | | | | |
|---|---|---|---|---|---|
| | 0 cm | 1 cm | 2 cm | 5 cm | 10 cm |
| 0.475 | 1.5 | 1.34 | 1.1 | 0.75 | 0.23 |
| 1.11 | 1.0 | 0.93 | 0.83 | 0.56 | 0.21 |
| 1.74 | 0.75 | 0.73 | 0.66 | 0.45 | 0.17 |
| 2.38 | 0.57 | 0.56 | 0.53 | 0.37 | 0.15 |
| 3.65 | 0.38 | 0.37 | 0.36 | 0.26 | 0.12 |
| 4.92 | 0.25 | 0.25 | 0.25 | 0.19 | 0.092 |
| 7.46 | 0.13 | 0.13 | 0.13 | 0.099 | 0.056 |

*Source dimensions are the same as in Fig. 6. The estimated accuracy of the dose-rate values is ± 20%.

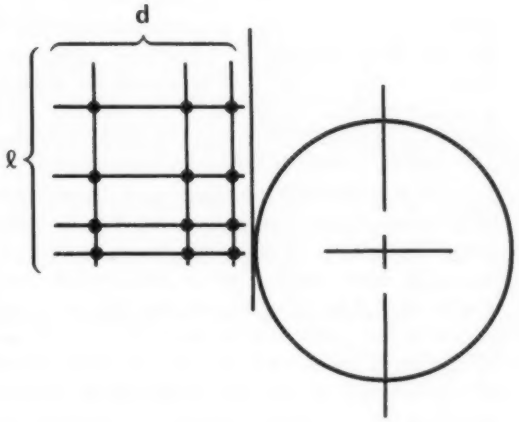


**Table 5 Dose-Rate Measurements (rads/hr) in Planes Parallel to the Source Axis***

| Tissue depth ($d$), cm | Lateral displacement ($l$) | | | | |
|---|---|---|---|---|---|
| | 0 cm | 1 cm | 2 cm | 5 cm | 10 cm |
| 0.475 | 1.5 | 1.5 | 1.3 | 0.58 | 0.22 |
| 1.11 | 1.0 | 0.99 | 0.81 | 0.47 | 0.20 |
| 1.74 | 0.75 | 0.73 | 0.62 | 0.38 | 0.18 |
| 2.38 | 0.57 | 0.57 | 0.47 | 0.30 | 0.16 |
| 3.65 | 0.38 | 0.37 | 0.32 | 0.23 | 0.13 |
| 4.92 | 0.25 | 0.25 | 0.22 | 0.16 | 0.097 |
| 7.46 | 0.13 | 0.13 | 0.12 | 0.10 | 0.072 |

*Source dimensions are the same as in Fig. 6. The estimated accuracy of the dose-rate values is ± 20%.

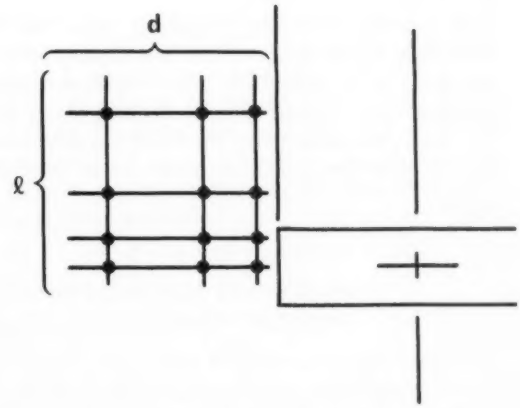




XUM

The data in Tables 3, 4, and 5 are condensed in Fig. 6, which profiles the dose rates in the perpendicular bisecting plane and in perpendicular planes 0, 2½, 5, 10, and 20 cm along the source axis. If this particular source were implanted in a patient, the dose accrued by any organ or organ system would be determined by consulting either the tabulated values or the profiles, once the distances from the source surface or center of geometry had been determined.

## Summary and Conclusions

This report presents the in-phantom predictions and measurements on two cylindrical $^{147}Pm_2O_3$ radioisotopic heat sources of nominal 15-watt rating and containing 0.25 and 3.5 ppm $^{146}Pm$ impurity. The protocol for characterizing the dose-rate fields is discussed. A comparison of two computer codes is included, the conclusion being that the more versatile QAD code is somewhat more accurate in predicting the measurements and, in fact, is capable of predicting the phantom measurements to within the experimental error of ± 20%. If the total source–shield weight is restricted to about 0.5 lb, the $^{146}Pm$ impurity would need to be reduced an order of magnitude or to about 0.02 ppm for promethium heat sources to be competitive with the estimated dose rates from electrorefined-$^{238}Pu$ heat sources. This comparison is for a promethium heat source of twice the thermal rating of a plutonium heat source. For a total source–shield weight of 1.2 lb (the full complement of shields utilized in the phantom measurements), the 0.25 ppm $^{146}Pm$ source produced dose rates at 20 cm into tissue (the approximate location of the spleen if the source is placed on the left ilium) of about 35 mrems/hr. This could be reduced to about 20 mrems/hr by rotating the source 90° and taking advantage of the dose reduction from source self-absorption.

It is perhaps misleading to compare "bare" sources rather than sources placed within a blood-pump subsystem since it is recognized that a significant dose reduction takes place by distance shielding alone. The first tissues encountered by the radiations emanating from a subsystem would probably be at distances greater than those in contact with a bare source. This will reduce the source-surface dose rate and thus the integrated dose rate in the body. However, the dose to any one organ, like the spleen, may not change appreciably unless there is an interposed thickness of higher-atomic-number materials from the subsystems.

A more logical comparison of promethium with plutonium would be the computation of dose rates accrued by tissue from sources placed within a subsystem. Once suitable prototypes are developed, this comparison should be made. (PSB)

## References

1. R. Paterson, H. M. Parker, and F. W. Spiers, A System of Dosage for Cylindrical Distributions of Radium, *Brit. J. Radiol.*, **9**: 487-508 (1936).
2. E. H. Quimby, Dosage Table for Linear Radium Sources, *Radiology*, **43**: 572-577 (1944).
3. R. J. Shalek, M. Stovall, and G. W. Batten, Jr., The M. D. Anderson Method for the Computation of Isodose Curves Around Interstitial and Intracavity Radiation Sources, *Amer. J. Roentgenol., Radium Ther. Nucl. Med.*, **102**: 662-672 (1968); 53 refs.
4. H. E. Johns, *The Physics of Radiology*, Charles C Thomas, Publisher, Springfield, Ill., 2nd ed., 3rd Printing, 1964.
5. *Physical Aspects of Irradiation, Recommendations of the International Commission on Radiological Units and Measurements*, National Bureau of Standards, Handbook 85, Superintendent of Documents, U. S. Government Printing Office, Washington, March 1964.
6. R. L. Engel, J. Greenborg, and M. M. Hendrickson, Isoshld—A Computer Code for General Purpose Isotope Shielding Analysis, USAEC Report BNWL-236, Pacific Northwest Laboratory, June 1966.
7. G. L. Simmons, J. J. Regimbal, J. Greenborg, E. L. Kelley, Jr., and H. H. Van Tuyl, Isoshld-II: Code Revision to Include Calculation of Dose Rate from Shielded Bremsstrahlung Sources, USAEC Report BNWL-236(Suppl.), Pacific Northwest Laboratory, March 1967.
8. R. E. Malenfant, QAD: A Series of Point-Kernel General-Purpose Shielding Programs, USAEC Report LA-3573, Los Alamos Scientific Laboratory, April 1967.
9. G. P. Lahti, QADHD Point-Kernel Radiation Shielding Computer Code To Evaluate Propellant Heating and Dose to Crew During Engine Operation, Report NASA-TM-X-1397, National Aeronautics and Space Administration, Lewis Research Center, June 1967.

Section

II

Isotopes and Radiation Technology

# Isotopes Around the World

## French Radioisotope Use Increases in 1968*

The production and sale of radioisotopes in France in 1968 increased 31% over 1967, which is the largest annual increase ever noted. Of the total of 73,046 sales made, 12,578 were to other countries, vs. 55,880 and 7458, respectively, in 1967. These deliveries represent a value of 14.250 million F† exclusive of taxes, of which 48% came from exports. Radioisotopes produced for the French Atomic Energy Commission's (CEA) own uses increased to 16.678 million F from 12.750 million F in 1967. The total 1968 production included

538 curies of $^{131}I$
531 curies of colloidal $^{198}Au$
112 curies of $^{32}P$
86 curies of $^{99m}Tc$
171 kilocuries of low-specific-activity $^{60}Co$
187 kr/hr (1 m) for $^{60}Co$ teletherapy
28 curies of $^{192}Ir$
85 kilocuries of $^{137}Cs$

The increase in sales was not due to an increase in the number of users (2.5%) but rather to an increase in medical uses (both $^{60}Co$ teletherapy and diagnostics), industrial radiation techniques, and the use of labeled molecules for chemical tracing (almost 50 new products have been put on the market), as well as to the initial production stages of radioisotope-powered thermoelectric generators fueled with $^{90}Sr$ titanate and promethium oxide sources.

In the development of radioisotope uses in industry, the CEA considers its role that of a public organization which makes its specialized services available for matters of national interest, especially in fields that relate to the nuclear program. Thus research is done on development of new apparatus that is eventually produced by industry; large-scale tracer experiments are carried out; and irradiator design and use are studied. In cooperation with the Technical Association for Nuclear Energy (A.T.E.N.), the CEA also publicizes radioisotope uses.

Some French achievements in 1968 were:

- Installation of a radioisotope-powered generator, the Marguerite II, in the Mediterranean to supply a luminous beacon and an ultrasonic beacon.
- Approval of potato irradiation to inhibit sprouting in storage.
- Use of radioactive tracers in water-pollution tests, e.g., measurement of polluted-water flow rates and of residence time in a water-purification plant.
- Development of a radioisotope-based X-ray-fluorescence analyzer for light elements (ARIEL).

The use of radioelements in French industry is estimated to have resulted in annual savings of the order of a hundred million francs. (MG)

*From CEA "Notes d'Information," No. 2, pp. 6-7, February 1969.

†One franc was approximately $0.24 at the time this report was written.

## "Understanding the Atom" in German

An East German brochure, *Radioaktive Isotope in der Industrie* (Radioactive Isotopes in Industry), is the counterpart of *Radioisotopes in Industry* of the USAEC's "Understanding the Atom" series. The 32-page German booklet has an attractive format, an easily readable text, and clear basic illustrations. The ordinary uses of radioisotopes—e.g., radiation sterilization, radiation-chemical processing, gaging, radiochemical analysis, leak detection, and tracing—are covered briefly. A number of organizations in East Germany concerned with peaceful uses of atomic energy assisted in preparation of the brochure, including the Zentralinstitut für Kernforschung (8051 Dresden, Postschliessfach 19). (MG)

## Tritium Labeling of Biochemicals by Modified Wilzbach Technique

A modification of the Wilzbach technique using microwave discharge is used routinely in the AB Atomenergi



XUM

laboratories at Studsvik, Nyköping, Sweden. The method is simple and rapid, and decomposition of the compound being labeled is low. A recent report* from the Swedish laboratory describes the tritium labeling of dihydrosterptomycine, tetracycline, and antipyrine.

(MG)

## Skinpreg Process Enhances Wood Properties

Skinpreg AB, Malmö, Sweden, reports the invention of a process for impregnating the "skin" of wood with a monomer and then polymerizing the monomer with radiation, heating, or heat and pressure. After pretreatment with a chemical solution for several hours, the wood is rinsed, then impregnated with monomer (or polymer) in a vacuum–pressure chamber in which depth of penetration is controlled. After a predrying step, the impregnation medium is polymerized by radiation or otherwise. A finished surface can be obtained by use of plastic-coated steel plates in a press.

Both softwoods and hardwoods can be used, and the surface may be colored by including a stain in the monomer. The floor-panel and window-line industries are particularly interested in the process, which will cost from $0.80 to $1.00 per square meter, including all pretreatment chemicals, monomer, and depreciation.

Further information is available from Skinpreg Aktiebolag, Torggatan 4, 211 40 Malmö, Sweden.

(PSB)

*T. Gosztonyi, Application of the Microwave Discharge Modification of the Wilzbach Technique for the Tritium Labelling of Some Organics of Biological Interest, Report AE-345 (1969).

Section

III

Isotopes and Radiation Technology

# Miscellaneous

## Availability of Isotopes and Services

### ORNL Stable-Isotope Inventory Augmented

Recent additions to the Oak Ridge National Laboratory (ORNL) enriched-stable-isotope saleable inventory include the following:

| Isotope | Purity, % | Amount available, g | Isotope | Purity, % | Amount available, g |
|---|---|---|---|---|---|
| $^{25}Mg$ | 98.2 | 43.3 | $^{124}Te$ | 91.0 | 1.4 |
| $^{26}Mg$ | 99.4 | 60.0 | $^{138}La$ | 7.8 | 0.1 |
| $^{26}Mg$ | 98.8 | 8.1 | $^{138}La$ | 1.2 | 0.5 |
| $^{57}Fe$ | 69.6 | 1.7 | $^{156}Dy$ | 21.6 | 0.4 |
| $^{57}Fe$ | 92.3 | 1.0 | $^{160}Dy$ | 69.5 | 3.3 |
| $^{74}Se$ | 28.7 | 1.5 | $^{162}Dy$ | 96.2 | 18.4 |
| $^{76}Se$ | 66.5 | 8.7 | $^{206}Pb$ | >99.98 | 1.7 |

### Lockheed-Georgia Gamma-Irradiation Facility

The primary facility for radiation processing by Lockheed-Georgia is a 250-thousand-curie $^{60}Co$ gamma irradiator (Fig. 1), completed in March 1967. The facility incorporates versatile features that make it particularly suitable for use in research and development programs requiring radiation processing of a wide range of materials.

The source plaque, 5 ft high and 9 ft wide, can provide uniform dose rates up to approximately $10^6$ rads/hr. Items or groups of items up to 9 ft wide, 10 ft high, and 45 in. thick and weighing up to 6000 lb can be mounted on a specimen carrier on each side of the source plaque during each irradiation cycle. Dose rates can be varied on each of the carriers by changing their distances from the source, and the carriers can be rotated 180° to provide a more uniform dose through thick specimens. Likewise, the cobalt can be rearranged on the plaque to provide varied dose rates in certain areas.

The irradiator is housed in an air-conditioned hot cell, 12 ft wide, 17 ft long, and 14 ft high, which is equipped with an access door, viewing windows, manipulators, water, electric power, and pneumatic, hydraulic, and instrumentation leads. When not in use, the source is stored in a pool of water below the cell floor, so that personnel may enter the cell.

Irradiation services are offered to government agencies and contractors and to commercial customers by the Lockheed-Georgia Nuclear Laboratory (Marietta, Ga.). Some of the products irradiated in the facility are the water-soluble polymers polyethylene oxide and polyethylene glycol; standard polyethylene film for use as a battery separator material in NASA spacecraft (a combination of cross-linking and grafting by gamma irradiation); and flour for disinfestation purposes (for eventual use by the U. S. Army).

(MG)



XUM

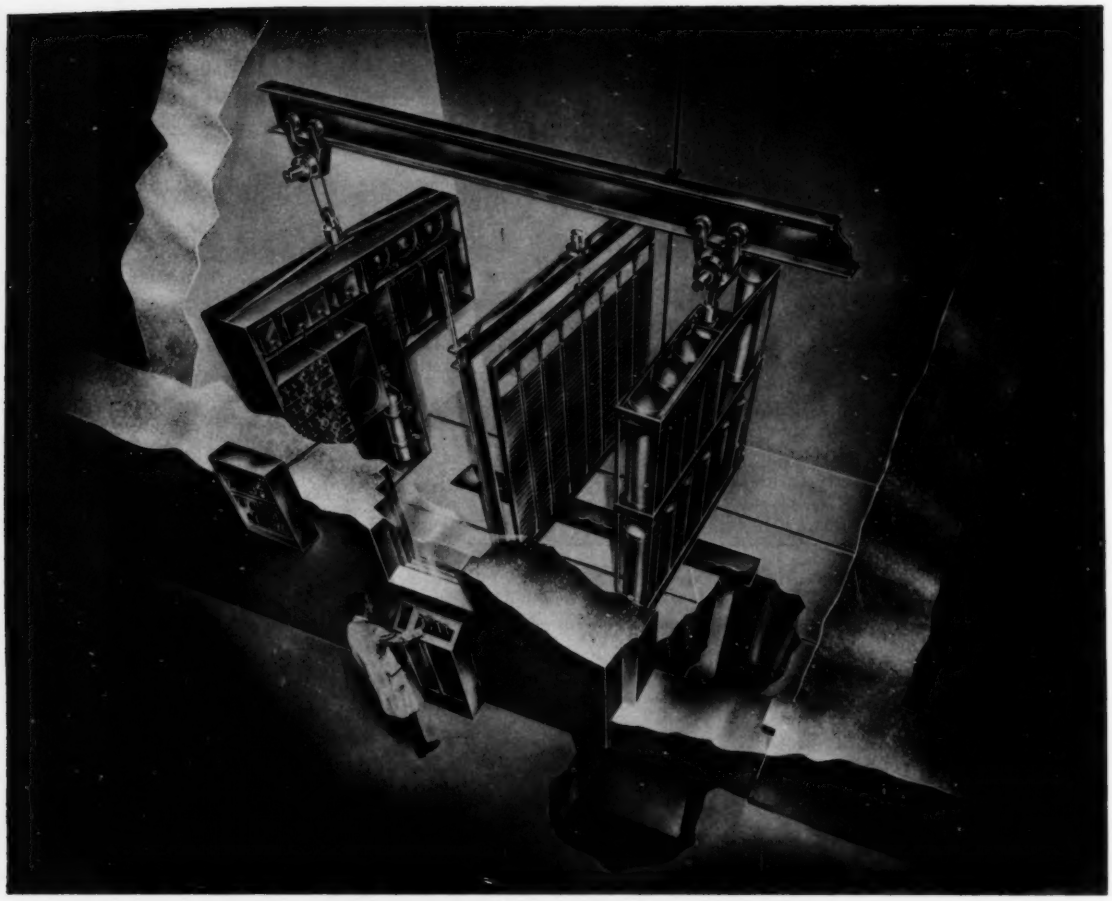

Fig. 1 Artist's cutaway view of the 250-thousand-curie $^{60}Co$ irradiator, with process and experimental irradiation taking place. When not in use, the plaque is turned 90° and lowered into the pool of water.

# AEC Activities

## Radioisotope-Fueled Power Generator Producing Electricity for Exhibit*

After continuously producing power for 8 years—4 of them under Arctic conditions—a radioisotope-fueled power-generator system has been incorporated into an operating exhibit now on display at Oak Ridge National Laboratory. This forerunner of the SNAP (Systems for Nuclear Auxiliary Power) series was manufactured by the Martin Company and fueled with 17,500 curies of $^{90}Sr$ titanate at ORNL's Isotopes Development Center in 1961.

The system was installed in an unmanned weather station on Axel Heiberg Island, about 40 miles from the North Pole, where it powered an automatic radiotransmitter that broadcast wind direction, velocity, and temperature data at 4-hr intervals. Between broadcasts, the power from the generator charged conventional batteries, which operated auto-

*For description see *Isotopes and Radiation Technology*, 4(2): 179-180 (Winter 1966–1967).

matic electronic weather-monitoring equipment. After 4 years, the generator was returned to ORNL, where an extensive examination showed it to be still operating normally. It has continued to produce power, the current output being about 60% of its original design level of 5 watts. (MG)

## Book: *Radioisotopes and Inquiry*

Bio-Atomic Research Foundation (North Hollywood, Calif.), *Radioisotopes and Inquiry*, Encyclopaedia Britannica Educational Corporation, Publishers, Chicago, 1968 (185 + xiv pp., $2.50).

*Radioisotopes and Inquiry* is the final version of a project administered by the Bio-Atomic Research Foundation of North Hollywood, Calif., under contract to the USAEC. The book is designed to bring fundamental radiological techniques within reach of the average high-school biology classroom, and special attention has been given to selecting experiments and investigations that can be done with simple and inexpensive materials. There is a student's edition in which probable results are not revealed. The teacher's edition contains a glossary, bibliography, and nuclear data. The bibliography and nuclear data, although not completely up to date, are sufficient for the audience for which the book is designed. (MG)

## Radioisotopes Identify Straight-Grain Timber

Elements dissolved in soil water enter a tree system through the roots and move upward in the trunk. If a radioisotopic tracer is present in the solution, the readings of a G–M counter passed over the trunk to detect the presence of radioisotopes will show the direction of the wood fibers, i.e., the grain, of the timber in the living tree. This interesting discovery was made by James L. Smith of the U. S. Forest Service in Berkeley, Calif., in the course of a study on moisture absorption by trees during the winter. The implications of the discovery may be far-reaching. For example, selective planting of seeds of straight-grain trees might breed out spiral grains.

## Texaco To Study $^{252}Cf$ for Oil-Well Logging

The first loan agreement with a commercial firm, Texaco, Inc., to use $^{252}Cf$ in applications studies has been announced. Two sources, to be fabricated at the U. S. Atomic Energy Commission's Savannah River Laboratory, will be provided to Texaco.

In the well-logging technique to be pursued by Texaco geologists, the $^{252}Cf$ is lowered into the borehole at a continuous rate of speed and the spontaneous-fission neutrons activate certain elements by neutron capture. A detector following the $^{252}Cf$ detects and records the presence of any short-lived radioactive elements. From this record the geologists are able to determine what elements are present and where an oil- or gas-bearing zone is located.

## Nuclear-Powered Cardiac Pacemaker Successfully Implanted in Dog

A compact nuclear-powered cardiac pacemaker designed to operate for a minimum of 10 years has been successfully implanted in a dog at the National Heart Institute, National Institutes of Health, Bethesda, Md. The device was developed by the U. S. Atomic Energy Commission through a contract with Nuclear Materials & Equipment Corporation, Apollo, Pa., a subsidiary of the Atlantic Richfield Company. The AEC has been developing and testing the device for 3 years under laboratory conditions simulating those in the human body. This implantment and others to follow in animals are intended to test the reliability of the device.

The nuclear pacemaker is about two-thirds the size of a pack of cigarettes and weighs 3.5 oz. It is $1\frac{3}{16}$ in. wide, $1\frac{7}{8}$ in. deep, and $2\frac{7}{16}$ in. long. Scientists hope that the device will eventually replace battery-operated devices currently used by about 20 thousand persons. In addition, about 5 thousand new heart-block patients receive pacemakers each year.

After completion of an extensive laboratory and animal test program, clinical studies of the pacemaker will be conducted at the Beth Israel Hospital, Newark, N. J., which serves as a consultant to the AEC.



XUM

# General

## Arizona Introduces Legislation To Join Western Interstate Nuclear Compact

Legislation allowing Arizona to become a member of the 11-state Western Interstate Nuclear Compact [see *Isotopes and Radiation Technology*, 7(1): 133 (1969)] has recently been passed by the Arizona State Legislature.

The Compact thus becomes a new program of the Arizona Atomic Energy Commission (AAEC). (The other 10 states involved are Alaska, California, Colorado, Idaho, Nevada, New Mexico, Oregon, Utah, Washington, and Wyoming.)

The AAEC, with Donald C. Gilbert as Acting Director, is a State Agency chartered to encourage the development and application of atomic energy in Arizona. Since its inception in 1965, the AAEC has been implemental in having Arizona become an Agreement State (March 1967) and presently serves as the regulatory group for the State. The Commission has also been active in sponsoring exhibits and symposiums related to nuclear energy and in developing a nuclear industry in the State. The AAEC also publishes a periodical, *Arizona Atomic Progress*. Information about the Commission and its program can be obtained from Donald C. Gilbert, The Arizona Atomic Energy Commission, 40 East Thomas Road, Suite 107, Phoenix, Ariz. 85012. (PSB)

## Babcock-Hart Award Honors Dr. S. A. Goldblith

The Babcock-Hart Award, which is sponsored by the Nutrition Foundation, Inc., and administered by the Institute of Food Technologists, is given annually to an individual who has distinguished himself by contributions to food technology which have resulted in improved public health through more nutritious food. The 1969 Award has been given to Dr. Samuel A. Goldblith, a professor in the Department of Nutrition and Food Science, Massachusetts Institute of Technology. Dr. Goldblith is a member of the American Institute of Biological Sciences' Advisory Committee to the Atomic Energy Commission's Food Irradiation Program and has been a contractor for many years of both the Division of Isotopes Development and the Division of Biology and Medicine of the U. S. Atomic Energy Commission. Many of his more than 170 publications deal with the effect of processing on the nutritional value of food, and he is a staunch champion of radiation preservation, which he believes can serve where other methods are ineffective. Freeze drying and microwave heating are two other techniques in which Dr. Goldblith is a recognized expert.

## ORNL Isotopes Information Center Publishes Review of Radio-Release and $^{85}$Kr Clathrates and Kryptonates

The Isotopes Information Center (IIC) at Oak Ridge National Laboratory has announced the availability of ORNL-IIC-18, "Radio-Release in Review, with Special Emphasis on $^{85}$Kr Clathrates and Kryptonates," by Joan E. Carden. The review discusses the development of the radio-release method, in which a nonradioactive component is determined indirectly by the quantitative release of a radioactive material from a radioactive reagent with which the sample is contacted. Eighteen successful radio-release techniques are discussed in detail with special emphasis on the highly versatile Kryptonates, and sensitivity data are presented. Discussions of the nonkrypton analytical tracer techniques, such as the determination of active hydrogen with lithium aluminum tritide, and of the $^{85}$Kr clathrates precede the discussion of the preparation, properties, and numerous applications of the Kryptonates. Single copies may be obtained gratis from the IIC, P. O. Box X, Bldg. 3047, Oak Ridge, Tenn. 37830.

## Dual-Purpose Radiation Facility Built in New Jersey

In Franklin Township, N. J., ground was broken in August 1969 for construction of a multiproduct radiation processing plant to be built by Radiation Technology, Inc. (Long Island City, N. Y.) and scheduled for early-1970 operation. This dual-purpose research and production complex will be used for both commercial radiation processing and for product research and development including the development of new composite materials, the improvement of basic chemical constituents, and the production of latex and organo-tin compounds using radiation synthesis. The plant is designed to contain more than a megacurie of $^{60}$Co and one or more electron accelerators, the latter to be used for such applications as the curing of coatings, cross-linking of polyethylene film and tubing, and the improvement of textiles.

### Radiosterilization of Human Tissues for Transplant Surgery

Radiation has proved effective in the sterilization of human bone, cartilage, heart valves, and tendons for transplant operations according to reports made at the first international panel meeting on the uses of radiation in human transplant surgery held in Budapest, June 1969. Twenty-one scientists—radiobiologists, surgeons, and specialists in irradiation techniques—from nine countries attended the 5-day meeting at the invitation of the International Atomic Energy Agency (IAEA).

Participants pointed out that radiation not only sterilizes biological tissues effectively for human transplants but beneficially influences their antigen character, thus making them less liable to rejection. They also stressed the importance of radiosterilization for the man-made materials of human implants. Since irradiation is a "cold" process, it is not harmful to man-made materials such as plastic.

The panel recommended an international cooperative program for the purpose of increasing the available information in this new field of nuclear medicine. It also suggested that training courses be established to acquaint various specialists with techniques of sterilization of human tissues and that the IAEA develop a code of practice that can be used as an international guideline for testing the sterility of graft tissue.

### Isotope Products Laboratories Provides Sealed Sources

Isotope Products Laboratories of Los Angeles has recently published a catalog that emphasizes their capability of processing both reactor- and cyclotron-produced radioisotopes into sealed sources. The product line consists of sealed sources at the low to intermediate level and is directed at users in the industrial and aerospace communities and, to some extent, universities. The company is also set up to fabricate special sources to meet customer specifications. Inquiries should be directed to Karl Amlauer, Technical Director, 920 N. Citrus Avenue, Los Angeles, Calif. 90038.

# Publications by Isotopes Information Center

Oak Ridge National Laboratory
Post Office Box X
Oak Ridge, Tenn. 37830

The Center has published the following reports, or Center personnel have made major contributions to their preparation:

*Isotopes and Radiation Technology*, a quarterly Technical Progress Review published by the U. S. Atomic Energy Commission. (Available from Superintendent of Documents, U. S. Government Printing Office, Washington, D. C. 20402; subscription $2.50 per year, $0.70 for individual issues; non-U. S. subscriptions $3.25 per year, $0.90 for individual issues)

TID-21620, List of AEC Radioisotope Customers with Summary of Radioisotope Shipments, FY 1964, P. S. Baker, March 1965. (Available from CFSTI*)

ORNL-3633, ORNL Radioisotopes Procedures Manual, coordinated by F. N. Case; compiled by D. A. Fuccillo, Jr., and Sylvia B. Ewing, June 1964. (Available from CFSTI)

ORNL-TM-1047, Research Materials Coordination and Planning Meeting, November 14–15, 1963, P. S. Baker (Comp.), April 1965. (Available from CFSTI)

ORNL-TM-1660, Two Machine-Printed, Camera-Ready Indexes for a Large Book, D. A. Fuccillo, Jr., Harry Katzen, Jr., and K. E. Nicholson, November 1966.

*Radioisotopes in Industry*, P. S. Baker, D. A. Fuccillo, Jr., Martha Gerrard, and Robert H. Lafferty, Jr., November 1965. (One of the USAEC's "Understanding the Atom" Series). (Available from Isotopes Information Center and from USAEC Division of Technical Information Extension, P. O. Box 62, Oak Ridge, Tenn. 37830, free)

ORNL-IIC-1, Publications on Isotopes at Oak Ridge National Laboratory, 1946–1963, Robert H. Laf-

*Clearinghouse for Federal Scientific and Technical Information, National Bureau of Standards, U. S. Department of Commerce, Springfield, Va. 22151. Full size $3.00; microfiche $0.65.



XUM

ferty, Jr., P. S. Baker, and Martha Gerrard, July 1964. (Available from CFSTI)

ORNL-IIC-2, Production of Calcium-47, with Literature Review of Uses, P. S. Baker, Martha Gerrard, and Robert H. Lafferty, Jr., May 1964. (Available from Isotopes Information Center, free)

ORNL-IIC-4, Iodine-132: Review of Properties, Uses, and Methods of Preparation, Martha Gerrard, John J. Pinajian, and P. S. Baker, November 1968. (Available from Isotopes Information Center, free)

ORNL-IIC-5, Proceedings of Symposium on Low-Energy X- and Gamma Sources and Applications, Held at Illinois Institute of Technology Research Institute, Chicago, Ill., Oct. 20–21, 1964, Philip S. Baker and Martha Gerrard (Eds.), November 1965. (Available from CFSTI)

ORNL-IIC-6, List of AEC Radioisotope Customers with Summary of Radioisotope Shipments, FY 1965, P. S. Baker, March 1966. (Available from CFSTI)

ORNL-IIC-7, Proceedings of Information Meeting on Irradiated Wood–Plastic Materials, Held at Conrad Hilton Hotel, Chicago, Ill., Sept. 15, 1965, R. E. Greene and P. S. Baker (Eds.), March 1966. (Available from CFSTI)

ORNL-IIC-8, Reactor Yield Calculations for 81 Radioisotopes Produced by $(n,\gamma)$ Reactions at Fluxes of $10^7$ to $10^{16}$ n/cm$^2$ · sec for Irradiation Times of 30 Minutes to One Year, T. C. Whitson and C. W. Friend, April 1966. (Available from CFSTI)

ORNL-IIC-9, List of AEC Radioisotope Customers with Summary of Radioisotope Shipments, FY 1966, P. S. Baker, Sept. 1967. (Available from CFSTI)

ORNL-IIC-10, Proceedings of Second Symposium on Low-Energy X- and Gamma Sources and Applications, Held at University of Texas, Austin, Tex., Mar. 27–29, 1967, Philip S. Baker, and Martha Gerrard (Eds.), Sept. 1967. (Available from CFSTI)

ORNL-IIC-11, Radiation Pasteurization of Fruits and Vegetables—A Bibliography, A. S. Abdel-Kader and E. C. Maxie (P. S. Baker, Ed.), September 1967. (Available from Isotopes Information Center, free)

ORNL-IIC-11 (Suppl. 1), Radiation Pasteurization of Fruits and Vegetables—A Bibliography, F. E. McKinney, August 1968. (Available from Isotopes Information Center, free)

ORNL-IIC-12, Special Sources of Information on Isotopes, F. E. McKinney, R. H. Lafferty, Jr., and P. S. Baker, January 1968. (Available from Isotopes Information Center, free)

ORNL-IIC-13, List of AEC Radioisotope Customers with Summary of Radioisotope Shipments, FY 1967, Ruth Curl (Comp.), March 1968. (Available from CFSTI)

ORNL-IIC-14, Radiation Processing of Food Products, L. V. Metlitskii, V.. Rogachev, and V. G. Krushchev (Martha Gerrard, F. E. McKinney, and P. S. Baker, Eds.), July 1968. (Available from Isotopes Information Center, free)

ORNL-IIC-15, Preservation of Bread by Means of Gamma Radiation, G. Stehlik and K. Kaindl (Translated by P. S. Baker), August 1968. (Available from Isotopes Information Center, free)

ORNL-IIC-16, Uses of Neutron Radiography—A Literature Review, Martha Gerrard, October 1968. (Available from Isotopes Information Center, free)

ORNL-IIC-17, List of AEC Radioisotope Customers with Summary of Radioisotope Shipments, FY 1968, Ruth Curl (Comp.), December 1968. (Available from CFSTI)

ORNL-IIC-18, Radio-Release in Review with Special Emphasis on $^{85}$Kr Clathrates and Kryptonates, Joan E. Carden, July 1969. (Available from CFSTI)

ORNL-IIC-19, Isotope User's Guide, F. E. McKinney, S. A. Reynolds, and P. S. Baker, September 1969. (Available from Isotopes Information Center, free)

ORNL-IIC-20, Centralized Processing of Fresh Meat and Poultry Including Pasteurization—A Bibliography, W. M. Urbain, P. S. Belo, and G. G. Giddings (F. E. McKinney, Ed.), April 1969. (Available from Isotopes Information Center, free)

ORNL-IIC-21, Isotopic Methods for Oceanographic Measurements, Martha Gerrard and Joan E. Carden. (In press)

ORNL-IIC-22(Pt. 1), Selected Abstracts of World Literature on Production and Industrial Uses of Radioisotopes (from *NSA*, January–March 1969), Martha Gerrard and P. S. Baker, June 1969. (Available from Isotopes Information Center, free)

ORNL-IIC-24, Isotopes Information Center Keyword Thesaurus, Robert H. Lafferty, Jr. (Ed.), July 1969. (Available from Isotopes Information Center, free)

ORNL-IIC-25, Preservation of Fish by Ionizing Radiation: An Annotated Bibliography, F. J. Weiss, F. E. McKinney, and L. M. Frye, September 1969. (Available from Isotopes Information Center, free)

No. 4, *Isotope Developments,* Ocean-Bottom Sediment Density Gauge, July 1967.

No. 5, *Isotope Developments,* Suspended-Sediment Concentration Gauge, October 1967.

No. 6, *Isotope Developments,* Eggshell Strength Gauge, May 1968.

No. 7, *Isotope Developments,* Hand Portable X-Ray Mineral Analyzer, August 1968.

*Selected Abstracts of Non-U. S. Literature on Production and Industrial Uses of Radioisotopes,* Martha Gerrard and P. S. Baker. (Available from Isotopes Information Center, free):

ORNL-TM-1356, January 1966
ORNL-TM-1356(Suppl. 1), March 1966
ORNL-TM-1505(Pt. 1), May 1966
ORNL-TM-1505(Pt. 2), October 1966
ORNL-TM-1505(Pt. 3), December 1966
ORNL-TM-1505(Pt. 4), February 1967
ORNL-TM-1940(Pt. 1), August 1967
ORNL-TM-1940(Pt. 2), February 1968
ORNL-TM-2223(Pt. 1), May 1968
ORNL-TM-2223(Pt. 2), August 1968
ORNL-TM-2223(Pt. 3), January 1969
ORNL-TM-2223(Pt. 4), February 1969

TID-24349, Division of Isotopes Development Research and Development Projects, 1967, Robert H. Lafferty, Jr., and Joan E. Carden (Eds.), May 1968. (Available from CFSTI and free from Isotopes Information Center)

TID-24823, Division of Isotopes Development Research and Development Projects, 1968, Robert H. Lafferty, Jr. (Ed.), January 1969. (Available from CFSTI and free from Isotopes Information Center)

**LEGAL NOTICE**

This journal was prepared under the sponsorship of the U. S. Atomic Energy Commission. Neither the United States, nor the Commission, nor any person acting on behalf of the Commission:

A. Makes any warranty or representation, expressed or implied, with respect to the accuracy, completeness, or usefulness of the information contained in this journal, or that the use of any information, apparatus, method, or process disclosed in this journal may not infringe privately owned rights; or

B. Assumes any liabilities with respect to the use of, or for damages resulting from the use of any information, apparatus, method, or process disclosed in this journal.

As used in the above, "person acting on behalf of the Commission" includes any employee or contractor of the Commission, or employee of such contractor, to the extent that such employee or contractor of the Commission, or employee of such contractor prepares, disseminates, or provides access to, any information pursuant to his employment or contract with the Commission, or his employment with such contractor.



XUM

# TECHNICAL PROGRESS REVIEWS

The United States Atomic Energy Commission publishes the Technical Progress Reviews to meet the needs of industry and government for concise summaries of current nuclear developments. Each journal digests and evaluates the latest findings in a specific area of nuclear technology and science. *Nuclear Safety* is a bimonthly journal; the other three are quarterly journals.

**Isotopes and Radiation Technology**
*P. S. Baker, A. F. Rupp, and associates*
Isotopes Information Center, Oak Ridge National Laboratory

**Nuclear Safety**
*Wm. B. Cottrell, W. H. Jordan, J. P. Blakely, and associates*
Nuclear Safety Information Center, Oak Ridge National Laboratory

**Reactor Technology**

**Reactor Materials**
*E. M. Simons and associates*
Battelle Memorial Institute, Columbus Laboratories

All are available from the U. S. Government Printing Office. See the back cover for ordering instructions.

The views expressed in this publication do not necessarily represent those of the United States Atomic Energy Commission, its divisions or offices, or of any Commission advisory committee or contractor.

# Availability of Reports Cited in This Review

**United States Atomic Energy Commission (USAEC)** reports are available at USAEC depository libraries and are sold by the Clearinghouse for Federal Scientific and Technical Information (CFSTI), National Bureau of Standards, U. S. Department of Commerce, Springfield, Va. 22151. All reports sold by CFSTI are $3.00 for printed copy and $0.65 for microfiche. Each separately bound part of a report is priced as a separate report. Some reports may not be available because of their preliminary nature; however, the information contained in them will generally be found in later progress or topical reports on the subject.

**Other U. S. Government agency** reports identified in this journal generally are available from CFSTI.

**Private-organization** reports should be requested from the originator.

**United Kingdom Atomic Energy Authority (UKAEA) and Atomic Energy of Canada Limited (AECL)** reports are available at USAEC depository libraries. UKAEA reports are sold by Her Majesty's Stationery Office, London; AECL reports are sold by the Scientific Document Distribution Office, Atomic Energy of Canada Limited, Chalk River, Ontario, Canada. UKAEA and AECL reports issued after March 1, 1967, are sold by CFSTI to purchasers in the United States and its territories.

XU

# Nuclear Science Abstracts

The U. S. Atomic Energy Commission, Division of Technical Information, publishes *Nuclear Science Abstracts (NSA)*, a semimonthly journal containing abstracts of the literature of nuclear science and engineering.

*NSA* covers (1) research reports of the U. S. Atomic Energy Commission and its contractors; (2) research reports of government agencies, universities, and industrial research organizations on a worldwide basis; and (3) translations, patents, books, and articles appearing in technical and scientific journals.

Complete indexes covering subject, author, source, and report number are included in each issue. These indexes are cumulated and sold separately.

# Availability of NSA

**SALE** *NSA* is available on subscription from the Superintendent of Documents, U. S. Government Printing Office, Washington, D. C. 20402, at $42.00 per year for the semimonthly abstract issues and $38.00 per year for the cumulated-index issues. Subscriptions are postpaid within the United States, Canada, Mexico, and all Central and South American countries, except Argentina, Brazil, Guyana, French Guiana, Surinam, and British Honduras. Subscribers in these Central and South American countries, and in all other countries throughout the world, should remit $52.50 per year for subscriptions to semimonthly abstract issues and $47.50 per year for the cumulated-index issues. The single-copy price for the abstract issues is $1.75 postpaid, with this exception: Add one-fourth of $1.75 for mailing to the countries to which the $52.50 subscription rate applies.

**EXCHANGE** *NSA* is also available on an exchange basis to universities, research institutions, industrial firms, and publishers of scientific information. Inquiries should be directed to the Division of Technical Information Extension, U. S. Atomic Energy Commission, P. O. Box 62, Oak Ridge, Tennessee 37830.

XUM

TECHNICAL PROGRESS REVIEWS may be purchased from Superintendent of Documents, U. S. Government Printing Office, Washington, D. C. 20402. *Nuclear Safety* at $3.50 per year (six issues) for each subscription or $0.60 per issue; *Reactor Technology* at $3.00 per year (four issues) for each subscription or $0.75 per issue; each of the other journals at $2.50 per year (four issues) or $0.70 per issue. The use of the order form below will facilitate the handling of your order.

POSTAGE AND REMITTANCE: Postpaid within the United States, Canada, Mexico, and all Central and South American countries except Argentina, Brazil, Guyana, French Guiana, Surinam, and British Honduras. For these Central and South American countries and all other countries: add, for each annual subscription, $1.00 for *Nuclear Safety* and $0.75 for each of the other journals; for single issues, add one-fourth of the single-issue price. Payment should be by check, money order, or document coupons, and MUST accompany order. Remittances from foreign countries should be made by international money order or draft on an American bank payable to the Superintendent of Documents or by UNESCO book coupons.

## *order form*

SUPERINTENDENT OF DOCUMENTS
U. S. GOVERNMENT PRINTING OFFICE
WASHINGTON, D. C. 20402

Please send — 1, 2, or 3 years

- ☐ Isotopes and Radiation Technology _____
- ☐ Nuclear Safety _____
- ☐ Reactor Technology _____
- ☐ Reactor Materials _____

Enclosed: document coupons ☐ check ☐ money order ☐

Charge: Superintendent of Documents No._____

SUPERINTENDENT OF DOCUMENTS
U. S. GOVERNMENT PRINTING OFFICE
WASHINGTON, D. C. 20402

(Print clearly)

_____
Name

_____
Street

_____
City, State, ZIP Code

XUM